Queensland University of Technology

Stream & Groundwater Responses to Episodic Recharge: Integrating Time-Series Analysis & Environmental Tracers

Clément Duvert

Thesis submitted in fulfilment of the requirements for the degree of
Doctor of Philosophy

Discipline: Hydrology/Hydrogeology

School of Earth, Environmental & Biological Sciences

Science & Engineering Faculty

Queensland University of Technology

2016

"(...)
Core of my heart, my country!
Her pitiless blue sky,
When sick at heart, around us,
We see the cattle die –
But then the grey clouds gather,
And we can bless again
The drumming of an army,
The steady, soaking rain.
(...)"

— **Dorothea Mackellar (My Country)**

Abstract

[INTRODUCTION] Understanding shallow groundwater systems is of fundamental importance globally, especially in environments where recharge is non-uniformly distributed in space and time. In particular, it is critical to develop methods that investigate climate-induced hydrological processes in such environments. The goal of this dissertation is to improve our understanding of the response of shallow aquifers and streams to episodic recharge at different spatial and temporal scales. A particular focus is on assessing the effects of episodic recharge on both inter-aquifer mixing and groundwater contribution to streams, a research area that has been largely ignored to date. To address these questions, the Teviot Brook catchment in subtropical southeast Queensland is examined in detail. This well-defined catchment is at the transition between an igneous mountain range and an alluvial valley, both overlying a sedimentary formation.

[RESULTS] Examination of the spectral signature of long-term precipitation and water level time-series demonstrates that the alluvial aquifer in its upstream section (i.e. close to the mountain front zone) is almost as responsive to inter-annual rainfall cycles as the stream, particularly during wet periods. By contrast, changes are less pronounced in the downstream section of the aquifer, even during multi-year droughts that led to the drying out of streams. The catchment hydrological dynamics are overall closely related to large-scale atmospheric circulations controlling rainfall patterns. By the use of an original sliding window cross-correlation technique, it is also inferred that diffuse recharge controls the short-term groundwater response in the downstream region.

Hydrochemical and isotopic tracers are studied pre- and post- a major storm event in the alluvial, sedimentary bedrock and fractured igneous rock aquifers, as well as the streams. These chemical methods suggest a strong connection between the main stream and underlying alluvium. Prompt recharge of the sedimentary bedrock aquifer near the mountain front via the fractured igneous rocks is evidenced by substantial changes in a range of indicators such as deuterium excess and carbon-13. In the downstream sections, the signature of some alluvial waters is suggestive of mixing with the sedimentary bedrock aquifer, but this process cannot be clearly established.

The assessment of changes in rare earth element signatures in each component enables evaluation of inter-aquifer mixing with more confidence. The contribution of freshly recharged waters to the deeper sedimentary bedrock groundwater flow via preferential pathways is confirmed along the mountain front, even in areas where more conventional tracers did not detect any variation. Post-flood contributions from sedimentary bedrock waters to the alluvium are revealed not only in the downstream part of the alluvial aquifer but also

at a location upstream, near the interface between the two formations.

The flowpaths of groundwater to the stream network are also investigated using time-series of a variety of tracers, including tritium. Results suggest that a substantial fraction of streamflow is contributed by old groundwater, likely to originate from the alluvial aquifer and/or the deeper sedimentary bedrock. The travel time of this older groundwater fraction is found to vary substantially over time; it is lower under low flow conditions, and increases shortly after major recharge events. This is attributed to the flushing out of older groundwaters by the recharge pulse. Also, while the travel time of groundwater stored in the catchment is generally longer than that of the groundwater contributing to stream baseflow, under high flow conditions the baseflow component has travel times that tend to approach those of stored groundwater.

[DISCUSSION & CONCLUSIONS] The findings described in this dissertation shed light on the hydrological response of catchments subjected to episodic recharge. Aside from providing a first qualitative assessment of mountain front recharge in a subtropical area, this work also identifies a number of nonlinear processes that had not been documented previously.

The connections between large-scale atmospheric circulations and catchment response are outlined, particularly for the groundwaters where mountain front recharge dominates. It is suggested that climatic cycles such as the El Niño Southern Oscillation may provide additional constraints on long-term groundwater level forecasting in eastern Australia.

It is also demonstrated that major recharge events can be a key control on inter-aquifer mixing. Due to the predominance of preferential pathways in this setting, groundwater flow is shown to be highly dynamic and to respond rapidly to a change in recharge conditions, both in the sedimentary bedrock and igneous rock formations. The need for a shift in thinking as to how bedrock aquifers are conceptualised in catchment studies is emphasised: rather than uniform and isotropic, such aquifers should be seen as highly preferential in character. Similarly, the interface between sedimentary bedrocks and overlying formations should be regarded as a dynamic zone with potentially significant interflow.

The finding that groundwater baseflow travel time estimates are positively correlated with antecedent precipitation is somewhat counterintuitive and contradicts previous observations. Importantly, it is suggested that the "old water" component in stormflow partitioning studies should not be regarded as one single, time-invariant entity, because its travel time varies considerably with varying recharge rates.

Significant outcomes from this work also include the development and refinement of methodologies related to the assessment of hydrological processes under changing recharge conditions. Of note is the use of rare earth elements as tracers of inter-aquifer transient mixing processes, as well as the collection of tritium time-series to outline variations in the travel time of the older groundwater fraction to streamflow. Benefits of conducting repeated sampling campaigns are also underscored for providing reliable assessments of the rate and timing of recharge effects on catchment hydrology.

A Glimpse of the Dissertation

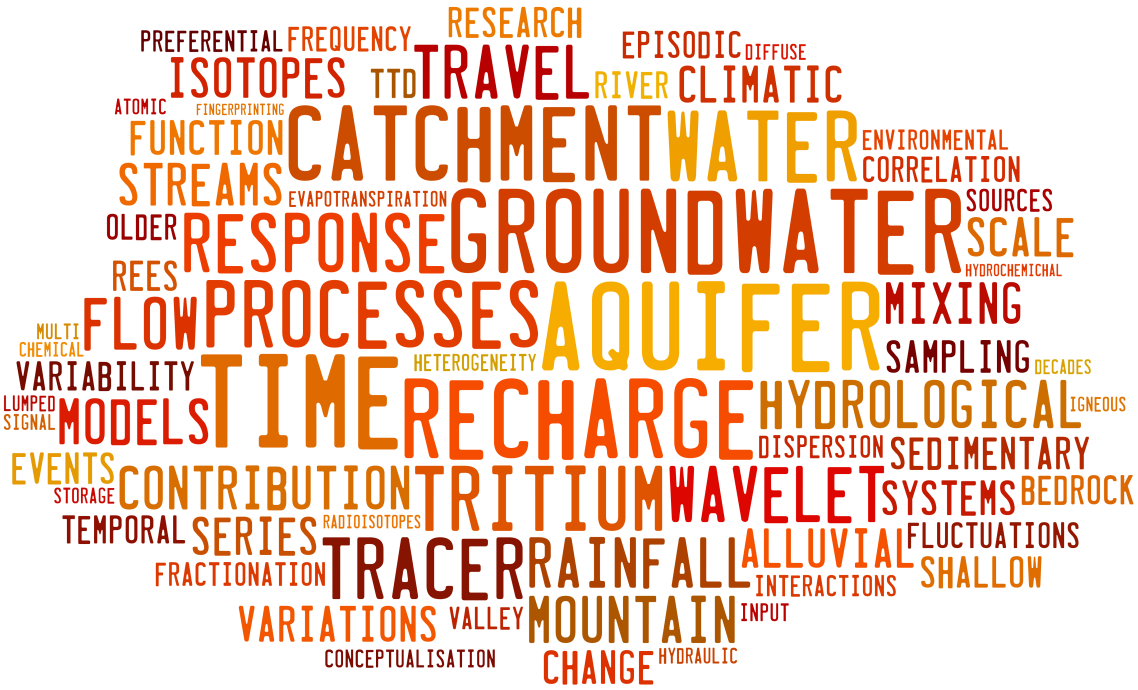

Acknowledgments

I owe my gratitude to all the people who have made this dissertation possible, and they are very many. Firstly, I would like to thank my Principal Supervisor, Malcolm Cox. I have been fortunate to have a supervisor who gave me the freedom to explore on my own. Thank you Mal for always supporting my ideas and research directions, even when I was departing from the group's research focus. I would also like to express my gratitude to Matthias Raiber, my Associate Supervisor. Thanks Matt for your enthusiasm and highly valuable guidance, particularly in the early stages of the PhD.

I am also thankful to my other supervisors, starting with Dioni Cendón. Apart from being a great host in Sydney, Dioni has brought his vast geochemical knowledge to the project, which I think has influenced my work and has been extremely beneficial. Hervé Jourde has been particularly helpful during my stays at the University of Montpellier, providing me with valuable expertise on time-series analysis, advice, and encouragement. My thanks also go out to other colleagues in Montpellier, in particular Christelle Batiot-Guilhe and Jean-Luc Seidel for many thought-provoking discussions. Lastly, I am grateful to Mike Stewart for kindly sharing his decades of wisdom in the field of catchment hydrology.

Besides my supervisors, I would like to thank my thesis committee, Christoph Schrank and Lucy Reading, for accepting to review my work and for the insightful comments. I am also thankful to the two referees who took time out from their schedule to serve as my external examiners. I extend my gratitude to the Head(s) of School at EEBS for continuous support: David Gust, Martin Sillence and, last but not least, Stuart Parsons. The administrative staff Sarie Gould, Courtney Innes, Noelene Davies and Samantha Talbot have also been an invaluable help throughout my candidature.

A very special thanks goes out to Des Owen, who has been an amazing friend and a great source of emotional support. Thanks Des for the endless debates on all sorts of topics, for allowing me to vent my frustration so many times, for teaching me the best strayan English, for the countless proof-reading sessions, and also for being such a great wordsmith. Thank you for the awesome time here and memorable trips overseas. Without your input, my thesis would definitely not look the way it does!

I am also thankful to other friends at QUT who made this experience exciting and fun. In particular, special thanks to Martin Labadz, Adam King, Coralie Siégel, Stefan Groflin and Irina Romanova for the rich scientific discussions and good moments outside of QUT. Thanks

also to my other fellows Zhenjiao Jiang, Bruce Napier, Jorge Martínez, Dareeju Biyanvilage, Padma Bollapragada, Mélina Celik, Alaa Haridi, Charmaine Cheah and Sharon Gray for the (caffeinated) time in R block 3rd floor, and to other folks for coping with our excessively noisy room.

Many people made my two summer stays at the Hydrosciences laboratory in Montpellier a very enjoyable experience; to name a few, Vivien Hakoun, Virgile Taver, Éléonore Resongles, Nicolas Briant, Jonathan Pourrier, and Pierre-Louis Legeay. I thank them for the fruitful discussions during the long coffee breaks. I extend my thanks to all the staff at the Hydrosciences laboratory for the good working atmosphere despite scorching temperatures and no air conditioning.

I am also indebted to my fieldwork assistants (Jackie, Giovanna, Andrea, Marica, Cora, Des, and I am probably missing some), thank you all for the fun times in the field and your hard work during data collection. I am very grateful to the landowners who let me sample their bores, thanks for not pulling out the rifle when you first thought I was a "dodgy foreigner sent by a mining company". The Landcare group (Lorraine Ternouth) and the Boonah council (Rick Stanfield) have also provided valuable information, which I greatly appreciate. Special thanks to Jiaorong Li for sharing her knowledge of the Teviot Brook catchment and for kindly providing me with the hydrochemical data she had collected twenty years ago. Because this thesis had a substantial laboratory component, I would like to warmly thank Shane, James, Aarshi, Irina, Sunny, Charlotte, Alice and Rachel at QUT, but also Robert, Chris and Brett at ANSTO, for much needed help at the bench and for good company.

I wish to dedicate this thesis to two academics who have been extremely influential in my young career. Ten years ago when I was still an undergraduate, Olivier Ribolzi made me discover catchment hydrology in the northern mountains of Laos. He has been such an inspiration, and I am indebted to him for sharing his tremendous knowledge of hydrochemistry and for teaching me his attention to detail. Then during my years in Mexico, Nicolas Gratiot was my advisor. I am yet to meet someone so trustful and supportive of my work; Nicolas became more of a friend than a supervisor. He has truly taught me how to become a researcher on my own, and he is the one who convinced me that I should pursue a career in research. I really feel lucky to have crossed paths with him!

I also recognise that this research would have been impossible without the financial support of the Endeavour Scholarship programme, the Australian Institute of Nuclear Science & Engineering, the Science & Engineering Faculty at QUT, and the French Embassy in Australia. I express my gratitude to those institutions.

Most importantly, all my good friends here and there have helped me stay – more or less – sane through these years despite the distance, and their friendship represents everything to me. And of course, I am forever indebted to my dear family for their love and support. *Merci !*

Contents

Statement of Original Authorship

The work contained in this thesis has not been previously submitted to meet requirements for an award at this or any other higher education institution. To the best of my knowledge and belief, the thesis contains no material previously published or written by another person except where due reference is made.

Signature: ..... **Date:** 03/04/2016

List of Publications

Chapter 4

C. Duvert, H. Jourde, M. Raiber, M.E. Cox, 2015. Correlation and spectral analyses to assess the response of a shallow aquifer to low and high frequency rainfall fluctuations.
Journal of Hydrology 527, 894–907.

Chapter 5

C. Duvert, M. Raiber, D.D.R. Owen, D.I. Cendón, C. Batiot-Guilhe, M.E. Cox, 2015. Hydrochemical processes in a shallow coal seam gas aquifer and its overlying stream–alluvial system: implications for recharge and inter-aquifer connectivity.
Applied Geochemistry 61, 146–159.

Chapter 6

C. Duvert, D.I. Cendón, M. Raiber, J.-L. Seidel, M.E. Cox, 2015. Seasonal and spatial variations in rare earth elements to identify inter-aquifer linkages and recharge processes in an Australian catchment.
Chemical Geology 396, 83–97.

Chapter 7

C. Duvert, M.K. Stewart, D.I. Cendón, M. Raiber, 2016. Time-series of tritium, stable isotopes and chloride reveal short-term variations in groundwater contribution to a stream.
Hydrology and Earth System Sciences 20, 257–277.

CHAPTER 1

Introduction

In this chapter, Sections 1.1 and 1.2 outline the background to the research developed in this thesis. Section 1.3 describes the general aims and provides details on the research questions to be addressed. Section 1.4 includes an outline of the thesis and its structure.

1.1 Significance of, and threats to, groundwater resources

Groundwater holds great social, ecological and economic importance. In particular, groundwater resources are an invaluable source of freshwater in areas where rainfall is not uniformly distributed throughout the year, such as in Mediterranean, wet/dry tropical, arid and semi-arid climatic regions. Groundwater is also comparatively less vulnerable to contamination than surface water bodies. As a result, two billion people worldwide rely on groundwater as their primary source of drinking water (Morris et al., 2003), and, just as importantly, groundwater extraction enables food security through supporting cropland irrigation (Shah et al., 2007).

The sustainability of groundwater resources depends on the rate of replenishment by recharge *versus* the rate of extraction. It is now widely accepted that both natural and human-induced factors are placing increasing pressure on groundwater resources, which may have significant effects on recharge rates (Taylor et al., 2013; Wada et al., 2014). First, aquifers are not isolated from climatic fluctuations (e.g. Tremblay et al., 2011; Kuss and Gurdak, 2014), and because climate change is likely to increase both the frequency and intensity of droughts and extreme rainfall worldwide (Bates et al., 2008), it may also im-

pact the recharge rates and groundwater processes (Green et al., 2011; Kløve et al., 2014). However, the magnitude of these changes remains unknown.

Other threats to aquifers stem from a range of anthropogenic activities that rely on groundwater extraction. Shallow groundwater and surface drainage systems are generally intricately connected (e.g. Hancock et al., 2005; Boulton et al., 2010). In these settings, overexploitation can lead to a reduction of river flows and negatively affect riparian ecosystems (Woessner, 2000). Overexploitation may also alter hydraulic gradients, which may in turn increase connectivity between aquifers and/or surface waters. This can become an issue where certain formations hold low-quality waters (e.g. brackish or saline), as mixing may lead to contamination of fresher resources. Particular examples are in areas where coal seam gas is exploited from coal-bearing deposits; large quantities of groundwater need to be extracted from the target formations, and concerns have been raised for potential impacts to both overlying aquifers and streams (Commonwealth of Australia, 2014).

Overall, in the context of increasing climatic and human-induced pressures, it is of major importance to improve our understanding of the response of groundwater as well as adjacent streams to external factors. A key issue is understanding the potential for connectivity between different water bodies, and the variations in connectivity over time. Because the response of hydrological systems can vary depending on the local climatological, morphological and geological settings, this goal first requires a better appreciation of how aquifers and streams operate at a catchment scale.

1.2 Catchment processes at the mountain front – alluvial valley transition zone

At a catchment scale, the processes governing aquifer dynamics can be complex. In mountainous areas, this complexity can be exacerbated by interactions between a range of aquifers from distinct geological formations. While mountainous areas cover a substantial part of the global land surface, mountain groundwater systems are still poorly understood. Greater recharge rates commonly occur in mountainous terrain because of higher precipitation, lower evapotranspiration and thinner soils (Maliva and Missimer, 2012). Recharge occurring at the mountain front – alluvial valley transition zone, i.e. the water that infiltrates into the subsurface fractures of the mountain rocks and piedmont formations, is believed to be a primary contributor to adjacent lowland rivers and aquifers (e.g. Alford, 1985; Wilson and Guan, 2004; Gleeson and Manning, 2008). Further downstream, diffuse recharge from precipitation over the alluvial plain may be the predominant recharge process (Stephens, 1995), but both mechanisms need to be clarified.

The seasonality of recharge is also an important factor (Jasechko et al., 2014), and under various climates, groundwater recharge occurs disproportionately from a few high intensity

rainfall events (e.g. Dripps and Bradbury, 2010; King et al., 2015); this is particularly true in tropical and subtropical regions (Jasechko and Taylor, 2015). In the current state of research, however, it is not fully clear how these highly intermittent rainfall events influence recharge in the mountain front – alluvial valley zone. The effect of episodic recharge on inter-aquifer mixing and travel time of water through catchments also remains poorly understood.

In order to advance our conceptual representation of catchment dynamics, the hydrological response of catchments to rainfall fluctuations needs to be investigated, including the role of aquifer recharge, potential inter-aquifer mixing, and discharge into lowland river systems. Such a study needs to encompass a wide range of temporal scales, from low frequency, multi-year climatic fluctuations to higher frequency rainfall variations up to individual storm events. Such conceptualisation of catchment processes is a necessary step towards effective and sustainable resource management.

1.3 Aims and scope of the study

The primary aim of this study is **to characterise the response of aquifers and streams to rainfall at different temporal scales**, with a particular focus on the mountain front – alluvial valley transition zone. To address this, the water pathways, mixing and travel times will be assessed in a study catchment located in southeast Queensland (Australia): this area was selected because it experiences many of the above-mentioned climatic and environmental issues. The catchment also features the interface between fractured igneous rock aquifers forming the headwaters and a sedimentary bedrock formation, both overlain by alluvial deposits. In particular, the three central research questions to be answered through this thesis can be stated as follows:

- How do shallow aquifers and associated streams respond to rainfall fluctuations at the mountain front – alluvial valley transition zone? (Chapters 4, 5, 6, 7)
- Can inter-aquifer mixing be triggered by episodic recharge? (Chapters 5, 6)
- Is the travel time of water through catchments affected by episodic recharge? (Chapter 7)

These questions will be addressed by first investigating the influence of climatic variability on shallow aquifers and streams using various time-series analytical techniques (Chapter 4). A combination of environmental tracers will then be used to explore the transient nature of hydrochemical processes, inter-aquifer mixing and recharge (Chapter 5), with a particular focus on an innovative tracer that shows promise for the examination of inter-aquifer processes (Chapter 6). Lastly, time-series of environmental tracers in streamwater will be used to assess the different groundwater contributions to streamflow and their age variations over time (Chapter 7).

Note that a more detailed statement of the hypotheses and sub-questions addressed in this dissertation is provided at the end of Chapter 2, which also clarifies how the research questions have been derived from knowledge gaps in the existing literature.

1.4 Thesis outline

While this thesis spans a broad range of investigations, all chapters are linked to the research aim formulated above. Chapter 2 provides a summary of the key aspects of the scientific background, establishes critical gaps in our understanding of catchment response to rainfall variations, and discusses the implications for this study. Chapter 3 gives a broad overview of the study area that was selected for this work, with details on its geology, climatology and catchment characteristics. Results are then presented through four separate chapters, each written in publication-formatted style (Chapters 4 to 7). These chapters correspond to stand-alone articles published in international scientific journals, and minor differences may exist between the version that appears in this thesis and the published versions.

In Chapter 4 (published in *Journal of Hydrology*), the response of the river and alluvial aquifer to both low and high frequency rainfall fluctuations that occurred in the past 25 years is investigated through time-series analysis. It is shown that the upstream parts of the alluvial aquifer, i.e. those closer to the mountain front zone, are responsive to low frequency rainfall fluctuations, whereas the downstream section of the shallow aquifer is less prone to change even during prolonged drought episodes. The short-term dynamics of response time also suggest that diffuse recharge prevails in the downstream part of the catchment.

Using a set of hydrochemical and isotopic tracers collected pre- and post- a major recharge event, Chapter 5 (published in *Applied Geochemistry*) provides an assessment of intra and inter-aquifer processes at shorter time scales. Rapid recharge of the sedimentary bedrock aquifer through the fractured rocks near the mountain front is evidenced, together with potential mixing between the sedimentary and downstream alluvial aquifers; however, not all lines of evidence are in agreement regarding the latter process.

Chapter 6 (published in *Chemical Geology*) takes a step further by investigating specifically the use of rare earth elements as a tracer of episodic recharge and inter-aquifer mixing. This less-conventional tracer allows more definitive assessment of inter-aquifer processes: the increasing influence of sedimentary bedrock waters in the downstream alluvium is confirmed, as is the recharge of the sedimentary bedrock aquifer via preferential pathways along the mountain front. In addition, post-flood contributions from sedimentary bedrock waters to the alluvium are revealed in the upstream part of the alluvial aquifer.

While the findings in Chapters 4, 5 and 6 have provided some foundation for understanding catchment response to rainfall variability, it remains unclear how the groundwater contribution to rivers responds to episodic recharge. Chapter 7 (published in *Hydrology and Earth System Sciences*) attempts to address this knowledge gap by exploring tracer time-series, including tritium, collected in streamwater. Results suggest that the travel time of discharging groundwater varies substantially over time; it is shown that shortly after flooding, the groundwater travel time can increase substantially, which is interpreted as the flushing out of older waters, possibly from the sedimentary bedrock aquifer, by pressure wave propagation.

Lastly, Chapter 8 summarises the findings and discusses them in relation to the overall aim of the thesis. It also provides a discussion of the implications of this study for hydrological process understanding in similar settings. Chapter 9 concludes the dissertation with some recommendations for future research.

CHAPTER 2

Scientific Background

In this chapter, an outline of the relevance of river–groundwater and inter-aquifer connectivity to catchment-scale hydrological processes is provided (Section 2.1). The current and emergent techniques used to investigate such processes are described and evaluated in Sections 2.2, 2.3 and 2.4. Lastly, Section 2.5 highlights the knowledge gaps identified from the review of literature, and the resulting research questions to be addressed in the dissertation.

2.1 Hydrological connectivity and its influence on catchment dynamics

2.1.1 River–groundwater and inter-aquifer connectivity

While surface water and groundwater have long been examined individually (Brunke and Gonser, 1997; Kalbus et al., 2006), these two entities are intimately connected in both space and time; hence the development of either resource can affect the quantity and quality of the other (e.g. Winter et al., 1998; Hancock et al., 2005; Boulton et al., 2010). The interactions between aquifers and rivers are controlled by the hydraulic gradient between the two components, and can occur in two ways: groundwater either flows as baseflow through the riverbed into the river (i.e. gaining stream), or surface water leaks through the riverbed into an underlying aquifer (i.e. losing stream) (Ladson, 2008). However, as such processes are at the interface between two scientific disciplines, river–groundwater interactions still pose major research challenges (Barthel, 2014).

Examination of subsurface hydrological processes can also be challenging, because interactions between individual aquifers with differing lithology may occur. Often the connectivity between different groundwater bodies is only partially studied, possibly due to a lack of widely available infrastructure for monitoring such processes. Inter-aquifer mixing has been observed in large sedimentary basins that comprise multi-layered aquifers (e.g. Négrel et al., 2012; Gonçalvès et al., 2013; Moya et al., 2015). For instance, upward flow from deep aquifers to shallower units has been documented (Dogramaci and Herczeg, 2002; Gassama et al., 2012). The mountain front zone can also bear significant inter-aquifer processes (Figure 2.1), particularly at the interface between the crystalline rocks forming the ranges and lowland sedimentary deposits (e.g. Hood et al., 2006; Smerdon et al., 2009; Andreu et al., 2011; Blumstock et al., 2015). Characterising inter-aquifer interactions in mountainous settings can be problematic, because fractured rock aquifers are often structurally complex, and mixing can occur locally along fractures (Sophocleous, 2002). In such settings, this complexity is likely to be compounded by interactions with the surface drainage network, especially where streams have eroded into the fractured rocks and where channels are made up of highly permeable, coarse-grained deposits (Maliva and Missimer, 2012). In order to better conceptualise how hydrological systems operate at the mountain front – alluvial valley interface, it is therefore crucial to consider both river–groundwater and inter-aquifer processes (Figure 2.1).

2.1.2 Understanding the timing of catchment response to rainfall

Because catchments are governed by temporally variable processes, assuming a steady state in conceptual models is too simplistic. It is now well recognised that climatic variations have a significant impact on river systems (e.g. Labat, 2010). Although aquifers are less

responsive than surface water bodies to a modification in external forcing, temporal changes can also be substantial. Where shallow aquifers are involved, there is clear evidence that climatic fluctuations, such as the El Niño Southern Oscillation (ENSO), are among the key drivers of groundwater variability (e.g. Hanson et al., 2004; Holman et al., 2009; Tremblay et al., 2011).

In catchments characterised by high seasonal and/or interannual climatic fluctuations, non-stationarity in the hydrological response becomes a fundamental consideration. This is particularly the case in areas where evapotranspiration rates typically exceed precipitation rates, hence limiting groundwater recharge (Maliva and Missimer, 2012). During minor rainfall events, most infiltrated water is lost to evapotranspiration, and the bulk of recharge occurs within a limited number of major events. Highly episodic recharge is common in arid to semi-arid environments (e.g. Cendón et al., 2010; Dogramaci et al., 2012), but has also been observed in temperate (Dripps and Bradbury, 2010) and humid subtropical settings (King et al., 2015). Factors such as low-frequency climatic fluctuations have been shown to influence interactions between aquifers (e.g. Cox and Wilson, 2006; Hofmann and Cartwright, 2013), but the effect of episodic recharge on inter-aquifer mixing remains largely undescribed.

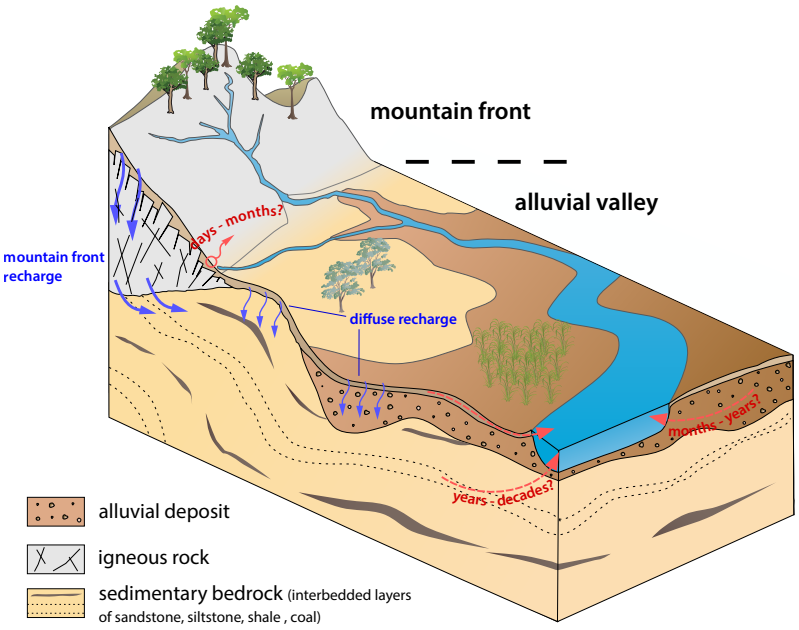

Figure 2.1: Conceptual diagram representing the mountain front – alluvial valley transition zone, and outlining the catchment processes to be studied as part of this thesis. Blue arrows represent recharge processes while red arrows represent discharge processes with an estimate of assumed travel times for each flow pathway.

River–groundwater interactions are another aspect of the catchment response that can be affected by climatic seasonality; e.g. a single river reach can transition from losing to gaining following a change in external forcing (Sophocleous, 2002). Where streams are gaining from an aquifer, the groundwater contribution to baseflow is essential in maintaining

riparian ecosystems (Woessner, 2000). Therefore, understanding the patterns of groundwater discharge to streams under changing rainfall conditions is of critical importance for the protection and management of water resources and ecosystems at the catchment scale. In particular, the travel time of groundwater contributing to baseflow is a key parameter that provides information on storage dynamics and flow pathways (McGuire and McDonnell, 2006; Figure 2.1). Baseflow waters can be very old (> 1000 years; Gardner et al., 2011; Frisbee et al., 2013), but it remains unclear how variable the age of baseflow waters is when catchments are subject to variations in recharge (Hrachowitz et al., 2013; Cartwright and Morgenstern, 2015).

Overall, addressing both spatial (i.e. from mountainous headwaters to lowland alluvial valleys) and temporal (i.e. event-based, seasonal and inter-annual) patterns of flow pathways is necessary for developing a comprehensive understanding of the catchment response to variable rainfall input (Schmidt et al., 2012). In particular, methods are needed for extrapolating results from small, instrumented settings to catchment scales (Sophocleous, 2002; Banks et al., 2011), and longer, higher resolution sampling schemes are also required to reduce uncertainties and better constrain fluxes (Hrachowitz et al., 2009).

To study the variability in water flow across catchments, a number of methods have been developed and tested in a wide range of settings. Firstly, methods relying on time-series analyses have proven useful in assessing the relationships between climatic variations and hydrological variables; these are outlined in Section 2.2. Secondly, a variety of hydrochemical and isotopic tracers has been used for the investigation of recharge, flowpaths and mixing in hydrological systems; these are described in Section 2.3. Thirdly, the travel time of water through catchments has been examined by adjusting environmental tracer time-series to lumped parameter models; these are evaluated in Section 2.4.

2.2 Time-series analyses to study catchment response to climatic variations

The occurrence of non-stationary patterns in hydrological time-series, such as trends and periodicities, has long been recognised, and in recent decades many tools have been developed to describe these patterns. While the response of streamflow to large-scale climatic fluctuations has been well investigated (e.g. Redmond and Koch, 1991; Cayan et al., 1999), most research on groundwater has overlooked climatic fluctuations and their relationship to groundwater flow (Barco et al., 2010). Only recently some studies have integrated regression, correlation and/or spectral analyses to reveal that climatic variations are among the main drivers of groundwater response (Hanson et al., 2004, 2006; Holman et al., 2009; Tremblay et al., 2011; Kuss and Gurdak, 2014). This section offers a succinct description of the time-series techniques relevant to this study.

2.2.1 Time-domain analyses

2.2.1.1 Detection of trends and shifts in time-series

Changes in hydrological time-series can occur either gradually (i.e. trends), abruptly (i.e. step changes), or in more complex forms (Kundzewicz and Robson, 2004). Various statistical tests have demonstrated their ability to detect such changes in hydrological records; monotonic trends are commonly investigated using the simple linear regression test or the Mann–Kendall test (Mann, 1945; Kendall, 1975). Step change tests are numerous and the most widely used are the Pettitt (Pettitt, 1982), Buishand or cumulative deviation (Buishand, 1982) and Worsley likelihood ratio (Worsley, 1979) tests.

Unlike the linear regression test, the Mann–Kendall test is a non-parametric test based on the correlation between the relative ranks of the data and their time order, which means little sensitivity to outliers. The Pettitt test is also a rank-based test (i.e. non parametric) that examines a change in the median of a record with the exact time of change unknown. The test is considered to be robust to changes in distributional form and relatively powerful (Kundzewicz and Robson, 2004). The Buishand test is based on the rescaled cumulative sum of the deviations from the mean, and is powerful in comparison with other tests for a shift that occurs towards the centre of the time-series (Buishand, 1982). The Buishand test is parametric as it assumes normally distributed data. The Worsley likelihood ratio also verifies whether the means in two parts of a record are different, for an unknown time of change. It is similar to the Buishand test but weights the deviation values depending on their position in the time-series.

Various reports in the literature outline the importance of using a combination of several tests to examine time-series, as they might not all provide the same response (Radziejewski and Kundzewicz, 2004; Machiwal and Jha, 2008). Published information clearly demonstrates that the concurrent use of a range of statistical tests is essential towards achieving reliable and more robust interpretations.

2.2.1.2 Correlation analyses

Correlation analyses have long been used to characterise the relationships between time-series. In particular, cross-correlation can allow identification of the transfer function between two signals. In hydrology, catchments can be considered as systems in which the input signal is rainfall, and the output signal (response) is groundwater level or stream discharge. In such cases, cross-correlation functions allow examination of the propagation of rainfall through the catchment, by assessing its response time (or lag time) and attenuation. If precipitation can be considered as a random process, the cross-correlation function represents the impulse response of the catchment to rainfall (e.g. Massei et al., 2006). The

cross-correlation between series x and y of length N is defined as (Box and Jenkins, 1976):

$$R_{xy}(k) = \frac{\sum_{i=1}^{N-k}(x_i - \bar{x})(y_{i+k} - \bar{y})}{\sqrt{\sum_{i=1}^{N}(x_i - \bar{x})^2 \sum_{i=1}^{N}(y_i - \bar{y})^2}} \tag{2.1}$$

where $R_{xy}(k)$ is the cross-correlation coefficient at lag k, and x and y are the arithmetic means over the N observations. By determining the value of k that maximises the correlation between the two series, noted τ, the method can yield an estimate of the average response time of the system:

$$\tau = \max_k R_{xy}(k) \tag{2.2}$$

Cross-correlation techniques have been primarily used for the study of karstic aquifers, as an alternative to more complex numerical models that may be less adapted to the high level of heterogeneity inherent to these systems. Different types of relationships have been established, including between rainfall and spring discharge (Mangin, 1975, 1984; Fiorillo and Doglioni, 2010), rainfall and groundwater levels (e.g. Larocque et al., 1998; Chen et al., 2004; Lee et al., 2006; Delbart et al., 2014), but also between rainfall and different chemical properties of water flow (Bouchaou et al., 2002; Massei et al., 2006). The use of correlation techniques in other hydrogeological settings has been very limited so far. Lee and Lee (2000) studied the rainfall–groundwater level relationships in a fractured bedrock aquifer, while Imagawa et al. (2013) investigated the same variables in an alluvial fan setting. Also lacking in the literature is an assessment of the seasonal variations in cross-correlation over extended time periods. Lee et al. (2006), Bailly-Comte et al. (2011) and Imagawa et al. (2013) were among the few who considered the seasonal variations in cross-correlation functions between rainfall and groundwater levels; all these studies found substantial differences in the groundwater response to contrasting climatic patterns.

The cross-correlation of a variable with itself is called autocorrelation (Box and Jenkins, 1976). Autocorrelation functions measure the linear dependency between successive values over a given period; in hydrology they have been used to describe the degree of persistence of a variable. The auto-correlogram of a de-trended time-series x is expressed as (Box and Jenkins, 1976):

$$r_x(k) = \frac{\sum_{i=1}^{N-k}(x_i - \bar{x})(x_{i+k} - \bar{x})}{\sum_{i=1}^{N}(x_i - \bar{x})^2} \tag{2.3}$$

Mangin (1975) first popularised the use of autocorrelation functions to karstic aquifers in an attempt to measure their inertia (persistence). Because individual rainfall measurements have little to no effect on neighbouring values, the autocorrelation function of rainfall would be expected to decrease quickly (Massei et al., 2006; Herman et al., 2009). By contrast, an aquifer with high storage capacity would present a much lower slope, indicating higher inertia than rainfall. Again, the use of autocorrelation function has been mostly limited

to the study of karstic aquifers (e.g. Larocque et al., 1998; Andreo et al., 2006; Valdes et al., 2006; Massei et al., 2006; Bailly-Comte et al., 2008; Herman et al., 2009). While these concepts have been rarely investigated in alluvial settings (Imagawa et al., 2013), they might be usefully applied to characterise shallow aquifers and how their persistence varies spatially and temporally.

2.2.2 Frequency-domain analyses

Spectral analyses have been used in hydrogeological studies for a few decades now (e.g. Mangin, 1984; Padilla and Pulido-Bosch, 1995). These techniques are complementary to correlation analyses, because they allow identification of the dominant oscillation modes in time-series that may be buried in noise. The Fourier transform is arguably the most widely used technique to decompose a signal into a frequency spectrum. However, because the standard Fourier analysis is based on the assumption that the signal is periodic in nature and of infinite length (Nakken, 1999), it is inadequate to translate non-stationary and finite signals, such as hydrological records, into the frequency domain.

Unlike the Fourier transform, wavelet analysis is a time-dependent spectral analysis that decomposes a time-series in the time–frequency space (Figure 2.2). The wavelet transform provides the ability to account for temporal variability in spectral character (Cooper and Cowan, 2008), which enables direct detection of discontinuities or trends in time-series (e.g. Torrence and Compo, 1998; Labat et al., 2004; Tremblay et al., 2011). To perform the transform, the technique involves shifting forward several scaled versions of an elementary (mother) wavelet along the time-series, and measuring the level of similarity between the wavelet and the signal at each step (Nalley et al., 2012; Figure 2.2). The continuous wavelet transform consists of the convolution of the time-series $x(t)$ with scaled and shifted wavelets $\psi_{a,\tau}(t)$:

$$C_x(a,\tau) = \int_{t=0}^{N-1} x(t)\,\psi^*_{a,\tau}(t)\,dt \qquad \text{with } \psi_{a,\tau}(t) = \frac{1}{\sqrt{a}}\,\psi\left(\frac{t-\tau}{a}\right) \tag{2.4}$$

where a is the parameter that governs the dilation ($a > 1$) or contraction ($a < 1$) of the wavelet, while τ is the parameter that governs the shifting of the wavelet along the time axis (Figure 2.2). $\psi_{a,\tau}(t)$ are the rescaled versions of the mother wavelet (when $a = 1$ and $\tau = 0$, $\psi(t)$ is the mother wavelet).

While the development of techniques based on wavelet transform in geoscience dates back from the early 1990s (e.g. Farge, 1992; Meyers et al., 1993), their introduction in hydrological studies has occurred later (Labat et al., 2000; Gaucherel, 2002; Andreo et al., 2006). Only recently wavelet analysis has been tested for the assessment of aquifer response to climatic variations (Slimani et al., 2009; Tremblay et al., 2011; Kuss and Gurdak, 2014). Very few studies have used the wavelet transform to address the spatial patterns in river and

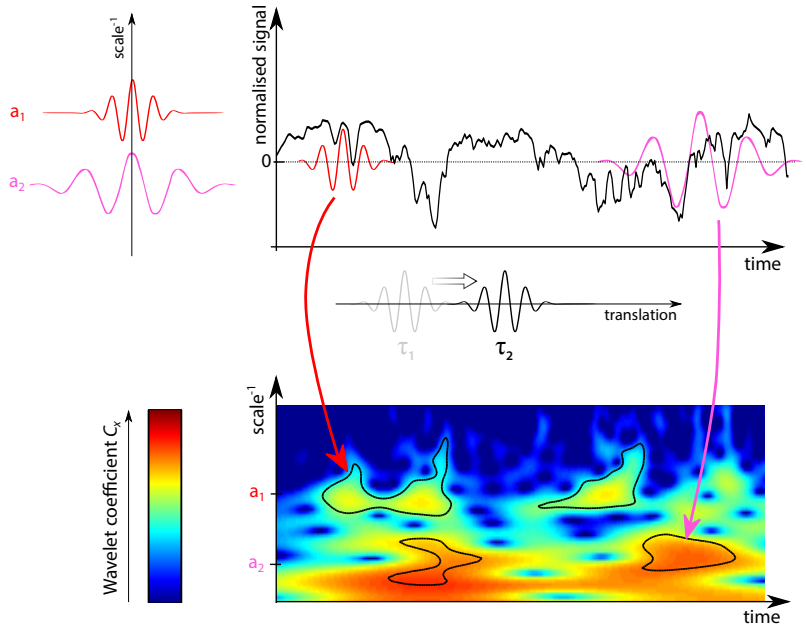

Figure 2.2: Illustration of the wavelet transform approach using the Morlet wavelet as a mother wavelet. Only the real parts of the wavelets are shown here. Daughter wavelets with $a = a_1$ (red) and $a = a_2$ (purple) are superimposed on the studied signal $x(t)$, represented by a continuous black line (top). The resulting wavelet coefficient spectrum $C_x(a, \tau)$ (bottom) measures the degree of correlation between $x(t)$ and the wavelet translated along the signal and defined at different scales a. The red and purple arrows point to areas where significant correlation exists between the two signals, emphasised by warmer colours on the wavelet spectrum.

groundwater response to rainfall, although this is needed to develop a sound understanding of the physical processes controlling shallow groundwater variability (Kuss and Gurdak, 2014).

2.3 Environmental tracers as fingerprints of recharge and mixing processes

Over the last few decades, environmental tracer techniques have been increasingly used for catchment process understanding. While artificial tracers can only be applied to local-scale studies, environmental tracers have the advantage of naturally labelling water molecules in the hydrological cycle, which allows for the study of water origin, flow pathways and travel times over a range of spatial and temporal scales. Environmental tracers can be especially useful for studying aquifers at the mountain front, where groundwater flow is complex and hydraulic data are often limited (e.g. Doyle et al., 2015).

A variety of tracers has been studied since the 1950s, the most common being the isotopes of the constituents of the water molecule itself. Along with the improvement of analytical techniques, many more tracers are now used in hydrological studies, and a substantial body of literature has demonstrated the added value of using multiple tracer data, rather than

relying on a single tracer, for better constraining flowpaths and inter-aquifer mixing (e.g. Kalbus et al., 2006; Cartwright et al., 2010; Négrel et al., 2012; Unland et al., 2013; King et al., 2015). This section provides a summary of the tracers relevant to this work, and describes how these can be used to investigate catchment-scale response to rainfall.

2.3.1 Stable isotopes of water

Isotopes of a particular element, e.g. the isotopes of oxygen ^{16}O and ^{18}O, have the same atomic number but varying numbers of neutrons in the nucleus, hence different atomic weights. Usually one of the isotopes is much more abundant than the other (e.g. ^{16}O more abundant than ^{18}O; Table 2.1). Stable isotope studies are based on the tendency of some isotopes to fractionate, i.e. to separate into light and heavy fractions. The isotopes of hydrogen and oxygen are very useful in hydrology because they can be considered as ideal tracers, i.e. "substances that behave in the studied system exactly as the material to be traced, but that have at least one property that distinguishes them from the traced material" (Zuber, 1986). In addition, the large variability of their isotopic ratios ^{2}H/^{1}H and ^{18}O/^{16}O can allow identification of a range of processes. The ratios measured in water samples are compared with a reference known as the standard mean ocean water (V-SMOW):

$$\delta^{2}\mathrm{H}(‰) = \frac{\left(\frac{^{2}\mathrm{H}}{^{1}\mathrm{H}}\right)_S - \left(\frac{^{2}\mathrm{H}}{^{1}\mathrm{H}}\right)_R}{\left(\frac{^{2}\mathrm{H}}{^{1}\mathrm{H}}\right)_R} \times 1000 \quad \text{and} \quad \delta^{18}\mathrm{O}(‰) = \frac{\left(\frac{^{18}\mathrm{O}}{^{16}\mathrm{O}}\right)_S - \left(\frac{^{18}\mathrm{O}}{^{16}\mathrm{O}}\right)_R}{\left(\frac{^{18}\mathrm{O}}{^{16}\mathrm{O}}\right)_R} \times 1000 \quad (2.5)$$

where R is for SMOW (reference) and S is for the studied sample. A positive δ value corresponds to enrichment with the heavy isotope relative to the standard, and *vice versa*. When δ^{2}H is plotted as a function of δ^{18}O for water in continental precipitation, an empirical linear relationship can be described, which is known as the global meteoric water line (Craig, 1961; Rozanski et al., 1993):

$$\delta^{2}\mathrm{H} = 8\ \delta^{18}\mathrm{O} + 10 \quad (2.6)$$

In local precipitation studies, slight deviations from the global meteoric line can occur that mainly depend on the local climate. Also, the deviation of δ^{2}H and δ^{18}O from equilibrium fractionation is referred to as the deuterium excess (Dansgaard, 1964). This value is useful because it cancels out the co-variations between the two isotopes.

Isotopic fractionation occurs during processes such as evaporation, chemical reactions or biological activity. Because of fractionation effects, waters develop a unique isotopic composition that can provide information on their origin and flow pathways (Clark and Fritz, 1997). In precipitation, considerable changes can occur due to altitudinal effects. Once on the ground surface, the isotopic content of water can vary widely depending on the amount of evaporation that occurs on the surface and in the shallow unsaturated zone, before the water infiltrates into the deeper ground. Evaporation systematically leads to an

Table 2.1: Natural abundance of the elements and isotopes used in this work.

Element	Isotopes	Natural abundance (%)	Half-life (yrs)
Hydrogen	^{1}H	99.9885	/
	^{2}H (deuterium)	0.0115	/
	^{3}H (tritium)	trace	12.32
Oxygen	^{16}O	99.76	/
	^{17}O	0.04	/
	^{18}O	0.2	/
Carbon	^{12}C	98.9	/
	^{13}C	1.1	/
	^{14}C	trace	5730
Strontium	^{84}Sr	0.56	/
	^{86}Sr	9.86	/
	^{87}Sr	7	/
	^{88}Sr	82.58	/

enriched δ^{2}H and δ^{18}O signature of water, hence to lower deuterium excess values. Once in groundwater systems, ^{2}H and ^{18}O behave conservatively and they become a characteristic property of the subsurface water flow. Under scenarios where a water sample is a mixture of two or more distinct components with different origins, and provided that the isotopic signature of each source can be described (e.g. direct runoff, subsurface water and deep groundwater), the analysis of stable isotopes allows identification of the sources and mixing patterns of the sample (e.g. Genereux, 2004; Lyon et al., 2009).

As it measures the deviation of a water sample from equilibrium, deuterium excess can be seen as a rate of evaporation index (Dansgaard, 1964). It has been used as a simple indicator of the processes driving groundwater salinisation, i.e. evaporation *vs* mineral weathering and/or transpiration (e.g. Huang and Pang, 2012). This can be usefully applied in settings where different aquifers have been affected by different salinisation processes, as a potential fingerprint of inter-aquifer mixing.

Apart from altitudinal effects, the isotopic signature of rainfall is also driven by important seasonal variations, and changes can be substantial even during single rainfall events. The collection of repeated samples covering different climatic patterns can therefore provide insight into episodic recharge processes. Under highly seasonal climates, the isotopic signature of groundwater, in particular its deuterium excess variations, can document the relative contributions of different rainfall events to recharge (Lee et al., 1999; Leybourne et al., 2006). Temporal variations of stable isotopes in rivers have also been used to determine the relative contributions of runoff and groundwater discharge to streamflow: variations would be expected to be large where runoff from recent precipitation is an important contribution, while the signal would be dampened where groundwater is the dominant contribution (Zuber and Maloszewski, 2000).

2.3.2 Carbon & strontium isotopic ratios

Carbon has two stable isotopes, ^{12}C and ^{13}C, which occur in a natural proportion of approximately 100 to 1 (Geyh and Mook, 2000; Table 2.1). Originally used to interpret ^{14}C data only, the $\delta^{13}C$ of dissolved inorganic carbon ($\delta^{13}C$-DIC) is now studied for its own tracing properties. In natural waters, the $\delta^{13}C$-DIC content is mainly driven by the isotopic composition of the carbon sources dissolved in the water. For recharging water, these sources are soil CO_2, living and dead organic matter in soils and rocks, methane, and carbonate minerals (Geyh and Mook, 2000). Because the source of organic carbon controls the state of fractionation of soil CO_2, information on the dominant vegetation types is required to determine the $\delta^{13}C$-DIC signature of recharge water. In groundwater, $\delta^{13}C$-DIC can range from –20‰ to +10‰ (Clark and Fritz, 1997). Specifically, positive $\delta^{13}C$-DIC values can be found in organic-rich systems where methanogenesis occurs, because this biogenic process preferentially removes the lighter ^{12}C from water (e.g. Schlegel et al., 2011; Sharma and Baggett, 2011; Golding et al., 2013). Recently, $\delta^{13}C$-DIC has shown potential for fingerprinting water origin and inter-aquifer mixing in regions where aquifers have contrasting $\delta^{13}C$-DIC signatures (Sharma and Frost, 2008; Frost et al., 2011; Meredith and Kuzara, 2012). However, there can be many overlaps between different potential water sources, which can make interpretation difficult in some particular cases.

In such situations, the use of strontium (Sr) isotopic ratio $^{87}Sr/^{86}Sr$ can help identify unique signatures from different sources. Strontium is a naturally occurring element that is principally derived from calcium-rich minerals through water/rock weathering reactions. Its isotopic composition in groundwater is mainly controlled by the mineralogy encountered along flowpaths. Among the four stable isotopes of strontium, only ^{87}Sr is radiogenic (Table 2.1); it is produced by decay from the radioisotope ^{87}Rb, which has a half-life of $4.88\,10^{10}$ years. High discrepancies exist in the $^{87}Sr/^{86}Sr$ ratios among minerals and rocks: ratios have values ranging from about 0.7 to greater than 4.0 (Faure, 1986). The use of Sr in hydrologic studies has been broadly documented in the last twenty years. When examined together with other tracers, the $^{87}Sr/^{86}Sr$ ratio has shown its efficiency for evaluating recharge processes and flowpaths (e.g. Négrel et al., 2001; Raiber et al., 2009; García-Veigas et al., 2013; Dogramaci and Skrzypek, 2015). In particular, the combined use of $^{87}Sr/^{86}Sr$ and $\delta^{13}C$-DIC has proved highly beneficial for the assessment of patterns and temporal scales in inter-aquifer mixing (Cartwright et al., 2010; Frost et al., 2011).

2.3.3 Rare earth elements

Rare earth elements (REEs) are a group of 15 elements called lanthanides (Figure 2.3), with atomic numbers ranging from 57 to 71, to which yttrium is commonly added (atomic number 39), because its chemical properties are identical to that of the heavier lanthanide series (Haxel et al., 2002). Interest in the use of REEs in hydrological studies originates

from their chemically coherent properties due to their trivalent charge and their similar ionic radius (Henderson, 1984). REEs exhibit strong fractionation as a group, but they also exhibit significant within-group fractionation resulting from the gradual decrease in their ionic radius with increasing atomic number (referred to as the lanthanide contraction; Johannesson et al., 2005). Of consideration is the dissimilar behaviour of cerium and europium compared to the other REEs because of their greater sensitivity to changes in redox conditions (Leybourne et al., 2000). These unique properties can assist in investigations of complex processes that single elements could not detect.

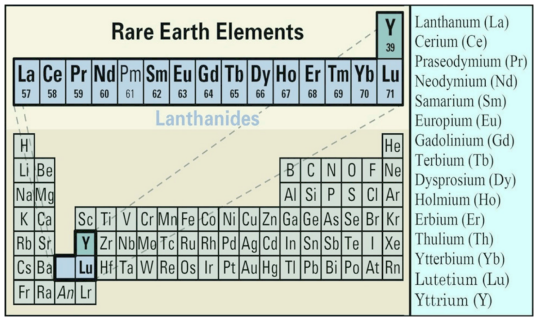

Figure 2.3: Periodic table with caption of REE (from Haxel et al., 2002).

The very low concentrations of REEs in natural waters (i.e. ppb levels) have long prevented their use as hydrological tracers (Dia et al., 2000). As a consequence of the recent developments in mass spectrometry, the past two decades have seen an increasing number of studies investigating REEs in hydrological systems. Waters commonly have REE fractionation patterns that closely resemble the REE fractionation patterns of the rocks through which they flow; therefore REEs can be another useful tracer of flowpaths and mixing within catchments (e.g. Johannesson et al., 1997; Tang and Johannesson, 2006; Biddau et al., 2009). In particular, REEs have been successful in describing inter-aquifer processes that were not revealed when using major ions and stable isotopes (Tweed et al., 2006).

However, the suite of elements can also behave non-conservatively in water–rock interaction. Factors such as pH, redox conditions, water chemical composition, and reactions with colloidal and particulate matter can control REE fractionation patterns (Tang and Johannesson, 2006; Pourret et al., 2007; Willis and Johannesson, 2011). Some studies suggest that REEs are released at an early stage during water–rock interaction in the recharge area, hence that they are indicators of recharge conditions (Tweed et al., 2006; Willis and Johannesson, 2011; Siebert et al., 2012). This is in disagreement with other work that argues that REE patterns represent the water–rock interactions occurring at a more recent stage, i.e. reflecting host rock conditions (Johannesson et al., 1997; Tang and Johannesson, 2006; Göb et al., 2013). These apparent contradictions underline the fact that more work is needed to better constrain the dynamics of REEs across catchments.

To understand the behaviour of REEs in groundwater, but also to appreciate the response of aquifers to rainfall events, capturing their seasonal variations is a fundamental step. While the temporal variability of REEs in rivers has been widely documented (e.g. Ingri et al., 2000; Shiller, 2002; Möller et al., 2014), little is known about their temporal variability in groundwater. The few studies that focused on this aspect have described substantial seasonal variations in the REE patterns of different groundwater systems (Gruau et al., 2004; Möller et al., 2006; Poh and Gasparon, 2011).

2.4 Travel time of water through catchments

2.4.1 Radioisotopes & tritium

Radioisotopes are isotopes that are unstable and release radiation when their nucleus loses neutrons. Radioactive decay is related to the degree of instability of the nucleus (Mook, 2000). It can be described as a purely statistical process, with a constant decay probability. The number of decays in a given time interval is proportional to the total number of atoms present:

$$\frac{dN}{dt} = -\lambda N \tag{2.7}$$

where N is the number of atoms and λ $[T^{-1}]$ is the decay constant. Integration of equation 2.7 gives the exponential decay rate, i.e. the rate at which the activity of a radioactive substance decreases with time (Freeze and Cherry, 1979):

$$A(t) = A_0\, e^{-\lambda/t} \tag{2.8}$$

where A_0 is the radioactivity level at some initial time and A the level of radioactivity at time t. It is a common and more intuitive practice to use half-life for describing the degree of instability of a radioisotope. Half-life $T_{1/2}$ is defined as the time required for half of the atoms initially present to decay, so that after one half-life $A/A_0 = 1/2$. It is written as:

$$T_{1/2} = \frac{\ln 2}{\lambda} \tag{2.9}$$

The half-lives of radioisotopes that are commonly used in hydrological studies cover a wide range of ages, from the very short-lived ^{222}Rn (3.8 days) to the long-lived ^{36}Cl (3.08×10^5 yr). Radioisotopes are valuable in the study of many hydrological processes because their decay provides a means of assessing times and rates (Mook, 2000). Dating is enabled by the observation of radioactive decay, but also in some cases by using records of time-varying input (e.g. for ^{3}H).

Tritium is a short-lived isotope of hydrogen which nucleus contains one proton and two neutrons. It decays into helium-3, and has a half-life of 12.32 yr (Table 2.1). The presence of

^{3}H in the hydrological cycle stems from both natural and anthropogenic sources. It is produced naturally in the atmosphere in small quantities, while it has been produced in higher proportions during the period of atmospheric testing of thermonuclear bombs, between 1950 and 1980. Tritium enters the hydrosphere as recharging precipitation. Although some ^{3}H may be produced naturally in the subsurface, its presence in groundwater most often refers to modern infiltration after the so-called bomb pulse (Clark and Fritz, 1997). Also, fractionation effects are small and can be ignored relative to measurement uncertainties and the larger change resulting from radioactive decay (Michel, 2005). In the southern hemisphere, the bomb pulse ^{3}H peak was several orders of magnitude lower than in the northern hemisphere (Freeze and Cherry, 1979; Clark and Fritz, 1997), and the ^{3}H concentrations of remnant bomb pulse water have already decayed well below that of modern rainfall (Morgenstern and Daughney, 2012). This characteristic allows for the calculation of unique ages from a single ^{3}H measurement (Stewart et al., 2010; Morgenstern and Daughney, 2012), which makes ^{3}H a very efficient and accurate tracer for travel time estimates over the last 100 years.

2.4.2 Calculation of travel times using lumped models

Tritium has long proven its value in studies that have focused on the travel time of water through catchments, both for estimating streamwater transit time and groundwater residence time (e.g. Eriksson, 1958; Maloszewski and Zuber, 1982; Michel, 1992; Stewart et al., 2007; Manning et al., 2012). In this thesis, the expression "transit time" refers to the time that has passed since a water molecule has entered a catchment until its exit through the stream network (McDonnell et al., 2010). By contrast, "residence time" describes water molecules resident within a catchment, rather than exiting it (Harman, 2015). In the literature, residence time is sometimes referred to as "groundwater age". Because the methods used for the evaluation of transit time and residence time are identical, the terminology "travel time" is used here to encompass both concepts.

Travel time is estimated by relating the tracer concentration – which can be ^{3}H, stable isotopes or chloride – measured in a sample to the history of the tracer input in water that fell over the catchment. Interpretation of travel time data is often problematic given that a single sample typically contains water parcels with different recharge histories, and thus with different ages. The mean age can vary considerably when distinct water sources are expected (Bethke and Johnson, 2002). This is especially true when the catchment is underlain by heterogeneous aquifers, as dispersion and mixing can lead to very broad spectra of ages (Weissmann et al., 2002). Rather than mean travel time, samples should therefore be characterised by a travel time distribution (TTD, i.e. probability density function of the travel times in the sample). Identifying the TTD of each sample is essential for deducing valuable information on recharge and storage processes (Eberts et al., 2012).

Several models, called lumped-parameter or black-box models, have been developed since the 1960s and applied to the interpretation of ^{3}H and other environmental tracers (Vogel, 1967; Eriksson, 1971; Maloszewski and Zuber, 1982). Each model is characterised by a TTD function that describes the transport of tracer particles from an input area to the output location (e.g. a borehole or the catchment outlet). Their use is based on the assumption that the shape of the TTD function is a priori known (Zuber and Maloszewski, 2000) and that the system is at steady state. Conceptually, if considering a conservative tracer that is instantaneously added at time t_e over the whole catchment area, the TTD function $g(t)$ describes the tracer concentration $C_{\text{out}}(t)$ at the outlet through time:

$$g(t) = \frac{C_{\text{out}}(t)}{\int_{t_e}^{\infty} C_{\text{out}}(t)\, dt} \tag{2.10}$$

This is equivalent to the probability density of the tracer leaving the catchment (Zuber, 1986); therefore the TTD function sums to unity in order to conserve mass:

$$\int_{t_e}^{\infty} g(t)\, dt = 1 \tag{2.11}$$

The mean travel time τ_m of a sample can then be derived from $g(t)$ by simply calculating the first moment of the function:

$$\tau_m = \int_{t_e}^{\infty} t\, g(t)\, dt \tag{2.12}$$

To resolve this conceptual approach mathematically, an inverse modelling method is applied where the catchment parameters are determined through adjustment of the TTD function to observations of tracer concentration data. For a steady state system, the relationship between the input and output concentrations is determined using a convolution integral, i.e. the amount of overlap of a TTD function as it is shifted over the input concentration function. The convolution integral is given by (e.g. Maloszewski and Zuber, 1982):

$$C_{\text{out}}(t) = [g * C_{\text{in}}](t) = \int_0^{\infty} C_{\text{in}}(t - t_e)\, g(t_e)\, e^{-(\lambda t_e)}\, dt_e \tag{2.13}$$

where t_e is time of entry; $C_{\text{out}}(t)$ is the output concentration; $C_{\text{in}}(t)$ is the input concentration; $e^{(-\lambda t_e)}$ is the factor to correct for decay if ^{3}H is used; λ is the decay constant; and $g(t_e)$ is an appropriate TTD function.

Various TTD functions have been developed to reproduce the effect of different recharge distributions and aquifer geometries (Cook and Herczeg, 2000). Some of these functions consider only the mechanical advection of water as driver of tracer transport, while others also account for the effects of dispersion–diffusion processes within the sub-surface. These models usually have one or two fitting parameters that are determined by calibrating the

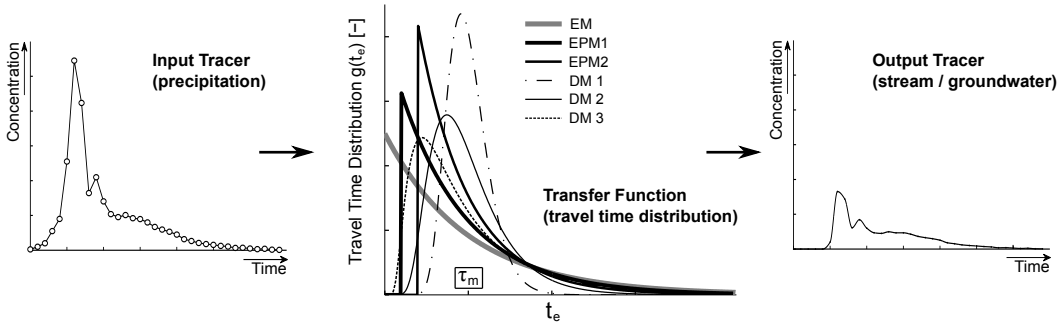

Figure 2.4: Outline of the inverse modelling method used to determine travel time distributions, together with the main TTD functions used in this study. EM stands for exponential model; EPM for exponential piston-flow model; DM for dispersion model. All distributions have a mean travel time τ_m of 10; EPM1 and EPM2 have piston flow parameters f of 0.8 and 0.6, respectively; DM1, DM2 and DM3 have dispersion parameters P_D of 0.03, 0.1 and 0.3, respectively.

model to the tracer records (Figure 2.4).

The piston flow model assumes that flow lines all have the same travel time, and the hydrodynamic dispersion and mixing are negligible. The TTD function for this model has one parameter (mean travel time τ_m) and is written as (Maloszewski and Zuber, 1982):

$$g(t_e) = \delta\left(t_e - \tau_m\right) \tag{2.14}$$

where δ is the Dirac delta function. In this model the traced water is assumed to have one single travel time. Tracers measured from confined aquifers with small recharge area might follow the piston flow model (Amin and Campana, 1996).

The exponential model (Figure 2.4) describes the TTD of a completely mixed reservoir, although transverse dispersion does not occur along flowlines and mixing occurs at the sampling point rather than within the system (Maloszewski and Zuber, 1996). Its TTD function also has one parameter (τ_m) and is as follows:

$$g(t_e) = \frac{1}{\tau_m}\, e^{-\frac{t_e}{\tau_m}} \tag{2.15}$$

This model can give an accurate description of TTDs in catchments underlain by homogeneous, unconfined aquifers receiving uniform recharge (Eberts et al., 2012).

The exponential piston flow model (Figure 2.4) describes a system that is exponentially distributed but delayed in time, since a portion of the system is piston flow (McGuire and McDonnell, 2006). Its TTD function has two parameters (τ_m and f) and is:

$$\begin{aligned} g(t_e) &= 0 \quad \text{for} \quad t_e < \tau_m(1-f) \\ g(t_e) &= \frac{1}{f\tau_m}\, e^{\left(-\frac{t_e}{f\tau_m}+\frac{1}{f}-1\right)} \quad \text{for} \quad t_e \geq \tau_m(1-f) \end{aligned} \tag{2.16}$$

where f is the ratio of the exponential volume to the total volume (= piston flow parameter). That model allows for a delay of the shortest flowlines, which may be suitable in certain settings. The exponential piston-flow model has been widely used for the interpretation of ^{3}H data in streamwater (e.g. Stewart and Thomas, 2008; Cartwright and Morgenstern, 2015).

The dispersion model (Figure 2.4) is an intermediate between the piston flow and the exponential models (Baudron et al., 2013). It assumes a tracer transport that is controlled by both advective and dispersive processes: a one-dimensional solution to the advection–dispersion equation is used as the TTD function (Maloszewski and Zuber, 1982), which has two parameters (τ_m and P_D):

$$g(t_e) = \frac{1}{t_e\sqrt{4\pi P_D \frac{t_e}{\tau_m}}}\, e^{\left[-\frac{(1-t_e/\tau_m)^2}{4P_D t_e/\tau_m}\right]} \tag{2.17}$$

where P_D is the dispersion parameter, which is the reciprocal of the Peclet number. P_D describes the relative width and height of the TTD and is a measure of the relative importance of dispersion to advection. The higher the value of P_D, the wider and the more asymmetrical the distribution of the travel times (Zuber and Maloszewski, 2000). The dispersion model has been extensively used in streamwater transit time investigations (e.g. Stewart et al., 2007; Stolp et al., 2010; Timbe et al., 2014) as well as groundwater residence time studies (e.g. Zuber et al., 2005; Blavoux et al., 2013; Lamontagne et al., 2015). It can give an approximate description of TTDs in samples from many system configurations (Baudron et al., 2013).

Lastly, several lumped-parameter models can be combined in order to represent more complex systems. For example, by using a combination of two dispersion models, Stewart and Thomas (2008) were able to identify two distinct groundwater components discharging to a spring in New Zealand.

Importantly, the effect of dispersion, diffusion and geochemical exchange can lead to unreliable estimates of TTDs when using lumped-parameter models (Bethke and Johnson, 2008). The combination of dispersion and decay of radioactive tracers can also lead to differences between the inferred apparent ages and the true mean travel times (Cornaton et al., 2011). However, these effects can be reduced by using ^{3}H and/or stable isotopes as tracers, which are constituents of the water molecule.

Unlike distributed-parameter models resolving the advection–dispersion equation, lumped-parameter models require minimal information concerning input and output tracer records (Einsiedl et al., 2009). While recent studies have developed non-parametric forms of TTD functions (Engdahl et al., 2013; Massoudieh et al., 2014a; McCallum et al., 2014), these novel techniques generally require a much higher amount of input data. Lumped-parameter

models, by contrast, can be easily validated with available data, and despite their straightforwardness, they have proven to yield valuable information about travel time within catchments that compare well to more complex approaches (Eberts et al., 2012; Green et al., 2014).

2.4.3 Capturing the non-stationary groundwater contribution to streams

Because catchment storage is not constant over time, the catchment response to rainfall is a temporally variable characteristic. This variability has been shown to affect substantially surface water transit times (McDonnell et al., 2010), but also groundwater residence times (Manning et al., 2012). Yet, the importance of temporal dynamics in travel times has often been overlooked in catchment hydrology (Hrachowitz et al., 2013). One of the reasons is that the widely used lumped-parameter model approach does not account for non-stationary processes. Only recently, the focus of many studies has transferred to developing time-variant forms of TTD, both in streamwater (e.g. Morgenstern et al., 2010; Roa-García and Weiler, 2010; Cvetkovic et al., 2012; Heidbüchel et al., 2012; Hrachowitz et al., 2013; Tetzlaff et al., 2014; Benettin et al., 2015; Harman, 2015) and groundwater studies (Massoudieh, 2013; Leray et al., 2014; Engdahl and Maxwell, 2015). While these studies have provided some foundation for investigating non-stationary travel times across catchments, the proposed approaches still require data-intensive computing, which largely limits their use for the time being (Seeger and Weiler, 2014).

There now seems to be consensus that theoretical developments have outpaced the plain observation of catchment processes, and that more experimental data is needed (McDonnell and Beven, 2014; Klaus et al., 2015a). In particular, high-resolution (event scale) sampling of environmental tracers may greatly assist in understanding time-variant catchment response (McDonnell et al., 2010; McDonnell and Beven, 2014). Travel time estimates are dependent on the chosen sampling frequency and length of records (Birkel et al., 2012; Massoudieh et al., 2014b), and it becomes increasingly clear that time-series of tracer data may improve the interpretation of highly seasonal hydrological systems.

The vast majority of research on streamwater transit time relies on the use of time-series of stable isotopes and/or chloride to inform lumped convolution models. Yet, the use of such tracers is likely to omit a significant portion of the TTD, i.e. older waters > 4 years (Stewart et al., 2007, 2010, 2012; Frisbee et al., 2013; Seeger and Weiler, 2014). This is a critical issue because the amount of older, deeper groundwater discharging to streams can be significant (Gardner et al., 2011; Smerdon et al., 2012; Bourke et al., 2014), and knowledge of the source and travel time of these delayed contributions is essential. Relating deeper groundwater flow processes to catchment response therefore requires addition of a tracer, such as ^{3}H, that is capable of fingerprinting water parcels with longer travel times (Figure 2.1).

Another important consideration is the extent to which the TTD of older groundwater contributions varies over time. Recent studies have shown that changes in recharge dynamics can activate different groundwater flowpaths, leading to significant modifications of the travel time of groundwater discharged to streams (Heidbüchel et al., 2013; van der Velde et al., 2015; Cartwright and Morgenstern, 2015). Storage within catchments is also a parameter that needs better appreciation, because storage water likely influences the dynamics of groundwater discharging into streams (Harman, 2015; van der Velde et al., 2015). A thorough assessment of the relationship between the travel time of groundwater stored in catchments and that of groundwater contributing to baseflow is therefore required. Overall, the development of experimental setups that combine sampling at high resolution (event scale), and analysis of tracers that can capture older water contributions, appears fundamental to obtain new insights into the variability of groundwater contribution to streamflow.

2.5 Implications – Derived research questions

The review of literature presented above has allowed identification of a number of gaps in knowledge, related to (i) the lack of understanding of catchment hydrological response to episodic recharge events, and (ii) some limitations and uncertainties in the techniques used to study such processes. The questions to be addressed in this study have therefore been divided into two categories, i.e. (i) those aimed at improving catchment process conceptualisation, and (ii) those aimed at improving observational and data interpretation techniques. In the following, the research questions to be addressed in each chapter are explicitly detailed consistent with this classification.

Chapter 4 – Response of a shallow stream–aquifer system to low and high frequency rainfall fluctuations

- *Questions on catchment process conceptualisation*
  - How do stream–alluvium systems respond to long-term rainfall fluctuations?
  - Are there connections between large-scale atmospheric circulations and catchment response?
- *Methodological considerations*
  - Is wavelet analysis a valuable tool to assess spatial and temporal patterns in aquifer response to rainfall?
  - Can time varying cross-correlation assist in detecting variations in short-term aquifer response to rainfall?

Chapter 5 – Transient hydrochemical processes in a river–alluvium–bedrock continuum and implications for recharge

- *Questions on catchment process conceptualisation*
  - Is mountain front recharge a significant process in aquifers of the mountain front –

alluvial valley?

– Can inter-aquifer mixing be triggered following major recharge events?

- *Methodological considerations*

  – Can a set of hydrochemical and isotopic tracers help resolve the location and seasonality of recharge in multi-aquifer settings?

Chapter 6 – Linking seasonal and spatial variations in rare earth elements with inter-aquifer processes

- *Questions on catchment process conceptualisation*

  – How do rare earth elements behave spatially and temporally in groundwater?

  – Is mountain front recharge a significant process in aquifers of the mountain front – alluvial valley?

  – Is inter-aquifer mixing triggered following major recharge events?

- *Methodological considerations*

  – Are rare earth elements effective tracers of episodic recharge and inter-aquifer mixing processes?

Chapter 7 – Tritium reveals temporal variations in the groundwater contribution to a stream

- *Questions on catchment process conceptualisation*

  – How does the travel time of older groundwater contribution to streams vary with varying recharge?

  – How do the travel time of water stored in catchments and that of groundwater contributing to baseflow relate?

- *Methodological considerations*

  – Is tritium beneficial to the evaluation of short-term variations in older groundwater contribution to streams?

CHAPTER 3

Features of Study Area

3.1 A natural laboratory setting with significant local issues

To address the research objectives formulated in the previous chapter, an area that provides a mountainous setting in which to explore river and groundwater responses to episodic recharge, as well as inter-aquifer connectivity, was required. The Teviot Brook catchment, located in Southeast Queensland, Australia, was found to meet all these criteria. The catchment headwaters, located in the Great Dividing Range, form steep gradients (Figure 3.1), and the area comprises a number of aquifers from a range of geological formations. Importantly, the region has a subtropical climate with highly variable rainfall, both seasonally and inter-annually. Hydrological monitoring infrastructure has been established in the catchment by government agencies in the 1980s, and long-term precipitation, discharge and groundwater level records are available at a number of locations.

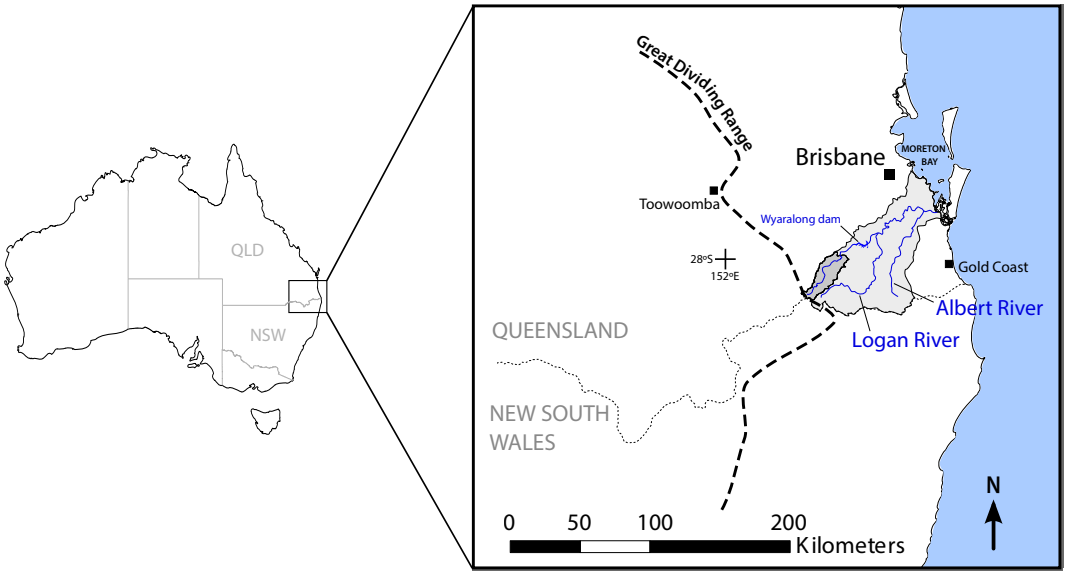

Figure 3.1: Location of the study area in southeast Queensland. The Teviot Brook catchment is represented in dark grey while the Albert-Logan catchment is in light grey.

The Teviot Brook catchment also experiences many of the issues outlined in the Introduction. The region has suffered from prolonged droughts in the 1990s and 2000s that were followed by extreme flooding during the summers of 2011 and 2013. There is no official metering of groundwater abstraction across the catchment, but the alluvial aquifer system supports intensive irrigated agriculture. Water shortages have been regularly experienced in the catchment during the past several decades, and as a result groundwater abstraction in the broader Albert-Logan area has increased by almost an order of magnitude between 1990 and 2010 (Sinclair Knight Merz, 2012). More recently, a major storm initiated by ex-tropical cyclone Oswald (January 2013) impacted on the headwaters of the Teviot Brook catchment, resulting in extensive damage to road networks and crops in the area.

In addition to climatic hazards, there is increasing environmental concern with regards to coal mining development in this general area. The Teviot Brook catchment overlies the Clarence–Moreton Basin, a regional sedimentary basin in which coal seam gas exploration has commenced in the mid 2000s and recently intensified. Exploration for coal seam gas requires drilling of deep wells that intersect the target coal-bearing formations, and gas production involves the extraction of large quantities of groundwater, which is likely to induce hydrodynamic changes in overlying aquifers and adjacent streams (Commonwealth of Australia, 2014). In some parts of the catchment, the coal-bearing sedimentary formation is in direct contact with the stream (Li and Cox, 1996), and groundwater discharge from the bedrock has been observed on stream banks at different locations (Li, 2001). In sections where the bedrock is likely to provide baseflow to the stream and seepage to the alluvium, coal seam gas activities may have a direct impact on both streamflow (i.e. loss of baseflow)

and alluvial groundwater flow. The Clarence–Moreton Basin is a region of considerable public opposition to coal seam gas, and the basin has been chosen as one of six nationwide priority regions for a "Bioregional Assessment", a Federal Government initiative aimed at increasing knowledge of the basin and its groundwater systems.

3.2 Geological setting

3.2.1 Regional geology

The Clarence–Moreton Basin is an intracratonic basin approximately 400 km in length and up to 120 km in width, which extends over 27 000 km^2 in southeast Queensland and northeast New South Wales (Wells and O'Brien, 1994; Figure 3.2). The Clarence–Moreton Basin overlies cratonised Paleozoic rocks and has been defined as part of the Great Australian Superbasin (Cook et al., 2013). Its regional sedimentary succession continues into the Surat Basin to the northwest, the separation between the two basins being represented by a broad basement high known as the Kumbarilla Ridge. The basin is bounded to the southwest by the Texas Subprovince, to the east by the Beenleigh Province, while it laps onto the Yarraman and South D'Aguilar Subprovinces and Esk Basin to the north (Figure 3.2).

The Clarence–Moreton Basin contains up to 3000 m of Late Triassic to Middle Jurassic non-marine sediments. Deposition is characterised by widespread, essentially fluvial sedimentation in broad depressions of the craton. Deformation within the basin is typically mild and the structural trends are generally inherited from the older basement rocks. Three major depocentres have been identified, i.e. the Cecil Plains, the Laidley, and the Logan Subbasins (Wells and O'Brien, 1994). The study area is within the Laidley Subbasin, and more specifically between the South Moreton Anticline and the Warrill Creek Syncline (Figure 3.2). These two structures, along with the West Ipswich Fault, are the major structural features in the area.

3.2.2 Local geology: structure & units

Situated on the western limb of the South Moreton Anticline and the eastern limb of the Warrill Creek Syncline, the Teviot Brook area has a general structure of north–south direction, with a flat-lying to very gentle west or east dipping appearance. The catchment bedrock is largely comprised of two sedimentary formations typical of the Clarence–Moreton Basin, the early Jurassic Marburg Sandstone in the northeast section, and to a much greater extent the middle Jurassic age Walloon Coal Measures. Both these formations are intruded by numerous Cenozoic rocks, which form substantial outcropping intrusions on the catchment floor, and in places capped by Cenozoic basalt flows. Igneous activity has also produced deformation of the sedimentary formations by dragging their beds upwards (Li, 2001). Quaternary sediments forming the alluvium have developed along streambeds as well as in the

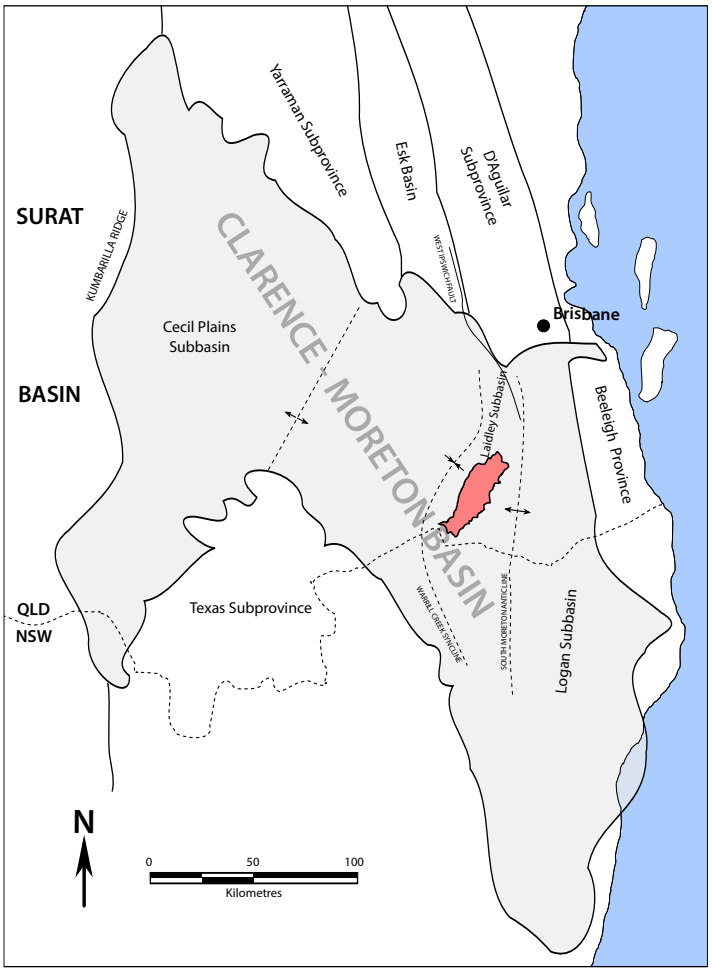

Figure 3.2: Regional structure of sedimentary basins, showing extent of the Clarence–Moreton Basin, which underlies the Teviot Brook catchment, shown in red. Map compiled from Wells and O'Brien (1994) and Li (2001).

lowland plain. Following is a summary description of each geological formation relevant to this study.

Sedimentary bedrock

The Walloon Coal Measures form the bedrock in most of the catchment (Figure 3.3). They consist of interbedded layers of sandstone, siltstone, mudstone, shale and coal (Wells and O'Brien, 1994). The sandstones are generally fine- to medium-grained and dominantly volcanic lithic in composition. The mudstones are usually associated with ironstone nodules, smectite and kaolinite being the prevalent clay minerals (Yago, 1989). The formation also includes thin coal seams (mostly less than 1 m thick) that are widely distributed, plus minor limestone, calcite veins and occasional beds of altered volcanic ash. The easily erodible rock types result in a low rolling topography and few outcrops (Cranfield et al., 1989). According to drilling logs, the thickness of the Walloon Coal Measures is 130 m at the north edge of

the study area (ESSO Australia, 1974), while Rassam et al. (2014) estimated an average thickness between 120 and 240 m throughout the catchment.

Igneous rocks

The Walloon Coal Measures are commonly intruded by Cenozoic dykes, sills and highly irregular intrusive rocks (Cook et al., 2013). Intrusions are broadly distributed throughout the Teviot Brook catchment, with a variety of formations ranging from trachyte to dolerite (Figure 3.3). Typical examples are Mt. Toowoonan (trachyte dyke), Mt. Minto Craig (alkali-rhyolite ring dyke), Mt. Moon and Mt. French (rhyolite dykes), Mt. Sugarloaf (andesite plug) and Mt. Alford (rhyolite ring-complex) (Li, 2001). Cenozoic extrusive rocks also occur in the catchment, mainly concentrated in the headwaters where a lava flow sequence that is part of the Main Range Volcanics extends over around 9 km^2. This sequence is an almost exclusively mafic formation, highly fractured and dominated by mildly alkaline basalt and hawaiite (Stevens et al., 1989; Cohen, 2012).

Alluvium

Deposits of Quaternary alluvium are well developed along Teviot Brook and its main tributaries (Figure 3.3). Where the stream flows through the Walloon Coal Measures, it has locally incised the soft sedimentary rocks, whereas in areas dominated by the more resistant igneous rocks, there is little alluvium formed, notably towards the headwaters. The thickness of the alluvial material ranges from 5 m in the headwaters to over 20 m in the central sections of the drainage system. Where it is well developed, the alluvium typically contains three horizontal layers: (i) a 1–3 m sandy/silty gravel layer at the base of the alluvium, which lies directly on the sedimentary bedrock; (ii) overlying this is a 10–16 m layer of firm clay; and (iii) a $\approx$ 1 m thick layer of black loamy soil at the top (Seccombe, 1989). The clay layer often comprises thin gravel and/or sand lenses, which suggests that different paleochannels formed when the river migrated across the valley.

3.3 Land use & morphology

The Teviot Brook catchment covers an area of around 550 km^2 before its waters flow into the recently built Wyaralong dam. Further downstream, Teviot Brook joins the Logan River, a major coastal drainage feature that discharges into the southern Moreton Bay (Figure 3.1). The population in the catchment amounts to approximately 3500, about one quarter of which lives in rural areas. The Boonah township in the lower section of the catchment is the main urban centre with around 2500 inhabitants. The area produces diverse agricultural products such as vegetables (carrots, beans, potatoes), cereal crops (lucerne, maize) and beef as well as dairy cattle. The valley largely supports irrigated crops, while cattle grazing extends on hillslopes and in upland areas. The headwaters are covered by native subtropical rainforest and form part of the Main Range National Park.

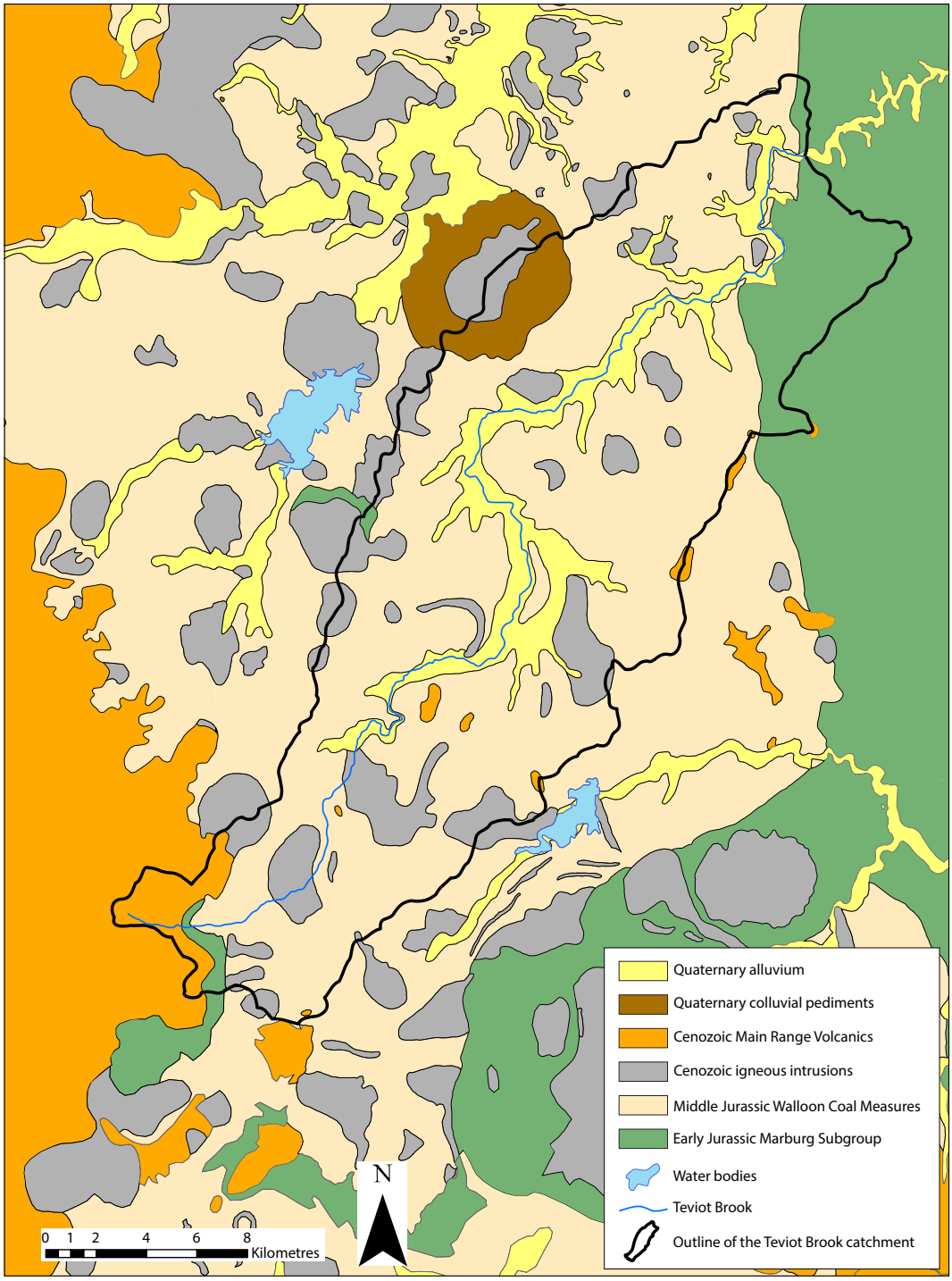

Figure 3.3: Geology of the Teviot Brook catchment and surrounding areas. Shapefile from the Geological Survey of Queensland (South-East Queensland GIS, Version 2, 2002).

The catchment is bounded by three mountain ranges: (i) the McPherson Range (a spur of the Great Dividing Range) in the headwaters, which reaches an elevation of 1375 mAHD at Mt. Superbus, highest peak of Southeast Queensland; (ii) the Dugandan Range in the east; and (iii) the Teviot Range in the west (Figure 3.4). Elevations rapidly decrease to the northeast, the outlet of the catchment lying at around 65 mAHD. The catchment is an elongate, roughly symmetrical valley along its southwest to northeast axis, and geology has played a major role in the morphology of the area: the more resistant igneous rocks form the steepest parts of the region, while the sedimentary formations have weathered to create low rounded hills with gentle slopes and broad alluvial valleys with dominantly fine-grained alluvium. The alluvial deposits typically form extensive flats and terraces adjacent to the main channel and within larger tributaries. Within these alluvial plains, the streams have built up embankments in places, and swampy areas are common in low-lying topography (Li, 2001).

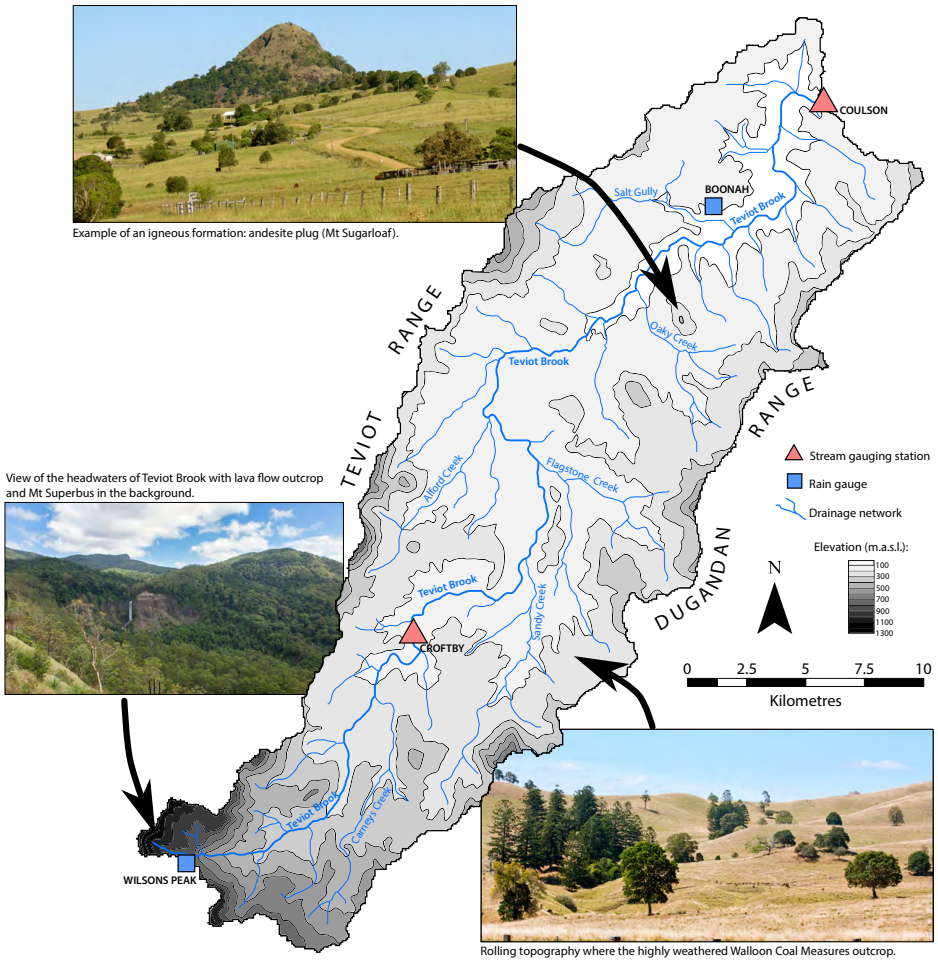

Figure 3.4: Topography of the Teviot Brook catchment, drainage network and location of monitoring stations. The photographs illustrate some morphological features typical of the catchment.

Teviot Brook, the main drainage feature, rises in the McPherson Range in the south. The stream then follows the centre of the valley floor and flows to the northeast. There are also a number of tributaries, most of which have their sources in the lateral ranges (Figure 3.4) and the sedimentary rocks have typical dendritic drainage patterns. Complex networks of gullies in the drainage system have developed as severely incised alluvium and sedimentary bedrock, and concerns have been expressed in regards to streambank erosion in the catchment (SEQwater, 2013).

3.4 Climatic setting

The climate in the area is humid subtropical (Köppen classification *Cfa*). Orographic effects largely control the rainfall pattern in the catchment, the annual precipitation in the headwaters being on average 50% higher than that in the lowland areas (Figures 3.5a and 3.5b). However, there can be considerable variations in rainfall from year to year. The annual precipitation at Boonah (downstream location; 110 mAHD; Figure 3.4) averages 840 mm for the 1965–2014 period, although the annual values range from 410 mm to 1260 mm (Figure 3.5a). At Wilsons Peak (upstream location; 850 mAHD; Figure 3.4) the average, minimum and maximum values are 1210, 700 and 1740 mm for the same period (Figure 3.5b).

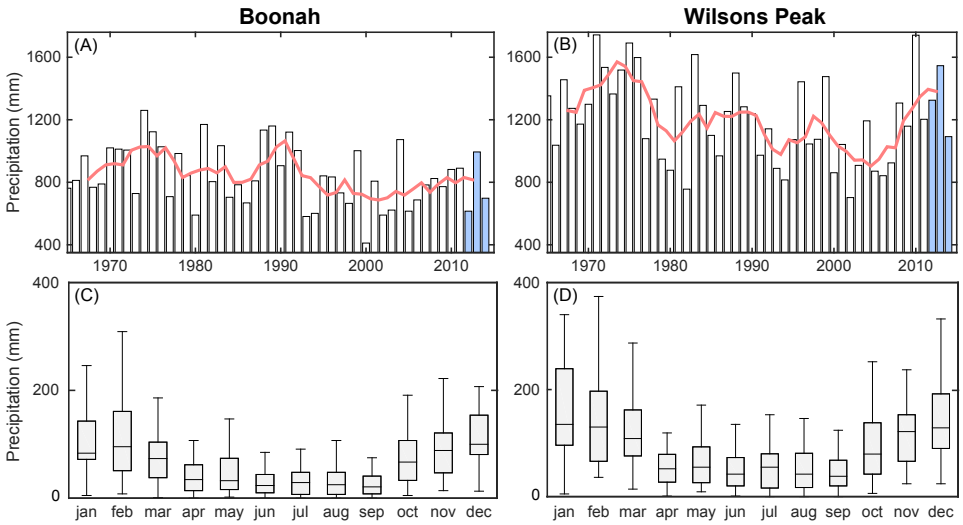

Figure 3.5: Annual precipitation from 1965 to 2014 at Boonah (a) and Wilsons Peak (b) (data from the Bureau of Meteorology). Red lines are five-year moving averages; the years of interest for this study are outlined in blue. Monthly variability in precipitation (mm) is shown for Boonah (c) and Wilsons Peak (d). Whiskers are for the quantiles 10, 25, 75, and 90, and the median values are shown as horizontal bars.

Seasonal patterns in rainfall are much better constrained, with the bulk of precipitation occurring between November and March, whereas June to September are mostly dry particularly in the lowlands (Figures 3.5c and 3.5d). Major rainfall events are not uncommon in summer, and daily rainfall in excess of 100 mm occurs on average every second year. Summer

thunderstorms triggered by atmospheric convection play a major role in the rainfall pattern of the area, as thunder is recorded 40 to 50 days per year (Li, 2001).

Evapotranspiration data are available at Beaudesert (25 km to the east of the Teviot Brook catchment). The average annual evapotranspiration rate is 1360 mm, with lowest values in June ($\approx$ 50 mm) and highest values in December or January ($\approx$ 190 mm). This confirms that evapotranspiration rates exceed precipitation rates in the Teviot Brook catchment during most of the year, the only exception being for major storm events.

3.5 Hydraulic properties of aquifers

Aquifers are associated with the three major geological components: (i) the Quaternary alluvium along Teviot Brook and its major tributaries; (ii) the Jurassic sedimentary formation underlying the alluvium; and (iii) the fractured Cenozoic intrusives and basalt flows. While much work has been done to describe the alluvial aquifer (Seccombe, 1989; Li, 2001), there is limited information on the Jurassic and Cenozoic formations.

Alluvial aquifer

The Quaternary alluvium forms a major groundwater resource, and according to a number of cross-sections compiled by Seccombe (1989), the gravel present in the basal layer of the alluvium is largely composed of resistant volcanic rocks. The gravel size varies from over 30 cm in the headwaters to less than 1 cm in the lower section. Because the clay layer that overlies these coarser elements has a much lower hydraulic conductivity, it locally confines the gravely aquifer. Li (2001) reassessed the pumping test data produced by Seccombe (1989), and found that the highest hydraulic conductivity occurs in the downstream sections of the aquifer (74–117 $\mathrm{m\,d^{-1}}$), where the gravel layer is wider and thicker than in other parts of the alluvium. High hydraulic conductivities also occur in the upper section of the alluvium (27–86 $\mathrm{m\,d^{-1}}$), where large size gravels and boulders act as aquifer materials. Lower values were found in the middle section of the alluvium (8 $\mathrm{m\,d^{-1}}$), which corresponds to a locally thinner basal layer.

Sedimentary bedrock

While the hydraulic conductivity of each constituting layer, when taken individually, may be low to very low, groundwater contained in the sedimentary formation can flow through joints and fissures, as well as in the bedding planes of coal seams, shales and sandstones (Li, 2001). By contrast, mudstone layers are poorly permeable and generally behave as aquicludes. Therefore, it is anticipated that groundwaters contained in the sedimentary formation flow mainly through preferential pathways. The spacing of bedding planes in the Walloon Coal Measures has been found to range from 2 to 20 mm (Eadie, 1985; Burton, 1988). As for aquifer productivity, the quantity of groundwater extracted from the formation is highly variable, but can be significant in places. The aquifer is often semi-confined to

confined, and water can be encountered from depths of 15 m, with most supplies being deeper than 30 m (Li, 2001).

Igneous rocks

All the Cenozoic formations present throughout the catchment are hard rocks with a low-porosity matrix, therefore groundwater movement may occur only via active conduits such as fractures and joints. Such features are typical within the catchment: open columnar joints of up to 1 m in width have been observed at the surface (Li, 2001), while in the subsurface, geotechnical investigations have shown that particularly basalts and trachyte are extensively fractured, with subvertical to vertical joints of 1 to 40 mm in width (Eadie, 1985; Burton, 1988). The size and density of fractures were also found to increase with the degree of weathering. More importantly, joints and bedding planes proved to be well developed where igneous rocks are in contact with sedimentary rocks (Burton, 1988). This feature suggests significant hydraulic connections between the two formations. Fractures are often partially filled with secondary minerals such as calcite (Li, 2001). Little is known about aquifer productivity in these igneous formations, but field observations indicate that some springs can have very substantial yields.

3.6 Overview of the catchment hydrology

Streamflow in Teviot Brook is dynamic and highly responsive to the local precipitation forcing. In the mountain front and upstream section of the alluvial valley, the stream is perennial, even after extended periods without rain, whereas in the downstream section of the catchment, Teviot Brook has occasionally dried up during prolonged droughts. It is unknown whether this mechanism is related to increased groundwater abstraction in the lowland plain during those dry spells. Most tributaries are intermittent and commonly dry up at the end of the dry season.

There are two gauging stations along the stream, and only the records from the upstream location are shown here because the records for the other station are very much alike. Interannual variations are significant (Figure 3.6a); of consideration are the two drought periods in the 1990s and the 2000s that led to record lows during most of these years (Figure 3.6b). By contrast, periods of high flow are in the 1970s, late 1980s and early 2010s. Annual runoff coefficient at this upstream station was highly variable between 1965 and 2014, ranging from 0.01 (severe drought in 2002) to 0.66 (highest storm event on record in 1976), with an average of 0.15. These values are comparable to other catchments in subtropical Australia (Peel et al., 2004), and most likely indicative of high evapotranspiration rates and/or deep drainage. Just as for rainfall, stream discharge is highly seasonal, with high flows from December to April followed by a long recession during the drier months (Figure 3.6c). Travel time of streamwater between the upstream and downstream gauging

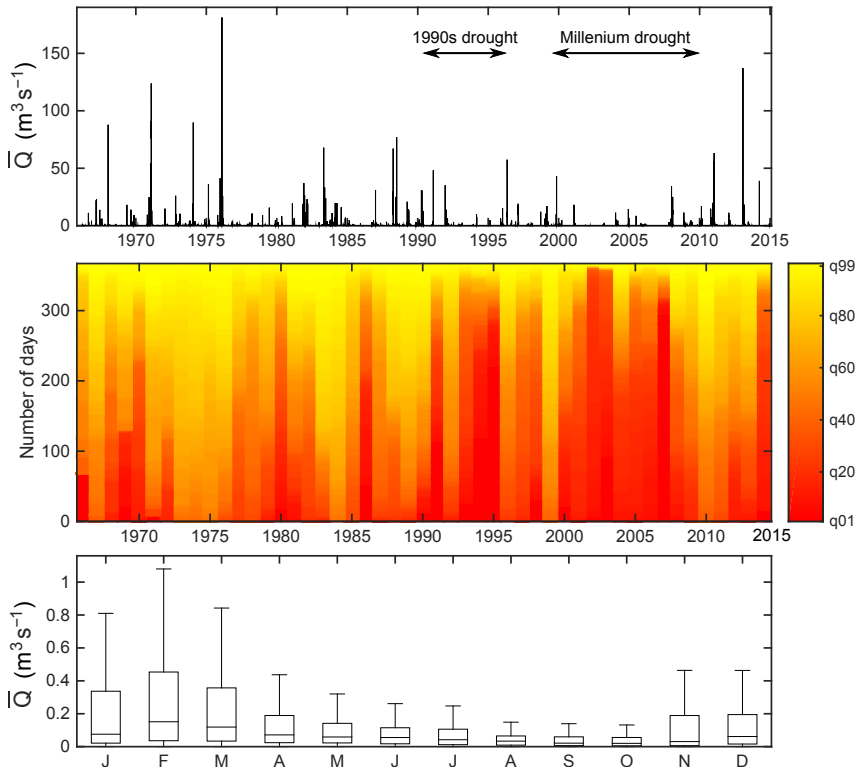

Figure 3.6: Mean daily discharge records at Croftby (upstream gauging station; DNRM station 145011A) for the 1965–2014 period (upper). Number of days exceeding the interannual quantiles (i.e. each bar represents the flow duration curve for a given year) (middle). Monthly variability in mean daily discharge at Croftby (lower). Whiskers are for the quantiles 10, 25, 75, and 90, and the median values are shown as horizontal bars.

stations is between five and 10 days depending on flow conditions.

The high discharge event that occurred in January 2013 (Figure 3.6a) is of high relevance for this work. It is the second highest value recorded since 1965, with a mean daily discharge at Croftby of $137\,m^3\,s^{-1}$. Chapters 5, 6 and 7 of this thesis examine in detail the response of different hydrological components to this extreme recharge episode.

CHAPTER 4

Response of a Stream–Aquifer System to Low and High Frequency Rainfall Fluctuations

This chapter has been published as:

C. Duvert, H. Jourde, M. Raiber, M.E. Cox, 2015. Correlation and spectral analyses to assess the response of a shallow aquifer to low and high frequency rainfall fluctuations.
Journal of Hydrology 527, 894–907. doi:10.1016/j.jhydrol.2015.05.054

Abstract

With the predicted acceleration of drought and flood frequency worldwide, it is critical to build knowledge on how shallow groundwater systems respond to rainfall variability. In this study, we characterise the hydrodynamic response of an agricultural catchment located in southeast Queensland, Australia, to the low and high frequency fluctuations in precipitation that occurred in the past 25 years. Strong interannual variations in the precipitation input affected surface water flow more substantially than groundwater levels (GWLs). There was also a likely influence of groundwater abstraction on stream baseflow and GWLs, although it was difficult to quantify. Several low frequency oscillations were apparent in the GWL records, particularly in the upstream section of the aquifer, which were neither detectable in rainfall nor in discharge records. Statistically significant episodes of coherence were found at the 2 to 4-yr band between the Niño3.4 index and GWLs for those upstream bores, especially during the 1995–2000 interval, which may be related to a strong La Niña event. In the downstream section of the catchment, higher groundwater persistence probably led to higher filtering of these low frequency oscillations. This paper also proposes a methodology for assessing the dynamic response time of GWLs in shallow aquifer systems to the precipitation input. Response time in a downstream borehole was highly variable temporally, ranging from 11 to 121 days. Rainfall amount was found to significantly affect the short-term dynamics of response time, with elevated rainfall leading to a decreased response time. Annually averaged response time was correlated with the annual number of days with rainfall > 30 mm, which was interpreted as the potential for diffuse recharge. Higher recharge potential induced longer response times, probably because of the larger amplitude in GWL variations.

4.1 Introduction

Shallow alluvial groundwater resources play an essential role in sustaining global agricultural activities through cropland irrigation. They generally provide good quality freshwater that is less vulnerable to contamination and climate unpredictability than surface water bodies. Alluvial aquifers are of strategic importance particularly in areas where rainfall is not uniformly distributed throughout the year, such as in Mediterranean, subtropical, arid and semi-arid regions. The recharge of shallow aquifers is therefore an important mechanism that needs to be well understood for effective management. Directly related to groundwater recharge are the fluctuations of groundwater levels (GWLs) (Dickinson et al., 2004; Zhang and Schilling, 2004; Cuthbert, 2010). With the acceleration of drought and flood frequency due to climate change (Bates et al., 2008; Taylor et al., 2013), expanding the knowledge on how shallow alluvial GWLs and associated streams respond to fluctuations in precipitation is fundamental. To fully understand these processes, the effects of both low and high frequency rainfall variations have to be investigated.

Examination of hydroclimatic time-series requires the use of appropriate analytical methods in order to account for non-stationarity and intermittent periodicities (Holman et al., 2011). Although spectral analyses have potential for detecting periodic patterns, most methods assume that signals are stationary in time and of infinite length. Unlike traditional spectral analyses, the wavelet transform method describes the frequency of a signal as a function of time, which allows detection of discontinuities and transient patterns (Grinsted et al., 2004). It is now well recognised that large-scale low frequency climatic fluctuations can have a substantial influence on GWL variability (e.g. Hanson et al., 2004; McNeil and Cox, 2007; Barco et al., 2010), and wavelet analysis has shown its value in identifying such relationships (Slimani et al., 2009; Holman et al., 2011; Tremblay et al., 2011; Perez-Valdivia et al., 2012; Kuss and Gurdak, 2014). As far as determined, however, few studies have concurrently applied wavelet transform to time-series of rainfall, streamflow, shallow GWLs and climate indices to assess the possible relationships amongst them. The delineation of spatial patterns in low frequency GWL variations within single aquifer systems has also been rarely addressed, although this is needed to develop a sound understanding of the physical processes controlling GWL variability (Kuss and Gurdak, 2014).

In addition to the study of low frequency periodicities in hydroclimatic records, an assessment of the response of shallow aquifers to high frequency rainfall fluctuations is required. Correlation analyses have been successfully used for this purpose (e.g. Chen et al., 2004; Massei et al., 2006; Fiorillo and Doglioni, 2010). The cross-correlation function can be used to determine an average response time between an input (rainfall) and an output (GWLs) signal. If precipitation can be considered as a random process, this cross-correlation represents the impulse response of the groundwater system to rainfall. Following the work by Larocque et al. (1998), Lee et al. (2006) subdivided multiannual time-series of rainfall and GWLs into seasonal datasets of 3-month duration, and analysed the variability of the impulse response by calculating cross-correlations for each period. Although this method yielded valuable information on the seasonal variability of groundwater response time, it may benefit from the addition of a more dynamic component. In particular, using sliding windows along the signals may allow acquisition of high-resolution time-series of GWL response times. An approach of this kind was first proposed by Beck et al. (1969) to determine flow velocity for manufacturing purposes. Latest applications in geosciences include the estimation of debris flow rate (Arattano and Marchi, 2005), assessment of transit time in karst systems (Bailly-Comte et al., 2008, 2011) and sewer flow monitoring (Dürrenmatt et al., 2013). Delbart et al. (2014) used time-varying cross-correlation functions to define the dynamic response time of shallow karstic GWLs to precipitation input. These authors successfully applied the sliding-window method to establish that response time was highly variable even at short time scales, and primarily a function of rainfall intensity. This approach proved useful in their case, and needs further testing in alluvial settings.

Another valuable correlation method is the autocorrelation function, which allows characterisation of the degree of persistence of a groundwater system. In the literature various terminologies have been proposed to refer to this particular character: the "memory effect" of an aquifer (e.g. Mangin, 1984; Valdes et al., 2006), its "inertia" (e.g. Bailly-Comte et al., 2008), or its "persistence" (e.g. Barco et al., 2010; the wording used in this paper). Following the pioneering work of Mangin (1984), persistence has been widely studied in karstic systems (Larocque et al., 1998; Andreo et al., 2006; Massei et al., 2006; Bailly-Comte et al., 2008), among others). In alluvial aquifers, however, the concept of persistence has to date been rarely investigated (Imagawa et al., 2013), and it might be usefully applied to characterise shallow aquifers and how their persistence varies spatially.

In this study, we examine time-series of rainfall, streamflow and shallow alluvial GWL in a subtropical agricultural catchment located in southeast Queensland, Australia. The region has been subjected to two extended periods of drought in the last 25 years that were preceded and followed by unusually wet conditions. The objectives are to use a set of correlation and spectral analyses in order to (i) characterise groundwater persistence and its variability within the aquifer system, (ii) assess the response of the stream-alluvial system to low frequency (inter-annual) fluctuations in precipitation, and (iii) assess the response of the aquifer to high frequency (daily) rainfall variations.

4.2 Methods

4.2.1 Study area

The Teviot Brook catchment is a tributary of the Logan River, southwest of Brisbane (Figure 4.1). It has its headwaters dominated by the basalts of the Main Range Volcanics, which form the crest of the Great Dividing Range. Elevations range between 65 m and 1375 m, and the climate is humid subtropical with extremely variable rainfall and an annual average precipitation of approximately 900 mm. Distribution of discharge is uneven throughout the year, with high flows occurring in summer followed by a long recession towards winter (Figure 4.1). The main stream and tributaries flow over alluvial material composed of weathered catchment materials, which range from cobble size and coarse-grained in the headwaters to fine-grained in the central and lower parts of the catchment. The alluvium has a thickness ranging between 5 m upstream and more than 20 m in downstream sections.

The general groundwater flow direction follows the alluvial flowpath and is essentially from the southwest to the northeast. Vertical hydraulic gradients indicate upward flow from the alluvium to the stream network. Groundwater levels are shallow across the alluvium, with values between 0.5 and 10 m below surface elevation. According to pumping test data (Seccombe, 1989), the aquifer transmissivity ranges between 0.9×10^{-3} and

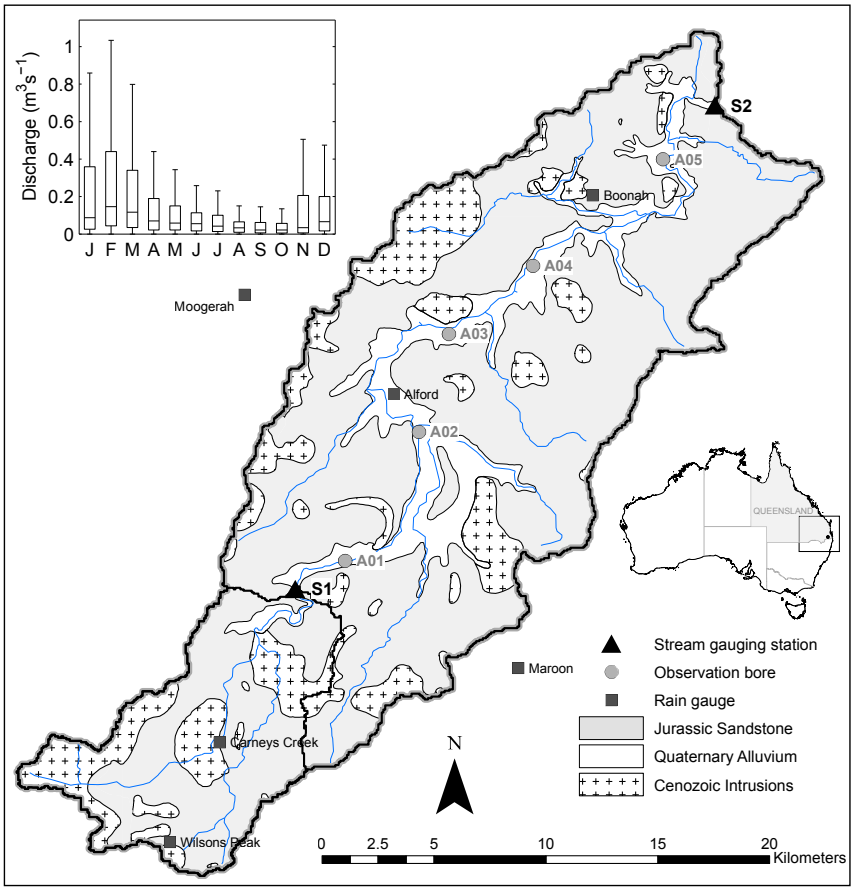

Figure 4.1: Location of the Teviot Brook catchment in southeast Queensland. Simplified geological map of the catchment with selected boreholes, rain gauges and stream gauging stations. Monthly distribution of mean daily discharge at S2.

$3.5 \times 10^{-3}\,\mathrm{m^2\,s^{-1}}$, with the lowest value found in a borehole located nearby A02, and highest values observed nearby A01 and A05 (Figure 4.1). The valley largely supports rural land use such as cattle grazing, fodder cropping and market gardening, and the primary sources for irrigation are alluvial groundwater and streamwater.

4.2.2 Datasets

Several observation boreholes have been drilled in the late 1980s by the Department of Natural Resources and Mines (DNRM), Queensland state government, in the alluvial valley of the catchment. Five boreholes with GWL records of substantial length were selected for this study; they are referred to as A01 to A05 from upstream to downstream (Figure 4.1). For these five bores, GWL time-series cover the period from 1988–2012, i.e. 25 years. Data were recorded on a monthly to quarterly basis at A01, A02, A03 and A05, while A04 is equipped with an automatic pressure logger and therefore has near-continuous data throughout the monitoring period. All the selected bores are known to intersect the alluvium. Field ob-

servations suggest that GWL time-series are more affected by groundwater abstraction at A02, A03 and to a lower extent A04, due to the occurrence of irrigation bores in the relative proximity of these monitoring bores. In contrast, A01 and A05 are located in areas of grassland where water extraction is much less likely. In addition to GWL data, two stream gauging stations administered by DNRM are located in both upstream and downstream parts of the Teviot Brook catchment (S1 and S2 in Figure 4.1). These stations represent drainage areas of 83 and 420 km^2, respectively. Both have been recording surface water discharge at a high frequency since 1966. Station S2 was closed in late 2010, while station S1 is still active. There is also a dense network of rain gauges of the Bureau of Meteorology (BoM), Australian Federal government, across the catchment (Figure 4.1). For much of this monitoring infrastructure, rainfall data has been recorded for over 50 years. In addition, the monthly series for selected climate indices were obtained through the Climate Explorer database of the Royal Netherlands Meteorological Institute (http://climexp.knmi.nl). The indices chosen for this study were the Pacific Decadal Oscillation (PDO) and the Niño3.4 index, which is defined as the average of sea surface temperature anomalies over the region 5°N – 5°S and 170°W – 120°W. Niño3.4 was used rather than Niño3 because it more closely reflects the Australian climate (Wang and Hendon, 2007).

4.2.3 Time domain analyses

4.2.3.1 Autocorrelation

Autocorrelation functions were calculated for each hydroclimatic time-series. These functions provide information on the degree of persistence of a variable, by measuring the linear dependency of successive values over a given period. The auto-correlogram of a time-series x is expressed as (Box and Jenkins, 1976):

$$r_x(k) = \frac{N^{-1}\sum_{i=1}^{N-k}(x_i - \bar{x})(x_{i+k} - \bar{x})}{\sigma_x^2} = \frac{\sum_{i=1}^{N-k}(x_i - \bar{x})(x_{i+k} - \bar{x})}{\sum_{i=1}^{N}(x_i - \bar{x})^2} \tag{4.1}$$

where $r_x(k)$ is the autocorrelation coefficient at lag k, N is the length of the series, and $\bar{x}$ is the arithmetic mean over the N observations. Mangin (1984) first applied autocorrelation to karstic systems in the Pyrenees, France, to measure the time a signal persists in the series. He showed that rainfall has a very low persistence whereas karstic springs with high storage have a much higher persistence. There are several ways of characterising the autocorrelation function. For instance, the slope of the auto-correlogram can be an indicator of persistence: the function drops off rapidly if values are of random nature, while a low slope illustrates high persistence in the series. As suggested by Massei et al. (2006), however, it is more appropriate to characterise the overall shape and magnitude of autocorrelation functions. For the purpose of this study, logarithmic fits were adjusted to each function:

$$r_x(k) \cong \alpha \log(k) + \beta \tag{4.2}$$

where k is the lag, α is a parameter that expresses the rate of decrease of the function, and β is a parameter related to the amplitude of the correlation for a unit lag.

4.2.3.2 Cross-correlation

Cross-correlation is commonly used to identify the transfer function between two signals. The cross-correlation between series x and y of length N is defined as (Box and Jenkins, 1976):

$$R_{xy}(k) = \frac{N^{-1}\sum_{i=1}^{N-k}(x_i - \bar{x})(y_{i+k} - \bar{y})}{\sigma_x \sigma_y} = \frac{\sum_{i=1}^{N-k}(x_i - \bar{x})(y_{i+k} - \bar{y})}{\sqrt{\sum_{i=1}^{N}(x_i - \bar{x})^2 \sum_{i=1}^{N}(y_i - \bar{y})^2}} \tag{4.3}$$

Considering a linear system and provided that the input signal is a pure white noise (i.e. a random process with no persistence), the cross-correlation function gives the impulse response of the system (Box and Jenkins, 1976). By determining the value of k that maximises the correlation between the two series, noted τ, the method can yield an estimate of the average transit time between the input and output signals:

$$\tau = \max_k R_{xy}(k) \tag{4.4}$$

In this study, an original approach was used that measures the time-variant cross-correlation between daily signals of precipitation and GWLs. Synchronised windows were shifted along the two series using a 1-day sliding interval, allowing determination of τ as a function of time. Considering a window of length ω, the combination of equations 4.3 and 4.4 gives:

$$\tau(t) = \max_k \left(\frac{\omega^{-1}\sum_{t-\omega/2}^{t+\omega/2}(x_i - \bar{x})(y_{i+k} - \bar{y})}{\sigma_x \sigma_y} \right) \quad t = \left[\frac{\omega}{2}, 1 + \frac{\omega}{2}, ..., i, ..., N - \frac{\omega}{2}\right] \tag{4.5}$$

The first value taken by t is $\omega/2$ so that computed τ values were centred on their time window. Lastly, a Tukey filter with ratio parameter 0.3 (see Tukey, 1968 for details) was applied to the moving windows in order to avoid edge effects during calculations. Only τ values for which the maximum of the cross-correlation function was statistically significant were kept. Likewise, values falling outside the expected [0–200] days lag were removed from the resulting τ series. Several window lengths were tested, which allowed acquisition of several high-resolution series of average transit time, and provided evidence on the uncertainties linked to the calculations.

4.2.4 Frequency domain analyses

4.2.4.1 Fourier transform

Spectral analyses are complementary to correlation analyses, as they may reveal certain characteristics present in a time-series that are buried in noise and not discernable otherwise

(Box and Jenkins, 1976; Percival and Walden, 1993). They provide a picture of the frequency content of the studied series, allowing for the dominant oscillation modes to be detected. Jenkins and Watts (1968) analytically demonstrated that the frequency spectrum of a time-series and its autocovariance function (i.e. the product of autocorrelation and variance) are linked by the general Fourier expression:

$$ps(f) = \sum_{k=-N}^{N-1} c_x(k)\, \mathrm{e}^{-2\pi i f k} \qquad \text{with } c_x(k) = r_x(k)\, \sigma_x^2 \tag{4.6}$$

where ps is the power spectrum of the time-series x, $c_x(k)$ is its autocovariance function, f is the frequency of the k^{th} mode (in cycles per sampling interval, i.e. days^{-1} or months^{-1} depending on the studied series), and i is the imaginary unit. In other words, the power spectrum of a time-series is the simple translation of its autocovariance function in the frequency domain. Due to one of the properties of the autocorrelation coefficient $r_x(k)$ which states that $r_x(k) = r_x(-k)$, equation 4.6 becomes:

$$ps(f) = \sigma_x^2 + 2 \sum_{k=1}^{N-1} c_x(k)\, \mathrm{e}^{-2\pi i f k} \tag{4.7}$$

In our case the time-series x, and hence $c_x(k)$, are real-valued. Therefore equation 4.7 can be re-written as:

$$ps(f) = \sigma_x^2 + 2 \sum_{k=1}^{N-1} c_x(k)\ \cos(2\pi f k) \tag{4.8}$$

As $ps(f)$ is symmetric against the $f = 0$ axis, power spectra were plotted on one side of the frequency axis only. Also, when a single spectrum is calculated from an entire time-series, variance in the estimate can be very high and hinder interpretations. To get around this issue, the Welch method was used (Percival and Walden, 1993), which consists of dividing the series into overlapping segments, computing a modified spectrum of each segment, and then averaging the spectra estimates. This substantially decreased the variance of the spectrum relative to the original estimate. Each averaged one-sided power spectrum was then examined in bi-logarithmic space in order to (i) identify the dominant periodicities for each signal and (ii) describe the variations in frequency such as breaks in slope that might reveal different behaviour modes (e.g. Herman et al., 2009).

4.2.4.2 Wavelet transform

Power spectra alone cannot fully describe non-stationary processes, because they do not account for changes in frequency content over time (Massei et al., 2006). The objective of the wavelet transform is to achieve a complete time-frequency representation of transient patterns occurring in the time-series (Labat, 2010). In this section, we do not intend to exhaustively describe the theory underpinning wavelet analysis, and refer the reader to

Torrence and Compo (1998) and Labat et al. (2000) for additional information. Instead, here we provide a succinct outline of the method.

To perform the transform, an elementary (mother) wavelet $\psi(t)$ is used, which is a finite-length and oscillating waveform, i.e. with a mean of zero. For this study, the Morlet wavelet was chosen due to its accurate localisation in the frequency domain (Torrence and Compo, 1998; Grinsted et al., 2004); Morlet is a complex wavelet defined as a sine wave modulated by a Gaussian distribution. The technique involves shifting forward the mother wavelet in a number of steps along the time-series, and measuring the level of similarity between the wavelet and the signal at each step through computation of the wavelet coefficient C_x. Several scaled versions of the mother wavelet are then generated, and the process is repeated for each scaled version of the wavelet, in order to produce sets of wavelet coefficients for each frequency (Nalley et al., 2012). Formally, continuous wavelet transform consists of the convolution of the time-series $x(t)$ with scaled and shifted wavelets $\psi_{a,\tau}(t)$:

$$C_x(a,\tau) = \int_{t=0}^{N-1} x(t)\,\psi^*_{a,\tau}(t)\,dt \qquad \text{with } \psi_{a,\tau}(t) = \frac{1}{\sqrt{a}}\,\psi\left(\frac{t-\tau}{a}\right) \tag{4.9}$$

where a is the parameter that governs the dilation ($a > 1$) or contraction ($a < 1$) of the wavelet (scale parameter), while τ is the parameter that governs the shifting of the wavelet along the time axis (translation parameter). t represents the sampling interval and * corresponds to the complex conjugate. $\psi_{a,\tau}(t)$ are the rescaled versions of the mother wavelet (when $a = 1$ and $\tau = 0$, $\psi(t)$ is the mother wavelet). Wavelet spectra are the expression of the wavelet coefficients against time and frequency. Resulting contour plots of the wavelet spectra were produced for each hydroclimatic time-series, where frequency (y-axis) and spectral power (i.e. absolute values squared of the wavelet coefficients; z-axis) were plotted against time (x-axis). On every plot, a cone of influence was drawn to reflect edge effects as proposed by Grinsted et al. (2004). Also, the series for which the Mann-Kendall test was positive at 95% confidence level were de-trended using a linear regression prior to applying the transform. Lastly, statistical significance of the wavelet power was calculated to estimate if periodic patterns are actually caused by non-stationary processes. More details on this procedure are available in Grinsted et al. (2004).

Given that our overall purpose was to look for relationships between climate indices and GWLs, a measure of the coherence between wavelet spectra was required. The selected method has been first proposed by Torrence and Webster (1999) and consists of identifying localised correlations between two spectra in the time-frequency domain. It is defined as:

$$\mathrm{WTC}_{xy}(a,\tau) = \frac{\left|a^{-1}C_{xy}(a,\tau)\right|^2}{\left(a^{-1}\left|C_x(a,\tau)\right|^2\right)\left(a^{-1}\left|C_y(a,\tau)\right|^2\right)} \qquad \text{with} \quad C_{xy} = C_x C_y^* \tag{4.10}$$

where WTC_{xy} is the wavelet coherence between time-series x and y, C_{xy} is the cross-

spectrum calculated from the two wavelet spectra, and a is the scale. The factor a^{-1} is used in order to convert spectra to energy densities (Torrence and Webster, 1999). Each term of equation 4.10 needs to be multiplied by a smoothing operator. It can be noticed that the formula is closely similar to that of the cross-correlation coefficient in the time domain. Again, the statistical significance level of wavelet coherence was estimated using the method presented by Grinsted et al. (2004). The wavelet coherence method was preferred to the calculation of cross-wavelet spectra only, because it appeared more conservative in identifying similarities between two spectra: cross-wavelet detects all areas with high common power whereas coherence is an accurate representation of the covariance between the two time-series (Torrence and Webster, 1999). Scripts used for all wavelet analyses were developed in Matlab and kindly provided by Grinsted et al. (2004).

4.3 Results and Discussion

4.3.1 Characterisation of the system as a time-invariant object

An assessment of the time-averaged system was initially conducted using autocorrelation functions and Fourier transform. The whole time-series were taken as input data, corresponding to 47 years of daily records for rainfall and discharge (1966–2012) and 25 years of daily records for GWLs (1988–2012). The Thiessen polygon method was used to compute an areal mean rainfall depth for the entire catchment from daily data captured at the five rainfall stations shown in Figure 4.1 ('Alford' station was excluded from the calculation because it contained extended periods with missing data).

Autocorrelation functions for the three types of hydroclimatic series are presented in Figure 4.2 together with their power spectra. The autocorrelation function of rainfall decreased rapidly for lag values close to zero (Figure 4.2a), which indicates that the rainfall signal was relatively random. This was further confirmed by the rainfall power spectrum (Figure 4.2b): apart from a peak located at a period of one year, the spectrum contained homogeneously distributed amplitudes and it remained flat across all frequencies. In contrast, discharge data at S1 and S2 showed a different structure, with a slightly longer memory effect with respect to rainfall (Figure 4.2c). An autocorrelation coefficient of 0.2 was reached in approximately 0.12 months i.e. four days for both discharge series. The spectrum for discharge also displayed a one-year periodicity (Figure 4.2d), but unlike rainfall it substantially decreased at high frequencies (i.e. low periods), reflecting a different behaviour mode.

Autocorrelation functions were also calculated on each of the five GWL time-series. As the data at A04 was recorded at a high frequency, a new series was generated for that location by sub-sampling the original series to obtain monthly frequency data. All series were also normalised using standard scores, i.e. by subtracting the mean and then dividing the result by the standard deviation. In order to eliminate the low-frequency component visible in the

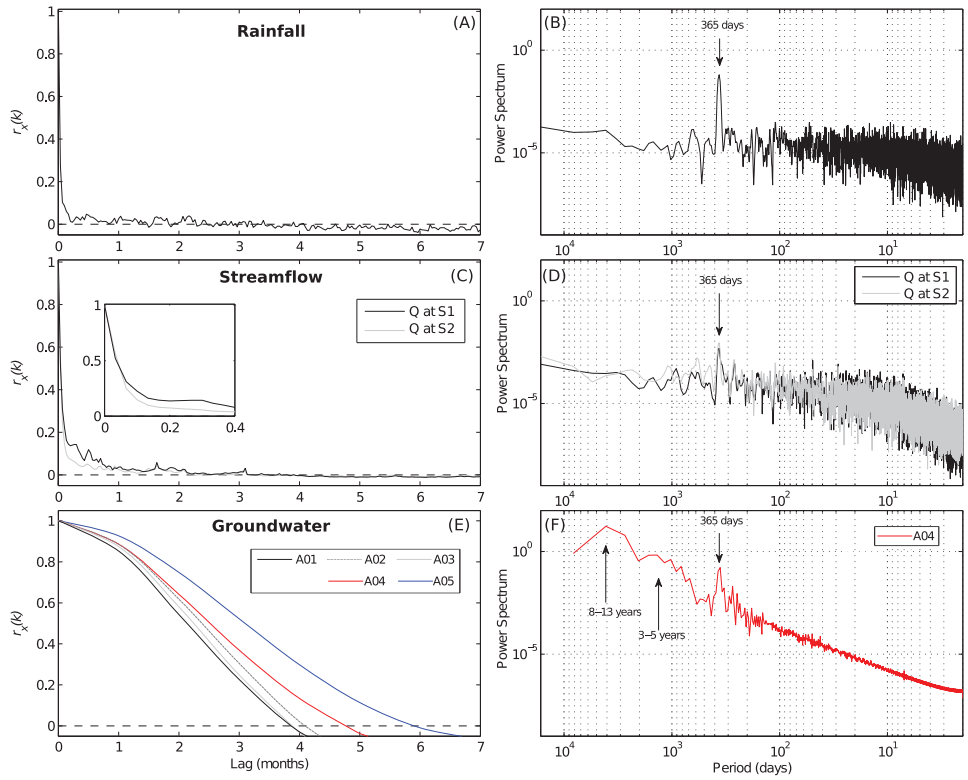

Figure 4.2: Autocorrelation functions for rainfall (A), discharge (C) and GWL time-series (E), and smoothed power spectra of the autocorrelation functions (B, D and F).

records, smoothed time-series were derived from the original time-series by fitting a locally weighted regression with a 3-yr smoothing window. This low-frequency trend line was then subtracted to the original time-series, which enabled achievement of stationary records. The five autocorrelation functions derived from each de-trended 25-yr record followed very gently decreasing slopes, where after a lag of three months autocorrelation coefficients still remained between 0.2 and 0.6 (Figure 4.2e). The frequency spectrum for A04 presented in Figure 4.2f had evident structure, with high amplitudes at lower frequencies (higher periods) and low amplitudes at higher frequencies (lower periods). A break in slope can be observed around the 10^{-3} frequency, and distinct peaks were discernable that suggest several oscillation modes in GWL data at one year, three to five years, and eight to 13 years.

Overall, with the exception of its annual component rainfall can be considered as a near white noise process, whereas discharge and to a much higher extent GWLs displayed significant persistence. The one-year oscillation observed in all spectra corresponds to the wet/dry seasonal cycles. The spectrum for GWLs showed a more complex structure: groundwater considerably amplified the low frequency fluctuations and smoothed out the high frequency fluctuations present in input precipitation. This suggests that the aquifer acted as a low-pass filter in the frequency domain, as previously reported in the literature (Molénat et al., 1999;

Imagawa et al., 2013).

Closer examination of the GWL autocorrelation functions can assist in documenting the spatial variability in groundwater persistence, as well as the physical processes controlling this variability. Distinct behaviour could be observed among the five functions, with various degrees of persistence. As proposed by Massei et al. (2006) and following equation 4.2, logarithmic fits were adjusted to each function to define more accurately the local inertia of the alluvial system.

Table 4.1: Parameters of logarithmic fits for the autocorrelation functions.

	A01	**A02**	**A03**	**A04**	**A05**
α **(1/month)**	-0.72	-0.69	-0.69	-0.59	-0.54
$k_{0.2}$ **(in months)**	3.1	3.4	3.2	3.8	4.5

$k_{0.2}$ is the lag needed to reach an autocorrelation coefficient of 0.2.

The α parameters of the functions are given in Table 4.1 together with the lags needed to reach an autocorrelation coefficient of 0.2. When taken together, these two figures provide a full picture of the autocorrelation functions. For a smoothing window of three years, the α parameter ranged between –0.72 and –0.54; it was lowest for A01 and highest for A05. There seemed to be a trend of increasing local persistence from boreholes located in the upstream part of the alluvium to boreholes located downstream. The $k_{0.2}$ values also generally increased from A01 (3.1) to A05 (4.5). The sensitivity of autocorrelation functions to the choice of a smoothing window was also assessed. Window lengths ranging from two to 10 years were tested. Although the degree of persistence was found to depend on the length of the selected window, the relative differences in persistence – hence in α values – between the five boreholes remained identical regardless of the window used.

To further understand the drivers responsible for this variability in persistence, α values were plotted against a number of local physical variables (Figure 4.3). Results are consistent with our previous assumptions: the variability in groundwater persistence was primarily related to the location of the boreholes from upstream to downstream (Figure 4.3a). Distance to river and alluvium thickness also partly explained the variance in α values (Figures 4.3b and 4.3c). As could have been anticipated, another variable that contributed to the variance in α was the maximum water table fluctuation (Figure 4.3d). However, the reduced amount of boreholes in our dataset limits the significance of correlations presented in Figure 4.3, and more data would be needed to provide better constraints on the physical processes controlling GWL persistence. Also, variations in local persistence can be due to other structural factors that we were not able to assess such as the change in grain size of the alluvial aquifer material or its degree of compaction, which can in turn lead to changes in hydraulic conductivities and thus in groundwater flow.

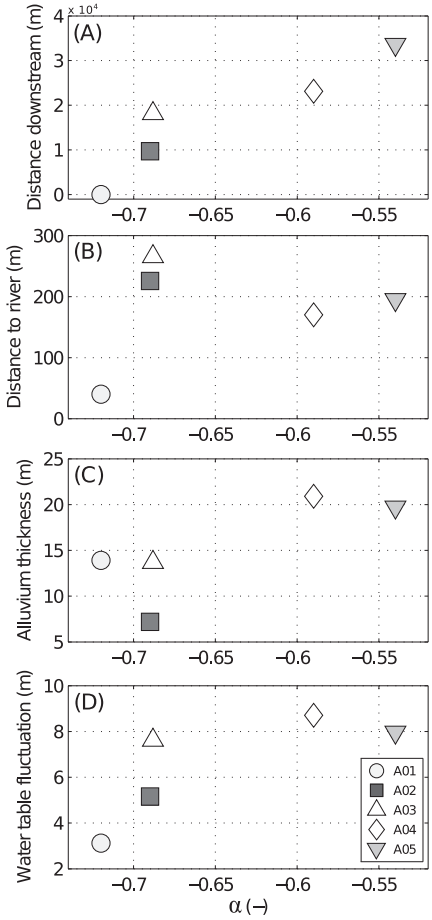

Figure 4.3: Relationship between the persistence parameter α and a set of physical variables. (A) Distance downstream taking A01 location as origin. (B) Distance from the borehole to the nearest stream. (C) Alluvium depth according to borehole logs. (D) Maximum water table fluctuation throughout 1988–2012 (i.e. minimum GWL subtracted to maximum GWL).

In their paper on the long-term dynamics of a chalk aquifer in Normandy, France, Slimani et al. (2009) related the persistence values calculated from four observation boreholes to the thickness of semi-permeable surficial formations overlying the aquifer. Where the surficial formations were thicker, persistence in GWLs was higher. More recently, Imagawa et al. (2013) studied the autocorrelation functions of two boreholes located at the apex and at the toe of an alluvial fan in Japan. They demonstrated that persistence was five times higher at the toe of the fan than at the apex. Assuming a similar hydraulic conductivity across the aquifer, the authors attributed the difference in persistence to a difference in outflow rate, which could be either downward flow, discharge to the stream network or seepage loss. In our study, the downstream part of the alluvium is characterised by a larger width ($\approx 2\,\mathrm{km}$ *vs* $\approx 1\,\mathrm{km}$ upstream), higher thickness (Figure 4.3c), and lower hydraulic gradient than in its upstream section; these features are consistent with greater storage in the downstream section. Following the suggestion of Imagawa et al. (2013), we infer that persistence can be

an indicator of the local storage capacity of alluvial aquifers, provided that the assumption of homogeneity in the hydraulic conductivity throughout the aquifer is respected. Overall, our findings indicate that autocorrelation functions can be usefully applied to assess persistence in shallow alluvial aquifers, and to document the spatial variability in groundwater persistence within single aquifers.

4.3.2 Response to low frequency rainfall fluctuations

4.3.2.1 Trends and relationships between hydroclimatic variables

As a preliminary approach, basic information was extracted from the datasets in order to achieve a conceptual representation of the catchment response to precipitation variability. The analysis focussed on the 1988–2012 period as the GWL records only cover this shorter 25-yr time span. The catchment was subject to a fairly high interannual variability in precipitation (Figure 4.4a). During this period, the Thiessen-averaged maximum annual rainfall depth for the Teviot Brook catchment was 1252 mm (1988), while the minimum value was 558 mm (2000) and the average value over the whole period was 891 mm/yr. There were two periods of intense drought, i.e. roughly from 1992 to 1996 (with an average precipitation of 740 mm/yr; period referred to as the "1990s drought") and from 2000 to 2008 (average precipitation 720 mm/yr; period referred to as the "Millennium drought"; Figure 4.4). As a result of these high fluctuations in input rainfall, stream discharge showed considerable variations (Figure 4.4b): the maximum, minimum and average annual runoff depth at S2 for the period 1988–2012 were 287 mm/yr (1988), 2 mm/yr (2003), and 77 mm/yr, respectively.

During the drought episodes, there was little to no surface water flow, although high flow events occurred on some occasions during these periods (Figure 4.4b). The main stream at S2 experienced an average of 175 d/yr with no discharge during the 1990s drought, and 202 d/yr with no discharge during the Millennium drought. In contrast, the average value for the remaining years (i.e. 1988–1991; 1997–1999; 2009–2012) amounted to 35 days without surface flow only. According to hydraulic gradient analyses, Teviot Brook was mostly a gaining stream in the valley, except during the two droughts when it dried up concurrently with significant drops in the GWLs.

The five normalised GWL time-series appeared to follow non-stationary dynamics, with consistent annual and inter-annual fluctuations amongst them (Figure 4.4c). The effects of the two droughts were visible on the five GWL records, as levels mostly decreased during these periods. As there is no official metering of groundwater abstraction across the Teviot Brook catchment, little is known about the extent to which the resource has been used during and between the drought periods. A recent study (Sinclair Knight Merz, 2012) on the Albert-Logan basin, which encompasses the Teviot Brook catchment, showed that groundwater abstraction for irrigation purposes was relatively constant from 1990 to 2000 despite the occurrence of the 1990s drought (0.5 mm/yr in 1990 increasing to 0.6 mm/yr in

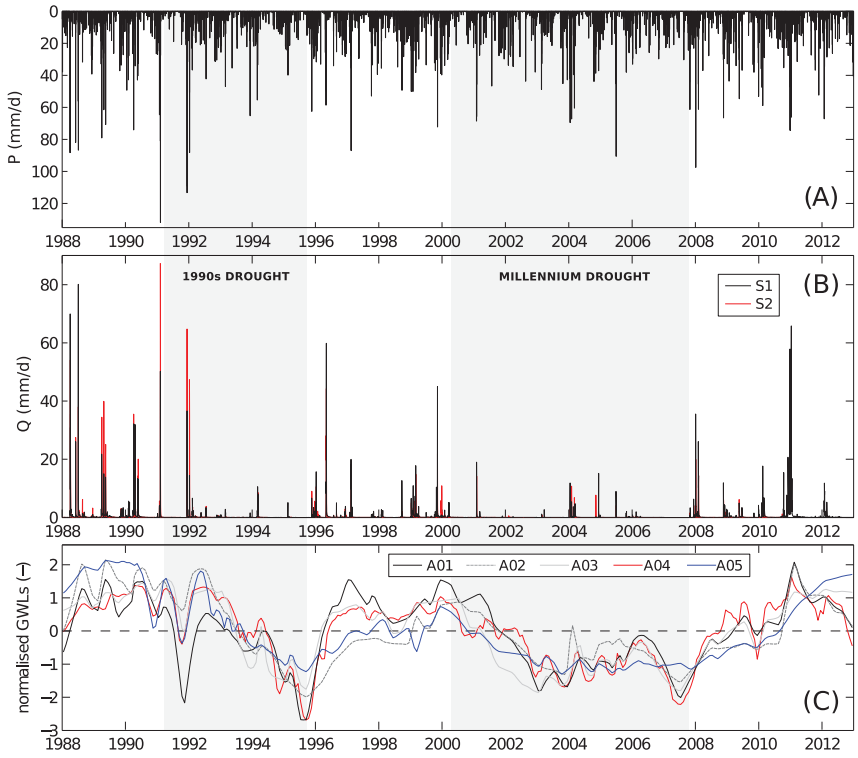

Figure 4.4: Time-series of the Thiessen-averaged daily precipitation (A), daily discharge at S1 and S2 (B), and monthly time-series of normalised groundwater levels at A01, A02, A03, A04 and A05 (C) for the 1988–2012 period. The grey shaded areas represent the time span of the two major droughts.

2000). At the onset of the Millennium drought, abstraction rates considerably increased to reach 1.9 mm/yr in 2005, and up to 3.0 mm/yr in 2010 when wet conditions returned. The last value equates to 4% of the average interannual streamflow in Teviot Brook, but to $> 100\%$ of streamflow during drought-affected years. However, there are also indications that groundwater usage in Teviot Brook is limited due to overall poor water quality (Department of Natural Resources, Mines and Water, 2006).

Possible gradual changes (i.e. monotonic trends) in the time-series were investigated using the Mann-Kendall test (Mann, 1945; Kendall, 1975), while abrupt changes were assessed with the cumulative deviation test (Buishand, 1982). According to the Mann-Kendall statistics, both annual precipitation depth and mean annual discharge at S1 and S2 followed a decreasing trend over the period at a 95% confidence level (decrease of 6 mm/yr and 0.4 mm/yr, respectively). Step changes were detected in 1992 for rainfall records and in 1991 for streamflow records (significance 95%). This is coherent with the onset of the first drought period. In contrast, mean annual GWL data showed neither significant monotonic trends nor step changes between 1988 and 2012 at any of the five studied boreholes.

Annual runoff coefficients were also calculated for the two stream gauging stations (Figure 4.5a). They correspond to the ratio of runoff to precipitation for each calendar year. Runoff coefficients ranged from < 0.01 to 0.23 at S2 (downstream), and from < 0.01 to 0.28 at S1 (upstream). Lowest values were concomitant with the drought episodes (< 0.01 in 1993, 2002, 2003 and 2006), while highest values occurred during high flow conditions (> 0.2 in 1988, 1991 and 2010). Peel et al. (2004) showed that Australian catchments have a lower runoff coefficient and much larger variability as compared to other catchments worldwide. Chiew et al. (2002) found runoff coefficients typically ranging between 0.2 and 0.3 for catchments located on the eastern coast of Australia. The slight disagreement between our values and the work of Chiew et al. (2002) is probably due to a negative bias induced by the extended dry conditions that occurred in the region during the study period.

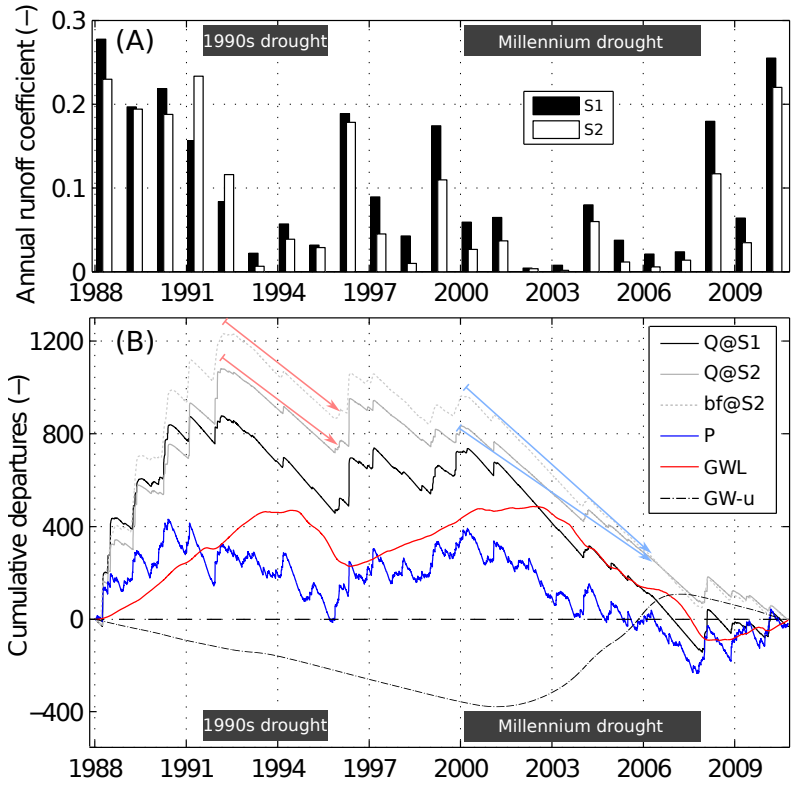

Figure 4.5: (A) Annual runoff coefficients at S1 and S2 from 1988 to 2010. (B) Variation of the standardised cumulative departures of the daily time-series of Thiessen-averaged rainfall depth, discharge at S1 and S2, GWLs at A04 and groundwater abstraction rates. GW-u is the assumed groundwater use according to Sinclair Knight Merz (2012). Black boxes represent the time span of the two major droughts.

To further compare trends and shifts among variables, standardised cumulative departures were calculated for rainfall, discharge at S1 and S2, baseflow at S2, and GWLs at A04. Baseflow, which is associated with water discharged from groundwater storage, was calculated by separating daily discharge time-series at S2 into baseflow and surface runoff using the recursive digital filter proposed by Eckhardt (2005). The calculations of cumulative departures involved (i) estimating standardised daily values, (ii) smoothing them out

using monthly moving windows, and (iii) computing the cumulative sum from the smoothed data.

The sustained declines in precipitation (blue line in Figure 4.5b) visible from 1991 to 1996 and from 2000 to 2008 confirm the occurrence of the two drought periods. The trends in discharge (black and grey lines) generally followed the observed trends in precipitation, although variations were largely exacerbated compared to precipitation. Trends were more pronounced in the whole catchment (S2) than in the upper valley (S1). Standardised cumulative departures for the baseflow values at S2 are plotted as dashed grey line in Figure 4.5b. During the 1990s drought, baseflow and total streamflow responded similarly to the decrease in precipitation (light red arrows in Figure 4.5b). Contrastingly, during the Millennium drought, the trend in baseflow was substantially amplified with respect to total streamflow (light blue arrows in Figure 4.5b). This indicates that during this second drought period, the shortage in precipitation had a correspondingly greater effect on groundwater discharge to streams than on runoff, which is likely a consequence of the enhanced groundwater pumping rates observed from 2000 to 2010 (Sinclair Knight Merz, 2012); dash–dot line in Figure 4.5b). Alternatively, this decrease in baseflow may be due to unsupplemented streamwater extraction during low flow conditions (Department of Natural Resources, Mines and Water, 2006). The return flow compound can be regarded as negligible because of the considerable evapotranspiration rates occurring in the area.

Variations in GWL departures at A04 (red line) generally followed comparable fluctuations as the ones for streamwater, however a substantial shift in time was observable in the downward trends: the first major decline began in late 1994, i.e. three years after the onset of the first drought, and the second decline began in late 2002, i.e. more than two years after the onset of the second drought. These findings can be compared to the work of van Dijk et al. (2013), who also showed a lag of several years for GWLs in responding to drought in the Murray Darling Basin. There was no significant difference in the behaviour of GWLs at A04 between the two drought periods.

The results obtained from Figure 4.5 can be conceptually interpreted as a series of processes that took place within the system in response to sustained dry periods: due to its rather low persistence, streamflow rapidly decreased as a result of lower input rainfall. This was further compounded by enhanced evapotranspiration rates in the lowland part of the catchment, as well as enhanced groundwater abstraction during the 2000–2008 period. By contrast, GWLs first maintained relatively close to pre-drought levels, because of higher storage capacity and continuing diffuse recharge over the catchment. Once the surface water network dried up (i.e. decoupling between surface and groundwater), it is likely that pumping from shallow alluvial boreholes increased considerably, hence generating the lagged decline in GWL data.

4.3.2.2 Wavelet spectra

The wavelet approach was used to develop our understanding of the low frequency variations and periodicities in hydroclimatic records. Wavelet spectra were calculated for Thiessen-averaged rainfall, discharge at S1 and S2, baseflow at S1 and S2, GWLs at A01 to A05, as well as for the climate indices PDO and Niño3.4 (Figure 4.6). The time-frequency spectrum for precipitation records (Figure 4.6a) showed a clear annual periodicity, represented by warmer colours, which was statistically significant during most of the study period regardless of the occurrence of droughts; this very likely corresponds to the annual wet/dry cycle. No significant oscillation modes were detected at lower frequencies.

The two discharge spectra were very much alike (Figures 4.6b and 4.6c), and there was no apparent cycle except at high frequencies. At S2, annual periodicity was expressed during the 1988–1992 and 2010–2012 intervals. When compared to the results from Figure 4.5, it appears that these two periods correspond to high flow conditions. With regards to climate indices, the PDO record (Figure 4.6d) was characterised by a strong annual periodicity. The limited length of records did not enable to detect potentially longer patterns such as 10-yr cycles. It presented two significant oscillations, the quickest one extending throughout the record (centred on the 16-month period, i.e. 1 to 2-yr band), and the slowest one, more powerful, extending from 1994 to 2000 and then from 2008 to 2012 (centred on the 48-month period, i.e. 2.5 to 5-yr band). This lower frequency oscillation mode is in line with the two intense La Niña events that occurred in eastern Australia within those time frames. It roughly corresponds to the periods for which precipitation was substantially higher (Figure 4.5b).

The spectra for the five observation boreholes (Figures 4.6f to 4.6j) showed somewhat distinct patterns. Unlike for rainfall and streamflow, a high amount of statistically significant periodicities were found at frequencies lower than one year. Of note is the dampening in spectrum amplitude and significance from upstream to downstream. The spectra for A01, A02 and A03 were comparable (Figures 4.6f, 4.6g and 4.6h), with three major oscillation modes: 1-yr (occurring intermittently throughout the study period), 2-yr (occurring mainly from 1988 to 1996), and 2.5-yr gradually changing to 5-yr periodicity (most powerful mode, occurring all throughout the record). The 1-yr mode was interpreted as the annual component observed in precipitation (Figure 4.6a) and PDO (Figure 4.6d). The driving forces behind the other two oscillation modes were not evident, and they may be related to complex processes such as occasional decoupling between surface and groundwater and/or enhanced groundwater abstraction (Section 4.3.2.1). Large-scale atmospheric patterns (e.g. the Niño3.4 index) might be another driving force for these low-frequency periodicities.

The spectrum for A04 (Figure 4.6i) also showed a consistent oscillation at the annual frequency, but lower frequency modes were more restricted in time than for upstream boreholes. A05 wavelet coefficients (Figure 4.6j) were even less significant, with almost no discernable

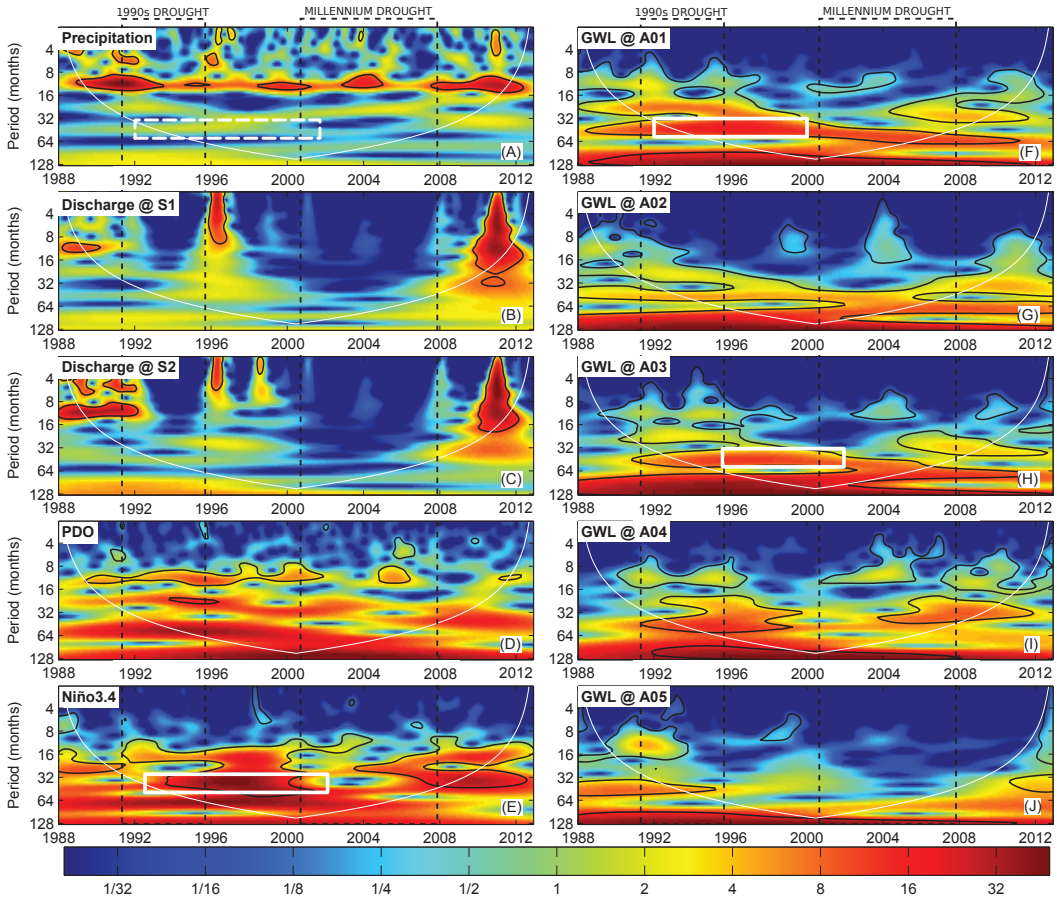

Figure 4.6: Continuous wavelet spectra for (A) Thiessen-averaged rainfall depth, (B) discharge at S1, (C) discharge at S2, (D) PDO and (E) Niño3.4 indices, and (F to J) for the five borehole GWL records. Spectral power is dimensionless, warmer colours denote higher power. Areas delineated by the black contours have significant wavelet power at a 95% confidence level. The cone of influence is represented by a thin white line, outside which edge effects may have influenced the calculation of the wavelet power. The white rectangles denote relevant periods discussed in the text.

pattern over the whole spectrum. At this location, one-year periodicity was only visible during the high flow conditions that occurred in the 1990–1992 period. For all five boreholes, significant fluctuations seemed to occur regardless of the hydroclimatic conditions, i.e. during both drought and inter-drought periods. Also, 10-yr variability was evident throughout much of the five GWL records (highly significant spectrum at the 128-month period; Figures 4.6f to 4.6j); however, due to its location outside the cone of influence this oscillation was not further interpreted.

The low frequency modes identified in the GWL series seemed to follow the ones apparent in the Niño3.4 index, particularly at the 2.5 to 5-yr band. Coherence was investigated between wavelet spectra following the methodology described in Torrence and Webster (1999), and the results are presented in Figure 4.7. Coherence spectra are shown for A01 and A03 only, because A01 and A02 yielded equivalent results, and A04 and A05 were not signifi-

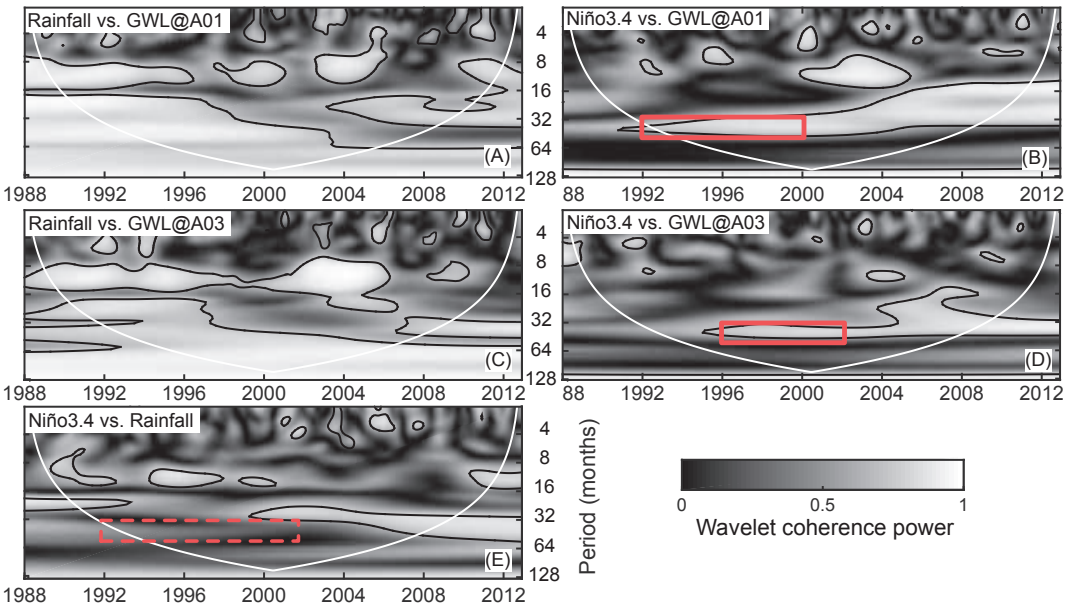

Figure 4.7: Wavelet coherence spectra between (A) rainfall and GWLs at A01, (B) Niño3.4 and GWLs at A01, (C) rainfall and GWLs at A03, (D) Niño3.4 and GWLs at A03, and (E) Niño3.4 and rainfall. Lighter colours denote higher coherence power, and areas delineated by the black contours have significant coherence at a 95% confidence level (as estimated by Grinsted et al., 2004). The cone of influence is represented by a thin white line. The red rectangles denote relevant periods discussed in the text.

cantly correlated with Niño3.4. Coherence between GWLs and rainfall was significant all throughout the records for A01 and A03, during both wet and dry periods, and for both lower (> 2 years) and higher frequencies (1 year and below) (Figures 4.7a and 4.7c). This indicates that rainfall and GWLs are strongly correlated, and that diffuse recharge from precipitation likely prevails in explaining GWL fluctuations.

Statistically significant episodes of coherence were found between the spectrum of Niño3.4 and the ones of A01 (Figure 4.7b), A02 (not shown) and to a lesser extent A03 (Figure 4.7d). In some instances, significant coherence index values were consistent with significant wavelet spectra values of both signals, such as during the 1992–2000 period for A01 and during the 1996–2002 period for A03 (2.5–4 yr periodicity; red rectangles in Figure 4.7 corresponding to white rectangles in Figure 4.6). Rainfall spectrum had lower coherence with Niño3.4 index than GWLs (Figure 4.7e), although various significant peaks were observable but that did not necessarily correspond to the episodes of strong coherence between Niño3.4 and GWLs (red dashed rectangle in Figure 4.7e).

The fact that the ENSO index appears to affect GWLs more significantly than rainfall may be interpreted as the combined effect of climate forcing and evapotranspiration on GWLs. For example, under high flow conditions such as during the massive La Niña event that preceded the Millennium drought, evapotranspiration was likely to be minor, and thus recharge was augmented; conversely, under drier conditions most rainfall may be lost through

evapotranspiration and/or groundwater abstraction. This combined influence may result in the enhanced correlation between Niño3.4 and GWLs that was observed. No long-term evapotranspiration data was available in the study area to confirm these assumptions.

The spectra for downstream locations A04 and A05 were less prone to cyclic patterns, and coherence with Niño3.4 was not significant for these boreholes. One explanation may be the higher persistence observed in the downstream valley, and therefore higher filtering out of not only high frequency but also low frequency oscillations. This is in accordance with our findings from Section 4.3.1 on the occurrence of higher storage capacity in the downstream section of the alluvium. Another explanation might be the occurrence of lower rates of groundwater abstraction downstream, or differences in evapotranspiration dynamics. The abstraction assumption holds for A05, as it is situated in a grassland area not directly affected by groundwater irrigation use; but it is unlikely for A04, as shown by our analyses in Section 4.3.2.1.

4.3.3 Response to high frequency rainfall fluctuations

4.3.3.1 Calculation of dynamic response time

This section focuses on the short-term relationships between the GWLs at A04 and precipitation at the closest rain gauge, corresponding to station 'Boonah' in Figure 4.1. Prior to applying the time-variant cross-correlation analysis, the two time-series were pre-processed. In order to obtain high cross-correlation coefficients and avoid instabilities, several subsets of precipitation and GWL series were computed by smoothing out the original series using a simple low pass filter (i.e. computation of moving average of original data). Aside from the original daily series, sub-series with moving average windows of two days, three days, a week, 10 days, a fortnight, a month, two months, three months, four months and six months were produced. One cross-correlation function was calculated for each of the 11 combinations and over the whole records (Figure 4.8). The peak coefficient was lowest for raw daily data (0.08) and gradually increased to reach a maximum for monthly data (0.20), before declining up to 0.12 for bi-annual data. The peak for monthly data was statistically significant at the 99% confidence level. Accordingly, monthly moving averages were chosen as an input for the dynamic analysis.

Moving cross-correlation functions were then calculated using a specific window length ω and a 1-day sliding interval shifted along the monthly-smoothed series. The maximum coefficient value was extracted for each time step as per equation 4.5. The most appropriate window length ω was defined through a trial-and-error process: windows ranging from 200 to 2000 days were tested, and the one that yielded the highest rate of significant R_{xy} peak values was selected. Note that the 200-day lower boundary was selected on the basis of Figure 4.8: as the most probable lag was found to be 90–100 days, data spanning at least twice the length of this lag was assumed to be necessary to obtain a reliable assessment of

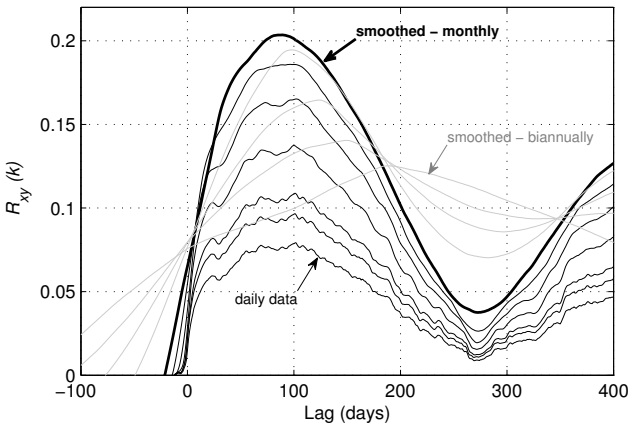

Figure 4.8: Selection of the smoothing window that maximises the cross-correlation peak between precipitation and GWLs at A04. Tested intervals were daily (original data), 2-day, 3-day, weekly, 10-day, fortnightly, monthly, 2-month, quarterly, 4-month, and bi-annually.

the cross-correlation. The highest number of significant correlation peaks was obtained for $\omega_1 = 1000$ days. To evaluate the sensitivity of the method to ω, two values surrounding ω_1 were also included in the analysis, i.e. $\omega_1 \pm 50\%$: $\omega_2 = 500$ days and $\omega_3 = 1500$ days.

Results for the three moving windows are represented in Figure 4.9. Apart from the sensitivity to ω, an assessment of the sensitivity to the smoothing interval used to modify the input time-series was also conducted; the black line in Figure 4.9 is for the monthly smoothing, while the grey shading is for the minimum and maximum values given by other smoothing intervals in the range of 15–45 days. Values for which the R_{xy} peak was not significant at a 99% confidence level were left out of the analysis, as well as τ values that fell outside the expected interval (i.e. $\tau > 200$ days). Statistical significance of the R_{xy} peak was calculated from the sample size alone according to $R_{\min} = 2.58/\sqrt{N}$ (2.58 is the critical value for the 0.995 probability of the normal distribution). This relies on the assumption that the series were normally distributed, which was approximately the case. The same significance test was used by Lee et al. (2006) and Delbart et al. (2014) to control the acceptability of cross-correlation coefficients.

The time span covered by statistically significant τ values was variable among the three tested windows; it was highest for ω_1 (75% of the whole series), while it reached 73% for ω_3 and 64% for ω_2. The actual values of response time were also highly variable over time and with respect to the computation window. The range of τ values was highest for ω_2 (11 to 115 days), with a mean value of 56 days (Figure 4.9a). It was lower for ω_3 (26 to 121 days) and ω_1 (13 to 109 days), with mean values of 67 and 59 days, respectively (Figures 4.9b and 4.9c). These results are in agreement with Delbart et al. (2014), who observed high variability in response time throughout their five-year record. The discrepancy between their values, which ranged between 0.2 and six days, and the ones presented here are likely due to the higher responsiveness of karstic aquifers.

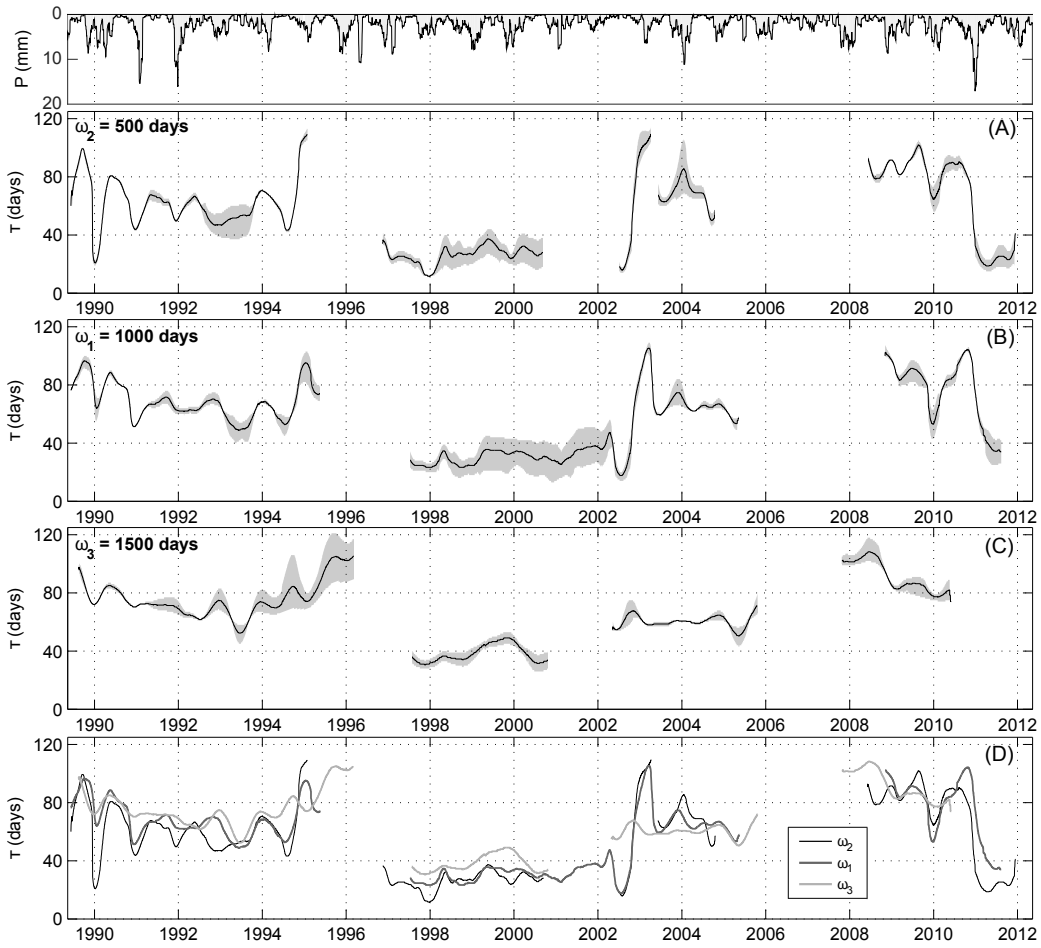

Figure 4.9: Dynamic response time of GWLs at A04 to precipitation according to (A) ω_2 (length 500 days), (B) ω_1 (length 1000 days) and (C) ω_3 (length 1500 days). (D) Comparison of the three reported series. Monthly smoothed precipitation is shown at the top of the figure.

The three series of response time calculated from three computation windows were generally consistent with each other, although anti-phasing was visible in some parts of the signal such as in 1995 between ω_1 and ω_3 (Figure 4.9d). Disagreements between ω_3 and the other two series were apparent on other occasions, as for instance in 2003; this may be due to excessive smoothing when using a 1500-day sliding window. When looking at longer time frames, there was a rather good agreement between the three simulations. The three windows provided comparable results in the 1989–1995, 1997–2001, 2003–2005 and 2009–2012 periods. Values were higher than average during the 1989–1996 period (τ around 70 days) and the 2008–2010 period (τ around 80 days). They were lower than average during the 1998–2002 and 2011–2012 periods (τ around 30 days), and close to average in 2003–2006 (τ around 60 days).

4.3.3.2 Drivers of the variability in response time

Response time at the event scale

As a first indication of the variability in τ, average GWL response times were calculated for the low frequency, interannual periods outlined in Section 4.3.2. Response time during the 1990s drought and the Millennium drought were on average 70 and 68 days, respectively. By contrast, the average GWL response time during the inter-drought periods was 49 days. Lee et al. (2006) were among the few authors who studied the seasonal variations in cross-correlation between precipitation and GWLs, by separating their series into 3-month periods. They showed that the seasonal variability in GWL response was mostly related to the thickness of the unsaturated zone, and that rapid response time occurred during the recharge period. Imagawa et al. (2013) also examined the change in GWL response according to three contrasting climate patterns. They established that the response time of GWLs in dry conditions was at least twice longer than during periods of elevated rainfall.

In the Teviot Brook alluvial aquifer, sustained rainfall periods seemed to generate a decrease in response time, as seen during late 1989 (average decrease from 95 to 65 days according to ω_1; from 100 to 20 according to ω_2; from 95 to 75 according to ω_3), late 2009 (average decreases: 90 to 55 (ω_1); 105 to 70 (ω_2); 90 to 80 (ω_3)), and most importantly in early 2011 (average decreases: 105 to 35 (ω_1); 90 to 20 (ω_2); no value for ω_3; Figure 4.9). Conversely, periods without significant rainfall events led to a substantial increase in response time, as observed during the second part of 1994, when τ increased from 45–70 to 85–110 days consistent with the three windows, as well as during early 2003 (increase 20 to 100 (ω_1); 20 to 105 (ω_2); no significant increase according to ω_3; Figure 4.9). Importantly, there were unexplained variations such as in early 1990 when response time followed a rising trend concurrently with elevated precipitation.

Overall, our results are in agreement with those of Lee et al. (2006) and Imagawa et al. (2013), and they illustrate the role of rainfall in the dynamics of GWL response time. By analysing their time-series of response time, Delbart et al. (2014) showed that rather than rainfall depth, the parameter with major influence on response time was rainfall intensity. They established that an increase in rainfall intensity led to a decrease in response time of the studied karstic aquifer, which they related to a quick saturation of the epikarst. As no data on rainfall intensity was available in this study, the relationship between this parameter and GWLs could not be assessed. However, it is unlikely that rainfall intensity was an important driver of response time variability in the Teviot Brook alluvial aquifer, owing to considerably lower hydraulic conductivities.

More generally, the incongruences in τ estimates point to an important limitation of the proposed method. They indicate that short-term variations were caused by a complex combination of mechanisms that were difficult to isolate from each other. As outlined by Lee

et al. (2006), the cross-correlation method can be used to reveal the occurrence of statistically significant correlations between high frequency precipitation and GWL records, but it does not provide information on what actually causes the GWL response. Other factors may contribute to the change in GWLs that are not directly related to rainfall, such as lateral flow from the drainage network and possible variations in groundwater abstraction rates. It is unlikely that the variations in GWL due to lateral flow would overprint the variations due to diffuse recharge, because daily GWLs at A04 were only weakly correlated with daily streamflow fluctuations. With regards to groundwater abstraction, pumping rates usually increase concomitantly with rainfall shortage. Information on potential groundwater pumping in the vicinity of borehole A04 was not available, therefore assessment of the relative dependence of τ to variations in precipitation and groundwater abstraction remained challenging. We note that these potential interferences have been subject of debate in the recent literature (e.g. Mair and Fares, 2010; Gemitzi and Stefanopoulos, 2011).

Response time at the annual scale

To obtain a broader appreciation of the mechanisms responsible for longer-term variations in response time, annually averaged response times were calculated and compared to a variety of other hydroclimatic variables. Explanatory variables were computed from daily records to obtain annual time-series. The tested series were (i) total rainfall, (ii) maximum daily rainfall, (iii) antecedent rainfall from previous year, (iv) number of days with P$>$ 5 mm, (v) number of days with P$>$ 10 mm, (vi) number of days with P$>$ 30 mm, (vii) mean discharge, (viii) maximum instantaneous discharge, (ix) mean discharge during the 30 consecutive wettest days ($\approx$ quantile 90), (x) mean discharge during the 30 consecutive driest days ($\approx$ quantile 10), (xi) baseflow index, and (xii) mean GWL. A simple correlation analysis was carried out using the annually averaged response times as the variable to be explained. Both Spearman and Pearson correlation coefficients were calculated for each set of variables (Table 4.2).

Two of the 12 tested variables exhibited significant correlation with the annual average response time, at a 90% confidence level and for both coefficients. They were the mean annual GWLs and the annual number of days with daily rainfall above 30 mm (Figure 4.10). Short response times occurred during years when average GWLs were low, while response times were usually longer when GWLs were closer from the ground surface (Figure 4.10a). This is in agreement with the findings from Lee et al. (2006), and can be seen as an increase in storage capacity due to an increase in aquifer thickness, the storage coefficient being the product of specific storage and aquifer thickness. It can also be attributed to the proportionally longer time needed for infiltrating water to reach the saturated zone when the GWL was low than when it was closer from the surface (Larocque et al., 1998).

Table 4.2: Pearson and Spearman rank coefficients between the annually averaged response times at A04 and 12 other variables.

	Pearson coefficient	Spearman coefficient
Annual P	0.08	0.11
Daily max P	0.02	0.00
Antecedent P	0.03	-0.14
Nb days with P> 5 mm	0.17	0.14
Nb days with P> 10 mm	0.28	**0.38**
Nb days with P> 30 mm	**0.34**	**0.35**
Mean annual Q	0.01	-0.08
Daily max Q	-0.16	-0.14
Q90	-0.06	-0.01
Q10	-0.26	-0.16
BFI	-0.15	-0.13
Mean annual GWL	***-0.41***	**-0.35**

Bolded and italicised coefficients have p values < 0.05; bolded coefficients have p values < 0.10. 'Q90' stands for the mean discharge during the 30 consecutive wettest days for each year, and 'Q10' stands for the mean discharge during the 30 consecutive driest days for each year. 'BFI' stands for annual baseflow index; BFI $= \frac{\sum_t b_t}{\sum_t Q_t}$ where b_t is the daily baseflow calculated using the Eckhardt filter and Q_t is the daily discharge.

Years with a higher number of days with elevated rainfall (P> 30 mm) generally had longer response times than years with a lower number of days with elevated rainfall (Figure 4.10b). Although the correlation was not strong (significant at 90% confidence level), these results indicate that a high number of severe precipitation events tended to generate higher averaged response time. The number of days with rainfall > 30 mm mm can be thought of as an indicator of diffuse recharge potential; this would suggest that higher recharge potential induced longer response time, probably because of higher magnitude in GWL variations. The timing of the alluvial aquifer response was therefore influenced by diffuse precipitation that directly contributed to its recharge. In a similar way, Barron et al. (2012) investigated the correlation between the annual sum of rainfall above a threshold and diffuse recharge. They found that, under some conditions, an increase in the sum of daily rainfall above a 20 mm threshold led to an increase in recharge. Although absolute recharge values were not calculated in this study, our results are likely in accordance with the findings from Barron et al. (2012).

The correlation analysis also indicates that flooding of the alluvial plain may not be a major driving force for recharge, as no significant correlation was found with annual maximum discharge series (Table 4.2). Overall, high data scattering in Figure 4.10 suggests that other processes were not accounted for, and more research is needed on the dynamics of GWL response time to better constrain the physical processes responsible for the observed variations.

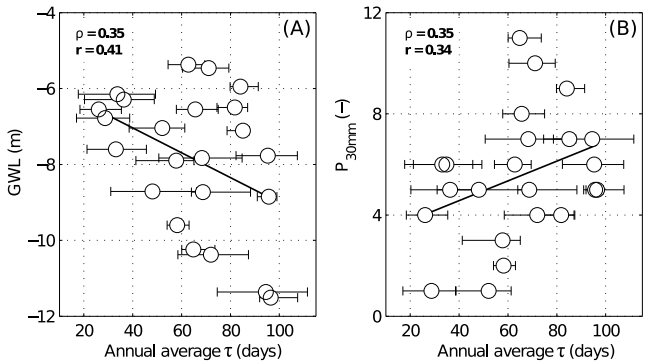

Figure 4.10: Relationship between annually averaged response times and (A) mean annual GWLs and (B) annual number of days with daily rainfall above 30 mm. Whiskers correspond to the highest and lowest response time values obtained from the calculations, without distinction of the window (500, 1000 or 1500 days) used to calculate them. ρ and r refer to the Spearman and Pearson correlation coefficients, respectively.

4.4 Conclusions

The research reported in this paper provides an analysis of the hydrogeological characteristics of a shallow alluvial aquifer located in southeast Queensland, Australia, and an examination of the inter-connections between climate indices, precipitation, discharge and shallow alluvial groundwater levels (GWLs) within the catchment. First, autocorrelation functions were used to characterise groundwater persistence at different locations within the alluvial aquifer. An upward trend in persistence was identified from upstream to downstream, which was attributed to a higher storage capacity in the downstream valley, related to drainage morphology. More generally, autocorrelation functions assisted in characterising shallow alluvial aquifers, and they were particularly useful in documenting the variations in persistence that can occur in heterogeneous groundwater systems.

Second, the response of the hydrological system to low frequency rainfall fluctuations was assessed. The region was subjected to two intense drought periods in the last 25 years, followed by periodic flooding, and surface water flow was more impacted than GWLs. There was a likely influence of groundwater abstraction on stream baseflow, especially during the Millennium drought; the impact of groundwater abstraction on GWLs was also apparent at some locations, although more difficult to quantify. Fourier and wavelet analyses revealed that most of the high frequency fluctuations found in precipitation and discharge were filtered out by the aquifer. In contrast, the low frequency fluctuations induced by large-scale atmospheric patterns were in some instances augmented in GWLs. Statistically significant episodes of coherence were found between the Niño3.4 index and GWLs in the upstream section, particularly during the 1995–2000 period. This corresponds to a massive La Niña event that preceded the Millennium drought, although other factors might be responsible for the low frequency oscillations in GWLs. Higher groundwater persistence in the downstream section probably led to higher filtering of the low frequency climatic variations. Overall,

this study demonstrates the usefulness of applying wavelet transform in order to assess the relationships between different climatic and hydrological records, and to delineate spatial patterns in GWL variations within single aquifer systems. Further work is required in the Teviot Brook catchment and elsewhere to assess more precisely the relative impact of anthropogenic groundwater abstraction on the dynamics of alluvial aquifers. Other efforts need to be directed to a more comprehensive and regional-scale investigation of the relationships between large-scale atmospheric forcings and GWLs.

Third, a method based on cross-correlation was proposed that measures the high frequency response time of GWLs to the precipitation input. Application of the method to our daily dataset at A04 indicates that response time was highly variable, and driven by a range of factors. Among them, rainfall amount was found to significantly affect short-term dynamics, with high rainfall reducing the aquifer response time. Annually averaged response time was consistently correlated with the annual number of days with high rainfall, which was interpreted as the potential for diffuse recharge. Higher recharge potential induced longer response times, probably because of the larger amplitude in GWL variations. More generally, the calculation of time-varying response time through cross-correlation provided promising information on the recharge dynamics of shallow alluvial aquifers, and future research will further examine the physical meaning of response time variations.

Acknowledgements

Thanks are due to DNRM and BoM for provision of the hydroclimatic data. This work largely benefited from discussions with N. Massei (University of Rouen), V. Hakoun and V. Taver (University of Montpellier), as well as Z. Jiang (Queensland University of Technology). The first author is supported by an Endeavour Scholarship awarded by the Australian Government. We also acknowledge financial support from the French Embassy in Australia during a visit to the University of Montpellier. Lastly, we would like to thank R.S. Crosbie, B.A. Zakhem and three anonymous reviewers for providing constructive comments that helped improve the quality of this manuscript.

CHAPTER 5

Hydrochemical Processes in a River – Alluvium – Bedrock Continuum and Implications for Recharge

This chapter has been published as:

C. Duvert, M. Raiber, D.D.R. Owen, D.I. Cendón, C. Batiot-Guilhe, M.E. Cox, 2015. Hydrochemical processes in a shallow coal seam gas aquifer and its overlying stream–alluvial system: implications for recharge and inter-aquifer connectivity.
Applied Geochemistry 61, 146–159. doi:10.1016/j.apgeochem.2015.05.021

Abstract

In areas of potential coal seam gas (CSG) development, understanding interactions between coal-bearing strata and adjacent aquifers and streams is of highest importance, particularly where CSG formations occur at shallow depth. This study tests a combination of hydrochemical and isotopic tracers to investigate the transient nature of hydrochemical processes, inter-aquifer mixing and recharge in a catchment where the coal-bearing aquifer is in direct contact with the alluvial aquifer and surface drainage network. A strong connection was observed between the main stream and underlying alluvium, marked by a similar evolution from fresh Ca–Mg–HCO_3 waters in the headwaters towards brackish Ca–Na–Cl composition near the outlet of the catchment, driven by evaporation and transpiration. In the coal-bearing aquifer, by contrast, considerable site-to-site variations were observed, although waters generally had a Na–HCO_3–Cl facies and high residual alkalinity values. Increased salinity was controlled by several coexisting processes, including transpiration by plants, mineral weathering and possibly degradation of coal organic matter. Longer residence times and relatively enriched carbon isotopic signatures of the downstream alluvial waters were suggestive of potential interactions with the shallow coal-bearing aquifer. The examination of temporal variations in deuterium excess enabled detection of rapid recharge of the coal-bearing aquifer through highly fractured igneous rocks, particularly at the catchment margins. Most waters collected from the coal-bearing aquifer also showed an enhanced influence of weathering during the wet season, which was likely triggered by the water–rock interaction with fresh recharge waters. An increase in both residual alkalinity and carbon isotopic ratios at two locations indicated inter-aquifer mixing between alluvium and bedrock during the wet season. The results of this study emphasise the need for conducting baseline hydrochemical surveys prior to CSG development in order to describe the transient nature of recharge and inter-aquifer mixing processes.

5.1 Introduction

Understanding interactions between different groundwater bodies is a crucial step towards sustainable management of water resources. Scientists have long attempted to trace groundwater flowpaths and aquifer interactions, and a range of tools have been developed for this purpose, including natural tracers such as major ions, trace elements and isotopes (e.g. Taylor et al., 1989; Schramke et al., 1996; Cartwright et al., 2006, 2010; Gassama et al., 2012; Martínez-Santos et al., 2012; Négrel et al., 2012; Hofmann and Cartwright, 2013; Brenot et al., 2015). At a catchment scale, aquifer connectivity can be complex and, where shallow aquifers are involved, the influences on groundwater may include subsurface processes as well as dynamic surface processes. In such instances, a combination of hydrochemical and isotopic tools is necessary to target specific processes. In areas where coal seam gas (CSG; also known as coal bed methane) is extracted from coal-bearing formations, understanding

interactions between aquifers and surface water is particularly important. Where they occur at shallow depths, coal-bearing aquifers may contribute baseflow to streams during low flow periods. Because large quantities of groundwater need to be extracted from the coal seams in order to release the adsorbed gas, concerns have been raised for potential impacts of CSG activities to both overlying aquifers and streamflow (Commonwealth of Australia, 2014). Under scenarios where the coal-bearing bedrock is in direct contact with alluvial aquifers and streams, the development of accurate conceptual models that consider seasonal influences is necessary to inform and develop sound numerical models for use in the CSG industry (Dahm et al., 2014).

In CSG environments, scientific attention has initially been directed to the chemistry of produced waters (e.g. Van Voast, 2003; Taulis and Milke, 2007; Alley et al., 2011; Dahm et al., 2014) and to their fate after extraction (e.g. Stearns et al., 2005; Healy et al., 2011; Sharma and Baggett, 2011; Meng et al., 2014). Along with the global expansion of the CSG industry (Moore, 2012; Hamawand et al., 2013), focus has more recently shifted towards developing a baseline understanding of interactions between the coal-bearing bedrock and adjacent aquifers and streams prior to CSG development. The hydrochemistry of CSG groundwater is typically characterised by sulfate, calcium and magnesium depletion, and sodium and bicarbonate enrichment (e.g. Van Voast, 2003). Recent studies have used these characteristics to delineate flowpaths associated with CSG aquifers (Healy et al., 2011; Moya et al., 2015). Other studies have shown that, because of variations in mineralogy of different formations, strontium isotopic ratios could be useful in identifying areas where mixed contributions of CSG groundwater and shallower systems occur (Frost et al., 2002; Campbell et al., 2008). Similarly, dissolved inorganic carbon (δ^{13}C-DIC) signatures were reportedly good indicators of the infiltration of produced CSG waters into adjacent systems (Sharma and Frost, 2008; Sharma and Baggett, 2011). This is due to the prevalence of enriched δ^{13}C-DIC values in organic-rich systems where methanogenesis occurs, because this biogenic process preferentially removes the lighter ^{12}C isotope from water (Schlegel et al., 2011). Some authors also used an integrated approach considering both hydrochemistry and isotopes to infer the degree of inter-aquifer mixing in different CSG settings (Grossman et al., 1989; Frost et al., 2011; Hofmann and Cartwright, 2013; Kanduč et al., 2014). While these previous studies provided some foundation for investigating aquifer connectivity associated with CSG groundwaters, few studies have been carried out in settings where the coal-bearing aquifers occur at shallow depths; as a result, the effects of recharge on CSG groundwaters have been largely overlooked. Another difficulty stems from the complex geology of the CSG aquifers: coal-bearing formations are typically heterogeneous and, consequently, not all these groundwaters may present a typical CSG water signature.

In this study, we test the value of a number of hydrochemical (major and trace elements) and isotopic (deuterium, oxygen, carbon, strontium, and tritium) tracers – and their com-

binations – for the delineation of inter-aquifer and stream–aquifer interactions in a CSG environment. A small catchment located in Southeast Queensland (Australia) was chosen for our research, because it features the interface between a coal-bearing sedimentary bedrock and a set of fractured Cenozoic rocks forming the headwaters and peripheral ranges. The overarching purpose of this study is to determine whether conventional hydrochemical and isotopic methods are sufficient to establish the interactions between fractured igneous aquifers, shallow coal-bearing sedimentary bedrock aquifers, exploited alluvial aquifers, and streams. In particular, the following research questions will be addressed: (1) what are the hydrochemical processes responsible for the chemical and isotopic facies in each hydrological component? (2) How do these facies vary pre/post a major flood event, and can seasonal variations help understand the recharge processes occurring in each aquifer? (3) What are the most effective tracer combinations to assess potential interactions between the coal-bearing aquifer and adjacent aquifers and streams?

5.2 Site description

5.2.1 Climate and geology

The Teviot Brook catchment is a sub-catchment of the Logan River (Southeast Queensland), with its headwaters in the Great Dividing Range (Figure 5.1). Elevations range between 65 and 1375 m above Australian Height Datum (m AHD), and climate in the region is humid subtropical (*Cfa* in Köppen classification) with extremely variable rainfall. The annual average precipitation for the 1966–2012 period is 1190 mm in the headwaters and 850 mm in the floodplain, most of which falls from November to April. Following the wet season, winter months are dominated by much drier conditions, although significant rainfall may occur from May to October. The headwaters support undisturbed subtropical rainforest, while the valley supports open woodland, grassland and irrigated agriculture.

Geologically, the catchment forms part of the Clarence–Moreton Basin, a Mesozoic sedimentary basin that covers about 38 000 km^2 at the border between Queensland and New South Wales. The Clarence–Moreton Basin contains fluvial sedimentary deposits that form interbedded sequences of aquifers and aquitards. The shallowest bedrock unit of the basin is a Jurassic sedimentary sequence named the Walloon Coal Measures, which outcrops over much of the Teviot Brook catchment (Figure 5.1). The Walloon Coal Measures consist of irregular beds of sandstone, siltstone, claystone, carbonaceous shale and coal (Wells and O'Brien, 1994), and their thickness is around 120–240 m in the study catchment (Rassam et al., 2014). A Quaternary alluvial formation composed of eroded catchment materials overlies the sedimentary bedrock. The alluvium has a thickness ranging between 5 m upstream and over 20 m downstream. The catchment headwaters feature a steep morphology with an outcropping Cenozoic basalt sequence known as the Main Range Volcanics. In addition,

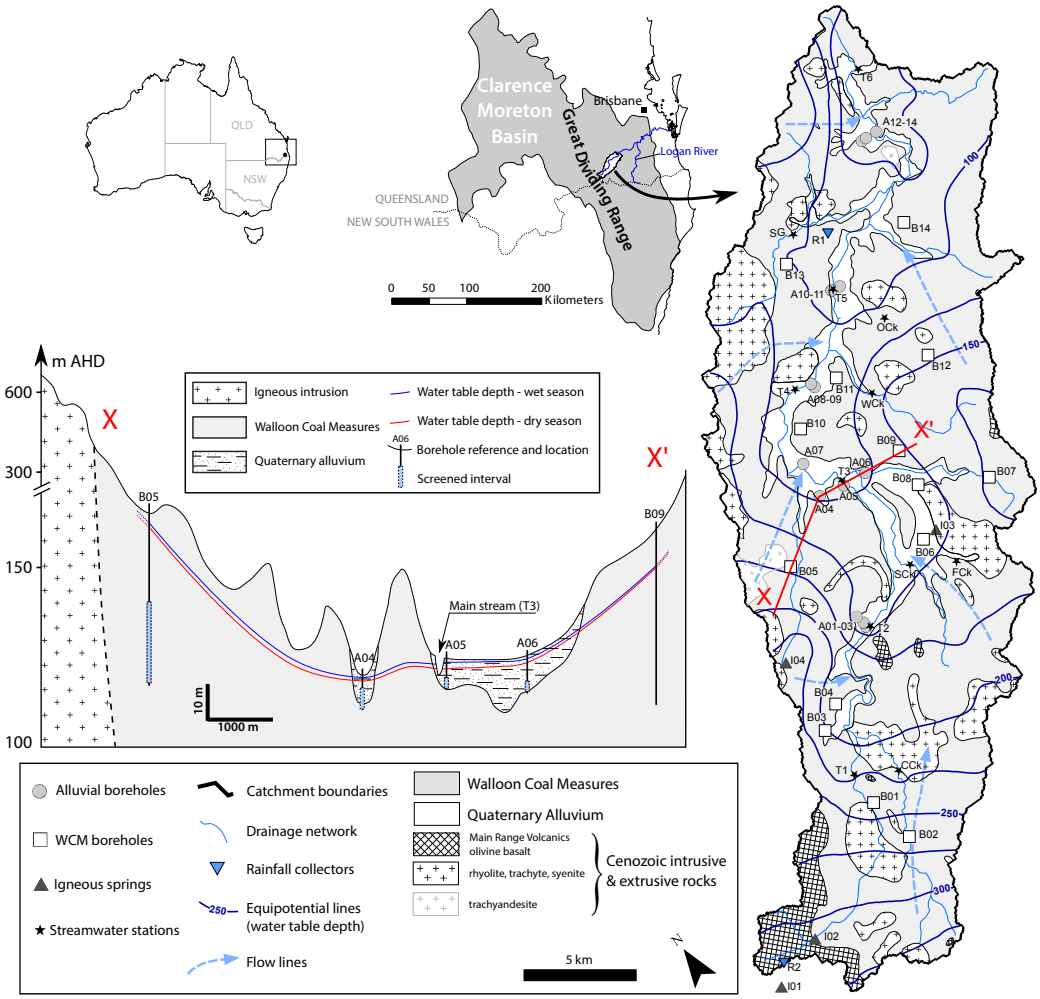

Figure 5.1: Location of the Teviot Brook catchment in Southeast Queensland. Geological map of the catchment with location of sampling sites and equipotential lines for the shallow aquifers (data obtained from the Queensland government (DNRM) database. Long-term median head values were calculated for each borehole, and data from neighbouring catchments were also used to draw the contour map). Geological cross-section along X–X' showing the depth of water table for the two sampling rounds. Samples were arranged in increasing order from upstream towards downstream for each component. 'B' is for bedrock boreholes, 'A' is for alluvial boreholes, 'I' is for igneous springs, 'T' is for the samples collected from the main stream, and 'R' is for the two rainfall collectors.

numerous intrusive dykes and sills associated to the Main Range Volcanics cap the ranges of the catchment as well as occur on the valley floor. The Walloon Coal Measures host a number of coal seams (Wells and O'Brien, 1994), and CSG exploration has commenced in the area and surrounding region about ten years ago and recently intensified.

5.2.2 Hydrogeological setting

Several water-bearing layers exist within the Walloon Coal Measures, and the formation is referred to as 'bedrock aquifer' in the following. It is assumed that recharge of the

bedrock and alluvial aquifers occur through a combination of mountain front recharge via the highly fractured igneous rocks and diffuse recharge over the catchment. The alluvium provides groundwater for irrigation, while the bedrock contains groundwater that is typically brackish (total dissolved solids up to 13 000 mg L^{-1}) and mostly used for livestock watering. Groundwater of medium to high salinity has been observed in sections of the alluvium as well as in the stream, which has been interpreted by some authors as the result of mixing between the different systems (Li and Cox, 1996). Vertical hydraulic gradients indicate upward flow from the bedrock aquifer to the alluvium and from the alluvium to the stream network, both under dry and wet conditions. The general groundwater flow direction follows the surface topography and is essentially from the southwest to the northeast (Figure 5.1). Regardless of the aquifer considered, groundwater levels are shallow across the catchment, and are commonly between 0.5 and 18.4 m below ground surface.

A major rainfall event occurred in the Teviot Brook catchment in late January 2013, i.e. between the dry and wet sampling rounds of this study. The Thiessen-averaged rainfall depth recorded over a three-day period reached 330 mm for this event. Heavy rainfall generated sustained high flows in the drainage network and temporary flooding of some parts of the floodplain, as well as a general increase in groundwater levels. Data indicate that the dry sampling round (October 2012) was conducted under low to very low head conditions, with levels amongst the 75% lowest on record (1988–2014 period). By contrast, the wet sampling round (March 2013) was conducted after groundwater levels had increased in all the boreholes that were accessed for this study (e.g. cross-section X–X' in Figure 5.1). This lends support to our postulation that the wet sampling round was conducted after recently recharged waters had reached the aquifers. There was no shift in the horizontal and vertical hydraulic gradients between the dry and wet monitoring periods.

5.3 Methods

5.3.1 Sample collection and analysis

Water samples were collected from each hydrological component previously identified. Twelve surface water sites (six locations along the main stream identified 'T1' to 'T6'; six tributaries) as well as 28 groundwater locations (14 boreholes from the alluvial aquifer identified 'A01' to 'A14', and 14 boreholes from the bedrock aquifer identified 'B01' to 'B14') and four springs (two draining basaltic rocks and two discharging from rhyolite or trachyte intrusions; identified 'I01' to 'I04') were investigated for hydrochemical and isotopic parameters (Figure 5.1). To evaluate the seasonal variations, samples were collected in October 2012 (dry season) and again in March 2013 (wet season). Temperature, pH and electrical conductivity were measured in the field. Immediately after collection, samples were filtered through 0.45 µm filters and kept refrigerated until analysed.

For groundwater boreholes, samples were collected after purging a minimum of three casing volumes with a stainless steel submersible pump (Hurricane XL, Proactive). The alluvial boreholes accessed for this study are part of the state government observation network (Department of Natural Resources and Mines), which have depths of 10–23 m, screen lengths of 3–6 m and are screened into the typically coarser basal layer of the alluvium. The 14 alluvial boreholes are distributed along five cross-sections that cover the whole alluvial flowpath. The alluvial borehole labelled A04, central to the valley (Figure 5.1), has a slightly longer screen interval that intercepts both the basal layer of the alluvium and the underlying bedrock formation. In this work, A04 was regarded as a potential "witness" of mixing between the two aquifers. The bedrock boreholes are exclusively private bores used for irrigation and/or livestock watering. As many bedrock boreholes have long screen intervals to maximise water yield (i.e. 5–17 m), only those that intercept the Walloon Coal Measures were sampled.

In addition, precipitation was sampled at two different locations in the headwaters (elevation 800 m AHD) and on the floodplain of the catchment (elevation 105 m AHD) on a monthly to fortnightly basis (Figure 5.1). In order to avoid water evaporation between two sampling rounds, rainfall collectors that adhere to IAEA standards were used (Gröning et al., 2012).

Cations and anions were measured at the Queensland University of Technology (QUT) using inductively coupled plasma optical emission spectrometry (Optima 8300, Perkin Elmer) and ion chromatography (ICS-2100, Dionex). Total alkalinity was measured by titrating water samples with hydrochloric acid to a pH endpoint of 4.5. Charge balance error for major ions was $< 10\%$ for all samples, and $< 5\%$ for 89% of the samples.

All samples were analysed for oxygen (δ^{18}O) and deuterium (δ^{2}H) stable isotopes at QUT using a Los Gatos Research water isotope analyser. Replicate analyses carried out during each run indicate that analytical error was $\pm 1.1‰$ for δ^{2}H and $\pm 0.3‰$ for δ^{18}O. The stable isotope composition of dissolved inorganic carbon (δ^{13}C-DIC) was measured at the University of Florida with an isotope ratio mass spectrometer (DeltaPlus XL, Thermo Finnigan) coupled with a universal on-line gas preparation device (GasBench II) on samples that had been filtered through 0.2 µm filters and stored in 12 mL Exetainer vials. Samples were run in three different batches and precision for all measured δ^{13}C-DIC values was estimated to range from $\pm 0.05‰$ to $\pm 0.09‰$.

Strontium isotopic ratios (^{87}Sr/^{86}Sr) were analysed at the University of Melbourne for samples collected during the dry sampling round. The ^{87}Sr/^{86}Sr ratios were measured by multi-collector inductively coupled plasma mass spectrometry on samples that had been acidified and loaded on Eichrom Sr resin columns. Instrumental mass bias was normalised to ^{88}Sr/^{86}Sr $= 8.37521$. Internal precision was < 0.00002, while external precision was

±0.00004. Tritium (^{3}H) was analysed at the Australian Nuclear Science and Technology Organisation in Sydney for samples collected during the dry sampling round. The 1 L samples were electrolytically enriched and analysed using a liquid scintillation counter. The limit of quantification was 0.05 tritium units (TU) for all samples, and uncertainty ranged between ±0.02 and ±0.07 TU.

5.3.2 Data analysis

Saturation indices were calculated using PHREEQC (Parkhurst and Appelo, 1999). In addition, a number of parameters were derived from the major ion and isotope data. In a recent paper, Owen and Cox (2015) defined the cation chloride ratio (CCR) index as:

$$\mathrm{CCR} = \frac{\mathrm{Ca_{meq}} + \mathrm{Mg_{meq}}}{\mathrm{Cl_{meq}}} - \frac{\mathrm{Na_{meq}} + \mathrm{K_{meq}}}{\mathrm{Cl_{meq}}} \tag{5.1}$$

where CCR is the dimensionless cation chloride ratio index, and $\mathrm{Ca_{meq}}$, $\mathrm{Mg_{meq}}$, $\mathrm{Cl_{meq}}$, $\mathrm{Na_{meq}}$, and $\mathrm{K_{meq}}$ are ionic concentrations in meq/L. The CCR index can be used to describe the hydrochemical processes affecting different groundwater systems, and particularly their possible evolutionary pathways towards CSG-type groundwaters.

Another useful indicator is the residual alkalinity r, which is a measure of the excess alkalinity that is not neutralised by calcium and magnesium (Van Beek and Van Breemen, 1973; Ribolzi et al., 1996):

$$r = \left(\mathrm{HCO_{3meq}} + \mathrm{CO_{3meq}}\right) - \left(\mathrm{Ca_{meq}} + \mathrm{Mg_{meq}}\right) \tag{5.2}$$

with r expressed in meq L^{-1}. This parameter can be relevant in describing the characteristics of CSG groundwaters, as they are generally enriched in (bi)carbonate ions even at high chloride concentrations (Van Voast, 2003).

Deuterium excess (d-excess) was proposed by Dansgaard (1964) as a "rate of evaporation index":

$$d_{\mathrm{excess}} = \delta^2\mathrm{H} - 8\,\delta^{18}\mathrm{O} \tag{5.3}$$

where d-excess is defined for a slope of 8 consistent with the global precipitation water line. This value is useful because it cancels out the co-variations between the two isotopes. It can be used to distinguish between the processes driving groundwater salinisation, i.e. evaporation *vs* mineral weathering and/or transpiration (e.g. Huang and Pang, 2012).

5.4 Results

5.4.1 Major ion chemistry

Total dissolved solids (TDS) contents increased from upstream to downstream, both in the main stream and alluvial aquifer (Appendix A.1). Upstream values ranged between 270–660 mg L^{-1} (dry season) and 230–370 mg L^{-1} (wet season) for streamwater, and between 550–660 mg L^{-1} (dry season) and 580–700 mg L^{-1} (wet season) for alluvial groundwater. By contrast, downstream values ranged between 2780–3630 mg L^{-1} (dry season) and 500–2500 mg L^{-1} (wet season) for streamwater and between 2030–3670 mg L^{-1} (dry season) and 1810–4210 mg L^{-1} (wet season) for alluvial groundwater. Salinity was highly variable in the samples collected from the bedrock aquifer (370–4800 mg L^{-1} in the dry and 490–6230 mg L^{-1} in the wet), while groundwaters from the igneous springs had TDS in the range 230–320 mg L^{-1} (dry) and 190–430 mg L^{-1} (wet).

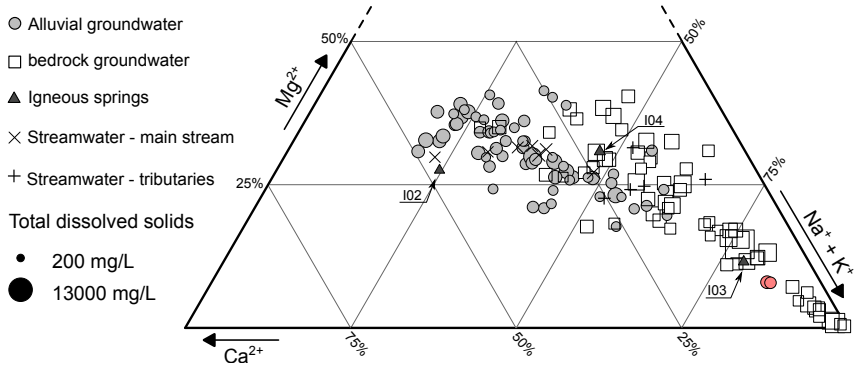

Figure 5.2: Ternary plot for major cations in each hydrological component of the Teviot Brook catchment (dry and wet season). Data are from this study and from Li (2001). The red circles correspond to values for A04.

Major ion chemistry revealed a wide variety of hydrochemical facies among the sampled waters (Appendix A.1). Generally, chemical types of the alluvial and igneous waters were Ca–Mg–HCO_3 to Ca–Mg–HCO_3–Cl, whereas the bedrock groundwaters predominantly had Na–Cl–HCO_3 facies. The range of hydrochemical facies encountered in the catchment is particularly reflected in their cation compositions (Figure 5.2). Na was the dominant cation in most bedrock waters, constituting from 30% to 99% of relative molar cation concentrations. In this aquifer, Cl and HCO_3 were the dominant anions, and some bedrock groundwaters had low to very low SO_4 concentrations (Appendix A.1). By contrast, Ca was the dominant cation in most alluvial waters, except for a few samples dominated by Na. Of note is the chemical composition of the waters taken from alluvial borehole A04, with a clear predominance of Na relative to Ca and Mg (Figure 5.2). This confirms that this monitoring bore very likely intercepts mixed contributions of alluvial and bedrock waters. Waters taken from the main stream channel had similar cation contents as alluvial waters, with Ca acting as the dominant cation. Tributaries of the Teviot Brook had slightly Na dominated waters,

which was consistent with the geological provenance of these streams, i.e. mainly draining the Walloon Coal Measures formation. Composition of waters that have flown through igneous rocks was widely variable: springs draining basalt (I01 and I02) had waters dominated by Ca and HCO_3 whereas the spring draining rhyolite (I03) had a Na–HCO_3 facies, and the spring draining trachyte (I04) had a mixed contribution of Ca, Mg and Na (Figure 5.2).

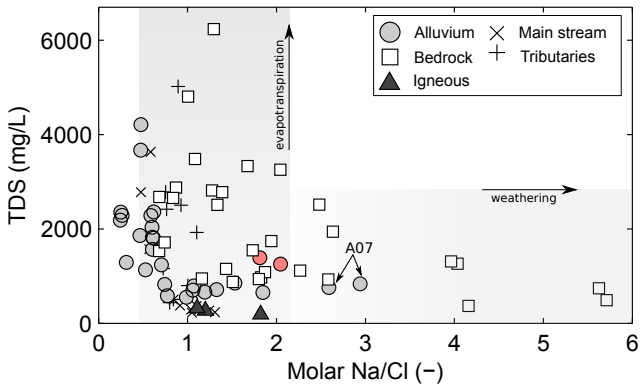

Figure 5.3: Variation in the molar Na/Cl ratio with increasing TDS in the Teviot Brook catchment (dry and wet season). The red circles correspond to values for A04. The vertical grey shaded area represents the Na/Cl ratios measured in local rainfall of 0.7 and 2.2.

Local rainfall had molar Na/Cl ratios between 0.7 (wet season) and 2.2 (dry season; Figure 5.3). Most alluvial groundwaters and all surface waters fell within the rainfall range. Notable exception is A07, with Na/Cl ratios of 2.9 during the dry season and 2.6 during the wet season. A04 also had relatively high values (1.8 and 2.1 for the dry and wet, respectively). Waters collected from the bedrock aquifer had molar Na/Cl ratios ranging between 0.7 and 5.8, and highest ratios were found in the bedrock groundwaters with TDS $< 1000\,\mathrm{mg\,L^{-1}}$. The four lowest Na/Cl ratios (< 0.5) were found for alluvial waters (Figure 5.3).

5.4.2 Oxygen and hydrogen isotopes

A local meteoric water line was derived from 29 samples taken from both R1 and R2, because no significant effect of elevation was observed on the isotopic signature of rainfall (Figure 5.4). The equation had an intercept of 15.8 and a slope of 8.4, which is comparable to that of Brisbane (intercept: 13.0 and slope: 7.9; Hughes and Crawford, 2012). The two main aquifers were not clearly distinguishable based on their isotopic signatures, as most waters were displaced to the right of the meteoric line (Figure 5.4). There was no direct correlation between TDS values and the position of samples on the evaporation trend. All igneous spring waters fell very close to the meteoric line, as did some bedrock waters (B01, B02 and B05). Of consideration is the high degree of evaporation for B14, which is identified by blue squares in Figure 5.4.

The calculated deuterium excess (d-excess) values for precipitation ranged between +8.3‰ and +18.4‰ throughout the study period. Most alluvial groundwater d-excess

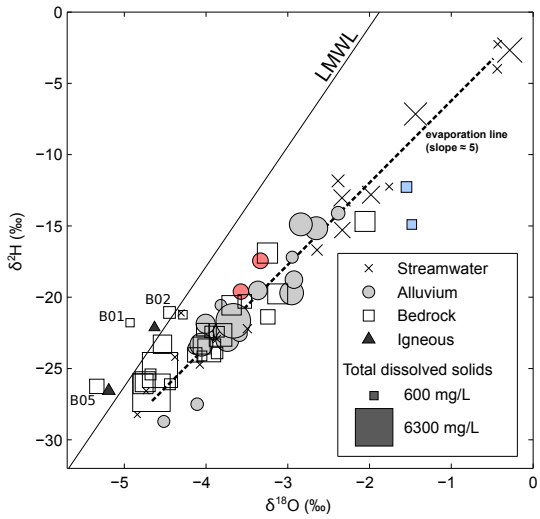

Figure 5.4: Stable isotopes of water for each hydrological component of the Teviot Brook catchment (dry and wet season). The size of markers refers to the TDS content in samples. The line noted LMWL is the local meteoric line calculated from 29 samples taken throughout an 18-month monitoring period ($\delta^2H = 8.4\,\delta^{18}O + 15.8$). The red circles correspond to data measured at A04, and the blue squares correspond to data measured at B14.

values were lower than those for rainfall (range +3.9–+10.2‰), with about 60% and 45% of them below +8‰ during the dry and wet seasons, respectively (Appendix A.3). By contrast, the bedrock groundwater *d*-excess values covered a wider range (–3.0–+17.7‰), with about 80% of them above +8‰ in the dry season, and 65% in the wet season. Values for igneous springs were generally higher than those for other groundwaters (median +11.9‰), except for I03 (spring draining rhyolitic rocks; *d*-excess = +4.4‰). The waters with highest evaporation were surface waters, particularly during the dry season (−0.5‰ < *d*-excess < +13.3‰, median +3.1‰). The only exception was for the bedrock borehole B14, which had a *d*-excess of –3.0‰ in the wet season (Figure 5.4).

5.4.3 Tritium, carbon and strontium isotopes

Monthly tritium (^3H) measurements in rainfall carried out by ANSTO at the Brisbane airport ranged between 0.9 and 1.8 TU during the monitoring period. For all groundwaters, salinity increased with decreasing ^3H. Values for alluvial groundwater fluctuated from < 0.05 to 1.22 TU, with only one sample (A11) presenting undetectable ^3H activities (Appendix A.3). Tritium values were systematically higher in the upstream part of the alluvium, and the lowest values were found in the downstream section (Figure 5.5). Values for the bedrock aquifer were generally lower than those in the alluvium, but the range of variation was high (< 0.05 < ^3H < 1.28 TU). Five boreholes (B03, B05, B10, B11, and B13) had values below detection limit (Appendix A.3; Figure 5.5). Borehole B14 had waters similar to rainfall values (^3H = 1.28 TU). The second highest value in the bedrock was found at B01 (^3H = 1.12 TU). The main drainage system had very modern water at T2, comparable

to precipitation (^{3}H = 1.28 TU), but no ^{3}H value was obtained for streamwater locations further downstream, where the contribution of older water to the stream network might have been identified.

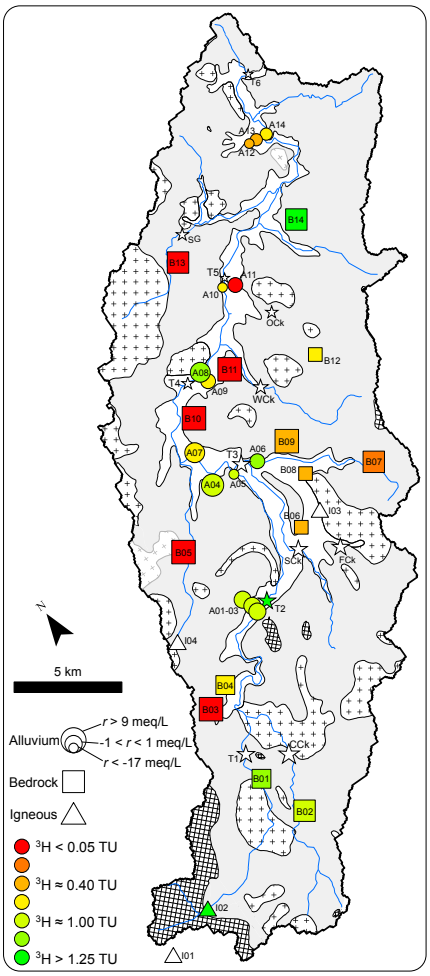

Figure 5.5: Map showing the distribution of tritium (^{3}H) activity (marker colour) and residual alkalinity (r) values (marker size) for the dry sampling round. 'I' is for igneous springs (triangles), 'A' is for alluvial bores (circles) and 'B' is for bedrock bores (squares). Streamwater locations are represented by stars. Legend for the geology is the same as in Figure 5.1. Values can be found in Appendices A.1 and A.3.

The δ^{13}C-DIC values in groundwaters of the Teviot Brook catchment varied from –14.6 to –3.2‰ during the dry season, and from –13.6 to –0.6‰ during the wet season (Appendix A.3). Samples from the bedrock and alluvial aquifers had similar ranges of δ^{13}C-DIC values (Appendix A.3). The δ^{13}C-DIC signature of igneous springs draining the Volcanics in the headwaters was low (–13.4 and –13.9‰ for I01 and I02, respectively). A few groundwater samples from the bedrock aquifer had higher δ^{13}C-DIC values, the most enriched value being for B05 (–3.2‰ and –2.7‰ during dry and wet season, respectively; Appendix A.3). Of consideration are the relatively enriched values for alluvial samples A05 and A12 during the wet season (δ^{13}C-DIC = −1.9‰ and –0.6‰, respectively), and to a

lower extent for alluvial samples A06, A09, A10, A13 and A14 ($-5.1‰ < \delta^{13}$C-DIC $< -4.2‰$).

The $^{87}Sr/^{86}Sr$ ratio of precipitation varies with distance to the coast; in this study we report the values measured by Ullman and Collerson (1994) and Raiber et al. (2009) in rainfall samples that were collected in Southeast Australia approximately 100 km from the coast ($^{87}Sr/^{86}Sr = 0.7131$ and 0.7107, respectively). Strontium isotopic ratios of surface and groundwaters in the Teviot Brook catchment were all considerably lower than precipitation. Values ranged from 0.7033 to 0.7054 (Appendix A.3), and the highest value was for I03, i.e. the spring draining a rhyolitic intrusion. All other samples fell within a narrower range of 0.7033 to 0.7043. The I01 and I02 springs had low $^{87}Sr/^{86}Sr$ ratios. The bedrock groundwaters generally had the most depleted values ($0.7033 < {}^{87}Sr/^{86}Sr < 0.7042$), while slightly higher ratios were found in the alluvial waters ($0.7038 < {}^{87}Sr/^{86}Sr < 0.7043$).

5.5 Discussion

5.5.1 Assessment of dominant hydrochemical processes

5.5.1.1 Salinisation as inferred by major ions and deuterium excess

Bedrock waters had a typical Na–Cl–HCO_3 facies, which is similar to the ones observed in other CSG groundwaters around the world (e.g. Van Voast, 2003; Kinnon et al., 2010; Hamawand et al., 2013). Some bedrock groundwaters had low to very low SO_4 concentrations (Appendix A.1), implying SO_4 reduction and/or gypsum precipitation. In contrast, waters draining the Main Range Volcanics (I01 and I02) were dominated by Ca and Mg cation composition. The alluvial and stream waters collected near the headwaters had a similar Ca–Mg–HCO_3 signature, suggesting an influence of the weathering of silicates mainly derived from the igneous rocks present in the headwaters.

The evolution towards more Na–Cl enriched stream and alluvial waters in the downstream section may be an indication of increased evapotranspiration, as reported in other parts of Australia (e.g. Cartwright et al., 2004; Cartwright and Weaver, 2005; Meredith et al., 2009; King et al., 2014). Any groundwater dissolving halite would inherit a Br deficiency compared to rainfall water (e.g. Cendón et al., 2004; Cartwright et al., 2006). However, molar Cl/Br ratios were all below 1000 for downstream waters, ruling out halite dissolution as an influence on salinity in these areas. In the absence of halite dissolution, the relationship between molar Na/Cl ratios and TDS contents (Figure 5.3) can be valuable in differentiating between the relative influence of evapotranspiration and rock weathering on water salinisation (e.g. Simpson and Herczeg, 1994; Cartwright et al., 2004; Raiber et al., 2009). Excess of Na/Cl ratios relative to the expected range for rainfall for some bedrock waters, particularly those with lower TDS, suggest the weathering of alkali feldspar (Appendix A.1). A04 had relatively high Na/Cl values (1.8 and 2.1 for the dry and wet, respectively), which

is indicative of mixing with bedrock waters for this bore (see Section 5.3.1). By contrast, evapotranspirative enrichment was the dominant process in groundwaters with higher salinity, both in the bedrock aquifer and in the stream–alluvial system (Appendix A.1). The low Na/Cl ratios (< 0.5) found for some alluvial waters indicate ion exchange of Na for Ca within the clays of the alluvium (Cartwright and Weaver, 2005) and/or the weathering of remnant igneous materials in the alluvial matrix.

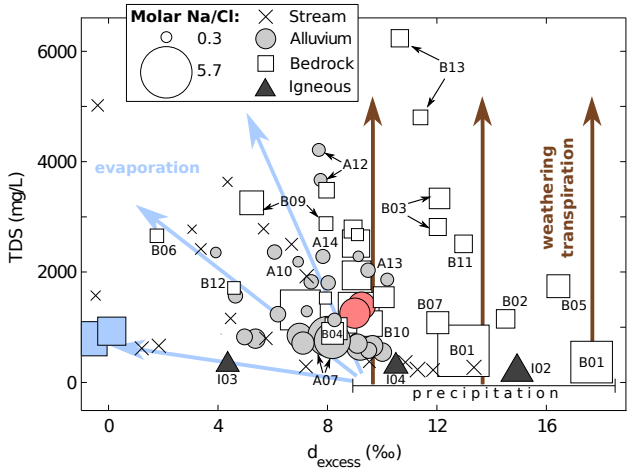

Figure 5.6: Relationship between TDS and deuterium excess for the waters of the Teviot Brook catchment (dry and wet season). The size of markers refers to the Na/Cl ratio for each sample. The range for deuterium excess in precipitation is from +8.3‰ to +18.4‰ based on the 29 samples taken throughout the study period.

Following recent work by Huang and Pang (2012) and Guo et al. (2014), the d-excess values are presented together with TDS contents to further document the processes driving groundwater salinisation (Figure 5.6). Two distinctive trends can be observed in Figure 5.6. First, rock weathering and/or transpiration were dominant processes for the waters with increasing TDS and d-excess values maintaining at a high level (brown arrows in Figure 5.6). Several of the bedrock waters were consistent with this first trend. Among these waters, the ones with higher Na/Cl ratios (i.e. larger makers) may have experienced higher rates of rock weathering, while ratios similar to rainwater (i.e. smaller markers) may indicate waters dominated by transpiration: many deep-rooted native plants can reach the water table of the coal-bearing bedrock aquifer. Second, evaporation was a dominant process for the waters with decreasing d-excess values and increasing TDS (blue arrows in Figure 5.6). This was the case for most alluvial waters and surface waters, and to a lower extent for some of the bedrock waters (B06, B09 and B12). Some samples that were consistent with this second trend and with d-excess values $\geq +6$‰ had high Na/Cl ratios, suggesting that for these samples there was a mixed contribution of mineral weathering and evaporation to the increase in TDS, e.g. the mixed waters in A04 (red circles in Figure 5.6). Other samples with potential mixed influences are A07, B04 and B10. The high degree of evaporation for B14 (Figures 5.4 and 5.6) most likely reflects seepage from evaporated dam water located

in the vicinity of the bore.

5.5.1.2 Residual alkalinity and CCR index to document evolutionary pathways

Residual alkalinity (r) values for streamwater and shallow alluvial groundwaters were close to zero in the upstream section of the catchment (Figure 5.7a, Cl values from < 1 to 5 meq L^{-1}; marker size in Figure 5.5). Ca and HCO_3 concentrations for these upstream waters were strongly correlated and followed a 1:2 trend, suggesting that calcite dissolution controlled their hydrochemistry (Herczeg and Edmunds, 2000; Cartwright et al., 2010). This is consistent with the presence of calcite as secondary minerals in the veins and fractures of the Main Range Volcanics and other intrusions, as reported by Li (2001). Further downstream, another process became apparent, with a decrease in r concomitant to a gradual increase in Cl. The addition of waters that underwent evapotranspiration probably occurred concurrently with carbonate precipitation due to supersaturation of these waters with regards to calcite and dolomite ($0.05 < SI_{calcite} < 1.06$ and $0.13 < SI_{dolomite} < 2.26$ for bores A12 to A14 and stream locations T4 to T6; Appendix A.1), which together led to salinisation (blue arrow in Figure 5.7a). There was a significant correlation between the increase in Cl concentrations through evapotranspiration processes and the decrease in r, probably because the alluvium had no major HCO_3 source.

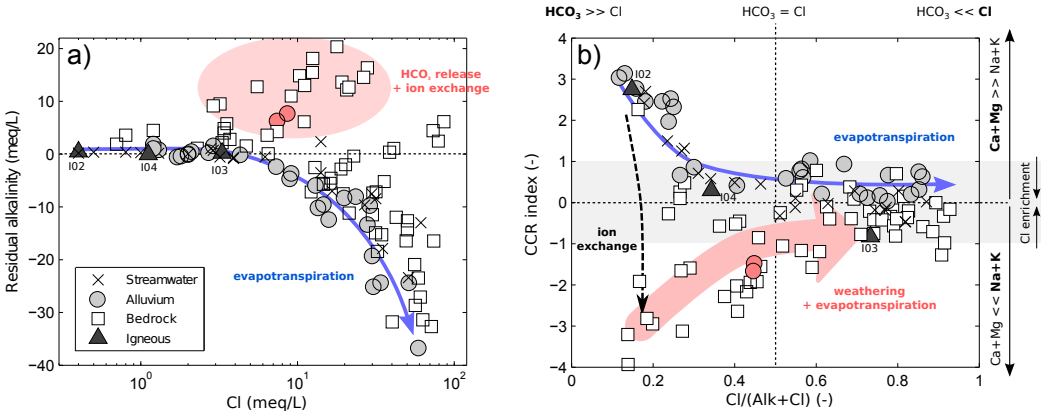

Figure 5.7: (a) Residual alkalinity (r) as a function of chloride concentrations for all hydrological components of the Teviot Brook catchment (dry and wet season). Residual alkalinity was calculated according to equation 5.2. (b) Cation chloride ratio (CCR) index versus the normalised ratio between chloride and total alkalinity (dry and wet season). The CCR index was calculated as expressed in equation 5.1 (Owen and Cox, 2015). CCR values between –1 and 1 indicate an enrichment of Cl relative to all major cations. Data are from this study and from Li (2001).

The CCR index of the stream–alluvium system was highly positive for upstream waters ($1 < CCR < 3$), reflecting the dominance of Ca and Mg and low Cl concentrations (Figure 5.7b). Concurrent to the downstream salinisation processes was a drop in CCR values to < 1, indicating the loss of Ca and Mg and increase in Na. However, because the CCR index maintained positive values ($0 < CCR < 1$; Figure 5.7b), some Ca and Mg must have continued to be released through silicate weathering and/or some localised carbonate

dissolution.

Due to the absence of systematic spatial variations in the bedrock aquifer, evolutionary pathways were assessed with variation in salinity, i.e. with the increase in Cl concentrations (Figure 5.7a). A substantial number of samples followed the evapotranspiration trend (decreasing r with increasing Cl), as previously described for stream and alluvial waters (marker size in Figure 5.5; Figure 5.7a). In contrast, some bedrock waters had significant excess in HCO_3 that tended to increase with salinity. Waters from the alluvial bore A04 (red circles in Figure 5.7) had similar ionic indexes to the majority of bedrock waters, with negative CCR values and positive r values.

The Na–HCO_3 facies characteristic of bedrock waters appeared to be evolving towards Na–HCO_3–Cl facies (red arrow in Figure 5.7b). These waters may have evolved via weathering of alkali feldspars contained in clays and sands of the Walloon Coal Measures, under saturation of clays such as kaolinite (Venturelli et al., 2003); kaolinite saturation was observed for all bedrock waters in the Teviot Brook catchment (Appendix A.1). In addition, the high HCO_3 concentrations may originate from bacterial SO_4 reduction, and possibly methanogenesis in some areas of the bedrock where coal seams occur (Papendick et al., 2011). High HCO_3 concentrations may facilitate carbonate precipitation and the depletion of Ca and Mg, which is consistent with oversaturation of most bedrock waters with respect to calcite and dolomite (Appendix A.1). Carbonate precipitation is typical in coal seams, including the Walloon Coal Measures (e.g. Ward et al., 1999; Chaffee et al., 2010), and this process may explain the persistence of positive r values as Cl increased for these waters.

Overall, the examination of CCR index together with other ratios confirmed the absence of a systematic evolutionary pathway for the coal-bearing bedrock groundwaters. Some bedrock waters had a consistent behaviour, with positive r and high Na content that both maintained with Cl enrichment. However, using these characters as simple tracers of interactions between the coal-bearing aquifer and the alluvial aquifer and streamwater was not realistic because of the high heterogeneity inherent to the Walloon Coal Measures complex geology. In the following section, other isotopic tracers (i.e. δ^{13}C-DIC and $^{87}Sr/^{86}Sr$) are tested together with an age tracer (^3H) to further constrain hydrochemical processes and possibly inter-aquifer relationships.

5.5.1.3 Additional insights using tritium, carbon and strontium isotopes

The δ^{13}C-DIC content of groundwaters reflects the signature acquired during recharge and all subsequent geochemical processes occurring in the saturated zone (Hofmann and Cartwright, 2013). Because the source of organic C controls the state of fractionation of soil CO_2, knowledge of the dominant vegetation types is required to determine the δ^{13}C-DIC signature of recharge water. According to Hattersley (1983), the proportion of C4 plants relative to C3 plants in Southeast Queensland is 74%. Given that C4 plants possess a δ^{13}C

signature (–15 to –9‰) distinct from that of C3 plants (–24 to –21‰) (Ladd et al., 2009), the soil δ^{13}C-CO_2 values would likely be between –17 and –14‰ in the study area (Clark and Fritz, 1997). As the soil CO_2 gets dissolved during recharge, and assuming a pH of 7 and a temperature of 20°C, recharge waters would acquire a δ^{13}C-DIC signature of around –10 to –7‰ (Figure 5.8a). In the headwaters, C3 vegetation (upland rainforest) is dominant, and therefore the δ^{13}C-DIC content of recharge waters would be between –16 and –14‰ in this part of the catchment as it is for instance in other temperate areas (e.g. Leybourne et al., 2006). Therefore, any δ^{13}C-DIC value higher than –14‰ in the headwaters and –7‰ in the valley may be indicative of either carbonate mineral dissolution or the product of biogenic processes, i.e. methanogenesis.

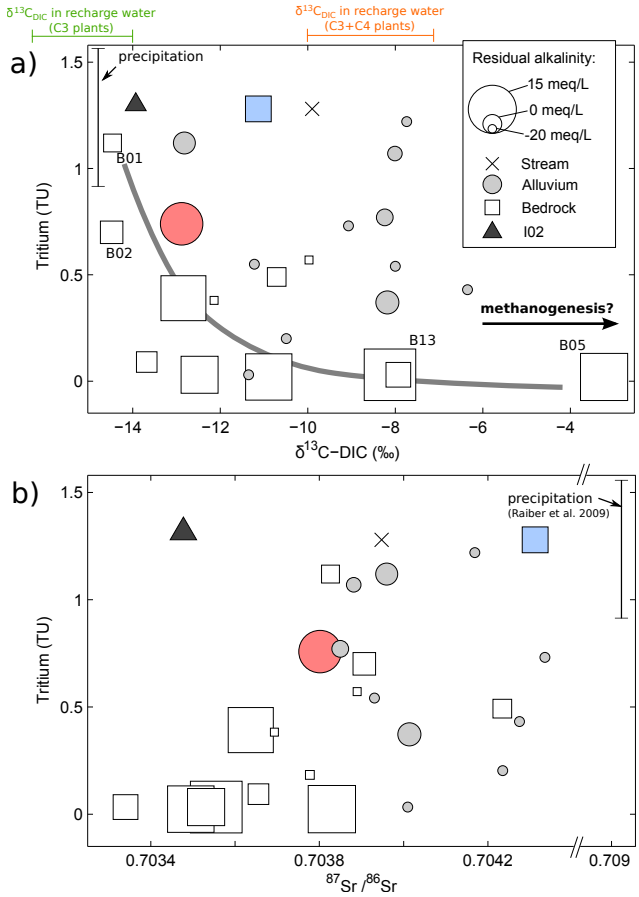

Figure 5.8: Variation of δ^{13}C-DIC (a) and $^{87}Sr/^{86}Sr$ ratios (b) relative to residence times expressed in tritium units (TU) for the dry season samples. The marker size reflects the value of residual alkalinity (smaller markers for negative values and larger markers for positive values). The red circle is for A04 and the blue square is for B14.

The depleted δ^{13}C-DIC content of igneous springs I01 and I02 draining the Volcanics is consistent with a C3-derived soil CO_2 source in the upland areas, as also reported in Cendón et al. (2014). Further downstream, the wide range of values found in alluvial and bedrock groundwaters indicates that there has been substantial evolution in DIC after the waters

reached the saturated zone. The δ^{13}C-DIC results for the dry sampling round are reported in Figure 5.8a together with the ^{3}H data. The five bedrock boreholes with ^{3}H values below detection limit were interpreted as groundwaters recharged over 60 years ago. Unlike the bedrock aquifer, alluvial waters contain a substantial modern component in most locations; however, there was no clear relationship between residence time and δ^{13}C enrichment for this aquifer. Borehole B14 had waters similar to rainfall values (^{3}H = 1.28 TU), which confirms that pond water contributed to the groundwater sampled at this location. If discarding B14 from the general trend (blue square in Figure 5.8a), a significantly negative correlation was found between ^{3}H and δ^{13}C-DIC data for samples collected from the coal-bearing aquifer. Older waters in the sedimentary bedrock generally had more enriched δ^{13}C-DIC signatures, and this was coherent with high r values (marker size in Figure 5.8a). Given the oversaturation of these waters with respect to calcite (SI = 0.23 and 0.15 at B05 and B13, respectively) and the occurrence of excess HCO_3 relative to Ca and Mg, carbonate dissolution was highly unlikely to occur. The higher δ^{13}C-DIC values, consistent with high r values and low SO_4 concentrations, may therefore be attributed to microbial methanogenesis (Figure 5.8a), as observed in similar settings (Leybourne et al., 2006; Sharma and Baggett, 2011; Kanduč et al., 2014). However, the range of δ^{13}C-DIC values reported by previous studies is significantly higher than the ones measured in this work. Such discrepancy may be explained by the occurrence of different methanogenic pathways such as acetate fermentation, which rarely produces δ^{13}C-DIC values $> 0‰$ (Aravena et al., 1995), although acetate fermentation has not been observed in the Walloon Coal Measures (Golding et al., 2013).

The $^{87}Sr/^{86}Sr$ ratios in groundwater change with the mineralogy of host rocks (e.g. Négrel et al., 2000). The highest $^{87}Sr/^{86}Sr$ value for I03 is consistent with higher values found in K-rich acidic material, due to the decay of ^{87}Rb to ^{87}Sr (Clark and Fritz, 1997). The low $^{87}Sr/^{86}Sr$ ratios in the I01 and I02 springs most probably reflect the release of Sr with a low $^{87}Sr/^{86}Sr$ ratio during the early stages of basalt mineral weathering, which likely overprinted the input rainfall signature (Figure 5.8b). The depleted values in the bedrock groundwaters may be due to the predominantly volcanic lithic composition of the Walloon Coal Measures (Wells and O'Brien, 1994). When relating the Sr isotopic ratios to groundwater age, it appears that the bedrock groundwaters with ^{3}H < 0.4 TU consistently had lower $^{87}Sr/^{86}Sr$ ratios (Figure 5.8b), while more modern waters falling in the range 0.49–1.12 TU had ratios similar to the ones of alluvial waters. The cluster of older waters with low Sr isotopic ratios also had the highest r values (large markers in Figure 5.8b).

The results obtained from isotopic analyses confirm that groundwaters from the studied aquifers followed distinct evolutionary pathways. In the bedrock aquifer, older waters were found to be relatively more enriched in ^{13}C and less enriched in ^{87}Sr relative to ^{86}Sr, concurrently with HCO_3 excess relative to Ca and Mg. This might be an indication of bio-

genic activity in the coal-bearing aquifer, although further measurements would be needed to confirm such a hypothesis. In the alluvium, there was considerable dispersion in isotopic data, but as a general rule waters had longer residence times and were more enriched in ^{13}C in the downstream section of the catchment, particularly during the wet season.

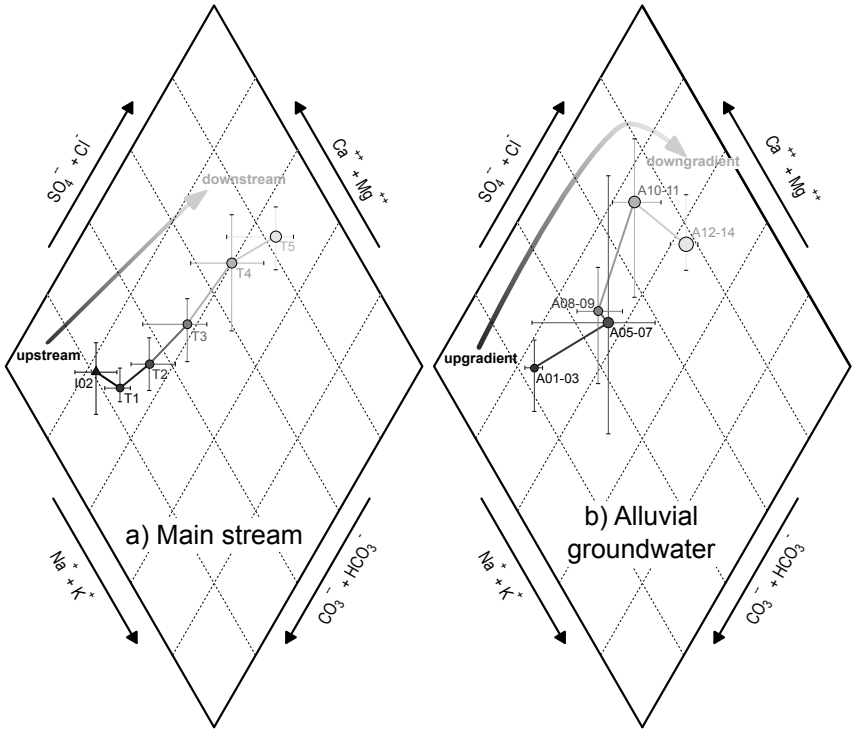

Figure 5.9: Piper diagrams of the evolution in major ion composition for the main stream (a) and alluvial groundwater (b). Values for the main stream correspond to the median values calculated from 18 samples collected at each location over the entire monitoring period, and whiskers correspond to minima and maxima. Values for the alluvium correspond to the median values calculated for each of the five cross sections (Figure 5.1), and whiskers correspond to minima and maxima. Note that A04 was excluded from the analysis of the second cross-section, because it was considered as an outlier.

5.5.2 Implications for recharge and inter-aquifer connectivity

5.5.2.1 Distinguishing between different recharge contributions to the stream–alluvial system

Major ion chemistry and its spatial evolution along the main drainage system were assessed for both alluvial waters and surface waters (Figure 5.9). In the surface waters (Figure 5.9a), there was a gradual evolution from Ca–Mg–HCO_3 waters in the headwaters to Ca–Na–Cl waters at the outlet of the catchment. Waters in the alluvium (Figure 5.9b) also became gradually Cl dominated and HCO_3 depleted along the alluvial flowpath, with higher dispersion in the data. The residual alkalinity (r) and CCR index values also followed similar evolutionary trends in the main stream and alluvial waters (Figure 5.7). The co-evolution in hydrochemical composition of both stream and alluvial waters suggests close interactions between the two components, or similar water sources and/or processes. According to the

examination of hydraulic gradients, the alluvial aquifer waters drained into the river at all five cross-sections, highlighting a strong stream–alluvium connection.

Waters draining the Main Range Volcanics (I01 and I02) were dominated by Ca and Mg (Appendix A.1), with r values close to zero and low Cl content (Figure 5.7a). Both the alluvial (A01 to A03) and stream waters (T1 and T2) collected in the upstream part of the catchment also had a Ca–Mg–HCO_3 signature and low to very low r values. This similarity in water facies suggests the occurrence of hydraulic connections between the fractured igneous rocks and the stream–alluvium system in its upstream part, i.e. mountain front recharge to the lowland shallow aquifer. Further downstream, the decrease in r concomitant to a gradual increase in Na and Cl in the stream–alluvium system is consistent with downstream addition of direct (diffuse) recharge waters that have undergone evapotranspiration before reaching the saturated zone. Slightly higher Sr ratios in the alluvial waters as compared to bedrock waters (Appendix A.3) might also reflect the stronger relative influence of Sr derived from rainfall through diffuse recharge in the alluvium. Alternatively, some authors have argued that the downstream salinisation of alluvial waters could be a result of the enhanced contribution of bedrock waters to the stream–alluvium system (Li and Cox, 1996), although this disregards the HCO_3 component generally present in the bedrock waters.

5.5.2.2 Influence of a major recharge event on bedrock and alluvial aquifers

According to fortnightly monitoring of stable isotopes in rainfall, d-excess was affected by important event-to-event variations throughout the study period (Figure 5.10). There was a sharp decrease in rainfall d-excess as a result of the January 2013 storm, with values dropping from +13.7 to +8.3‰ at R1 and from +14.7 to +8.8‰ at R2. The following samples rapidly returned to pre-flood levels, i.e. between +13 and +18‰ (Figure 5.10b). Of interest are the groundwater level dynamics recorded in alluvial boreholes A01 and A08 (Figure 5.10c). Series were normalised using standard scores, and data indicate that the dry sampling round was conducted under low depth conditions, while the wet sampling round was conducted after recently recharged waters had reached the water table. We therefore hypothesised that the January 2013 rainfall event had a pronounced influence on the general aquifer recharge dynamics in the catchment that potentially overwhelmed the effects of evaporation. The relatively depleted d-excess values that occurred during that rainfall event were considered a proxy for recently recharged waters that did not undergo further evaporation. This assumption is supported by the slight depletion in d-excess observed at A01 and A08 after the January 2013 storm (Figure 5.10d), although this depletion was attenuated relative to the depletion in rainfall d-excess. Note that the drop in d-excess occurred one month later at A08, which might be an indication of a lagged response time to recharge in A08 relative to A01.

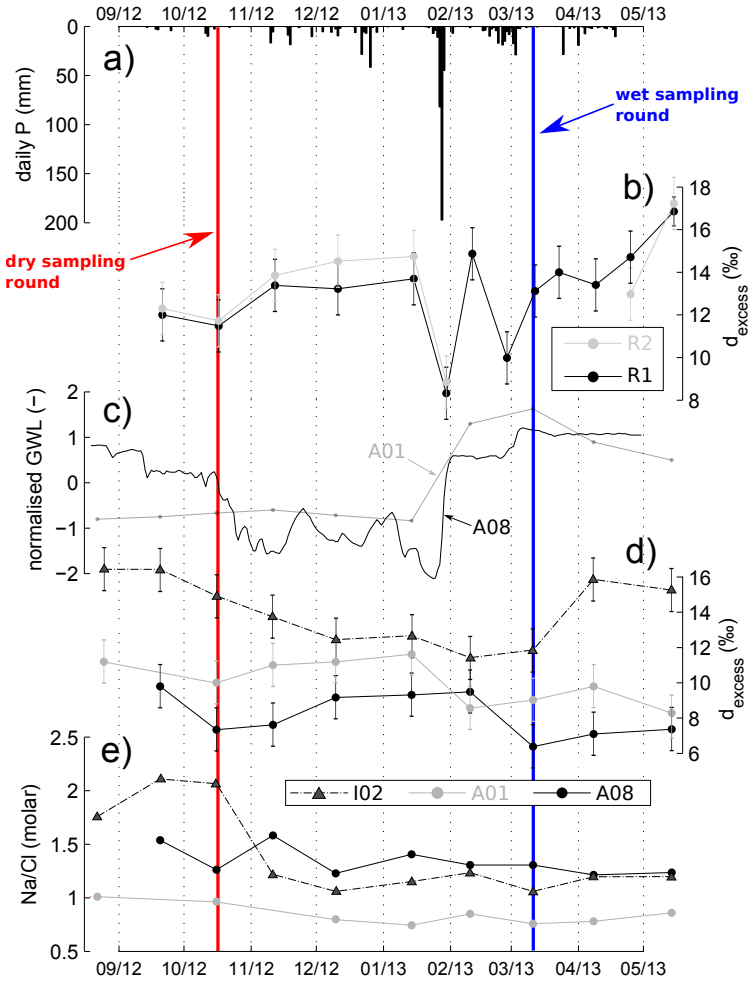

Figure 5.10: Seasonal evolution of (a) Thiessen-averaged precipitation, (b) deuterium excess in precipitation for the two rainfall collectors, (c) normalised groundwater levels at A01 and A08, (d) deuterium excess at I02, A01 and A08, and (e) Na/Cl ratios at I02, A01 and A08. Absolute error range for deuterium excess was calculated as $u_d = \sqrt{(u_{\delta^2\mathrm{H}})^2 + 8\,(u_{\delta^{18}\mathrm{O}})^2}$ with $u_{\delta^2\mathrm{H}} = \pm 1.1‰$ and $u_{\delta^{18}\mathrm{O}} = \pm 0.3‰$, which yielded $u_d = \pm 1.39‰$.

For a majority of locations, the variation in *d*-excess between the two sampling rounds was substantial (Figure 5.11). Five of the bedrock boreholes (B01, B02, B05, B07 and B11) with highly enriched initial *d*-excess values (+12.0‰ < *d*-excess < +17.7‰) underwent a significant decrease during the wet season towards values (+9.0‰ < *d*-excess < +13.0‰) comparable to the ones recorded in rainfall for the major recharge event (represented by the grey shaded area in Figure 5.11). Three of the alluvial boreholes (A09, A10 and A11) with more depleted dry season *d*-excess values (+3.9‰ < *d*-excess < +6.2‰) showed an increase during the wet season towards values comparable to the ones of the major recharge event (+6.9‰ < *d*-excess < +9.1‰). All the bores identified by blue shaded areas were very likely directly influenced by the isotopic signature of the January recharge waters. Of significance is the location of four of the bedrock boreholes falling within this category, either in close proximity to igneous intrusions (B01, B02 and B05) or proximal to the catchment

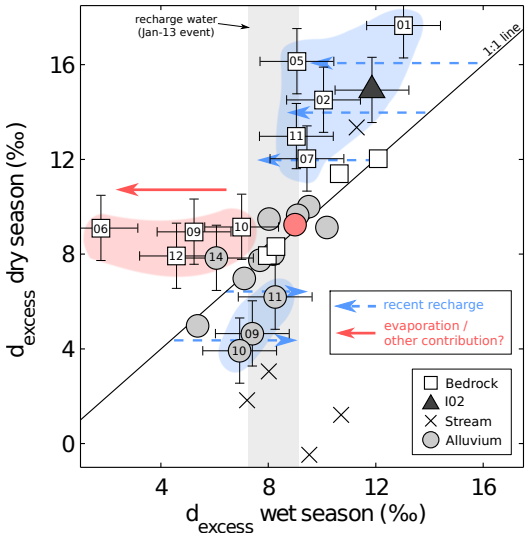

Figure 5.11: Relationship between dry and wet season deuterium excess values for each studied borehole. The grey shaded area corresponds to the deuterium excess signature for the late January rainfall event. The red circle corresponds to A04, while B14 was discarded of this figure. Whiskers are for absolute uncertainties on deuterium excess calculations; they are shown only for the samples for which a significant seasonal difference was recorded. The error range was calculated as in Figure 5.10.

edges (B07) (Figure 5.1). The same four boreholes had high d-excess values and Na/Cl ratios similar to rainwater (Figure 5.6). For these waters, the effect of evaporation during recharge was overall very limited. This lends further support to our assumption that recharge of the bedrock predominantly occurred via preferential pathways through the fractured intrusions, facilitating rapid recharge with less potential for evaporative fractionation than diffuse recharge through soils. The two boreholes located closest to the headwaters (B01 and B02) also had high ^{3}H values coupled with low "igneous-like" δ^{13}C-DIC ratios, which confirms that recently recharged waters contributed to the bedrock at these locations.

Contrastingly, the d-excess values in four bedrock boreholes (B06, B09, B10 and B12) and one alluvial borehole (A14) were not affected by direct recharge processes, as they evolved towards more depleted values after the January flood in the range $+1.8‰ < d\text{-excess} < +6.0‰$ (Figure 5.11). Other processes such as enhanced evaporation before recharge and/or mixing with more evaporated waters might have occurred in those mostly low-lying bores (identified as red shaded area in Figure 5.11). Seven alluvial boreholes and four bedrock boreholes plotted on the 1:1 line (including A04), suggesting that no significant change in water source or recharge process has occurred at these locations. Despite the potential effects of evaporation on d-excess temporal variations, this parameter showed potential as a tracer of transient recharge processes in both the alluvial and bedrock aquifers. Our results can be compared to earlier work by Lee et al. (1999) who, after acknowledging that summer and winter precipitation had very distinct d-excess signatures, used the values measured in groundwater samples of a Korean island to quantify the relative contributions of

summer and winter rainfall to recharge. Likewise, Leybourne et al. (2006) assumed that the similitude between the d-excess measured in winter precipitation and the d-excess derived from groundwater in a shallow aquifer of Canada is a reflection of the predominance of winter rainfall to recharge.

5.5.2.3 Inter-aquifer mixing induced by transient recharge processes

The pre- and post-flood changes in Na/Cl were relevant to this study because they can provide insight into inter-aquifer interactions that may be further accelerated during recharge. The percent seasonal variations (i.e. normalised gains and losses) in Na/Cl ratios and Cl/HCO_3 ratios were calculated for all repeated samples (Figure 5.12). Only five alluvial boreholes, all located in the downstream section of the catchment (A09, A10, A12, A13 and A14), and two bedrock boreholes (B10 and B12), plotted close to the origin of the plot, indicating that there was no apparent effect of recharge on these groundwaters. This is in agreement with Figure 5.11, which showed that isotopic variations in the two bedrock groundwaters were unrelated to the signature of recharge waters. Five alluvial boreholes (A01, A02, A07, A08 and A11) had significantly lower Na/Cl ratios during the wet season (normalised loss between –13% and –29%). As this change was not related to a significant shift in the chloride/alkalinity ratio, it may be the result of simple mixing with Ca-rich recently recharged waters. Values for most streamwater samples and one bedrock groundwater (B04) showed a decrease in the chloride/alkalinity ratio together with a consistent Na/Cl ratio. This was also interpreted as dilution by Ca–Mg–HCO_3 recharge waters (black arrows in Figure 5.12).

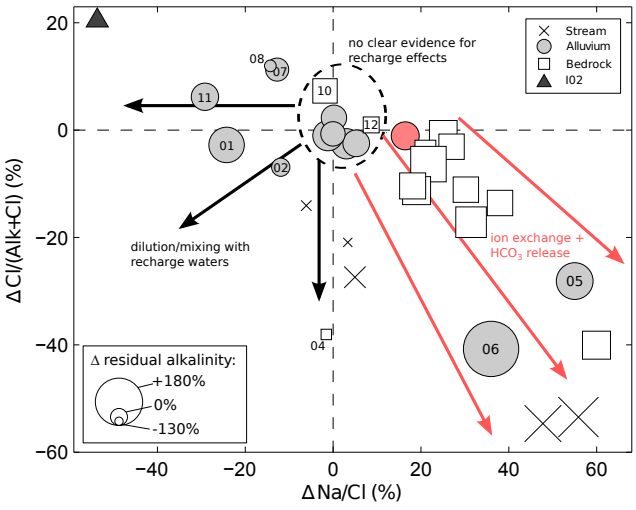

Figure 5.12: Seasonal percent variations in chloride/alkalinity ratios versus seasonal percent variations in molar Na/Cl ratios for all repeated samples. The marker size reflects the seasonal percent variations in residual alkalinity (small markers: seasonal decrease in r; large markers: seasonal increase in r). The red circle is for A04, and B14 was not included. A positive change reflects an increase from dry to wet seasons. The pattern identified with red arrows only applies to groundwater; for streamwater the driving process was rather different water contributions.

More importantly, all but three bedrock boreholes followed a consistent trend with increasingly positive Na/Cl variations and increasingly negative chloride/alkalinity variations (red arrows in Figure 5.12). This trend was coherent with increasingly positive r values from dry to wet periods. The described changes most probably reflect enhanced silicate weathering by recharge waters, but it may also be related to enhanced ion exchange following the addition of recharge waters that became enriched in Ca during earlier flow through calcite-rich igneous fractures. These processes have been previously described as the hydrochemical processes typically occurring in the bedrock aquifer (Section 5.5.1); our findings suggest that the addition of large quantities of recharge waters contributed to boosting these mechanisms. Interestingly, three alluvial boreholes followed the same trend as the one described for bedrock waters, one of them A04 (red circle) and the other two A05 and A06. Concomitant to the evolution at A05 and A06 was a substantial enrichment in δ^{13}C-DIC from –9.1‰ to –1.9‰ at A05, and from –7.7‰ to –5.1‰ at A06 (Appendix A.3). This seasonal shift in both hydrochemistry and carbon isotopic ratios might be an indication of transient mixing with HCO_3-rich, methanogenic waters such as the ones found in the Walloon Coal Measures.

To our knowledge, there are few reports in the literature that describe the use of temporal variations in ionic ratios to infer on potential inter-aquifer mixing. A study of a multi-layered aquifer in southern India examined the seasonal changes in Ca/Mg and Mg/K, and identified transient mixing between different aquifers that was related to the intensity of monsoon recharge (Gassama et al., 2012). Although further research will need to better constrain the temporal variations and processes behind them, our approach may be valuable in delineating the areas where seepage of coal-bearing aquifers into alluvial waters occurs following recharge events.

5.5.2.4 Using multiple tracers to assess alluvium–bedrock connectivity

Generally, alluvial waters in the downstream section of the catchment had higher TDS values and with enriched Na composition, yet slightly positive CCR values (boreholes A10 to A14; Appendix A.1 and Figure 5.7b). Li and Cox (1996) observed similar increases in TDS for downstream alluvial waters and proposed that it was the result of discharge of brackish bedrock waters to the alluvium. Other authors in other catchments nearby have also proposed that alluvial salinisation could be influenced by interactions with the bedrock (Huxley, 1982; Dafny and Silburn, 2014). Yet, while a few bedrock groundwaters in the downstream areas were brackish (B11, B13) and were proximal to the brackish alluvial waters, evapotranspiration is also a typical salinisation process in alluvial aquifers (e.g. Cartwright and Weaver, 2005; King et al., 2014).

All alluvial waters maintained low to very low r values and positive CCR (Figure 5.7), which suggests that evapotranspiration was dominant in the alluvium. However, if brackish

bedrock waters with positive r and negative CCR index were discharging to the alluvium, the combination of bedrock-derived HCO_3 and positive CCR of alluvial waters would facilitate carbonate precipitation, hence masking increases in r. It is therefore difficult to determine if the increase in TDS in the downstream areas was driven by inter-aquifer mixing using r and CCR alone (Table 5.1). Furthermore, the composition of bedrock waters was highly variable due to aquifer heterogeneity, and the similar hydrochemical composition observed between some bedrock waters and alluvial waters (Figure 5.7) further limits the ability to describe mixing based on r and CCR alone.

The analysis of d-excess revealed that most alluvial groundwaters located downstream mimicked the d-excess signature of bedrock waters, i.e. relatively high d-excess in the range $+3.9‰ < d\text{-excess} < +9.5‰$ and medium to high TDS for boreholes A10 to A14 (Figures 5.6 and 5.11). This might be again an indication of seepage from the coal-bearing aquifer into the downstream part of the alluvial aquifer. However, significant overlap between and within the two systems limits the applicability of d-excess as a definitive tracer of inter-aquifer connectivity (Table 5.1). Tritium tended to provide further evidence for an increased influence of the bedrock water type to the downstream section of the alluvium, because the alluvial waters were generally older than further upstream (Figure 5.5). In the bedrock, older (low ^3H) groundwaters also coincided with enriched $\delta^{13}C$-DIC values, and in the alluvium a similar trend of increasing ^{13}C and decreasing ^3H in a downstream direction (boreholes A09 to A14 excluding A11) was observed, particularly in the wet season (Figure 5.8a and Appendix A.3). This potential influence of the bedrock on the alluvial aquifer may reflect flushing of the bedrock waters to the alluvium during recharge periods. Noticeably, the examination of percent variations in Na/Cl and Cl/HCO_3 ratios did not confirm inter-aquifer mixing following the January recharge event in these downstream alluvial boreholes (Figure 5.12).

Overall, interactions between the alluvium and the groundwaters contained in the Walloon Coal Measures were difficult to isolate, although they could be inferred in the downstream section of the catchment. Importantly, salinisation was not an obvious or useful indicator of this interaction (Table 5.1). Despite a combined multi-isotope and hydrochemical approach, the delineation of mixing between bedrock and alluvial waters remains speculative in the current state of research. This underlines the need to conduct further studies that test other tracers, such as dissolved methane and rare earth elements, which might provide additional insight into inter-aquifer mixing.

5.6 Conclusions

The combination of major ion hydrochemistry and isotopic tracers, used in conjunction with a repeated sampling strategy, allowed a better understanding of groundwater flow-

Table 5.1: Summary of the value of each tracer for the assessment of hydrochemical processes and the delineation of alluvium–bedrock connectivity.

Tracer	**Standard notation (unit)**	**Distinguishing between distinct evolutionary pathways**	**Delineating alluvium–bedrock interactions**
Total dissolved solids	TDS (mg/L)	In combination with other major ions, TDS may help identify specific processes; however, TDS on its own was a poor proxy for within-aquifer processes.	TDS was a poor proxy for aquifer interactions. Increases in TDS may relate to within- or between-aquifer processes and may show seasonal variation.
Sodium-chloride ratio	Na/Cl (–)	The Na/Cl ratio had some value for identifiying salinisation processes within aquifers, but needed to be used in combination with other tracers.	Consistent Na/Cl ratios in adjacent aquifers may suggest connectivity, but combinations of other tracers were needed to reach this conclusion.
Cation chloride ratio	CCR (–)	The CCR index, when compared with alkalinity/Cl ratios, was useful in conceptualising processes that influence all major ions within aquifers.	The CCR index had some value in identifying potential aquifer interactions; however, it had to be combined with isotopic tracers to provide some confidence in interpretations.
Residual alkalinity	r (meq/L)	Residual alkalinity was useful in distinguishing between the potential influence of coal degradation and other processes where HCO_3 ions are reduced (e.g. carbonate precipitation).	The use of r for investigating aquifer interaction was complicated because the saturation index of carbonates may differ between aquifers, thus masking r.
Stable isotopes of water	d-excess (‰)	d-excess has some value for delineating between different evapotranspiration processes, particularly when combined with ionic ratios.	Repeated sampling for d-excess was highly beneficial when investigating aquifer interactions, and highlighted some unexpected seasonal changes related to recharge events.
Carbon-13 in dissolved inorganic carbon	δ^{13}C-DIC (‰)	δ^{13}C-DIC and ^{3}H were particularly useful for distinguishing between different processes within the coal-bearing bedrock aquifer.	The combinations of δ^{13}C-DIC and ^{3}H allowed aquifer interactions to be inferred with a higher degree of confidence than using other tracers alone.
Tritium	^{3}H (TU)		

paths, geochemical processes and recharge patterns in the Teviot Brook catchment, South-east Queensland (Australia). A number of intra and inter-aquifer processes were identified, including: (i) strong connection between the main stream and its underlying alluvial aquifer; (ii) different evolutionary pathways in the coal-bearing bedrock aquifer, with considerable spatial variability; (iii) rapid recharge of the bedrock aquifer through the highly fractured igneous intrusive and extrusive rocks; (iv) potential interactions between the bedrock and the alluvial aquifers in its downstream section; and (v) enhanced weathering triggered by recharge waters in the bedrock aquifer and in some areas of the alluvial aquifer.

Ionic ratios such as the cation chloride index and residual alkalinity proved useful in distinguishing between processes leading to salinisation, although individual processes were not unique to specific aquifers and heterogeneity of the coal-bearing bedrock led to highly variable hydrochemistry. As a result, these tracers could not provide definitive assessments of inter-aquifer connectivity. Tritium, carbon and strontium isotopes provided insights into the evolutionary pathways of the bedrock waters, with older waters having lower $^{87}Sr/^{86}Sr$ ratios and relatively enriched δ^{13}C-DIC, which was interpreted as a result of potential interactions with coal seams. Deuterium excess was valuable in revealing that the bedrock waters were less affected by evaporation than the stream–alluvial system. These results led us to hypothesise that recharge of the sedimentary bedrock aquifer predominantly occurred through the fractured intrusive and extrusive igneous rocks. The examination of seasonal variations in d-excess and ionic ratios also assisted in documenting the effects of recharge on both the alluvial and bedrock aquifers.

Overall, this study demonstrates that the hydrogeology in shallow alluvial and bedrock systems is dynamic, and may exhibit variability between distinct wet and dry periods. This suggests that seasonality is an important consideration when studying inter-aquifer interactions in shallow systems, particularly where mixing with CSG aquifers is investigated; an issue that has been largely overlooked in the recent literature. Results also demonstrate that simple ionic ratios used concurrently with isotopic tracers have potential to better constrain flowpaths and possibly identify interactions with shallow coal-bearing aquifers. However, this study also illustrates the limitations of using conventional tracers to delineate inter-aquifer mixing, mostly because of the considerable heterogeneity observed in the coal-bearing aquifers and complex recharge processes. In these cases, other innovative tracers need to be tested in order to confirm inter-aquifer interactions in CSG environments.

Acknowledgments

Thanks are due to the Department of Natural Resources and Mines (Queensland) for access to the government borehole network, and to landowners for giving access to sampling sites. S. Russel, J. Brady, A. Bargav, R. Chisari and S. Hu are acknowledged for assistance with laboratory work. We also wish to thank N. Briant, A. King, J. Martinez, J. Pourrier, É. Resongles and M. Taulis for helpful discussions. The Australian Institute of Nuclear Science and Engineering is acknowledged for funding the tritium analyses

(research grant ALNGRA14026). This work was greatly improved by the thoughtful review of I. Cartwright, Associate Editor, and the comments of an anonymous reviewer. The first author is receiving an Endeavour Scholarship from the Australian Commonwealth Government.

CHAPTER 6

Linking Seasonal & Spatial Variations in Rare Earth Elements with Inter-Aquifer Processes

This chapter has been published as:

C. Duvert, D.I. Cendón, M. Raiber, J.-L. Seidel, M.E. Cox, 2015. Seasonal and spatial variations in rare earth elements to identify inter-aquifer linkages and recharge processes in an Australian catchment. **Chemical Geology** 396, 83–97. doi:10.1016/j.chemgeo.2014.12.022

Abstract

With the aim of elucidating the seasonal behaviour of rare earth elements (REEs), surface and groundwaters were collected under dry and wet conditions in different hydrological units of the Teviot Brook catchment (Southeast Queensland, Australia). Sampled waters showed a large degree of variability in both REE abundance and normalised patterns. Overall REE abundance ranged over nearly three orders of magnitude, and was consistently lower in the sedimentary bedrock aquifer (18 ppt $< \sum$REE $<$ 477 ppt) than in the other hydrological systems studied. Abundance was greater in springs draining rhyolitic rocks ($\sum$REE = 300 and 2054 ppt) than in springs draining basalt ranges ($\sum$REE = 25 and 83 ppt), yet was highly variable in the shallow alluvial groundwater (16 ppt $< \sum$REE $<$ 5294 ppt) and, to a lesser extent, in streamwater (85 ppt $< \sum$REE $<$ 2198 ppt). Generally, waters that interacted with different rock types had different REE patterns. In order to obtain an unbiased characterisation of REE patterns, the ratios between light and middle REEs ($R_{(M/L)}$) and the ratios between middle and heavy REEs ($R_{(H/M)}$) were calculated for each sample. The sedimentary bedrock aquifer waters had highly evolved patterns depleted in light REEs and enriched in middle and heavy REEs ($0.17 < R_{(M/L)} < 1.00$ and $-0.16 < R_{(H/M)} < 0.93$), whereas the springs draining intrusive and extrusive rocks had relatively flat patterns ($0.20 < R_{(M/L)} < 0.38$ and $-0.16 < R_{(H/M)} < 0.09$). Surface waters were generally enriched in middle REEs (median $R_{(M/L)} = 0.35$ and median $R_{(H/M)} = -0.04$), and waters from the shallow alluvial aquifer had very diverse patterns with important spatial variations. Samples collected from the alluvium exhibited an increasing influence of the sedimentary bedrock from upgradient to downgradient; typically they showed flat patterns in the upstream section of the alluvium (median $R_{(M/L)} = 0.21$ and median $R_{(H/M)} = 0.06$) gradually evolving towards patterns depleted in light REEs and enriched in middle and heavy REEs downgradient (median $R_{(M/L)} = 0.48$ and median $R_{(H/M)} = 0.38$). To document the seasonal variations in REE patterns, the difference in ratios between dry and wet sampling campaigns was determined for each repeated sampling location. Contributions from the sedimentary bedrock water to the alluvium during the wet season were identified at two locations (increase from $R_{(H/M)} = 0.03$ and 0.35 to $R_{(H/M)} = 0.62$ and 0.89). The effect of recharge through fractured igneous rocks was also observed in two boreholes intercepting the sedimentary bedrock, where the freshly recharged waters likely contributed to the deeper groundwater flow during the wet season (decrease from $R_{(M/L)} = 0.81$ and 0.56 to $R_{(M/L)} = 0.46$ and 0.17). Results from this study suggest that REEs may be usefully applied as indicators of recharge processes and inter-aquifer mixing. They also underline the importance of conducting seasonal sampling campaigns to capture possible short-term variations in REE patterns and abundance, which is essential to enable a better understanding of hydrological and hydrochemical processes in complex geological settings.

6.1 Introduction

Rare earth elements (REEs) form a group of 14 trace metals with gradually increasing atomic number that behave coherently and predictably (Henderson, 1984). Because of their potential use as tracers of groundwater origin and mixing processes, these elements have received much attention over the last several decades (Smedley, 1991; Johannesson et al., 1997; Dia et al., 2000; Gruau et al., 2004; Willis and Johannesson, 2011; Noack et al., 2014). REEs have been successful in describing processes that are not revealed when using conventional hydrochemical methods such as major ions and stable isotopes (Tweed et al., 2006). Where there is contrasting geology, and so contrasting mineralogy, REEs can be useful fingerprints of host aquifers or catchment geology (Playà et al., 2007). However, there is still some debate as to whether REE concentrations and their shale-normalised patterns represent the water-rock interactions occurring at a recent stage, i.e. reflecting host rock conditions (Johannesson et al., 1997; Tang and Johannesson, 2006; Göb et al., 2013), or at an earlier stage, i.e. reflecting recharge conditions (Möller et al., 2006; Tweed et al., 2006; Willis and Johannesson, 2011). This controversy stems from the considerable number of factors controlling REE concentrations and patterns in groundwater. Processes such as sorption, colloidal organic matter-mediated complexation and co-precipitation have been shown to occur after the dissolution of REEs from rocks following changes in pH and/or redox conditions (Johannesson et al., 1997, 2000; Biddau et al., 2002; Pourret et al., 2007). Preferential adsorption of light REEs relative to heavy REEs has also been observed (e.g. Johannesson et al., 2000; Leybourne et al., 2000; Tweed et al., 2006). Overall, the factors influencing geochemical reactions and thus REE fractionation patterns in aquifers are still not fully understood.

While spatial variations of REEs have been studied extensively and in a variety of aquifer systems (e.g. Biddau et al., 2009; Guo et al., 2010; Hagedorn et al., 2011; Siebert et al., 2012; Göb et al., 2013), the assessment of seasonal variations of REEs in groundwater systems is still lacking in the literature. Acquisition of temporally discretised data is important because single samples may not reflect the usual state of a system due to temporarily unusual conditions (e.g. Shiller, 1997). More importantly, capturing seasonal variations in REEs appears essential to appreciate the possible linkages between different aquifers as well as possible variations in driving mechanisms. Due to the ease of surface water sampling, several authors have reported on the temporal variability of REEs in rivers (Ingri et al., 2000; Shiller, 2002; Bagard et al., 2011; Möller et al., 2014). All such studies showed that fluctuations in REE concentrations and patterns could be substantial over time. In groundwater studies, however, temporal variability has been poorly examined so far: Olivié-Lauquet et al. (2001), followed by Gruau et al. (2004) and Pourret et al. (2010), investigated the temporal evolution of REE concentrations and patterns in the shallow groundwaters of wetland areas in Brittany, France. Pourret et al. (2010) showed that patterns were remarkably stable

over their 7-yr sampling record, whereas Gruau et al. (2004) described pronounced seasonal variations in absolute REE concentrations. Similarly, Poh and Gasparon (2011) found that REEs responded rapidly to recharge in boreholes intercepting a wetland aquifer of Southeast Queensland, Australia. In a deeper aquifer setting, Möller et al. (2006) reported substantial seasonal variations in the REE patterns from two bores drilled in a limestone aquifer system in Jordan; the authors concluded on inter-aquifer linkages with an underlying sandstone unit. Overall, little is known about the temporal variability of REEs in groundwater, and this particularly applies to mountainous areas where systems can be highly responsive to seasonal changes. There is, therefore, a need not only to document the spatiotemporal variability of REEs in groundwater bodies, but also to test their effectiveness as an indicator of inter-aquifer linkages as well as recharge processes. No such research has been undertaken to assess the impact of recharge on groundwater REE patterns.

In this study, we investigate the geochemical behaviour of REEs within a catchment located in Southeast Queensland, Australia (Figure 6.1). The Teviot Brook catchment has been selected because it comprises a number of aquifers from a range of geological formations, which provide an ideal setting in which to explore inter-aquifer interactions. A Jurassic sedimentary formation forms the bedrock underlying much of the Quaternary alluvium, and recharge is expected to occur mainly through numerous Cenozoic intrusive and extrusive rocks scattered throughout the catchment. In some parts of the catchment, the sedimentary bedrock is in direct contact with the drainage network, and linkages between different aquifers and the river system can be anticipated. Here we test the hypothesis that REEs can be a valuable tracer of the spatial and temporal changes taking place within hydrological units and, consequently, of the linkages between streams and shallow and deeper aquifers. The detailed objectives of this study are (i) to define the REE concentrations and patterns for each hydrological unit (i.e. drainage system, igneous 'recharge' water, shallow alluvial groundwater, and deeper sedimentary bedrock aquifer), (ii) to explore the spatial and seasonal variability of REE signatures, and (iii) to use our findings to assess the usefulness of REEs as tracers of the linkages between aquifers and recharge processes.

6.2 Geologic and geochemical setting

Teviot Brook is a tributary of the Logan River, to the southwest of Brisbane (Australia). Precipitation and discharge data in the catchment indicate a pronounced seasonality. Intense rainfall triggering elevated flows occurs in summer from December through April, and this is followed by a much drier period from May to November. The Teviot Brook catchment forms part of the Clarence–Moreton Basin (CMB), a large sedimentary basin that covers the southeast region of Queensland and northeastern New South Wales (Figure 6.1). The CMB contains fluvial sedimentary deposits of Triassic, Jurassic and Cretaceous age, which form interbedded sequences of aquifers and aquitards. In the study catchment, a Jurassic

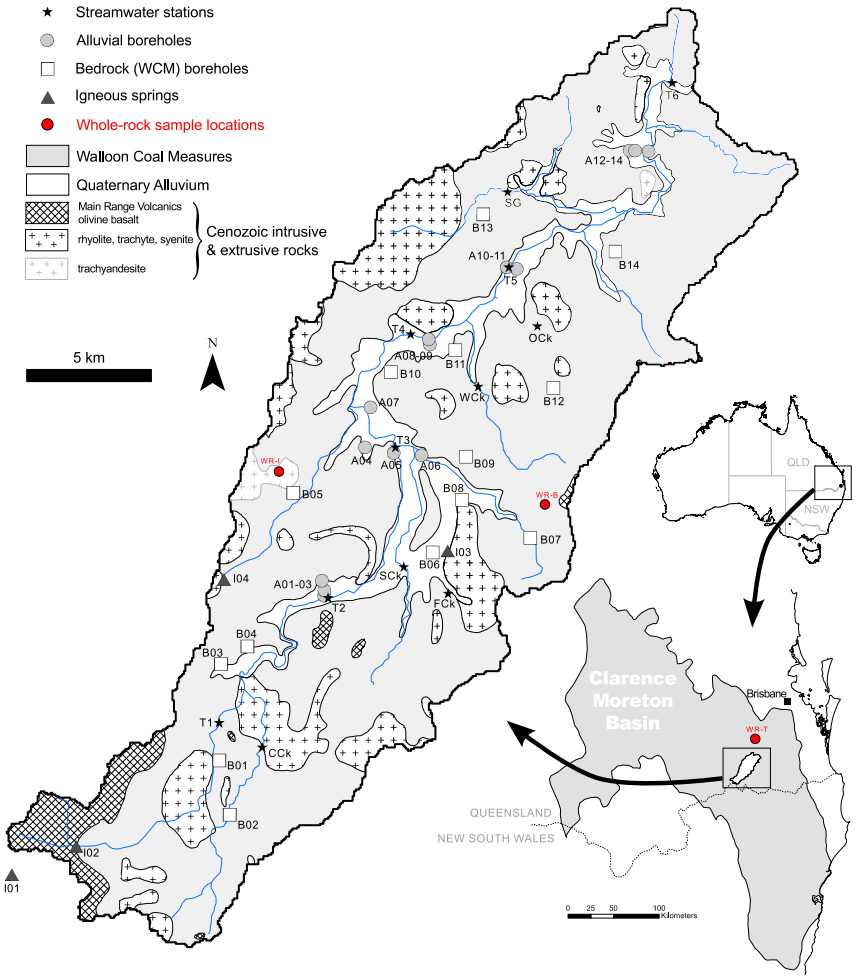

Figure 6.1: Location of the Teviot Brook catchment within the Clarence-Moreton Basin. Geology of the catchment and location of boreholes, springs and surface water samples. Samples were arranged in increasing order from upstream towards downstream for each hydrological component. 'B' is for WCM boreholes, 'A' is for alluvial boreholes, 'I' is for igneous springs, 'T' is for the samples collected from the main stream, and 'WR' is for the whole-rock sample locations (WR-I and WR-T are from Ewart et al., 1985). The geological map is provided by the Geological Survey of Queensland (South-East Queensland GIS, Version 2, 2002).

sedimentary sequence named the Walloon Coal Measures (WCM) forms the bedrock for much of the catchment and outcrops largely along its edges. The WCM consist of non-continuous beds of sandstone, siltstone, claystone, carbonaceous shale and coal (Wells and O'Brien, 1994), and have a thickness of around 120–240 m in the Teviot Brook catchment (Rassam et al., 2014). In the catchment headwaters, a Cenozoic lava flow sequence that is part of the Main Range Volcanics (MRV) extends over around 9 km^2. This is an almost exclusively mafic formation dominated by mildly alkaline basalt and hawaiite (Stevens et al., 1989; Cohen, 2012). Associated with this volcanic sequence are several intrusions of predominantly felsic composition (i.e. mainly rhyolite), which produce local plugs and dykes, and in places cap the lateral ranges of the catchment. Lastly, the Quaternary alluvium composed of weathered catchment materials overlies the WCM, which typically contains a

basal sandy gravel layer overlain by a thicker layer of firm blue clay. The alluvium has a thickness ranging between 5 m upstream and over 20 m in the central sections and lowlands; there is no significant variability in the alluvium lithology from upstream to downstream.

The alluvial aquifer supports intensive irrigated agriculture. The WCM also provide supplies of groundwater that is commonly brackish, and is typically used for livestock watering. Groundwater of elevated salinity has also been observed in sections of the alluvium as well as in the stream (Li and Cox, 1996), indicating that the different geological layers are likely to be hydraulically connected. It is assumed that most of the recharge of aquifers occurs as mountain front recharge through the highly fractured igneous rocks outcropping in the headwaters and along the lateral ranges.

In a recent study, Duvert et al. (2015a) used major ion and isotope hydrochemistry to interpret the hydrochemical processes within each hydrological unit of the Teviot Brook catchment. They demonstrated that alluvial groundwater and streamwater had a Ca–Mg–HCO_3 facies in the upstream section of the catchment, predominantly obtained through the weathering of silicates and carbonates. Silicates were mainly derived from the mafic rocks present in the headwaters, whereas carbonates were available as secondary minerals recrystallised in veins and fissures of the basalts. Weathering mechanisms were followed by gradual salinisation from upstream to downstream as a result of the influence of evapotranspiration in the unsaturated zone prior to recharge. In contrast, waters contained in the WCM were classified as Na–HCO_3–Cl type waters influenced by three concurrent processes, i.e. (i) evapotranspiration, (ii) the leaching from albite and Na-rich clay minerals of the WCM, and (iii) the anaerobic decomposition of organic matter (i.e. methanogenesis).

Environmental isotope data showed substantial seasonal variations even in WCM waters, highlighting the significance of temporal changes in the groundwater systems of this area. Due to a comparable signature and a similar longitudinal evolution, Duvert et al. (2015a) also inferred the occurrence of a strong connectivity between the alluvial groundwater and the drainage network. However, conventional hydrochemical methods were not sufficient to clearly conclude on a linkage between the shallow alluvial aquifer and deeper WCM groundwater.

6.3 Methods

6.3.1 Sample collection

To explore the spatial variability of the system and the contrasts between different end-members, a total of 63 samples were collected from 44 surface, spring and groundwater locations throughout the catchment (Figure 6.1). Twelve streamwater sampling locations were selected along the main stream and in tributaries where direct seepage from the WCM

Table 6.1: Number of samples collected from different hydrological units of the Teviot Brook catchment.

Sampling round	Streamwater	Alluvial groundwater	WCM groundwater	Igneous groundwater
Oct-2012 (dry)	9	9	6	2
Mar-2013 (wet)	7 (4)	13 (8)	14 (6)	3 (1)

The figures in parentheses correspond to the number of repeated samples.

was expected due to elevated levels of salinity. Four springs draining either the volcanic rocks located in the headwaters or the lateral felsic intrusions were sampled as well (referred to as 'igneous groundwater'). In addition, 14 boreholes intercepting the shallow alluvial aquifer and 14 boreholes intercepting the WCM aquifer were accessed (Figure 6.1). The alluvial boreholes used for this study are monitoring bores from the Queensland Department of Natural Resources and Mines (DNRM), and all of them are screened into the coarse basal layer of the alluvium. One alluvial borehole (A04) also intercepts the top of the WCM formation. The WCM boreholes are exclusively private infrastructure, which are constructed to maximise water yield, i.e. with long screen intervals. However all those bores intercept the WCM geological unit only.

To explore the seasonal variability of the catchment waters, samples were collected during two different periods: sampling round 1 was conducted in late October 2012 during a drought that occurred from June to December 2012. Data from sampling round 1 are referred to as 'dry' in the subsequent sections. Sampling round 2 was carried out in March 2013 after significant flooding of the Teviot Brook that occurred in late January 2013. Data from sampling round 2 are referred to as 'wet' in the subsequent sections. In total, four streamwater locations, eight alluvial boreholes, six WCM boreholes and one igneous spring were sampled during both dry and wet conditions (Table 6.1), hence allowing an assessment of the seasonal variations in REE data.

Groundwater samples were collected using a submersible pump (Stainless Steel Hurricane XL, Proactive). Before sampling, all boreholes were purged at least three well volumes, and sampling was conducted after pH, temperature and electrical conductivity had stabilised. All samples were filtered in the field through 0.2 µm in-line filters and collected in HDPE bottles that had been thoroughly acid-washed in the laboratory prior to collection. Collected samples were acidified to 0.6% with ultrapure nitric acid (RCI Labscan Limited) within 48 h of collection in a clean laboratory setting, and stored refrigerated until they were analysed.

6.3.2 Analytical procedure

In order to obtain an approximation of the range of REE concentrations to be expected in the catchment, all samples were first analysed at the Queensland University of Technol-

ogy, Brisbane ('lab 1' in Figure 6.2). They were diluted two to three times prior to analysis with an inductively coupled plasma mass spectrometer (ICP-MS; 8800 Triple Quadrupole, Agilent). The isotopes selected for analysis were ^{139}La, ^{140}Ce, ^{141}Pr, ^{146}Nd, ^{147}Sm, ^{153}Eu, ^{157}Gd, ^{159}Tb, ^{163}Dy, ^{165}Ho, ^{166}Er, ^{169}Tm, ^{172}Yb and ^{175}Lu. Internal standard (Be, Rh, In, Bi) was added to each aliquot for drift correction. To verify the accuracy of measurements, digested USGS reference materials W-2, BIR-1 and AGV-2 were analysed in parallel. Samples with REE concentrations falling below the quantification limits at lab 1, i.e. 35 out of 63 samples, were analysed in another laboratory at ANSTO, Sydney ('lab 2' in Figure 6.2), using an online pre-concentration system prior to detection by ICP-MS. Samples were injected into a mixed-resin column (seaFAST, ESI) that chelates REEs but allows matrix ions to be rinsed out; this allows a roughly 20-fold increase in concentration, while also cleaning mobile phases and reducing background levels. The use of a pre-concentration column also allows reduction of oxide and hydroxide production in the plasma, particularly BaO and BaOH, which can cause polyatomic interferences with MREEs (Dulski, 1994). Potential BaO production was found to be negligible after column treatment. Production of REE oxides was also monitored in each run for all REEs from single REE stock solutions, and a correction factor was used for each potential oxide. Accordingly, quantification limits were reduced to < 0.1 ppt. The isotopes selected for analysis were the same as at lab 1, complemented by ^{89}Y. Accuracy and reproducibility of measurements were monitored with the analysis of SLRS-4 standard material.

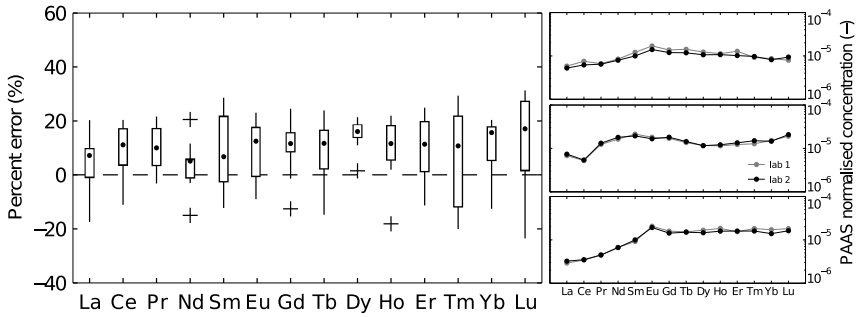

Figure 6.2: REE analytical precision and accuracy. Left: distribution of errors for each REE between the results from two laboratories for 16 samples. Black circles correspond to median values, boxes correspond to q10 and q90, whiskers to minima and maxima, and crosses are for outliers. References are the results for lab 2 (ANSTO); yttrium is not included in the analysis, as it was not measured at lab 1 (QUT). Right: examples of differences in REE patterns for the two laboratories for three different samples after Eu correction (top: T5; middle: I03; bottom: B11).

In addition, 16 of the samples with high REE concentrations were analysed at both laboratories for an appraisal of the degree of agreement between the two analytical procedures. Results from lab 2 were considered as the reference values against which the accuracy of results from lab 1 was assessed through relative error calculations. The distribution of errors for the 16 samples and for each REE – excluding Y – can be observed in Figure 6.2, together with examples of normalised REE patterns as determined by the two laboratories. Measured

concentrations of the 16 replicate samples were generally slightly higher at lab 1, as attested by the positive errors in Figure 6.2. However, almost all errors fell within the ±20% range, with median values between zero and 10%. Given the overall good agreement between the results from lab 1 and lab 2, we included some analyses that were only conducted at lab 1, providing they yielded high enough concentrations and smooth REE patterns. Twelve samples analysed at lab 1 only were integrated into our dataset, which corresponds to 19% of the whole batch of 63 samples.

Core samples for analysis of whole-rock REEs of the WCM were collected from the DNRM core library from the Wild Horse-1 coal seam gas exploration well located within the Teviot Brook catchment (WR-B in Figure 6.1). Core samples were taken from three different depth intervals (Appendix A.4) to obtain a representative overview on the heterogeneity within the sedimentary sequence of the WCM. Whole-rock REE analyses were conducted at the University of Melbourne. Sample powders (approx. 100 mg) were dissolved at high pressure, using HF–HNO_3 and HNO_3. After repeated refluxing with HNO_3, no residues other than rare low-density carbon particles were observed. Sorption of REEs to the organic fraction pelitic and psammitic sediments may compromise the yield of these elements in our bulk rock analyses (e.g. Whitford et al., 1994). However, the amount of insoluble carbon was very small and trace element sorption to organic matter was considered unlikely in 5M HNO_3. Following dilution, a weighed aliquot was equilibrated with a multi-isotope spike (Eggins et al., 1997) and analysed for REEs on an Agilent 7700s Quadrupole ICP-MS. The USGS reference material W-2 was used for calibration. Typical reproducibility of the REEs is on the order of ±1%.

6.3.3 Data analysis

All measured REE concentrations were normalised by their average concentrations in the post-Archean Australian average shale composite (PAAS), as revised by Pourmand et al. (2012). The series of elements were plotted on semi-logarithmic axes, and Y was included between Dy and Ho when data were available. The degree of fractionation from lighter to heavier metals was then expressed by the normalised concentration of medium elements (MREEs) ratioed to the normalised concentration of light elements (LREEs), and by the normalised concentration of heavy elements (HREEs) ratioed to the normalised concentration of MREEs. Noack et al. (2014) reported on the usefulness of comparing those two ratios to allow for a succinct and unbiased characterisation of REE patterns. Following these authors, ratios were calculated as an average over multiple elements as opposed to single weight group representatives. Here ratios were computed as follows:

$$R_{(M/L)} = \log\left(\frac{\mathrm{MREE}_N}{\mathrm{LREE}_N}\right) = \log\left(\frac{(\mathrm{Gd}_N + \mathrm{Tb}_N + \mathrm{Dy}_N)/3}{(\mathrm{La}_N + \mathrm{Pr}_N + \mathrm{Nd}_N)/3}\right) \tag{6.1}$$

$$R_{(H/M)} = \log\left(\frac{\mathrm{HREE}_N}{\mathrm{MREE}_N}\right) = \log\left(\frac{(\mathrm{Tm}_N + \mathrm{Yb}_N + \mathrm{Lu}_N)/3}{(\mathrm{Gd}_N + \mathrm{Tb}_N + \mathrm{Dy}_N)/3}\right) \tag{6.2}$$

where $R_{(M/L)}$ is the ratio between medium and light elements, $R_{(H/M)}$ is the ratio between heavy and medium elements, and HREE_N, MREE_N and LREE_N are PAAS-normalised concentrations in HREEs, MREEs and LREEs, respectively. Both Ce and Eu were excluded from the calculation of ratios as they can exhibit different oxidation states. Ce and Eu anomalies were calculated using the geometric method, i.e. assuming that the nearest neighbour concentrations behave linearly on log-linear plots (Lawrence et al., 2006). Anomalies were expressed as follows:

$$\mathrm{Ce/Ce^*} = \frac{\mathrm{Ce}_N}{(\mathrm{La}_N \times \mathrm{Pr}_N)^{1/2}} \qquad \text{and} \qquad \mathrm{Eu/Eu^*} = \frac{\mathrm{Eu}_N}{(\mathrm{Sm}_N \times \mathrm{Gd}_N)^{1/2}} \tag{6.3}$$

where Ce/Ce* and Eu/Eu* are a measure of the anomaly of these elements, and where values more than unity are commonly termed positive and values less than unity are commonly termed negative. In addition, the sum of REEs was calculated for each sample from absolute concentration values, excluding Y from calculations because this element was not determined in the 12 samples analysed at lab 1 and included into the dataset.

6.4 Results

6.4.1 REE patterns and concentrations in waters

The REE concentrations in streams and groundwaters from the Teviot Brook catchment are presented in Appendix A.4, together with field measurements (i.e. pH and electrical conductivity). When normalised to PAAS, different hydrological units showed distinctive REE patterns (Figure 6.3). All samples collected from the WCM aquifer had rising REE patterns, i.e. gradual increase from LREEs to HREEs, with reasonable consistency among samples (Figure 6.3a). These waters were all strongly fractionated, with LREE depletion for all of them and HREE enrichment for most of them. Another characteristic feature of WCM waters was the positive Y anomalies relative to Ho (Figure 6.3a). Y/Ho ratios ranged between 32 and 51; the reference PAAS ratio is ≈ 26 (Pourmand et al., 2012). Of consideration is also the rather low overall REE content in these waters ($18\,\mathrm{ppt} < \sum\mathrm{REE} < 477\,\mathrm{ppt}$; median 61 ppt). Lastly, WCM samples had either slightly positive or slightly negative Eu anomalies.

In contrast, igneous-sourced waters had much flatter normalised REE patterns with noticeably low fractionation (Figure 6.3b). This applied to all springs regardless of the type of rocks they drained. A wide range of concentrations characterised the four samples, with the springs draining felsic rocks (I03 and I04, in grey) presenting higher concentrations ($\sum$REE: 2054 ppt and 300 ppt, respectively) than the springs draining mafic rocks (I01

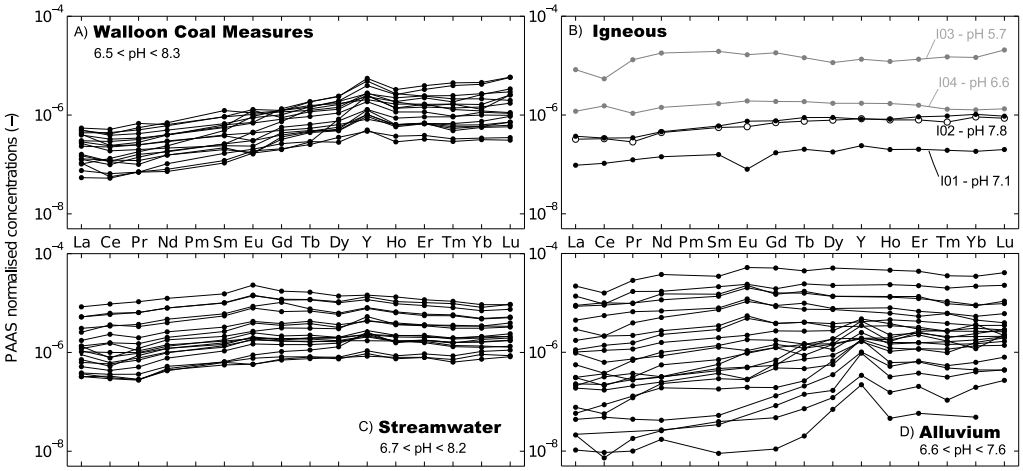

Figure 6.3: REE normalised patterns for each hydrological unit together with their pH range. In (B), the springs draining rhyolite rocks are plotted in grey while the springs draining the basaltic MRV are plotted in black. The two profiles for I02 correspond to the dry (white circles) and wet (black circles) sampling rounds.

and I02, in black; $\sum$REE: 25 ppt and 83 ppt, respectively). A negative Ce anomaly was found in the I03 sample (Ce/Ce* = 0.55), whereas a negative Eu anomaly was found at I01 (Eu/Eu* = 0.48).

For streamwater (Figure 6.3c), normalised REE patterns had relatively low fractionation, and some samples showed evidence for a slight LREE depletion. Enrichment in MREEs was apparent in several streamwater samples, as indicated by the various concave patterns with their point of inflexion located around Eu or Gd (Figure 6.3c). Lastly, the shallow alluvial groundwater (Figure 6.3d) exhibited a very wide range of concentrations and patterns (16 ppt $<$ $\sum$REE $<$ 5294 ppt; median 189 ppt). Patterns differed considerably from one borehole to another, with evidences for both flat profiles (similar to waters discharging from igneous rocks) and fractionated rising profiles (similar to WCM waters). Several alluvial samples had a positive Y anomaly relative to Ho (26 $<$ Y/Ho $<$ 78), and various samples had a negative Ce anomaly.

6.4.2 Whole-rock REE patterns

Whole-rock data for igneous rocks were obtained from Ewart et al. (1985) (Appendix A.4; Figure 6.4a). The rhyolite sample is from a ring dyke located in the Teviot Brook catchment (WR-I in Figure 6.1), whereas the trachyte samples are from the Flinders Peak – an intrusive feature located around 20 km north of the catchment, and geochemically similar to the trachyte plugs that occur in the study area (WR-T in Figure 6.1; Ewart, 1982). Whole-rock data for the WCM were collected and measured as part of this current study (Appendix A.4; Figure 6.4b). The three WCM samples were obtained from different depths of one exploration bore drilled in the sedimentary bedrock and located in the eastern part

of the study area (WR-B in Figure 6.1). An outstanding feature of the normalised REE patterns for igneous rocks is the negative Eu anomaly, particularly for the rhyolite sample (Eu/Eu* = 0.13; Figure 6.4a). Eu anomaly was also significant for the trachytic rocks, although less pronounced (0.71 < Eu/Eu* < 0.93). Conversely, the three patterns from the WCM had positive Eu anomalies (1.38 < Eu/Eu* < 1.48; Figure 6.4b). In terms of REE fractionation patterns, the rhyolitic rock was slightly depleted in HREEs, whereas the trachytic rocks revealed substantial MREE enrichment (Figure 6.4a). No whole-rock data was available for the MRV basalts; however, Ewart et al. (1988) reported that hawaiites and alkaline basalts of Southern Queensland such as the ones forming the MRV commonly exhibit lower REE fractionation as compared to other igneous rocks. For the WCM rocks, by contrast, important depletion in LREEs was observed in all three samples, and HREE enrichment was observed in one sample whereas the two other had no noticeable HREE enrichment relative to MREEs (Figure 6.4b).

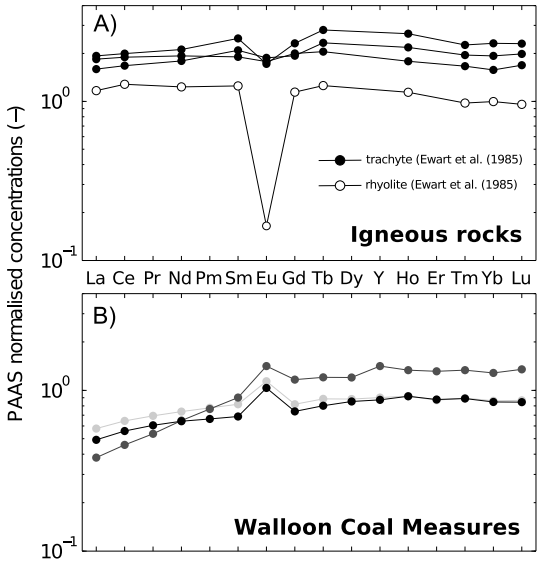

Figure 6.4: REE normalised patterns for different whole-rock samples. (A) Igneous rocks; the four profiles were taken from Ewart et al. (1985). (B) Walloon Coal Measures; the three profiles were measured as part of this study.

6.4.3 REE normalised ratios

The $R_{(M/L)}$ ratios as expressed in equation 6.1 were plotted against the $R_{(H/M)}$ ratios as expressed in equation 6.2, for all the samples (Figure 6.5). Because values were log-transformed, a flat REE pattern would have (0;0) coordinates. Positive values correspond to fractionation patterns enriched in heavier elements relative to lighter elements (i.e. enrichment in MREEs for $R_{(M/L)}$ and in HREEs for $R_{(H/M)}$), whereas negative values correspond to fractionation patterns enriched in lighter elements relative to heavier elements (i.e. enrichment in LREEs for $R_{(M/L)}$ and in MREEs for $R_{(H/M)}$). Also, the higher the absolute

value, the steeper the slope of the shale-normalised pattern. All samples had positive $R_{(M/L)}$ values, indicating that no MREE depletion occurred (Figure 6.5). Waters collected from igneous aquifers had near-flat patterns ($0.20 < R_{(M/L)} < 0.38$ and $-0.04 < R_{(H/M)} < 0.02$), whereas almost all WCM waters had positive to highly positive ratios ($0.17 < R_{(M/L)} < 1.00$ and $-0.16 < R_{(H/M)} < 0.93$). As anticipated, alluvial waters were highly scattered on the bi-logarithmic plot ($0.10 < R_{(M/L)} < 1.42$ and $-0.27 < R_{(H/M)} < 0.89$). Similar to the spring waters, igneous rock samples plotted very close to the origin of the graph (red triangles in Figure 6.5; $0.01 < R_{(M/L)} < 0.13$ and $-0.09 < R_{(H/M)} < -0.04$), confirming the near-flat patterns for these formations. The WCM rock samples also depicted low $R_{(H/M)}$ values, but they had $R_{(M/L)}$ values greater than the ones for igneous rocks (red squares in Figure 6.5; $0.37 < R_{(M/L)} < 0.58$ and $0.01 < R_{(H/M)} < 0.05$). Although positive, these ratios remained lower than the values found for WCM waters.

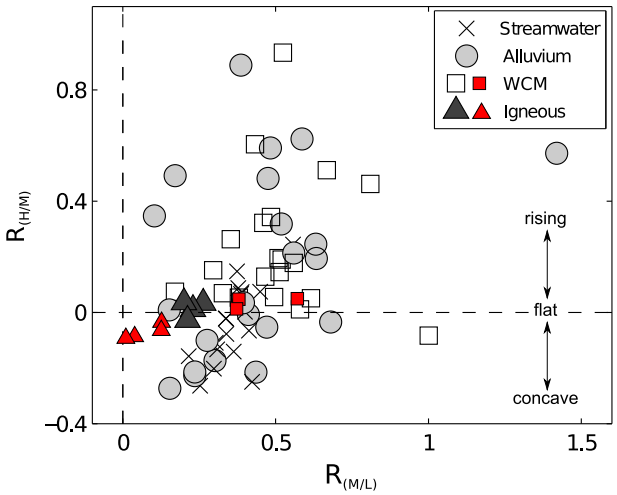

Figure 6.5: REE patterns as ratios of middle over light REEs ($R_{(M/L)}$) and heavy over middle REEs ($R_{(H/M)}$). Red markers are for whole-rock values.

6.4.4 Seasonal variations in REE concentrations

In order to evaluate the seasonal variation of REE chemistry in the Teviot Brook catchment, samples were collected under both dry and wet conditions. In general, absolute concentrations of the REEs were higher in the dry season than in the wet season (Figure 6.6). Among the four streamwater locations that were sampled twice, three exhibited decreasing trends and one had similar REE concentrations for both sampling rounds (Figure 6.6a). In alluvial water (Figure 6.6b), total REE concentrations changed substantially from dry to wet conditions, and all eight boreholes sampled twice showed a decrease in REE abundance. In the WCM (Figure 6.6c), the six boreholes that were accessed during both sampling rounds followed distinctive variations: three of them had decreasing concentrations whereas the remaining three had increasing concentrations from dry to wet conditions. Lastly for waters

from igneous aquifers (Figure 6.6d), I02 was the only spring sampled twice; its total REE concentration was remarkably similar for both sampling events.

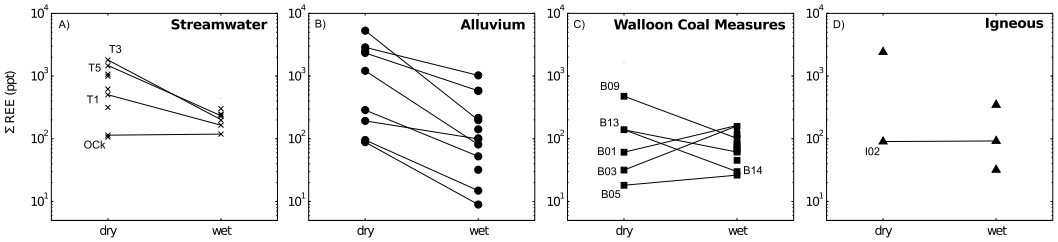

Figure 6.6: Seasonal differences in REE concentrations for each hydrological unit.

6.5 Discussion

6.5.1 Characteristics of REE patterns for each hydrological unit

All samples collected from the WCM aquifer had strongly fractionated REE patterns, and the majority exhibited LREE depletion (Figures 6.3a and 6.5). Leybourne et al. (2000) showed that depleted LREEs are commonly found in groundwaters with higher pH due to the adsorption of LREEs, whereas HREEs are more stable as dicarbonato complexes. However, in our case there was no evidence of a correlation between pH and the REE fractionation patterns. The positive Y/Ho anomalies found in the WCM aquifer may indicate progressive REE sorption to iron oxyhydroxides or particulate matter that preferentially affects Ho (Bau, 1999; Tweed et al., 2006). Alternatively, it may be due to the effect of carbonate precipitation in the WCM (Bau et al., 1996; Zhou et al., 2008). WCM samples also had either positive or negative Eu anomalies, but the reasons for this were not clear and they may reflect local physico-chemical conditions. There was no evidence of an anomaly with regard to Ce, which supports the findings of other authors who found no or only weak Ce anomalies in groundwater originating from deep sedimentary bedrock aquifers (e.g. Göb et al., 2013; Yan et al., 2013). Altogether, the fractionation patterns between LREEs and HREEs in WCM waters were in agreement with comparable work conducted by Raiber (pers. comm.) in the same sedimentary bedrock formation from adjacent catchments.

Igneous-sourced waters had relatively flat normalised REE patterns (Figures 6.3b and 6.5). MREE enrichment was detected in I03, and this is a well-known feature of low pH waters (Johannesson and Zhou, 1999). A negative Eu anomaly was found at I01, which originates from the basalts of the MRV. The occurrence of negative Eu anomalies in waters draining basaltic rocks has been well documented in the literature, as for instance by Lawrence et al. (2006) in a similar setting. The higher REE concentrations found in springs draining felsic rocks as compared to springs draining mafic rocks might be attributed to

the higher acidity of felsic formations such as rhyolite, which likely generated more weathering and therefore higher REE water content (e.g. Leybourne et al., 2000). However, in our case there was a poor statistical correlation between pH values and the sum of REE concentrations (Figure 6.3b).

A significant number of streamwater samples were enriched in MREEs (Figures 6.3c and 6.5). In their study on the REE variability in Southeast Queensland rivers, Lawrence et al. (2006) showed that MREE enrichment was common in streams, and it was associated with preferential weathering of phosphatic minerals. Davranche et al. (2004, 2011) suggested that complexation with humic substances in organic-rich waters could yield MREE enriched patterns. In addition, surface waters typically display negative Ce anomalies due to the precipitation of dissolved Ce^{3+} as particulate Ce^{4+} in oxidising conditions (Leybourne and Johannesson, 2008). As REEs are strongly complexed by organic matter (e.g. Pourret et al., 2007; Tang and Johannesson, 2010a), the absence of negative Ce anomalies in our samples may be explained by the complexation of Ce by organic colloids that may have occurred concomitantly (Dia et al., 2000; Hagedorn et al., 2011).

Unlike other hydrological units, the shallow alluvial groundwater exhibited a wide range of patterns, with both flat profiles (i.e. igneous- or "recharge-like" pattern) and fractionated rising profiles (i.e. "WCM-like" pattern) (Figures 6.3d and 6.5). The high degree of fractionation observed in several alluvial samples, as well as the positive Y/Ho anomalies, might be an indication of mixing with WCM water. More generally, and in the absence of carbonate or evaporite formations in the area, highly fractionated patterns may reflect a higher residence time in host rocks and thus a longer period of water–rock interaction leading to more evolved waters. Various alluvial samples also had a negative Ce anomaly, which can be seen as a good indicator of the oxidising conditions that may occur in various parts of the alluvial aquifer (e.g. Göb et al., 2013). Another explanation for the negative Ce anomalies may be the trapping of this element by Fe oxyhydroxides in the upper soil horizon (Pédrot et al., 2015).

6.5.2 Comparison between whole-rock and water REE patterns

Ewart et al. (1985) interpreted the negative Eu anomaly found in igneous rock samples (Figure 6.4a) as the effect of feldspar-dominated fractionation during crystallisation. Such a pattern is also typical of rhyolitic volcanic rocks (Johannesson et al., 2005 and references therein). Contrastingly, the positive Eu anomalies found for the WCM rock samples (Figure 6.4b) may be attributed to the high amount of albite minerals accumulated in the sedimentary bedrock. When comparing the whole-rock patterns with the ones found in surface and groundwaters, it appeared that:

(i) There was no consistency between the Eu anomalies found in rocks and those found

in waters that interacted with those rocks. Only I01 had a negative Eu anomaly for springs discharging from igneous rocks, and only two out of 14 WCM waters had a slightly positive Eu anomaly.

(ii) There was reasonable agreement between the overall fractionation patterns of waters and their host rocks. The WCM rock samples had rising REE patterns that were remarkably similar to those previously identified in the WCM groundwaters (Figures 6.3a and 6.4b). The igneous formations had less fractionated patterns, which did not greatly differ from the near-flat patterns observed in the springs draining these formations. Of note is the slight enrichment in MREEs identified for the rhyolitic whole-rock sample, which was also observed at the I03 spring.

6.5.3 Spatial variations along the alluvial flowpath

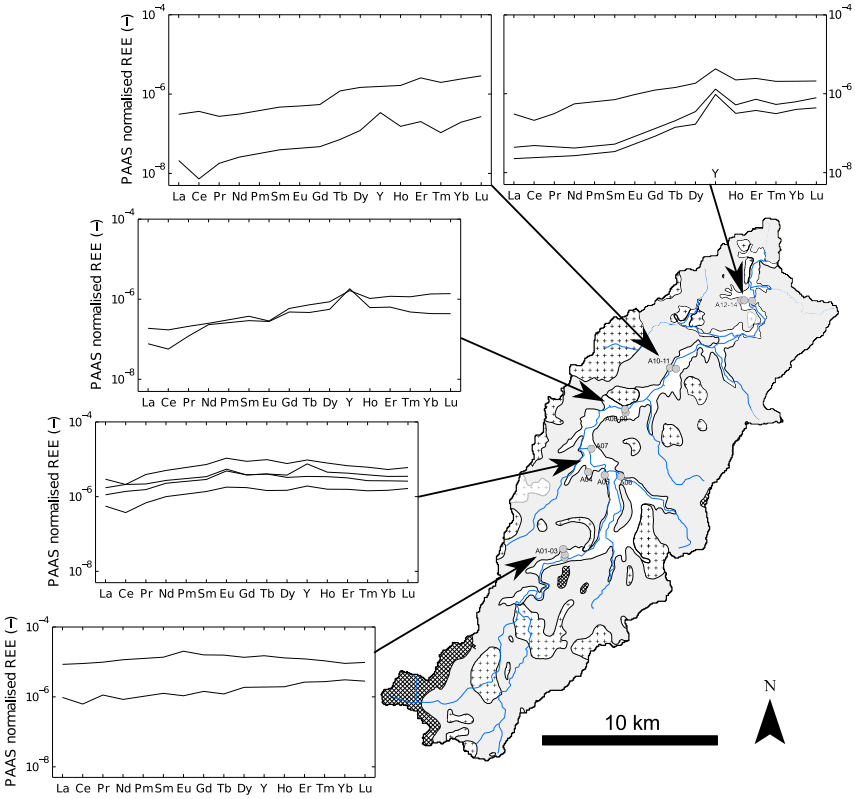

Figure 6.7: Evolution of the REE patterns in alluvial groundwaters from upgradient (Southwest) to downgradient (Northeast). Legend for the map is the same as in Figure 6.1.

The spatial variations in REE patterns were studied for the hydrological units where a reasonable number of measurements (> 5 values) exist, i.e. for the main stream, the alluvial water and WCM waters. There was no clear spatial pattern in the WCM aquifer due to relatively high similarity among REE patterns – apart from the differences observed in Eu anomaly. In the alluvium, however, an evolution in REE signatures was detected

from upstream to downstream. The REE patterns measured at different locations along the alluvial flowpath during the dry sampling round are shown in Figure 6.7. Normalised REE patterns gradually evolved from relatively flat profiles in the upstream part of the alluvium to LREE-depleted profiles with positive Y anomalies in the lowlands. Based on the assumptions made in Sections 6.5.1 and 6.5.2, our findings support a longitudinal evolution of the shallow alluvial groundwater from igneous recharge-like patterns upstream to WCM-like patterns downstream. This might be attributed to an increase in residence time as water flows downstream (Duvert et al., 2015a), which may contribute to an increase in REE fractionation. However, prior studies showed that even in sedimentary aquifers containing old groundwater, REE fractionation along flowpaths was not substantial (Willis and Johannesson, 2011; Siebert et al., 2012). Another interpretation of the fractionation between upstream and downstream alluvial waters may be an increased discharge of WCM water to the alluvial aquifer towards the lower section of the catchment, as opposed to the overwhelming contribution of waters discharging from igneous rocks further upstream. Two elements tend to support this second interpretation:

(i) A number of studies showed that LREEs are preferentially adsorbed on solid mineral phases compared to HREEs, especially when (bi)carbonate ions are present in solution (Biddau et al., 2002; Quinn et al., 2006; Tang and Johannesson, 2010b). This mechanism likely occurred in WCM waters, as residual alkalinity (i.e. the excess alkalinity that is not neutralised by calcium and magnesium) was found to be particularly high in the WCM aquifer only (Duvert et al., 2015a).

(ii) Investigations of estuarine processes at the saltwater – freshwater interface showed that fractionation of REEs commonly occurs during mixing (Lawrence and Kamber, 2006). In most cases, mixing with brackish water leads to the flocculation of dissolved organic matter in colloidal form, and this is followed by the removal of LREEs from groundwater (Duncan and Shaw, 2003; Tang and Johannesson, 2005). It is questionable whether similar mechanisms took place at the alluvium – sedimentary bedrock interface in the Teviot Brook catchment. Here we postulate that the salinity gradient, which results from WCM water seepage into the alluvial aquifer, triggered the flocculation of organic matter hence the removal of LREEs in the downstream section of the alluvium (Figure 6.7). However, further data on REE speciation in these alluvial waters and the kinetics of REE complexation with colloidal organic matter (e.g. Pédrot et al., 2008) are necessary to confirm such a hypothesis.

The $R_{(M/L)}$ and $R_{(H/M)}$ ratios were used to further quantify the visual interpretations from Figure 6.7. Particular focus was directed to the spatial variations identified in the main stream and alluvial aquifer (Figures 6.8a and 6.8b, respectively). The change from green to yellow colours depicts the upstream to downstream movement, and the values in Figure 6.8b are median values calculated from each borehole transect. Normalised REE

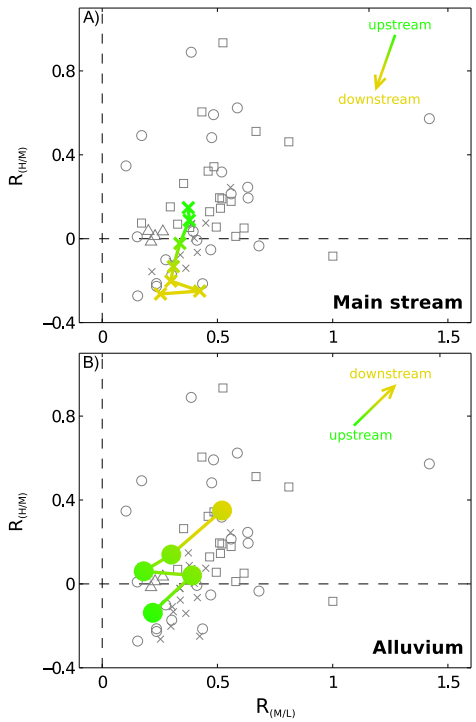

Figure 6.8: Spatial evolution of REE normalised ratios. (A) Along the main stream. (B) Along the alluvial flowpath (plotted values are median values for each bore transect, from upstream to downstream). Green markers are for upstream while yellow markers are for downstream.

patterns in streamwater were always relatively close to flat shapes, with a gradual enrichment in MREEs occurring from upstream to downstream (Figure 6.8a). The ratio between MREEs and LREEs remained at a similar level along the flow path, i.e. showing a slight LREE depletion with regard to MREEs. By contrast, alluvial waters evolved from near-flat REE patterns in the upstream part of the catchment (median $R_{(M/L)} = 0.21$ and median $R_{(H/M)} = -0.06$) to more LREE depleted and more HREE enriched patterns in the downstream part of the catchment (median $R_{(M/L)} = 0.48$ and median $R_{(H/M)} = 0.38$; Figure 6.8b). Such a discrepancy between the spatial variations in shallow groundwater and the drainage network can be attributed to the different mechanisms that affect the REE chemistry in those systems. As suggested by several authors (Pourret et al., 2007; Tang and Johannesson, 2010a), the influence of discharge areas in changing redox conditions and the presence of organic colloids in surface water were likely responsible for gradual MREE enrichment relative to HREEs in the downstream part of the Teviot Brook.

In terms of absolute REE content, a significant increase was apparent along the main stream (from 85ppt $< \sum$REE $<$ 252ppt upstream, to 849ppt $< \sum$REE $<$ 2198ppt downstream). These figures are in disagreement with the results from Lawrence et al. (2006) who reported a 75% decrease in REE abundance along a stream channel. In the shallow groundwater, by contrast, there was a significant decrease along the alluvial flowpath (from

2498 ppt $< \sum$REE $<$ 5294 ppt upstream to 88 ppt $< \sum$REE $<$ 287 ppt downstream). This decrease with flow downgradient is consistent with an earlier study of REE evolution in a shallow alluvial aquifer (Johannesson et al., 1999), but it is inconsistent with the positive salinity gradient observed in the Teviot Brook alluvial aquifer (Duvert et al., 2015a). This apparent contradiction outlines the fact that evaporative enrichment was not the main driver of REE abundance variations in the alluvial aquifer. More generally, REE spatial variations were not governed by the same mechanisms as the ones governing major ion chemistry variations, as previously noted by Tweed et al. (2006). These authors argued that major ions are tracers of the accumulative effects of water–rock interaction, whereas REE concentrations reflect mineral dissolution that preferentially occurs during recharge.

6.5.4 Linking the seasonal variations with inter-aquifer processes

The generally higher REE concentrations measured in the dry season as compared to the wet season (Figure 6.6) were attributed to enrichment due to enhanced evapotranspiration during the dry season, coupled with dilution with rainwater or recently recharged water during the wet season. The decreasing trends in streamwater (Figure 6.6a) are in agreement with the findings from Hagedorn et al. (2011), who found higher REE concentrations during the dry season in rivers draining the Australian Alps. The decreasing trends in alluvial water (Figure 6.6b) are consistent with the study by Poh and Gasparon (2011), who revealed a substantial decrease in REE concentrations from dry to wet periods in a wetland groundwater system in Southeast Queensland. Reasons for the lack of consistent variations in the WCM (Figure 6.6c) were not evident, but may be related to their location: the three increasing trends were found in boreholes located in the upstream section of the catchment (i.e. B01, B03 and B05). Unlike most WCM locations, these three bores were also characterised by a substantial increase in total dissolved solids from dry to wet (Duvert et al., 2015a). Overall, the seasonal changes in REE abundance evidenced in almost all the studied systems underline the importance of carrying out several sampling rounds that capture the temporal variability of such highly responsive systems.

Although concentrations proved to vary substantially between dry and wet periods, fractionation patterns were relatively preserved for most locations. Among all the locations sampled twice, only two WCM boreholes, two alluvial boreholes and one tributary of the Teviot Brook exhibited pronounced changes in their dry/wet fractionations. The seasonal differences in PAAS-normalised REE patterns for these five locations are reported in Figure 6.9. Note that temporal changes in REE patterns are marked in Figure 6.9 by blue arrows for flattening trends and by red arrows for increasingly fractionated trends. Considerable increase in LREEs and to a lesser extent MREEs was observed in the WCM borehole B01, whereas HREEs remained at a similar level between dry and wet seasons (Figure 6.9a). At B05, there was a slighter increase in LREEs coupled with substantial decreases in MREEs

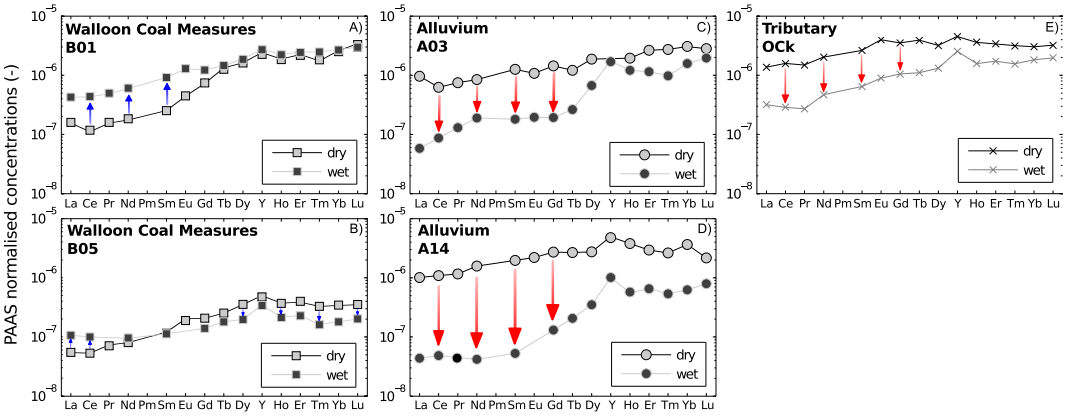

Figure 6.9: Evolution of REE patterns from dry to wet conditions for four boreholes and the Oakley Creek, a tributary of Teviot Brook. Temporal changes in REE patterns are marked by blue arrows for flattening trends and by red arrows for increasingly fractionated trends.

and HREEs (Figure 6.9b). In other words, both REE patterns evolved from a "WCM-like" fractionation to an "igneous-like" fractionation, hence suggesting an effect of recharge to the sedimentary bedrock aquifer. This assumption is further supported by the position of these two boreholes near the headwaters of the catchment and in the vicinity of highly fractured igneous outcrops, where recharge most likely occurred during and after the summer rainfall events (Figure 6.1). If confirmed, our findings would indicate that the WCM aquifer was recharged through the outcrops of the MRV as well as from other intrusions that have penetrated the WCM in various locations throughout the catchment.

Patterns in the alluvial boreholes A03 and A14 followed opposite behaviour: a substantial decrease in LREEs was detected at both locations (Figures 6.9c and 6.9d), coupled with a slight decrease in MREEs and HREEs at A14 (Figure 6.9d). In other words, these two patterns evolved from a near-flat normalised profile to a "WCM-like" fractionated profile. This very likely corresponds to an enhanced seepage from the WCM groundwater towards the alluvial aquifer during the wet season. A03 is located upstream whereas A14 is located in the downstream section of the alluvium (Figure 6.1), but both boreholes are less than a hundred metres from the boundary with the WCM. As previously shown in Figure 6.6, overall concentrations were much lower during the wet season for the two alluvial groundwaters.

The variation in REE pattern was also assessed for the Oakley Creek tributary (OCk in Figure 6.1), which mainly drains the WCM (Figure 6.9e). As for A14, the overall REE concentration decreased from dry to wet season, with a more extensive depletion in LREEs and MREEs. An increase in the Y anomaly was also observed at OCk (Y/Ho = 32 and 43 in dry and wet periods, respectively; Figure 6.9e). This finding may indicate an increased contribution of the LREE-depleted WCM waters to the surface drainage during the wet season. Given that OCk was the only tributary where repeated sampling was conducted, our assumption of increased seepage from the WCM is disputable, and the REE seasonal

variation emphasised here would need to be compared with REE dynamics from other tributaries before we can confirm it. Lawrence et al. (2006) proposed that in catchments with distinctive lithology, the REE pattern in rivers could be used as a fingerprinting tool for evaluating the origin of streamwater. However, we should also emphasise that several other processes might contribute to changes in the REE fractionation of surface water. If a more detailed investigation is carried out on the factors controlling REE fractionation, the approach from Lawrence et al. (2006) might be usefully applied to the Teviot Brook catchment to quantify bedrock seepage to the drainage network.

Several hypotheses can explain the changes in REE patterns described in Figures 6.9a and 6.9b. Flushing out of the more evolved WCM "resident" water and replacement by freshly recharged water may have occurred during the rainy season. Duvert et al. (2015a) reported no significant change in major ion chemistry; therefore, the likelihood of a mixed contribution of resident water and recharge water in the wet period, rather than complete replacement of the WCM water, is greater. Mixing most likely changed the fractionation patterns by inducing a concentration of LREEs together with a dilution of HREEs. In addition, mixing of the two end-members may have triggered chemical reactions that further affected the REE fractionation patterns. Although pH values increased only slightly at the two locations (circumneutral waters with $7.7 < \text{pH} < 8.3$), a four-fold increase in dissolved Fe was observed at B01 (from 0.03 to 0.11 meq L^{-1}) and the increase was twofold at B05 (from 0.07 to 0.12 meq L^{-1}). The reduction of insoluble Fe^{3+} to dissolved Fe^{2+} can be explained by oxygen-depleted conditions that probably occurred during flooding. The process of REE fractionation induced by iron-mineral scavenging has been broadly reported in the literature (e.g. Leybourne and Johannesson, 2008). In addition, Davranche et al. (2011) showed that the reduction of Fe^{3+} actually results in organic matter desorption, which in turn gives rise to the release of REEs. Such mechanism may have occurred in the WCM during recharge, however this hypothesis was not sufficient to explain the depletion in MREEs and HREEs that was concomitantly observed at B05.

Overall, other complexing ligands and processes may have occurred during mixing of the two end-members, and more data would be necessary to further interpret these processes. In particular, the excess HCO_3 relative to Ca and Mg in most WCM waters would be likely to facilitate carbonate precipitation upon mixing with Ca-rich recharge waters, which might have an effect on the REE behaviour. In the case of the alluvial boreholes shown in Figures 6.9c and 6.9d, no substantial change either in Fe concentrations or in pH values were recorded. The depletion in LREEs was attributed to the mixing with HREE depleted waters from the WCM aquifer, as already discussed in Section 6.5.3.

6.5.5 Towards a typology of inter-aquifer processes

The study of seasonal differences in REE normalised patterns allowed for detection of two distinctive processes. First, the possible effect of recharge on sedimentary bedrock water has been observed at two locations in the WCM. Second, the likely seepage of water from the WCM into the shallow alluvium has been observed at two locations of the alluvial aquifer. The seasonal change in $R_{(M/L)}$ and $R_{(H/M)}$ for the two boreholes screened in the WCM, i.e. B01 and B05, can be observed in Figure 6.10a. Values under dry conditions were typical of rising REE patterns ($R_{(M/L)}$ = 0.81 and 0.56 and $R_{(H/M)}$ = 0.46 and 0.18, respectively). Both signatures then clearly evolved towards the origin of the plot, i.e. towards flatter patterns ($R_{(M/L)}$ = 0.46 and 0.17 and $R_{(H/M)}$ = 0.32 and 0.07, respectively). Conversely, the two alluvial boreholes A03 and A14 evolved from lower ratios ($R_{(M/L)}$ = 0.10 and 0.39 and $R_{(H/M)}$ = 0.35 and 0.03, respectively) to higher ratios ($R_{(M/L)}$ = 0.39 and 0.59 and $R_{(H/M)}$ = 0.89 and 0.62, respectively), outlining the change from flatter patterns to more fractionated patterns (Figure 6.10b). It is worth highlighting the high degree of similarity between the respective orientations of the two blue arrows and two red arrows in Figures 6.10a and 6.10b.

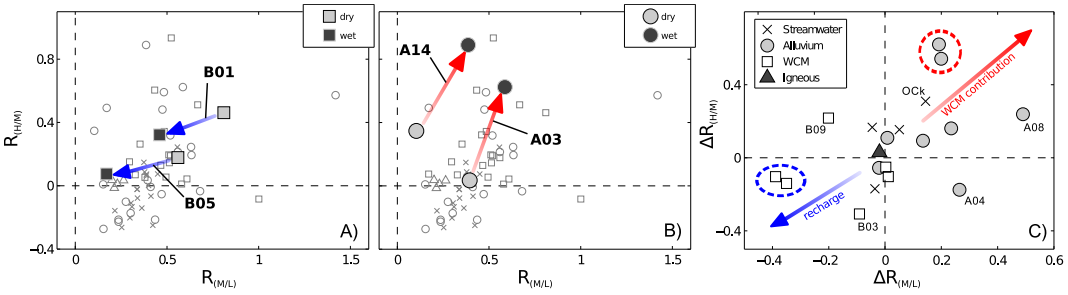

Figure 6.10: Temporal evolution in the $R_{(M/L)}$ and $R_{(H/M)}$ ratios for various boreholes of the Teviot Brook catchment. (A) Temporal change at the WCM boreholes B01 and B05. (B) Temporal change at the alluvial boreholes A03 and A14. (C) Conceptual typology of the temporal variations in normalised REE patterns. The values for boreholes B01 and B05 are surrounded by a blue circle, and the values for boreholes A03 and A14 are surrounded by a red circle.

A conceptual typology of the different seasonal changes identified in this study is provided in Figure 6.10c. Data plotted in the figure are the differences over time of the values presented in Figure 6.5 for each of the groundwater, springs and streamwater locations that were repeatedly sampled. The blue circle identifies the values for boreholes B01 and B05 ($\Delta R_{(M/L)}$ = –0.35 and –0.40; $\Delta R_{(H/M)}$ = –0.14 and –0.10, respectively) and the red circle locates the values for boreholes A03 and A14 ($\Delta R_{(M/L)}$ = 0.19 and 0.19; $\Delta R_{(H/M)}$ = 0.54 and 0.59, respectively; Figure 6.10c). The position of these circles confirms that the evolution towards higher ratios (i.e. increase in fractionation) indicates an influence of highly evolved sedimentary bedrock water, and the evolution towards lower ratios (i.e. flattening) indicates an influence of recently recharged water.

As a general rule, $\Delta R_{(M/L)}$ was slightly more efficient than $\Delta R_{(H/M)}$ in discriminat-

ing between alluvial and sedimentary bedrock samples, because most alluvial samples had positive $\Delta R_{(M/L)}$ ratios whereas most WCM samples had negative $\Delta R_{(M/L)}$ ratios (Figure 6.10c). All eight $\Delta R_{(M/L)}$ values from the alluvial boreholes ranged from near zero to significantly positive, with A08 showing the highest value (0.53). This may indicate that seepage from the WCM aquifer occurred at A08 as well, although visual examination of the dry and wet REE patterns at A08 did not allow for detection of a significant change (Section 6.5.4). The only alluvial borehole with a negative $\Delta R_{(H/M)}$ value (–0.22) was A04, reflecting a larger depletion in HREEs relative to the depletion in MREEs, which we were not able to explain. As outlined previously, A04 is the only alluvial borehole with a screen interval that intercepts both the basal layer of the alluvium and the top of the WCM; this might be a reason for the different seasonal change observed at A04. In contrast, the igneous spring and most streamwater samples showed no substantial change. The only streamwater location presenting a significant temporal shift was OCk ($\Delta R_{(M/L)} = 0.14$ and $\Delta R_{(H/M)} = 0.51$; Figure 6.10c). These values are reasonably similar, although lower, to the ones from A03 and A14, which tends to confirm the likely increased contribution of WCM waters to the creek discharge during the high flow season. The sedimentary bedrock groundwater had mainly negative values, apart from the $\Delta R_{(H/M)}$ value at B09 (–0.20). The two studied boreholes B01 and B05 were the ones with the lowest values, hence the highest evidence for an influence of recharge.

Overall, this typology provides a way of discriminating between areas where the effect of WCM waters on the alluvial aquifer is apparent, or where recharge into the sedimentary bedrock may occur. However, there are still a number of limitations to its broader applicability. First, only six of the 14 WCM boreholes and eight of the 14 alluvium boreholes could be repeatedly sampled, and results might have differed with a more comprehensive dataset. Second, samples were collected on a seasonal basis, and detailed understanding of the temporal changes in REE patterns would require the collection of samples at a higher temporal resolution, e.g. at a monthly frequency. In its current state this typology is a promising tool to identify inter-aquifer mixing and recharge processes, but it still needs to be further tested.

In order to confirm our assumptions, the stable isotope data presented in Duvert et al. (2015a) were reassessed, with a closer examination of boreholes B01, B05, A03 and A14 (Figure 6.11). Values for the two WCM boreholes (Figure 6.11a) lie close to the meteoric line, indicating little enrichment hence little evaporation and rapid infiltration, which is consistent with the location of these two boreholes close to the headwaters. Duvert et al. (2015a) showed that waters sampled from igneous rocks and springs were typically freshly recharged waters with nil to little isotopic fractionation compared to rainwater. When looking at the seasonal variation in groundwaters, a significant change was observed from dry to wet for both boreholes (blue arrows in Figure 6.11a). Rather than being related to evaporation, this

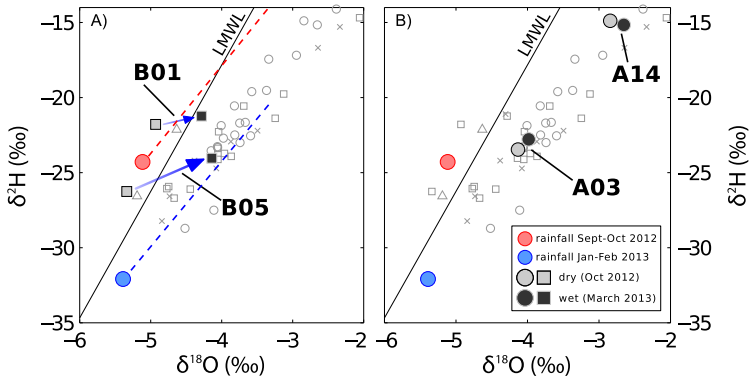

Figure 6.11: Stable isotopes of oxygen and hydrogen data for the four previously identified bores. The two rainfall isotopic values are weighted averages calculated from samples collected fortnightly at two locations in the Teviot Brook catchment. The dashed lines are inferred evaporative trend lines. LMWL stands for local meteoric water line (modified from Duvert et al., 2015a).

shift was probably indicative of a larger contribution of isotopically depleted recharge waters: the major rainfall events that occurred in January and to a lower extent in February, i.e. prior to the wet season sampling round, had depleted weighted average isotopic values relative to earlier rainfall events (blue and red circles in Figure 6.11, respectively). This suggests that recharge water contributed to the WCM groundwater hydrochemical evolution at these locations, and this is in full agreement with our previous interpretations based on REE data. The two alluvial groundwaters at A03 and A14 conserved very similar isotopic signatures from dry to wet periods (Figure 6.11b). These results again underline the potential of REE patterns to identify processes that cannot be detected with conventional hydrochemical tools alone.

6.6 Conclusions

In this study, we examined the potential of rare earth elements (REEs) to trace the spatial and temporal variability of different surface water and groundwater systems located within a drainage catchment in Southeast Queensland, Australia. Patterns were normalised to the post-Archean Australian average shale composite and compared between each hydrological and/or lithological component, i.e. groundwater from a sedimentary bedrock formation known as the Walloon Coal Measures (WCM), springs draining basaltic and felsic igneous rocks, the alluvial aquifer and the surface drainage system. Distinct signatures were observed in waters that have interacted with different rocks. The WCM aquifer had highly evolved, LREE depleted and HREE enriched patterns, whereas the springs draining intrusive and extrusive igneous rocks had relatively flat patterns. Surface waters were generally enriched in MREEs, and waters collected from the shallow alluvial aquifer had very diverse patterns with important spatial variations. The spatial variations of REEs were assessed along the alluvial flowpath and the main drainage stream. The behaviour of REEs between the two systems did not appear to be related. REE patterns collected from the alluvial

groundwater exhibited an increasing influence of the WCM-like REE pattern (i.e. depleted in LREEs and enriched in MREEs and HREEs) from upgradient to downgradient. In terms of abundance, total REEs in the alluvial waters decreased towards the outlet of the catchment, which was consistent with a gradual sorption of elements in the aquifer matrix. By contrast, there was an increase in the REE concentrations in the main stream, and REE patterns did not change significantly from upstream to downstream, suggesting that other processes controlled the REE chemistry in surface water and masked possible contributions of the WCM to the stream.

Based on the investigation of REE seasonal variations and of the changes in ratios between LREEs, MREEs and HREEs, we concluded on the occurrence of two types of inter-aquifer linkages. First, contributions from WCM waters to the alluvium were evidenced during the wet season at two locations in the alluvial aquifer. Second, the effect of mountain front recharge was revealed in areas where the fractured igneous formations likely contributed to WCM aquifer recharge during the wet season. Overall, our findings have several implications for studies assessing connectivity between aquifers:

(1) It shows that REEs can be used to elucidate complex hydrological processes occurring in catchments, such as rapid recharge through fractured rocks and inter-aquifer mixing.

(2) It confirms that REE chemistry and major ion hydrochemistry are not controlled by the same processes, and that REE behaviour in aquifers still requires further understanding.

(3) It underlines the importance of conducting seasonal sampling rounds to identify possible short-term variations in REE patterns, even for shallow bedrock aquifers. This is critical to improved understanding of hydrological and hydrochemical processes.

Further investigation is required in the Teviot Brook catchment and other settings to better quantify the seasonal fluctuations in REE patterns and abundance. This is particularly important in areas where conventional hydrochemical methods alone do not accurately describe the temporal changes occurring in hydrological systems. For such settings, we showed that REEs have potential for providing additional insight into nonlinear hydrological processes.

Acknowledgments

Thanks are due to the Queensland DNRM for providing access to the government borehole network, and to all Teviot Brook landowners for giving access to sampling sites. Irina Kinaev, Brett Rowling and Chris Dimovski are thanked for assistance with laboratory work. Discussions with Charlotte Allen, Christelle Batiot-Guilhe and Des Owen helped improve this manuscript. We also would like to acknowledge the Australian Institute of Nuclear Science and Engineering for funding part of this project. Lastly, our thanks go to Karen Johannesson, Aline Dia and an anonymous reviewer for their comprehensive review of our manuscript, as well as to the Editor-in-Chief Michael Böttcher. The first author is supported by an Endeavour Scholarship provided by the Australian Federal Government.

CHAPTER 7

Tritium Reveals Temporal Variations in the Groundwater Contribution to a Stream

This chapter has been published as:

C. Duvert, M.K. Stewart, D.I. Cendón, M. Raiber, 2016. Time-series of tritium, stable isotopes and chloride reveal short-term variations in groundwater contribution to a stream.
Hydrology and Earth System Sciences 20, 257–277.

Abstract

A major limitation to the assessment of catchment transit time (TT) stems from the use of stable isotopes or chloride as hydrological tracers, because these tracers are blind to older contributions. Yet, accurately capturing the TT of the old water fraction is essential, as is the assessment of its temporal variations under non-stationary catchment dynamics. In this study we used lumped convolution models to examine time-series of tritium, stable isotopes and chloride in rainfall, streamwater and groundwater of a catchment located in subtropical Australia. Our objectives were to determine the different contributions to streamflow and their variations over time, and to understand the relationship between catchment TT and groundwater residence time. Stable isotopes and chloride provided consistent estimates of TT in the upstream part of the catchment. A young component to streamflow was identified that was partitioned into quickflow (mean TT ≈ 2 weeks) and discharge from the fractured igneous rocks forming the headwaters (mean TT ≈ 0.3 yr). The use of tritium was beneficial for determining an older contribution to streamflow in the downstream area. The best fits between measured and modelled tritium activities were obtained for a mean TT of 16–25 yr for this older groundwater component. This was significantly lower than the residence time calculated for groundwater in the alluvial aquifer feeding the stream downstream ($\approx$ 76–102 yr), emphasising the fact that water exiting the catchment and water stored in it had distinctive age distributions. When simulations were run separately on each tritium streamwater sample, the TT of old water fraction varied substantially over time, with values averaging 17 ± 6 yr at low flow and 38 ± 15 yr after major recharge events. This counterintuitive result was interpreted as the flushing out of deeper, older waters shortly after recharge by the resulting pressure wave propagation. Overall, this study shows the usefulness of collecting tritium data in streamwater to document short-term variations in the older component of the TT distribution. Our results also shed light on the complex relationships between stored water and water in transit, which are highly nonlinear and remain poorly understood.

7.1 Introduction

Catchment transit time (TT) can be defined as the time water spends travelling through a catchment, from infiltrating precipitation until its exit through the stream network (McDonnell et al., 2010). Because this parameter integrates information on storage, flow pathways and source of water in a single value, it has been increasingly used as a generic indicator of catchment dynamics (McGuire and McDonnell, 2006). Accurate quantification of TT is of prime importance for water resource management issues, in particular for the assessment of catchment sensitivity to anthropogenic inputs such as fertilizers or herbicides (e.g. van der Velde et al., 2010; Benettin et al., 2013), and for the provision of additional constraints on catchment-scale hydrological models (e.g. Gusyev et al., 2013). TT is estimated by relating

the signature of a tracer measured in a sample taken at the outlet of a catchment to the history of the tracer input in rainfall-derived recharge water. Interpretation of TT data is often problematic because a single sample typically contains water parcels with different recharge histories, different flowpaths to the stream and thus different ages. This is exacerbated when the catchment is underlain by heterogeneous aquifers, as dispersion and mixing of different water sources can lead to very broad spectra of ages (Weissmann et al., 2002). Rather than a single scalar value, samples are therefore characterised by a TT distribution (i.e. probability density function of the TTs contained in the sample). The residence time (RT) distribution is another useful indicator that refers to the distribution of ages of water resident within the system, rather than exiting it. RT distributions are generally used to characterise subsurface water or deeper groundwater that is stored in the catchment.

In the last two decades, a great deal of effort has been directed to the determination of catchment TTs in a variety of streams and rivers worldwide (e.g. Maloszewski et al., 1992; Burns et al., 1998; Soulsby et al., 2000; Rodgers et al., 2005; Dunn et al., 2010). Attempts have been made to correlate the TTs to catchment characteristics such as topography (McGuire et al., 2005; Mueller et al., 2013; Seeger and Weiler, 2014), geology (Katsuyama et al., 2010) or soil type (Tetzlaff et al., 2009, 2011; Timbe et al., 2014). Assessment of the relationship between groundwater RT and catchment TT has also been undertaken occasionally (Matsutani et al., 1993; Herrmann et al., 1999; Reddy et al., 2006). Because catchment storage is highly non-stationary, catchment TTs are known to vary over time (McDonnell et al., 2010), yet the importance of temporal dynamics in TT distributions has been overlooked until recently. One of the reasons is that this non-stationarity is not accounted for in the models commonly used in catchment TT research. In the last five years, an ever-growing number of studies has transferred its focus to assessing dynamic TT distributions (Hrachowitz et al., 2010, 2013; Roa-García and Weiler, 2010; Rinaldo et al., 2011; Cvetkovic et al., 2012; Heidbüchel et al., 2012, 2013; McMillan et al., 2012; Tetzlaff et al., 2014; Birkel et al., 2015; van der Velde et al., 2015; Benettin et al., 2015; Harman, 2015; Klaus et al., 2015a; Kirchner, 2015). Most of these studies agreed on the importance of considering storage dynamics, because the RT distribution of storage water and the TT distribution of water transiting at the outlet of the catchment are likely to be very different. Concurrently to these recent advances in catchment hydrology, groundwater scientists have also developed new theoretical bases for the incorporation of transient conditions in RT distribution functions (Massoudieh, 2013; Leray et al., 2014). Nonetheless, the determination of time-variant TT and RT distributions requires data-intensive computing, which still largely limits their use in applied studies (Seeger and Weiler, 2014).

A simple, yet still widely used alternative to more sophisticated models is the lumped-parameter modelling approach, which has been developed since the 1960s to interpret age tracer data (Vogel, 1967; Eriksson, 1971; Maloszewski and Zuber, 1982). Lumped models

require minimal input information, and are based on the assumptions that the shape of the TT or RT distribution function is a priori known and that the system is at steady state. The relationship between input and output signatures is determined analytically using a convolution integral, i.e. the amount of overlap of the TT or RT distribution function as it is shifted over the input function. Some of the lumped models consider only the mechanical advection of water as driver of tracer transport (e.g. exponential model), while others also account for the effects of dispersion–diffusion processes (e.g. dispersion model). Non-parametric forms of RT distribution functions have recently been developed (Engdahl et al., 2013; Massoudieh et al., 2014b; McCallum et al., 2014), but again, these more recent approaches require a higher amount of input data, which makes the standard lumped-parameter approach a method of choice for the time being.

Commonly used to determine TT distributions using such models are the stable isotopes of water (^{2}H and ^{18}O). Because they are constituents of the water molecule itself, ^{2}H and ^{18}O follow almost the same response function as the traced material, hence are generally referred to as "ideal" tracers. Another tracer that behaves relatively conservatively and has been often used in the literature is chloride. An important issue with using ^{2}H, ^{18}O and/or chloride as TT indicators is that detailed catchment-specific input functions are needed (ideally at a weekly sampling frequency for several years), and such data are rare globally. More importantly, Stewart et al. (2010, 2012) criticised the use of these tracers to assess catchment TTs, arguing that TT distributions are likely to be truncated when only ^{2}H and/or ^{18}O are used. In an earlier study, Stewart et al. (2007) reported differences of up to an order of magnitude between the TTs determined using stable isotopes as compared to those determined using tritium (^{3}H). Later works by Seeger and Weiler (2014) and Kirchner (2015) reinforced the point that "stable isotopes are effectively blind to the long tails of TT distributions" (Kirchner, 2015). The effects of older groundwater contributions to streamflow have largely been ignored until recently (Smerdon et al., 2012; Frisbee et al., 2013), and according to Stewart et al. (2012), new research efforts need to be focused on relating deeper groundwater flow processes to catchment response. Accounting for potential delayed contributions from deeper groundwater systems therefore requires the addition of a tracer, such as ^{3}H, that is capable of determining longer TTs.

^{3}H is a radioactive isotope of hydrogen with a half-life of 12.32 yr. Like ^{2}H and ^{18}O it is part of the water molecule and can therefore be considered an "ideal" tracer. Fractionation effects are small and can be ignored relative to measurement uncertainties and to its radioactive decay (Michel, 2005). The bomb pulse ^{3}H peak that occurred in the 1960s was several orders of magnitude lower in the southern hemisphere than in the northern hemisphere (Freeze and Cherry, 1979; Clark and Fritz, 1997), and the ^{3}H concentrations of remnant bomb pulse water have now decayed well below that of modern rainfall (Morgenstern and Daughney, 2012). These characteristics allow the detection of relatively older groundwater

(up to 200 yr) and, importantly, the calculation of unique TT distributions from a single ^{3}H value, provided the measurement is accurate enough (Morgenstern et al., 2010; Stewart et al., 2010). Other age tracers such as chlorofluorocarbons and sulfur hexafluoride have shown potential for estimating groundwater RT (e.g. Cook and Solomon, 1997; Lamontagne et al., 2015), however these tracers are less suitable for streamwater because of gas exchange with the atmosphere (Plummer et al., 2001).

Long-term evolution of ^{3}H activity within catchments has been reported in a number of studies, both for the determination of RT in groundwater systems (e.g. Zuber et al., 2005; Stewart and Thomas, 2008; Einsiedl et al., 2009; Manning et al., 2012; Blavoux et al., 2013) and for the assessment of TT in surface water studies (Matsutani et al., 1993; Stewart et al., 2007; Morgenstern et al., 2010; Stolp et al., 2010; Stewart, 2012; Gusyev et al., 2013; Kralik et al., 2014). Most of these studies had to assume stationarity of the observed system by deriving a unique estimate of TT or RT from ^{3}H time-series data, in order to circumvent the bomb pulse issue. Benefiting from the much lower ^{3}H atmospheric levels in the southern hemisphere, Morgenstern et al. (2010) were the first to use repeated streamwater ^{3}H data to assess the temporal variations in TT distributions. Using simple lumped parameter models calibrated to each ^{3}H sample, they established that catchment TT was highly variable and a function of discharge rate. Following the same approach, Cartwright and Morgenstern (2015) explored the seasonal variability of ^{3}H activities in streamwater and their spatial variations from headwater tributaries to a lowland stream. They showed that different flowpaths were likely to have been activated under varying flow conditions, resulting in a wide range of TTs. To the extent of our knowledge, shorter term (i.e. less than monthly) variations in streamwater ^{3}H and their potential to document rapid fluctuations in the older groundwater component in streamflow have not been considered in the literature.

This study investigates the different contributions to streamflow in a subtropical headwater catchment subjected to highly seasonal rainfall, as well as their variations over time. The overarching goal is to advance our fundamental understanding of the temporal dynamics in groundwater contributions to streams, through the collection of time-series of seasonal tracers, i.e. tracers subject to pronounced seasonal cycles (^{2}H, ^{18}O and chloride), and ^{3}H. We postulate that ^{3}H time-series data may provide insight into the nonlinear processes of deeper groundwater contribution to rivers. Specifically, the questions to be addressed are:

(i) Can simple lumped models provide reliable estimates of catchment TTs in catchments characterised by intermittent recharge and high evapotranspiration rates?

(ii) Can short-term variations in older (5–100 yr) groundwater contributions be captured by ^{3}H time-series data?

(iii) How dissimilar are the RT of aquifers adjacent to streams (i.e. storage water) and the TT of streamwater (i.e. exiting water)?

7.2 Study area

7.2.1 Physical setting

The upper Teviot Brook catchment is located southwest of Brisbane (Southeast Queensland, Australia), with its headwaters in the Great Dividing Range (Figure 7.1). It covers an area of 95 km^2, and elevations range between 160 and 1375 metres above sea level. Climate in the region is humid subtropical with extremely variable rainfall: mean annual precipitation for the catchment is 970 mm (1994–2014 period), of which 76% falls from November to April. While Teviot Brook is a perennial stream, the distribution of discharge is uneven throughout the year: the mean annual discharge is 120 mm (1994–2014 period), with highest and lowest streamflow occurring in February (average 40 mm) and September (average 2 mm), respectively. The headwaters support undisturbed subtropical rainforest, while the valley supports open woodland and grassland.

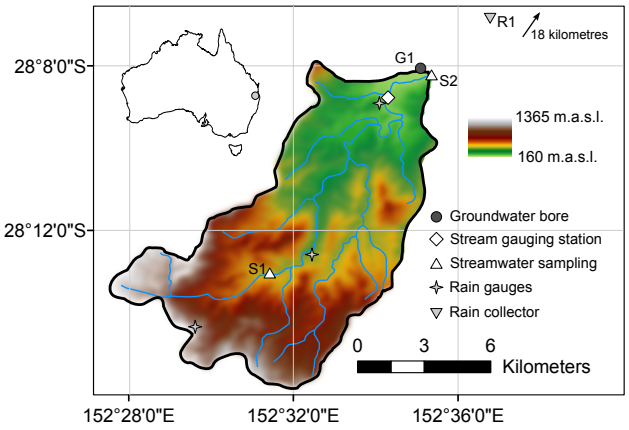

Figure 7.1: Upper Teviot Brook catchment and location of sampling sites. The stream gauging station corresponds to Teviot Brook at Croftby (145011A; operated by the Queensland Department of Natural Resources and Mines). The rainfall gauges correspond to Wilsons Peak Alert (040876), Carneys Creek The Ranch (040490) and Croftby Alert (040947), all run by the Bureau of Meteorology.

The first sampling location (S1) is situated in a steep, narrow valley where the stream erodes into the fractured, silica-rich igneous rocks forming the headwaters. At this upstream location, boulders, gravel and sand constitute the streambed substrate as well as near-channel deposits. The second sampling location (S2) lies further downstream where the valley is flatter and forms a wide alluvial plain. At this downstream location the stream is incised into the alluvial deposits, which at G1 are composed of fine-grained material, i.e. mostly gravel and silty clay. Underlying the alluvial deposits is a sedimentary bedrock formation (Walloon Coal Measures) consisting of irregular beds of sandstone, siltstone, shale and coal, some of which contain significant volumes of groundwater. Duvert et al. (2015a,b) reported high Fe concentrations and low ^{3}H activities for some groundwaters of the sedimentary bedrock.

Hydraulic gradient analysis indicates that the alluvium mostly drains into the stream; hydrochemical and isotopic data also revealed a close connection between the alluvium and surface water in the Teviot Brook catchment (Duvert et al., 2015a). Borehole G1 is 13.9 m deep and it is screened from 12.3 m to its bottom, i.e. entirely within the alluvial stratum. The horizontal distance between G1 and S2 is 60 m.

7.2.2 Catchment hydrology

The monitoring period spans over two years, from mid-2012 to late 2014. Daily streamflow data were obtained from a gauging station operated by the Queensland Department of Natural Resources and Mines (Croftby station; 145011A) and located 2 km upstream of S2 (Figure 7.1). Daily precipitation data were available at three rain gauges spread across the catchment and operated by the Australian Bureau of Meteorology. Average precipitation was calculated from the three records using the Thiessen method. Annual precipitation amounted to 1010 mm in 2012, 1190 mm in 2013 and 960 mm in 2014. The rainfall depths recorded in the headwaters were 100 to 250 mm higher than those in the floodplain. The maximum daily rainfall amount was 275 mm and occurred in late January 2013, with a weekly value of 470 mm for this same event (Figure 7.2a). This intense episode of rainfall generated a daily peak flow of 137 $m^3 s^{-1}$ upstream of S2 (Figure 7.2b), which corresponds to a 22-yr return period event at that station – calculated by fitting long-term data to a Galton distribution. Earlier work has shown that this major event contributed significantly to recharge of the alluvial and bedrock aquifers in the headwaters (Duvert et al., 2015a,b). Another high flow event occurred in late March 2014, with a daily peak flow of 39 $m^3 s^{-1}$. Generally, examination of the hydrograph reveals that extended recession periods followed peak flows. Low flow conditions ($Q < 0.01\ m^3 s^{-1}$) occurred towards the end of the dry season, i.e. approximately from November through to January (Figure 7.2b). The stream did not dry up during the study period although very low flow ($Q < 0.001\ m^3 s^{-1}$) occurred for 30 consecutive days in February–March 2014.

7.3 Methods

7.3.1 Sample collection and analysis

Bulk samples of precipitation were collected at R1 (Figure 7.1) at fortnightly to monthly intervals using a Palmex RS1 rainfall collector, which allows virtually evaporation-free sampling (Gröning et al., 2012). Streamwater and groundwater samples were collected at S1 and S2 (stream sampling locations) and G1 (alluvial aquifer) following the same sampling design as the rainfall samples. Samples at G1 were taken after measuring the water table level and purging a minimum of three casing volumes with a stainless steel submersible pump (Hurricane XL, Proactive). All samples were filtered through 0.45 µm membrane filters, and

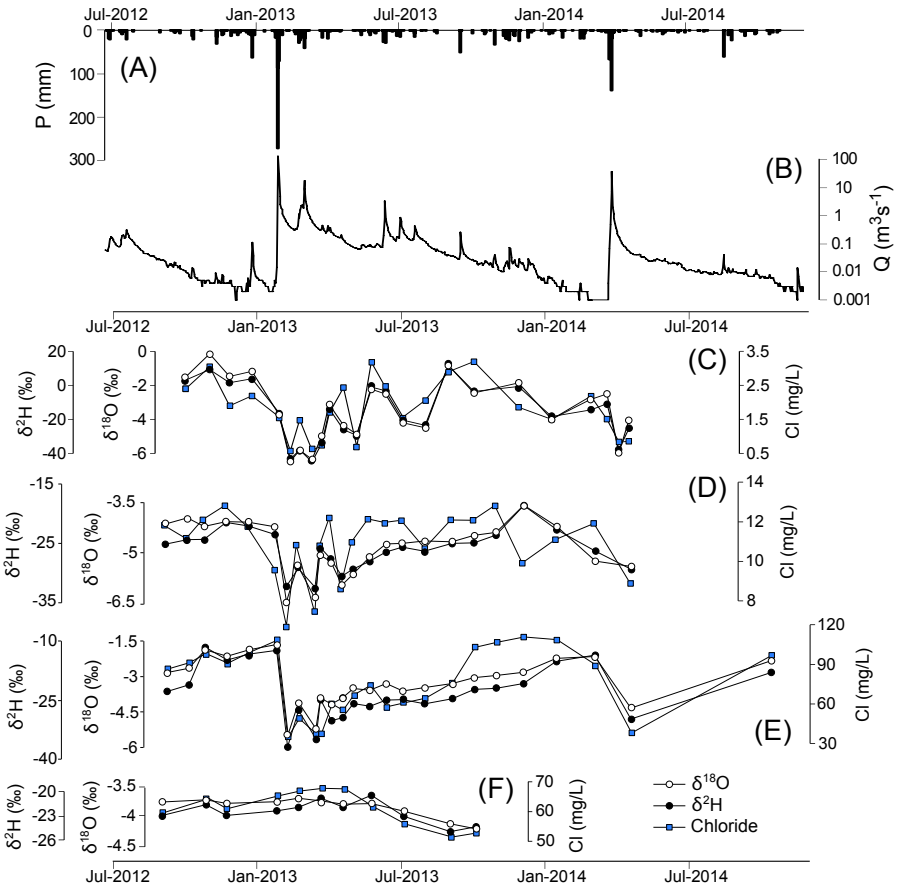

Figure 7.2: Time-series of Thiessen-averaged precipitation (a), daily discharge at Croftby (DNRM station 145011A) (b), and δ^2H, δ^{18}O and chloride at R1 (rainfall) (c), S1 (d) and S2 (streamwater) (e), and G1 (groundwater) (f). Note that the y-axes of δ^2H, δ^{18}O and chloride have different scales for each individual plot.

care was taken to seal the bottles and vials tightly to avoid evaporation.

Stable isotopes and chemical elements were measured for all samples at R1, S1, S2, and G1. ^{3}H activity was determined at S2 for most samples, and at G1 for one sample. Chloride concentrations were measured using ion chromatography (ICS-2100, Dionex), while iron and silicon were measured using inductively coupled plasma optical emission spectrometry (Optima 8300, Perkin Elmer). Total alkalinity was measured by titrating water samples with hydrochloric acid to a pH endpoint of 4.5. Major ions were assessed for accuracy by evaluating the charge balance error, which was $< 10\%$ for all samples and $< 5\%$ for 93% of the samples. Samples were also analysed for ^{2}H and ^{18}O, using a Los Gatos Research water isotope analyser (TIWA-45EP). All isotopic compositions in this study are expressed relative to the VSMOW-standard (δ notation). Between-sample memory effects were minimised by pre-running all samples and subsequently re-measuring them with decreasing isotopic ratios, as recommended in Penna et al. (2012). Replicate analyses indicate that analytical error was

±1.1‰ for δ^2H and ±0.3‰ for δ^{18}O. All these analyses were conducted at the Queensland University of Technology (QUT) in Brisbane. In addition, ^{3}H was analysed at the Australian Nuclear Science and Technology Organisation (ANSTO) in Sydney. Samples were distilled and electrolytically enriched 68-fold prior to counting with a liquid scintillation counter for several weeks. The limit of quantification was 0.05 tritium units (TU) for all samples, and uncertainty was ±0.06TU. A sample collected in August 2013 was excluded from the dataset since it was analysed twice and yielded inconsistent results.

7.3.2 Tracer-based calculation of transit and residence times

7.3.2.1 Using stable isotopes and chloride

Mean TTs were determined through adjustment of a TT distribution function to observations of fortnightly input and output signatures (here the term 'signature' is meant to encompass either an ionic concentration or an isotopic composition). An input recharge function was initially computed from the measured input data that accounts for loss due to evapotranspiration (e.g. Bergmann et al., 1986; Stewart and Thomas, 2008):

$$C_{\mathrm{r}}(t) = \frac{R(t)}{\overline{R}}(C_{\mathrm{p}}(t) - \overline{C_{\mathrm{r}}}) + \overline{C_{\mathrm{r}}} \tag{7.1}$$

where $C_{\mathrm{r}}(t)$ is the weighted input recharge signature at time t; $\overline{C_{\mathrm{r}}}$ is the average recharge signature (taken at G1); $C_{\mathrm{p}}(t)$ is the input rainfall signature; $R(t)$ is the fortnightly recharge as calculated by the difference between precipitation and evapotranspiration; and $\overline{R}$ is the average recharge amount.

The weighted input was then convoluted to the selected TT distribution function (g) to obtain output signatures (Maloszewski and Zuber, 1982):

$$C_{\mathrm{out}}(t) = [g * C_{\mathrm{r}}](t) = \int_0^\infty C_{\mathrm{r}}(t - t_e)\, g(t_e)\, e^{(-\lambda t_e)}\, dt_e \tag{7.2}$$

where t_e is time of entry; $C_{\mathrm{out}}(t)$ is the output signature; $C_{\mathrm{r}}(t)$ is the weighted input signature; $g(t_e)$ is an appropriate TT distribution function; and $e^{(-\lambda t_e)}$ is the term that accounts for decay if a radioactive tracer is used ($\lambda = 0$ for stable isotopes and chloride). In this study we used both the exponential and dispersion models; the reader is referred to Maloszewski and Zuber (1982) and Stewart and McDonnell (1991) for a detailed overview of TT distribution functions.

In some instances, two models were combined to represent more complex systems on the basis of our understanding of the catchment behaviour (Figure 7.3). This was to distinguish between a shallower and a deeper flow component with shorter and longer TT, respectively.

Bimodal models were obtained by linearly combining two TT distributions:

$$C_{\mathrm{out}}(t) = \phi \int_0^{\infty} C_{\mathrm{r}}(t-t_e)\, g_{\mathrm{o}}(t_e)\, e^{(-\lambda t_e)}\, dt_e + (1-\phi) \int_0^{\infty} C_{\mathrm{r}}(t-t_e)\, g_{\mathrm{y}}(t_e)\, e^{(-\lambda t_e)}\, dt_e \quad (7.3)$$

where ϕ is the fraction of the older component ($0<\phi<1$), and $g_{\mathrm{o}}(t_e)$ and $g_{\mathrm{y}}(t_e)$ are the TT distribution functions of the older and younger components, respectively (Figure 7.3). Bimodal distributions combined either two dispersion models or one exponential and one dispersion model. The mean TTs, noted τ, were then derived from the fitted distributions by calculating their first moment:

$$\tau = \int_0^{\infty} t\, g(t)\, dt \quad (7.4)$$

In the following the mean TT of the younger component is referred to as τ_{y} (subdivided into τ_{y1} and τ_{y2}), while the mean TT of the older component is referred to as τ_{o}, and the mean RT of storage groundwater is referred to as τ_{r} (subdivided into τ_{r1} and τ_{r2}) (Figure 7.3).

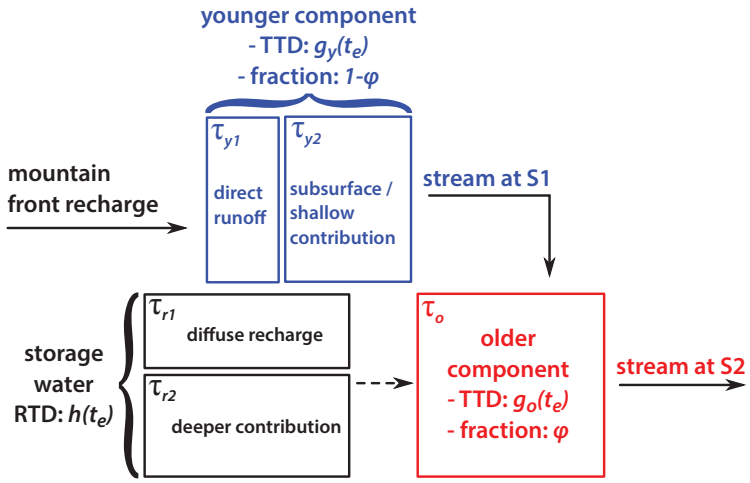

Figure 7.3: Conceptual diagram showing the flow components and their transit times to be characterised in this study.

For chloride, the measured input and output series were highly dissimilar due to the significant effect of evaporative enrichment in soils. To get around this issue, a correction factor was applied to the predictions obtained using equations 7.2 and 7.3: $C_{\mathrm{out}}(t)$ values were multiplied by $F = \frac{P}{(P-ET)}$ (i.e. ratio between precipitation and recharge over the preceding 12 months). The reasoning behind the use of this correction factor was that all chloride ions find their way through the soil, whereas much of the rainfall is evaporated off.

To estimate the fraction of older water that contributed to streamflow, a simple two-component hydrograph separation was carried out (Sklash and Farvolden, 1979) based on fortnightly data of each of the three seasonal tracers. This allowed obtaining time-varying

values of ϕ:

$$\phi(t) = \frac{\delta_{S1}(t) - \delta_{R1}(t)}{\overline{\delta_{G1}} - \delta_{R1}(t)} \tag{7.5}$$

where δ_{S1}, δ_{R1} and δ_{G1} are the tracer values of streamflow, rainfall and groundwater, respectively. The use of a chemical mass balance approach to partition streamflow was preferred over recursive digital filtering (Nathan and McMahon, 1990), because the former method is less likely to include delayed sources, such as bank return flow and/or interflow, in the older water component (Cartwright et al., 2014).

7.3.2.2 Using tritium

The occurrence of seasonal variations in rainfall ^{3}H concentrations has been widely documented (e.g. Stewart and Taylor, 1981; Tadros et al., 2014). These variations can be significant and have to be considered for achieving reliable estimates of TT distributions. Monthly ^{3}H precipitation data measured by ANSTO from bulk samples collected at Brisbane Aero were used to estimate the ^{3}H input function for the Teviot Brook catchment. Because Brisbane Aero is *ca.* 100 km northeast of Teviot Brook, the rainfall ^{3}H concentrations are likely to be significantly different between these two locations due to oceanic and altitudinal effects. According to Tadros et al. (2014), ^{3}H values for Toowoomba (i.e. located in the Great Dividing Range near Teviot Brook) were about 0.4 TU above those for Brisbane Aero for the period 2005–2011. Based on this work, an increment of +0.4 TU was applied to values measured at Brisbane Aero in order to obtain a first estimate of rainfall ^{3}H concentrations for Teviot Brook (input series A2 in Table 7.1). A second estimate was obtained by comparing the historical ^{3}H data between Toowoomba and Brisbane Aero for the period with overlap between the two stations, i.e. 1968–1982. All monthly values with precipitation > 100 mm, corresponding to rainfall likely contributing to recharge, were included in the analysis ($n = 31$). A scaling factor of 1.24 was derived from the correlation between the two stations ($R^2 = 0.80$). This factor was used to compute input series B2 (Table 7.1).

Table 7.1: Description of the different ^{3}H input series computed for the Teviot Brook catchment.

Input series	Description of input parameters
A1	A2 −25%
A2	Brisbane Aero ^{3}H values +0.4 TU
A3	A2 +25%
B1	B2 −90% CI slope
B2	Brisbane Aero ^{3}H values ×1.24 TU
B3	B2 +90% CI slope

CI refers to the confidence interval on the Toowoomba *vs* Brisbane Aero regression slope.

To account for losses due to evapotranspiration as rainfall infiltrates into the ground, a weighting procedure similar to the one reported by Stewart et al. (2007) was developed. Monthly ^{3}H recharge was estimated by subtracting monthly evapotranspiration from monthly precipitation, and weighting the ^{3}H rainfall concentrations by the resulting recharge. Instead of calculating single annual values, 6-month and 1-yr sliding windows were used to obtain monthly values as follows:

$$C_i = \frac{\sum_{i-t}^{i} C_j r_j}{\sum_{i-t}^{i} r_j} \tag{7.6}$$

where C_i is the monthly ^{3}H recharge for the i^{th} month, C_j and r_j are the monthly ^{3}H precipitation and monthly recharge rate for the j^{th} month, and t is 6 or 12 depending on the span of the sliding interval used. To avoid edge effects, a Tukey filter (Tukey, 1968) with coefficient 0.6 was applied to the sliding windows.

Input (recharge) and output (streamwater) ^{3}H concentrations were then related using the same convolution integral as the one used for stable isotopes (equations 7.2 and 7.3), with λ the ^{3}H decay constant such that $\lambda = 1.54 \cdot 10^{-4}\,\mathrm{d}^{-1}$. To account for the uncertainty in input parameters and to assess the sensitivity of TT distribution calculations to the input function, four additional input series were derived from A2 and B2 (Table 7.1), and all six input series were subsequently used in the calculations. Least square regressions were used, and root mean square errors (RMSE) were calculated to find the best data fit for each simulation using a trial and error process. All data processing and analyses were performed using Matlab version 8.4.0 (R2014b), with the Statistics toolbox version 9.1.

7.4 Results

7.4.1 Seasonal tracers in precipitation, streamwater and groundwater

Description. Stable isotope ratios and chloride signatures in precipitation were highly variable throughout the study period (Figures 7.2c; 7.4). The δ^2H and δ^{18}O rainfall values ranged between -41‰ to $+12$‰ (average -12‰) and -6.5‰ to -0.1‰ (average -3.1‰), respectively, while chloride concentrations ranged between 0.6 to 3.2 mg L^{-1} (average 1.8 mg L^{-1}). Generally, the most significant rainfall events had isotopically depleted signatures. As an example, there was a considerable drop in all tracers during the January 2013 event (e.g. for δ^2H: decrease from -16‰ to -41‰; Figure 7.2c). The local meteoric water line derived from rainfall samples had an intercept of 15.8 and a slope of 8.4 (Duvert et al., 2015a), similar to that of Brisbane (Figure 7.4a). The stable isotope ratios measured in streamwater at S1 (Figure 7.2d) and S2 (Figure 7.2e) also covered a wide range of values, and followed similar temporal patterns to those for rainfall. However, the overall variations were less pronounced in streamwater with evident dampening of input signals. Average val-

ues were lower for S1 (δ^2H = −25‰ and δ^{18}O = −4.9‰) than for S2 (δ^2H = −20‰ and δ^{18}O = −3.7‰), both locations having lower average values than rainfall. All S1 samples aligned close to the meteoric water line, whereas most S2 samples plotted along a linear trend to the right of the line (Figure 7.4a). Chloride concentrations in streamwater ranged between 6.4 and 12.8 mg L^{-1} at S1, and between 35.1 and 111.1 mg L^{-1} at S2 (Figures 7.2d; 7.2e; 7.4b). At S2, higher chloride values were consistent with higher δ^{18}O values and *vice versa*, whereas there was a weaker correlation between the two tracers at S1 (Figure 7.4b). The fluctuations in stable isotopes and chloride in groundwater were considerably attenuated as compared to rain and streamwater (Figures 7.2f; 7.4). The δ^2H, δ^{18}O and chloride values recorded at G1 tended to slightly decrease during the rainy season, although they stayed within the ranges −22 ± 3‰, −3.9 ± 0.4‰ and 60 ± 10 mg L^{-1}, respectively (Figure 7.2f). Consistent displacement to the right of the meteoric line was observed for all G1 samples (Figure 7.4a).

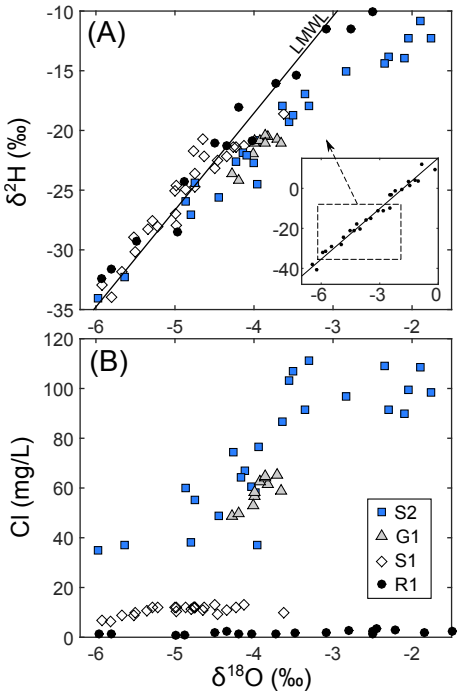

Figure 7.4: Relationships between (a) δ^2H and δ^{18}O and (b) chloride and δ^{18}O for rainfall, streamwater and groundwater of the Teviot Brook catchment. The local meteoric water line plotted in (a) follows the equation $\delta^2\text{H} = 8.4 \cdot \delta^{18}\text{O} + 15.8$ (Duvert et al., 2015a).

Interpretation. The large temporal variability observed in rainfall isotopic and chloride records (Figure 7.2c) may be attributed to a combination of factors. First, there was an apparent seasonal cycle as values were higher in the dry season and tended to decrease during the wet season. These are well-known features for rainfall that can be related to the 'amount effect' (Dansgaard, 1964) where raindrops during drier periods experience partial evaporation below the cloud base, typical in tropical to subtropical areas (Rozanski et al.,

1993). Second, more abrupt depletions of ^{2}H and ^{18}O occurred during significant precipitation events (Figure 7.2c), as has been reported in other parts of eastern Australia (Hughes and Crawford, 2013; King et al., 2015). In streamwater, isotopic ratios were generally lower for S1 and S2 than for rainfall, which most likely reflects the predominant contribution of depleted rainfall to recharge (Duvert et al., 2015a). Also, the position of S1 and S2 samples relative to the meteoric line (Figure 7.4a) indicates that fractionation due to evaporation occurred at S2, because unlike those measured at S1, isotopic ratios measured at S2 followed a clear evaporation trend. Elevated chloride concentrations are further evidence of the occurrence of evaporative enrichment downstream, with values one order of magnitude higher at S2 than at S1 (Figure 7.4b). These results are in line with field observations, showing that the streambed at S2 featured a gentler slope and that lateral inflows from evaporation-prone tributaries may have contributed to streamflow at this location. It can also be noted that the enrichment of chloride at S2 was much higher than that of stable isotopes (Figure 7.4b). This is a common observation in Australian catchments, largely attributed to high rates of evapotranspiration that concentrate cyclic salts in the unsaturated zone, thereby increasing the salinity of subsurface water before it discharges into streams (e.g. Allison et al., 1990; Cartwright et al., 2004; Bennetts et al., 2006).

7.4.2 Tritium in precipitation, streamwater and groundwater

Description. The groundwater sample collected at G1 in October 2012 yielded a ^{3}H activity of 1.07 ± 0.06 TU. Additional data was obtained from Please et al. (1997), who collected a sample at the same location in 1994. This earlier sample had an activity of 1.80 ± 0.20 TU. The 20 samples of streamwater collected at S2 showed variable ^{3}H activities ranging between 1.16 ± 0.06 TU and 1.43 ± 0.06 TU (Figure 7.5).

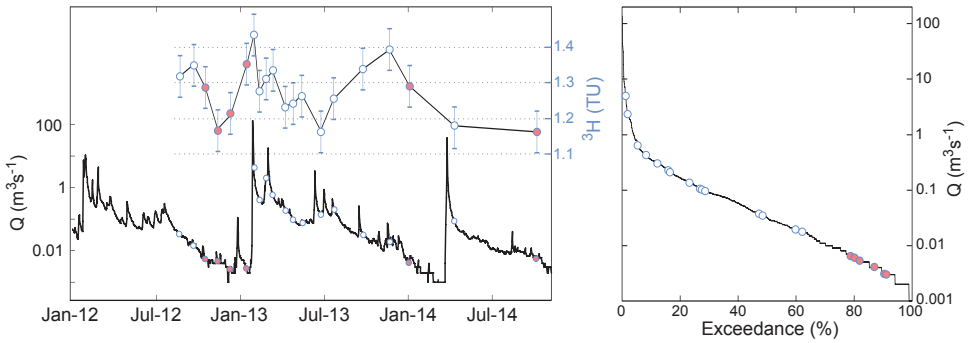

Figure 7.5: Time-series of ^{3}H activity at S2 and daily discharge data (left). Flow duration curve at S2 (right). The six red circles correspond to samples used to fit the low baseflow model (see Figure 7.9). The whiskers correspond to measurement uncertainty (±0.06 TU for all samples).

In order to estimate a ^{3}H input signal for the Teviot Brook catchment, several precipitation time-series were calculated from Brisbane Aero monthly ^{3}H dataset, as detailed in Table 7.1. Recharge time-series were then derived from these precipitation time-series using

equation 7.6. An example of the calculated monthly precipitation and recharge time-series for the 2003–2014 period is presented in Figure 7.6 for scenario A2. While the ^{3}H activity in rainfall ranged between 1.1 and 6.4 TU for A2, most of the rainfall events contributing to recharge (i.e. for which monthly precipitation prevailed over monthly evapotranspiration; red circles in Figure 7.6) remained in the narrower range 1.5–2.5 TU.

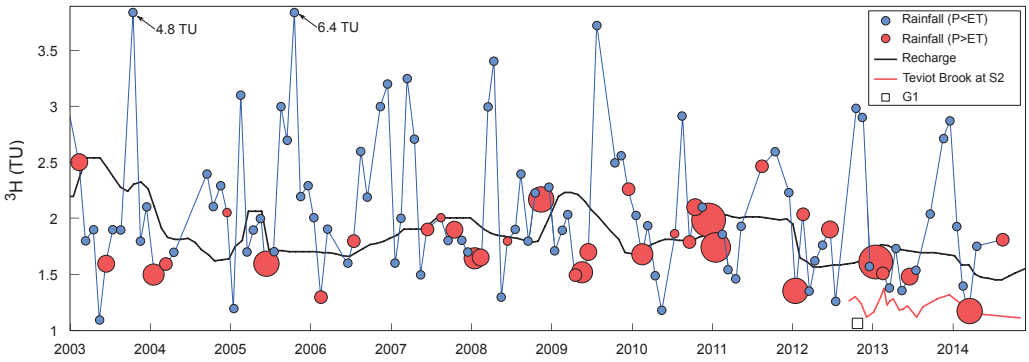

Figure 7.6: Temporal evolution of input ^{3}H in precipitation (circles) and recharge (black line) for the Teviot Brook catchment considering the A2 scenario. The plotted circles correspond to rainfall collected at Brisbane Aero and adjusted to Teviot Brook according to A2. The recharge time-series was obtained using equation 7.6 and a 12-month sliding window. The marker size for rainfall contributing to recharge (red circles) reflects the recharge rate.

Interpretation. The ^{3}H activity in rainfall showed considerable month-to-month variability. Winter (dry season) values generally were higher than summer (wet season) values, consistent with results from Tadros et al. (2014). Among the 20 ^{3}H values obtained at S2, higher values tended to coincide with higher flow conditions, although it was not systematic (Figure 7.5). For instance, the sample collected in January 2013 under low flow conditions yielded 1.35 ± 0.06 TU; by contrast, the sample collected in April 2014 during the falling limb of a major runoff event yielded 1.19 ± 0.06 TU, i.e. among the lowest values on record. Kendall's rank correlation and Pearson's coefficients were calculated between the ^{3}H measurements in streamwater and other hydrological, hydrochemical and isotopic variables (Table 7.2). ^{3}H activity was not significantly correlated with any of the other variables. Unlike in Morgenstern et al. (2010) and Cartwright and Morgenstern (2015), there was no strong linear relationship between flow rate and ^{3}H activity in the stream. The lack of strong correlation between ^{3}H and variables such as antecedent wetness conditions and the number of days since the last high flow event occurred, implies that more complex mechanisms governed the short-term fluctuations of ^{3}H in streamwater.

7.4.3 Residence time estimate for storage water

The sample collected at G1 in October 2012 ($^3\text{H} = 1.07 \pm 0.06$TU) suggests that alluvial groundwater contains a substantial modern component, because its ^{3}H concentration was only slightly below that of modern rainfall. An earlier ^{3}H value reported by Please et al.

Table 7.2: Kendall's τ and Pearson's r correlation coefficients between ^{3}H and other variables at S2.

Variable	r	τ
Mean daily discharge ($m^3\,s^{-1}$)	0.47	0.06
δ^2H (‰)	−0.27	−0.06
δ^{18}O (‰)	−0.23	0.02
Cl ($mg\,L^{-1}$)	−0.12	0.03
Si ($mg\,L^{-1}$)	0.35	0.11
Alkalinity ($mg\,L^{-1}$)	−0.32	−0.13
Fe ($mg\,L^{-1}$)	0.25	0.11
Antecedent P in the last 15 days (mm)	0.32	−0.01
Last day with $P > 2$ mm (–)	0.11	0.03

No value was statistically significant at $p < 0.05$ for both tests.

(1997) was re-interpreted and combined with our more recent measurement to provide additional constraints on the RT at G1. Two steady-state models were adjusted to the data points. The first model to be tested was a unimodal dispersion model while the second one was a bimodal exponential–dispersion model. For the bimodal model, the mean RT of younger components τ_{r1} was constrained to 1 yr, and the fraction of younger water was constrained to 57% as these parameters provided best fits on average.

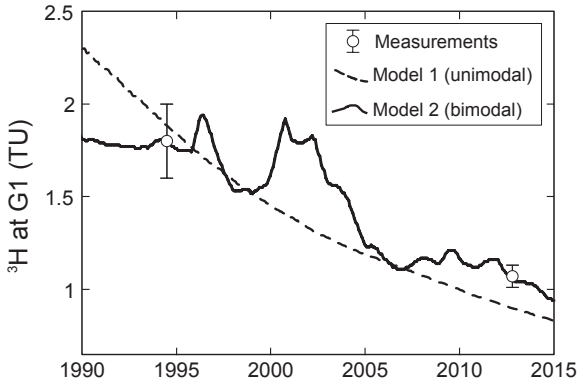

Figure 7.7: Fits of two models at G1 using A2 as input ^{3}H series. The unimodal model is a dispersion model with first moment 48.2 yr and dispersion parameter 0.71. The bimodal model is an exponential–dispersion model: a younger component (exponential distribution; fraction 57%) with first moment 1 yr and an older component (dispersion distribution; fraction 43%) with first moment 82.9 yr and dispersion parameter 0.30. The 1994 measurement is from Please et al. (1997).

Results for both models are presented in Table 7.3 and the two fits using A2 as an input function are shown in Figure 7.7. As expected, mean RTs varied as a function of the input function chosen: values were generally lowest with A1 and B1 and highest with B3. Both models provided reasonably good fits, although for all simulations the bimodal distri-

Table 7.3: Results of model simulations of residence time for G1 using ^{3}H.

	Unimodal DM			Bimodal EM–DM			
Input series	τ_r (yr)	D_P	RMSE (TU)	τ_{r1} (yr)	τ_{r2} (yr)	D_P	RMSE (TU)
A1	46.9	0.70	±0.19	1	75.8	0.29	±0.02
A2	48.2	0.71	±0.18	1	82.9	0.30	±0.01
A3	39.8	0.71	±0.18	1	89.0	0.28	±0.03
B1	48.5	0.69	±0.22	1	86.8	0.30	±0.06
B2	61.6	0.70	±0.20	1	95.0	0.29	±0.05
B3	54.6	0.69	±0.21	1	102.5	0.29	±0.05

DM stands for dispersion model; EM–DM stands for exponential–dispersion model; D_P stands for dispersion parameter. For the EM–DM, τ_{r1} was constrained to 1 yr, and the fraction of younger water was constrained to 57%.

bution described more accurately the measured data (median RMSE 0.04 TU *vs.* 0.20 TU; Table 7.3). Unimodal distributions had τ_r ranging between 40 (using A3 as input series) and 62 yr (using B2 as input series), with a standard deviation of 7 yr among all simulations. The older water fraction of bimodal models had τ_{r2} between 76 (using A1 as input series) and 102 yr (using B3 as input series), with a standard deviation of 9 yr.

7.4.4 Transit time estimates using seasonal tracers

Lumped parameter models were adjusted to the stable isotope and chloride time-series at S1. Due to the limited number of fortnightly data, all values were included in the analysis, i.e. samples collected under both low baseflow and higher flow conditions. Two models were tested and compared for this purpose, a unimodal exponential model and a bimodal exponential–dispersion model (Table 7.4; Figure 7.8).

While both models provided reasonably low RMSE, unimodal models were less successful in capturing the high-frequency variations observed in output measurements (e.g. lowest values in late January and late February 2013; blue lines in Figure 7.8). All three tracers yielded comparable exponential TT distribution functions, with τ_y ranging between 65 and 70 days (Table 7.4). The bimodal models provided slightly more satisfactory fits for all tracers (black lines in Figure 7.8), with lower RMSE overall. Bimodal TT distribution functions derived from data at S1 had a younger fraction (27%) with τ_{y1} between 14 and 16 days, and an older fraction (73%) with τ_{y2} between 113 and 146 days (Table 7.4) depending on which tracer was used.

Calibration was also carried out on the tracer time-series collected at S2 and following the same procedure (Table 7.4). When considering a unimodal exponential distribution, all three tracers yielded comparable TT distribution functions, with τ_y ranging between 71 and

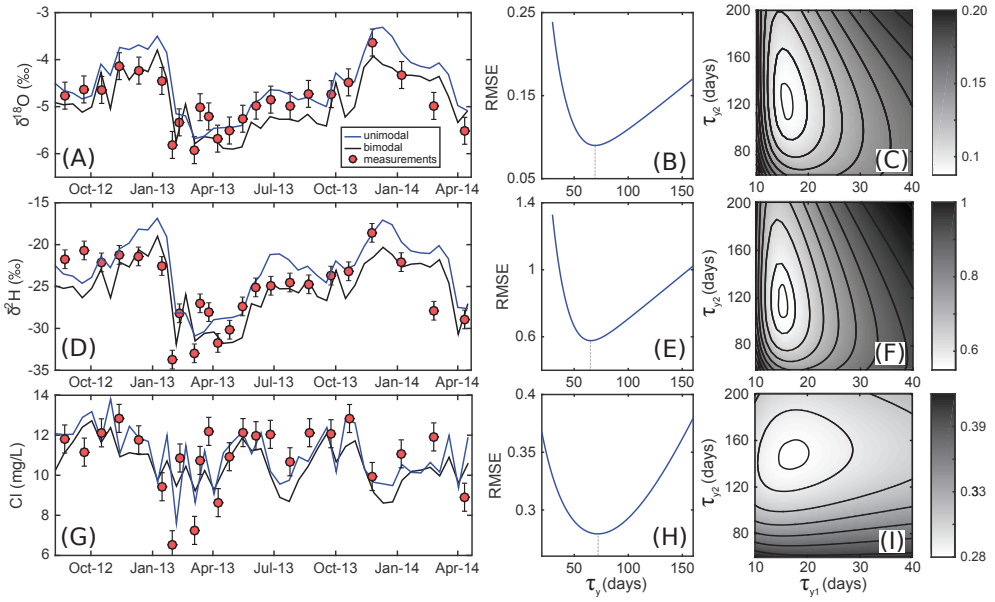

Figure 7.8: Exponential (blue) and exponential–dispersion (black) models calibrated to the δ^{18}O (a), δ^{2}H (d) and chloride (g) time-series at S1. Whiskers correspond to the measurement uncertainty as given in the Methods section. Root mean square errors (RMSE) of the exponential model as a function of τ_y for the three tracers (b, e, h). RMSE of the exponential–dispersion model (27% younger component; dispersion parameter 0.3) as a function of mean transit times of the younger (τ_{y1}) and older (τ_{y2}) fractions for the three tracers (c, f and i). Lighter colours are for lower RMSE, and the smallest contours correspond to the range of acceptable fit, arbitrarily defined as the values for which the RMSE are lower than the lowest RMSE obtained with the exponential models. Results for these simulations are reported in Table 7.4.

85 days, which was slightly longer than the mean TTs calculated at S1. When considering a bimodal exponential–dispersion distribution, the younger fraction had τ_{y1} of 23 to 24 days while the older fraction had τ_{y2} of 99 to 109 days (Table 7.4).

7.4.5 Transit time estimates using tritium

7.4.5.1 Model adjustment to low baseflow samples

A lumped parameter model was fitted to the six ^{3}H samples that were taken under low baseflow conditions, i.e. $Q < 0.01\,\mathrm{m^3\,s^{-1}}$. The model chosen for this purpose was a bimodal exponential–dispersion model; the fitting procedure was as follows:

- The dispersion parameter of the older component was loosely constrained to around 0.3 in order to mimic the shape of the TT distribution identified at G1 (Section 7.4.3). The old water fraction ϕ was constrained to 82%, i.e. the average value obtained for the six baseflow samples using tracer-based hydrograph separation following equation 7.5.
- Initial simulations were run using the six input series with no further model constraint. For the six scenarios, τ_y consistently converged to 0.33 ± 0.08 yr.
- All models were then re-run while adding the additional constraint as noted above, so that the only parameter to be determined by fitting was τ_o.

Table 7.4: Results of model simulations of transit time for S1 and S2 using ^{2}H, ^{18}O and chloride.

		Unimodal EM		Bimodal EM–DM		
Sampling location	Tracer	τ_y (days)	RMSE	τ_{y1} (days)	τ_{y2} (days)	RMSE
S1	δ^{18}O	69	±0.09‰	15	121	±0.08‰
	δ^{2}H	65	±0.58‰	15	113	±0.52‰
	chloride	70	±0.28 mg L^{-1}	16	146	±0.26 mg L^{-1}
S2	δ^{18}O	85	±0.16‰	23	109	±0.16‰
	δ^{2}H	71	±0.75‰	24	99	±0.72‰
	chloride	76	±4.89 mg L^{-1}	24	106	±4.68 mg L^{-1}

EM stands for exponential model; EM–DM stands for exponential–dispersion model. For the EM–DM, the dispersion parameter of the second mode was 0.3 and the fraction of younger water was 27%.

Figure 7.9 provides an example of the adjustment using A2 as input ^{3}H function. Reasonably good fits were obtained for all simulations (0.14 TU < RMSE < 0.16 TU), with τ_o between 15.8 and 24.5 yr, average 20.1 ± 3.9 yr (Table 7.5).

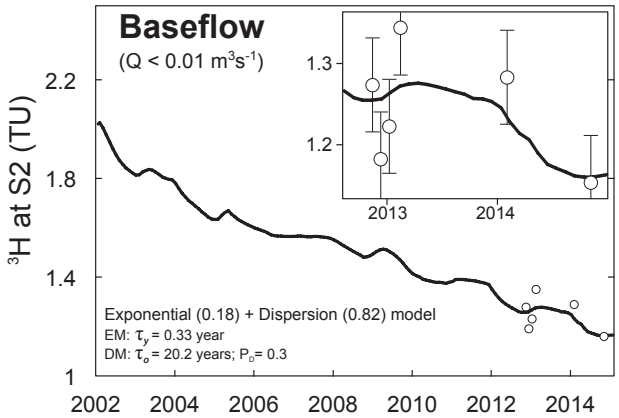

Figure 7.9: Bimodal model fitted to the ^{3}H activities at S2 under low baseflow conditions (i.e. daily $Q < 0.01\,\mathrm{m^3\,s^{-1}}$). A2 was used as input ^{3}H series for this case. Results using other input series are listed in Table 7.5.

7.4.5.2 Model adjustment to single tritium values

Unlike for rainfall ^{3}H values where high temporal variability was observed, the derived time-series for recharge was relatively constant over the last decade (Figure 7.6). This characteristic in principle allows reliable assessment of catchment TTs with single ^{3}H measurements, providing the ^{3}H remaining in the hydrosphere is too small to cause ambiguous ages, as it is in the southern hemisphere (Morgenstern et al., 2010; Stewart et al., 2010). All 20 samples collected at S2 were fitted separately using the same lumped model for each point, so that the only parameter to be determined by fitting was the TT of the old water

Table 7.5: Results of model simulations of transit time for S2 under low baseflow conditions (i.e. daily $Q < 0.01\,m^3\,s^{-1}$), using ^3H and an exponential–dispersion model.

Input series	τ_o (yr)	RMSE (TU)
A1	15.8	±0.15
A2	20.2	±0.15
A3	24.5	±0.15
B1	15.8	±0.14
B2	19.8	±0.16
B3	24.4	±0.16

The mean TT of younger components (τ_y) was constrained to 0.33 yr, the dispersion parameter of older components was constrained to 0.3, and the ratio of older water was constrained to 82%.

fraction (τ_o). The model parameters were chosen according to the best fit obtained for baseflow samples (i.e. mean TT of young component τ_y 0.33 yr, dispersion parameter of old component 0.3; Section 7.4.5.1). In addition, for each sample the fraction of old water ϕ was constrained to the value obtained using tracer-based hydrograph separation according to equation 7.5. Conceptually, this approach appeared more meaningful than another option that would have consisted in constraining τ_o and subsequently determining the old water fractions ϕ, because there was no indication that τ_o remained constant over time. Simulations were carried out for all three hydrograph separation tracers and all six input series, and the sensitivity of simulations to both the ^3H measurement uncertainty (±0.06 TU) and the error related to the hydrograph separation procedure were also calculated.

Time-series of τ_o were derived for each input function, and Figure 7.10 shows the results obtained with A2 as an input series. The old water fraction ϕ varied between 0.39 and 1, and while there was a good agreement between the three tracers, hydrograph separation based on chloride generally yielded lower variations in ϕ over time (Figure 7.10a). Generally, the older component was lowest during high flow conditions and greatest during recession periods. The simulated τ_o values varied considerably over time, and variations exceeded the uncertainties related to measurement uncertainties, chemical mass balance calculation errors and input estimates (Figures 7.10b; 7.10c; 7.10d). ^{18}O was the least accurate in evaluating the variations in τ_o (wider range for the red shaded area in Figure 7.10c), while chloride was the most accurate despite less pronounced τ_o variations (narrower range for the red shaded area in Figure 7.10d). Yet, all three tracers provided comparable results, with a consistent shift in values either upwards or downwards. As a general rule, there was a negative correlation between ϕ and τ_o. When using A2 as input function, τ_o fluctuated between 11.9 and 58.0 yr (^2H; Figure 7.10b), 11.6 and 63.2 yr (^{18}O; Figure 7.10c) and 11.5 and 42.1 yr (chloride; Figure 7.10d). For clarity purposes the τ_o values reported in the text do not consider errors related to measurement uncertainty. Values were highest after the

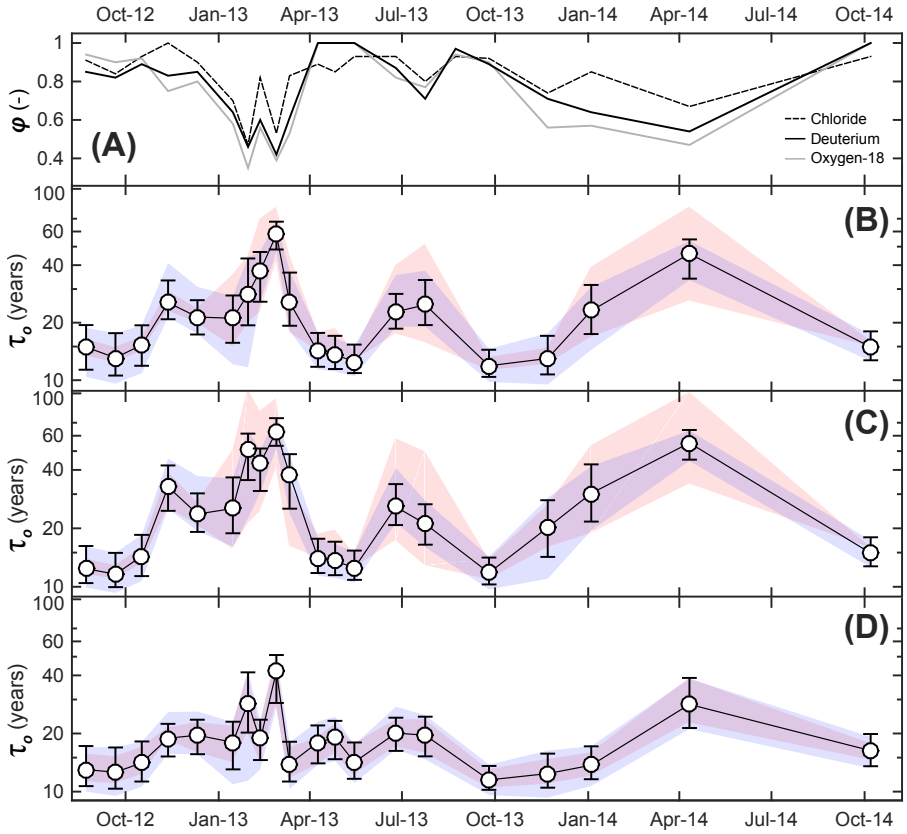

Figure 7.10: Variations in the older component fraction ϕ according to the three seasonal tracers (using equation 7.5) (a). Variations in the TT of older fraction τ_o at S2 based on hydrograph separation using ^{2}H (b), ^{18}O (c) and chloride (d). Values in (b), (c) and (d) were obtained through the adjustment of exponential–dispersion models to each ^{3}H sample separately, and using A2 as input series and a 12-month sliding window. Whiskers represent the error range due to the measurement uncertainty on each sample (i.e. ±0.06 TU). The blue shaded areas represent the range of values due to uncertainties in the estimation of recharge input (i.e. for the six ^{3}H input time-series), while the red shaded areas represent the range of error related to the calculation of ϕ, which was estimated according to the method described in Genereux (1998) and propagated to the calculation of τ_o.

major recharge events that occurred in January and February 2013, with τ_o between 26.8 and 63.2 yr in late February, and in April 2014, with τ_o between 28.3 and 55.1 yr. They were lowest during periods undergoing sustained low flow such as in September 2012 (τ_o between 11.6 yr for ^{18}O and 13.1 yr for ^{2}H) and in September 2013 (τ_o between 11.5 yr for chloride and 11.9 yr for ^{2}H). Of note is the timing of the highest τ_o value in late February 2013, i.e. one month after the major recharge episode.

7.5 Discussion

7.5.1 Conceptual framework

According to our conceptual understanding of the upper Teviot Brook catchment, we have partitioned streamflow into two major components (Figure 7.3). The first end-member represents the contribution of younger waters from rapid recharge through the highly frac-

tured igneous rocks forming the mountain front, as outlined in previous studies (Duvert et al., 2015a,b). This younger component was further divided into (i) quick flow and (ii) relatively delayed contribution of waters seeping from the rock fractures (Figure 7.3). We assume that the TTs of the younger end-member can be accurately described through analysis of the seasonal tracers' signal dampening. Waters originating from this component typically had low total dissolved solid (TDS) concentrations, although high Si concentrations at high flow.

The second end-member we postulate contains older waters derived from the aquifer stores located in the lowland section of the study area (Figure 7.3). Specifically, these are waters discharging from both the alluvial aquifer and the underlying sedimentary bedrock aquifer. Although a distinction between the two groundwater stores would be ideal, the lack of clear differentiation between both water types led us to consider one single "older water" component. We assume that the TTs of the older end-member may be accurately described through ^{3}H data analysis. The ^{3}H activities in both aquifers were generally lower than those in surface water; the sedimentary bedrock aquifer had on average lower ^{3}H values than the alluvial aquifer, and waters from both aquifers had varying but generally high TDS concentrations (Duvert et al., 2015a). Furthermore, higher Fe concentrations were observed in the sedimentary bedrock waters shortly after recharge (Duvert et al., 2015b).

In the next sections of the Discussion, a stepwise approach is followed to evaluate the accuracy of the conceptual model outlined above. In particular, the younger and older components in streamflow are assessed and discussed in Sections 7.5.2 and 7.5.3, respectively. Section 7.5.4 considers the relationships between the older streamflow component and groundwater stored in the catchment. The variations over time of the TTs of the older component τ_o are then quantified and elucidated (Section 7.5.5). Lastly, Section 7.5.6 addresses the limitations of the current methodology and raises new questions for future research.

7.5.2 Identification of a younger component in streamflow

The younger end-member was defined by adjusting lumped models to the seasonal tracer time-series (Section 7.4.4; Figure 7.8). Among all the TT distributions described in the literature, the exponential model was selected because it considers all possible flowpaths to the stream – the shortest flowpath having a TT equal to zero and the longest having a TT equal to infinity (e.g. Stewart et al., 2010). Importantly, this distribution assumes heavy weighting of short flowpaths, which in our case may accurately replicate the prompt response of streamflow to rainfall inputs in the headwaters.

At S1, the bimodal distribution provided the most accurate simulations (Table 7.4), which lends support to the occurrence of two end-members contributing to streamflow at

this upstream location. The first (exponential) component may reflect quick flow and subsurface waters feeding the stream (τ_{y1} between 14 and 16 days), while the second (dispersion) component may be attributed to the contribution of waters discharging from the highly fractured igneous rocks (τ_{y2} between 113 and 146 days; Figure 7.8). Results at S2 were also slightly more accurate when using a bimodal distribution, suggesting a dual contribution to streamflow at S2 as well. More importantly, the fits for S2 were not as accurate as those for S1, regardless of the distribution and tracer used (Table 7.4). This reflects the likely importance of other concurrent processes in the downstream section of the catchment. Among them, evaporation may be a major limitation to applying steady-state lumped models at S2. It has been reported that ^{18}O is generally more sensitive to the effects of evaporation than ^{2}H (Klaus and McDonnell, 2013; Klaus et al., 2015b). However, in this study there were no significant differences between TT distributions derived from the two stable isotopes. Calibration of the models on chloride measurements did not yield as accurate results as those for stable isotopes at S1 and to a higher extent at S2, which may be attributed to the higher effects of evaporative enrichment on chloride. Based on flux tracking methods, Hrachowitz et al. (2013) showed that processes such as evaporation can result in considerable biases in TT distribution estimates when using chloride as a tracer.

It is increasingly recognised that stable isotopes cannot provide realistic estimates of longer TT waters, regardless of the lumped model used (Stewart et al., 2012; Seeger and Weiler, 2014; Kirchner, 2015). In this study, it is very likely that older water (i.e. $> 5\,yr$) contributed to streamflow at S2 (see Section 7.5.3) but also possibly at S1, and only using stable isotopes and chloride does not allow detection of such contribution. Therefore the ages defined above should be regarded as partial TTs that reflect the short-term and/or intermediate portions of the overall TT distribution for the system, i.e. τ_y rather than τ (Seeger and Weiler, 2014).

7.5.3 Identification of an older component in streamflow

The transfer function that provided the most accurate estimates of TT for the baseflow samples at S2 was an exponential–dispersion model (Section 7.4.5.1). While other distributions could have been tested, there is a large body of literature that has reported good agreement between exponential, exponential-piston flow and dispersion models calibrated to ^{3}H data (e.g. Maloszewski et al., 1992; Herrmann et al., 1999; Stewart et al., 2007; Cartwright and Morgenstern, 2015). The good fits obtained using this bimodal function (Figure 7.9; Table 7.5) confirm that two major water sources contributed to streamflow at S2. It can be argued that the exponential component captured all young contributions from upstream, i.e. quick flow + soil water + discharge from fractured igneous rocks, as identified in Section 7.5.2 ($\tau_y = 0.33\,yr$), while the dispersion component encompassed the delayed groundwater flowpaths (τ_o between 15.8 and 24.5 yr). This older contribution to stream-

flow may originate from the alluvial aquifer, potentially supplemented by seepage from the bedrock storage, as discussed in Section 7.5.1.

A number of studies were carried out in the last four decades that also used ^{3}H to assess TTs of the baseflow component to streams. For catchment areas in the range 10–200 km^2, TT estimates were between 3 to 157 yr (n = 39; median 12 yr; data presented in Stewart et al. (2010) supplemented with later papers by Morgenstern et al. (2010), Kralik et al. (2014) and Cartwright and Morgenstern (2015)). While our results compare relatively well to the literature, estimates can vary greatly even within single catchments (e.g. Morgenstern et al., 2010). Also, all reported studies were conducted in temperate regions, this work being the first one carried out in a subtropical setting.

7.5.4 Storage water and its relationships with the older streamflow component

Simulations of groundwater RT using ^{3}H as a tracer are generally insensitive to the type of lumped parameter model chosen, given that ambient ^{3}H levels are now almost at pre-bomb levels (e.g. Stewart and Thomas, 2008). At G1, better fits were obtained for bimodal functions (Figure 7.7; Table 7.3). This may be interpreted as the probable partitioning of groundwater into one contribution of younger waters by diffuse recharge or flood-derived recharge ($\tau_{r1} \approx 1$ yr) coupled with a second contribution of older waters, potentially seeping from the underlying sedimentary bedrock aquifer ($\tau_{r2} \approx 80$ to 100 yr).

While the older component to streamflow as identified in Section 7.5.3 was characterised by relatively old waters with TT in the range $15.8 - 24.5$ yr, this contribution could not be directly related to the RT of storage waters (i.e. $\tau_o \neq \tau_r$). Despite the exclusive use of samples taken under low baseflow conditions to determine τ_o, the obtained values were significantly lower than the estimates of τ_{r2} for the alluvial aquifer (average 20.1 ± 3.9 yr *vs.* 88.7 ± 9.3 yr, respectively). This confirms that water stored in the catchment (resident water) and water exiting the catchment (transit water) are fundamentally different and do not necessarily follow the same variations, as recognised in recent work (e.g. Hrachowitz et al., 2013; van der Velde et al., 2015). Results from a dynamic model of chloride transport revealed that water in transit was generally younger than storage water (Benettin et al., 2015). Differences between RTs and TTs also indicate that the assumption of complete mixing was not met for the Teviot Brook catchment. This corroborates the findings from van der Velde et al. (2015), who established that complete mixing scenarios resulted in incorrect TT estimates for a catchment subjected to high seasonal rainfall variability. For instance, shallow flowpaths may be activated or deactivated under varying storage. Among the few studies that investigated the relations between catchment TT and groundwater RT based on ^{3}H measurements, Matsutani et al. (1993) reported that streamwater was formed by a mixture of longer RT groundwater (19 yr) and shorter RT soil water (< 1 yr). Overall, more work is needed to better define the two distributions and to assess how they relate to

each other under non-stationary storage conditions.

7.5.5 Drivers of the variability in the older component transit time

When fitting models to each ^{3}H value in streamwater, τ_o was found to vary substantially over time (Figure 7.10). In order to better apprehend the factors influencing the variations in τ_o, the obtained values were compared to other hydrological and hydrochemical variables, particularly the antecedent wetness conditions, dissolved Fe concentrations and the old water discharge rate (Figure 7.11). Under sustained dry conditions ($P_{15} < 5$ mm), there was no consistent relationship between τ_o and the amount of precipitation during the 15 days prior to sampling, with τ_o ranging between 14.9 and 23.1 yr ($n = 3$; Figure 7.11a). For higher values of P_{15} (i.e. $P_{15} \geq 10$ mm), there was a positive correlation between the two variables ($n = 17$, R^2 for power law fit = 0.47, p-value = 0.002). The TT of the old water fraction was lowest for P_{15} between 10 and 50 mm (τ_o 11.9 to 25.5 yr), and it increased when antecedent precipitation increased (τ_o 25.6 to 58.0 yr for $P_{15} > 100$ mm). Generally, values averaged 17.0 ± 5.6 yr at low flow and 38.3 ± 14.7 yr after major high flow events. This was in accordance with results from Figure 7.10, and suggestive of the predominant contribution of older alluvial and/or bedrock waters shortly after recharge episodes.

There was also a positive relationship between τ_o and Fe concentrations at S2 ($n = 20$, R^2 for power law fit = 0.48, p-value = 0.001), with all the values > 0.2 mg L^{-1} corresponding to $\tau_o > 30$ yr (Figure 7.11b). In contrast, no significant relationship was observed at S1, as Fe values at this station ranged between < 0.01 to 0.96 mg L^{-1}. Duvert et al. (2015b) reported increasing Fe concentrations after a major recharge event for some groundwaters of the sedimentary bedrock. The increase in streamflow Fe might therefore be a result of enhanced discharge of these waters into the drainage network, which is coherent with older τ_o values. However, other chemical parameters distinctive of the bedrock groundwaters did not produce a characteristic signature in streamflow during high flow conditions. Or else, high Fe concentrations may be simply due to higher weathering rates at higher flows, although this hypothesis disregards the high value measured for the April 2014 sample (Fe = 4.15 mg L^{-1}) despite relatively low discharge ($Q = 0.095$ m^3 s^{-1}).

As discussed previously, a modification in storage due to a change in recharge dynamics may have activated different groundwater flowpaths and hence water parcels with different RTs (Heidbüchel et al., 2013; van der Velde et al., 2015; Cartwright and Morgenstern, 2015). When the rate of recharge was highest, flushing out of waters located in the deeper, older bedrock aquifer may have been triggered by the resulting pressure wave propagation. By contrast, the relatively younger τ_o observed during lower flow conditions may be attributed to waters that originate from shallower parts of the alluvium and/or from subsurface layers. This is reflected in the relationship between τ_o and Q_o, i.e. the portion of streamflow provided by the older component ($Q_o = Q \cdot \phi$; Figure 7.11c). In this figure the groundwater end-

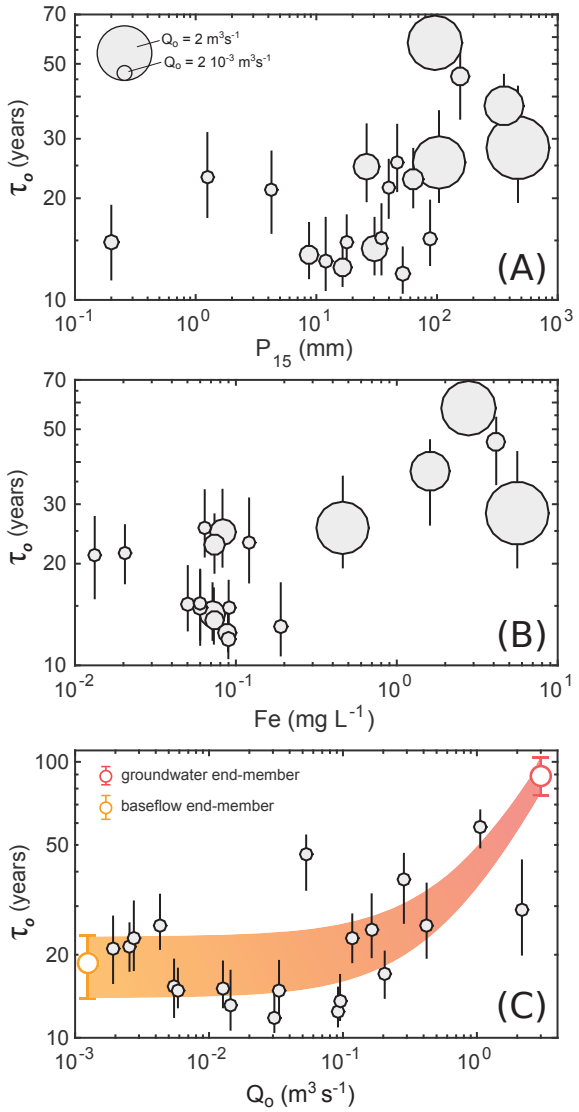

Figure 7.11: Relationship between the transit time of old water fraction (τ_o) and antecedent precipitation P_{15}, i.e. precipitation depth over the catchment during the 15 days prior to sampling (a). Relationship between τ_o and dissolved Fe concentrations (b). Relationship between τ_o and Q_o ($Q_o = Q \cdot \phi$) (c). Values were obtained using A2 as input series and ^{2}H as a hydrograph separation tracer. Whiskers correspond to simulations using upper and lower measurement uncertainty errors. The size of markers in (a) and (b) provides an indication on the value of Q_o during sampling. In (c), the groundwater (red) end-member corresponds to the RT calculated at G1, while the baseflow (orange) end-member corresponds to the TT of the old water fraction calculated at S2 using the six baseflow samples. The shaded area in (c) represents simple linear mixing between the two end-members.

member corresponds to τ_r (using the highest recorded Q_o through the study period), while the baseflow end-member corresponds to the τ_o value calculated using the six baseflow samples. The two end-members were linearly connected in an area that represents the extent of possible fluctuations of τ_o, from lower old water contributions to higher old water contributions. The individual τ_o values broadly followed this mixing trend (Figure 7.11c), which lends support to the assumptions that (i) the TT of the older end-member may not be

characterised by a single value but rather by a range of possible ages that fluctuate depending on flow conditions, and (ii) during and shortly after higher flows, a near steady-state was reached in which the TT of the old water fraction increased and approached the RT of stored water (i.e. $\tau_o \rightarrow \tau_r$). Overall, the large scattering observed in Figure 7.11 suggests that many processes led to the variations in τ_o, and that these processes were largely nonlinear.

Importantly, the finding that TTs of the old water component increased with increasing flow has not been reported before. Our results are in stark contrast with the previous observation by Morgenstern et al. (2010) and Cartwright and Morgenstern (2015) that ^{3}H-derived TTs were higher at low flow conditions and lower at high flow conditions. However, these two studies did not account for a younger component to streamflow (i.e. ϕ was effectively constrained to 1 for all samples), which may explain the disagreement with our results. Hrachowitz et al. (2015) reported an increase in storage water RT at the start of the wet season in an agricultural catchment in French Brittany, which they related to changes in storage dynamics (i.e. more recent water bypassing storage at higher flow). The authors did not comment on potential changes in streamwater TT during the same period, however.

We also recognise that the results reported here might be due to partially incorrect interpretation of the obtained dataset: underestimation of the old water fraction ϕ during high flow events might be responsible for the apparent positive correlation between Q_o and τ_o, although this is unlikely because the three seasonal tracers yielded very similar flow partitions. Another potential bias in our calculations is the possible lack of representation of the discharge from the fractured igneous rocks in the headwaters, which might contribute significantly to the young component during high flow events. Such enhanced contribution might result in slightly longer τ_y, hence shorter τ_o. Because no ^{3}H measurement was conducted at S1, this hypothesis could not be tested further (see Section 7.5.2). More generally, our work emphasises the current lack of understanding of the role and dynamics of deeper groundwater contributions to streams, and suggests that more multi-tracer data is needed to better assess the TTs of the old water fraction. Our findings also indicate that the so-called "old water fraction" (also referred to as "pre-event water" or "baseflow component" in tracer studies; e.g. Klaus and McDonnell, 2013; Stewart, 2015) should not be regarded as one single, time-invariant entity, but rather as a complex component made up of a wide range of flowpaths that can be hydrologically disconnected – and subsequently reactivated – as recharge and flow conditions evolve.

7.5.6 Limitations of this study and way forward

Several assumptions have been put forward in this study that need to be carefully acknowledged. Firstly, there are limitations related to the use of seasonal tracers (i.e. stable isotopes and chloride):

1. The lumped convolution approach used for the assessment of TTs of the younger contribution to streamflow relied on assumptions of stationarity. Such assumptions are very likely not satisfied in headwater catchments, particularly those characterised by high responsiveness and high seasonal variability in their climate drivers (Rinaldo et al., 2011; McDonnell and Beven, 2014). Unfortunately, the dataset obtained as part of this study did not enable characterisation of time-varying TT distribution functions, since this approach would require longer tracer records (e.g. Hrachowitz et al., 2013; Birkel et al., 2015) and/or higher sampling frequencies (e.g. Birkel et al., 2012; Benettin et al., 2013, 2015). Nonetheless, Seeger and Weiler (2014) recently noted that in the current state of research, the calculation of time-invariant TT distributions from lumped models still represents a useful alternative to more complex, computer-intensive modelling methods.

2. Using tracers that are notoriously sensitive to evapotranspiration in environments where this process commonly occurs can be problematic. Hrachowitz et al. (2013) established that evaporation can severely affect the calculations of TTs when chloride is used as an input-output tracer. Although evapotranspiration was considered in our recharge calculations (equation 7.1), a detailed analysis of catchment internal processes would be needed to verify whether evapotranspiration modifies the storage water RTs and subsequent catchment TTs. Using data from a catchment subjected to high rainfall seasonal variability, van der Velde et al. (2015) showed that younger water was more likely to contribute to evapotranspiration, which tended to result in longer catchment TTs.

3. The partitioning of streamflow relied on the assumption that two main components contributed to streamwater, although this may not be the case at S2 because soil water may explain the higher chloride concentration and more enriched $\delta^{18}O$ observed at this location (Klaus and McDonnell, 2013; Figure 7.4). However, we hypothesise that the occurrence of this third end-member would not significantly affect the calculation of τ_o, because the TT of soil water is likely to be considerably shorter than that of the older streamflow component (e.g. Matsutani et al., 1993; Muñoz Villers and McDonnell, 2012).

Secondly, there are a number of limitations related to the use of ^{3}H:

1. The most significant uncertainties were those related to the computed ^{3}H input functions. These may be reduced by regularly collecting rainfall ^{3}H on site. The accuracy of ^{3}H measurements was another source of uncertainty, and further improving analytical precision of ^{3}H activity in water samples may allow more rigorous assessment of short-term TT variations (e.g. Morgenstern and Daughney, 2012).

2. Changes in ^{3}H concentrations due to phase changes such as evaporation are commonly ignored, however, high evaporation environments such as that of the lower Teviot Brook catchment might significantly affect ^{3}H activity in streamwater. Future research is needed to examine more thoroughly the potential interferences on ^{3}H due to evaporation (Koster et al., 1989).

3. While stationarity may be a reasonable assumption for groundwater, inter-annual variations in recharge can affect RTs substantially (Manning et al., 2012). Further work aimed at providing additional constraints on RT variability is therefore required, by routinely collecting age tracer data in groundwater. Massoudieh et al. (2014a) showed that using multiple years of tracer records can allow more realistic quantification of the uncertainty on RT distributions. Also uncertain in our work is the spatial representativeness of waters collected at G1.

4. Despite yielding longer TTs than seasonal tracers, the use of ^{3}H did not preclude the potential omission of any older contribution (i.e. > 100 yr) to the stream. Frisbee et al. (2013) argued that even studies based on ^{3}H measurements might miss a significant part of the TT distributions rather than just their tail. In our case, the likelihood of waters with much longer RTs seeping from the sedimentary bedrock could not be verified using ^{3}H only. Other tracers that can capture older water footprints, such as terrigenic helium-4 (Smerdon et al., 2012) or carbon-14 (Bourke et al., 2014) would need to be tested for that purpose.

5. Another issue that has been raised recently is the potential aggregation biases affecting the calculation of TT distributions in complex systems (Kirchner, 2015). Based on the use of seasonal tracers, the author demonstrated that mean TTs are likely to be underestimated in heterogeneous catchments, i.e. those composed of subcatchments with contrasting TT distributions. A similar benchmark study should be undertaken for ^{3}H in order to verify whether TTs derived from ^{3}H measurements in heterogeneous catchments are also biased.

7.6 Conclusions

Based on time-series observations of seasonal tracers (stable isotopes and chloride) and ^{3}H in a subtropical mountainous catchment, we assessed the different contributions to streamflow as well as the variations in catchment TT and groundwater RT. Calibrating lumped parameter models to seasonal tracer data provided consistent estimates of TTs in the upstream part of the catchment, where evaporation was not a major process. In the downstream location, lumped models reproduced the tracers' output signals less accurately, partly because evapotranspiration complicated the input-output relationships, but also because of the increased hydrological complexity at this scale (i.e. interactions with deeper storage waters).

In this context, the use of ^{3}H time-series was highly beneficial for (i) determining an older groundwater contribution to streamflow in the downstream area, and (ii) providing insight into the temporal variations of this old water fraction. The old water fraction TT was significantly younger than the RT of groundwater stored in the catchment, which outlines the necessary distinction between transit and storage waters in catchment process conceptualisation. When simulations were run separately on each ^{3}H streamwater sample, the TT of old water fraction was found to vary substantially over time, with values averaging 17 ± 6 yr at low flow and 38 ± 15 yr after major recharge events – other parameters being held constant. These variations were interpreted as the activation of longer, deeper flowpaths carrying older waters when the rate of recharge was highest.

Overall, this study suggests that collecting high-resolution ^{3}H data in streamwater can be valuable to document short-term variations in the TT of old water fraction. If confirmed by further studies and corroborated by the use of other dating tracers, the occurrence of fluctuations in older contributions to streamflow may have important implications for water resource management and particularly contamination issues, because these fluctuations may control the time scales of retention and release of contaminants. It is therefore essential to collect longer-term experimental data that will contribute to identifying older groundwater contributions and to quantifying them with more confidence.

Acknowledgments

Funding for the tritium analyses was provided by the Australian Institute of Nuclear Science and Engineering (ALNGRA14026). Continuous financial support from the School of Earth, Environmental & Biological Sciences and M.E. Cox (QUT) are greatly appreciated. We would like to thank A. Bonfanti, M. Citati, G. Destefano, J. López and C. Ranchoux for their assistance with fieldwork. R. Chisari (ANSTO) and J. Brady (QUT) carried out most laboratory analyses. The Brisbane Aero tritium rainfall dataset was kindly provided by S. Hollins (ANSTO). Insightful discussion with S. Lamontagne (CSIRO) during the course of this study is gratefully acknowledged. D. Owen (QUT) is thanked for assistance with English. Comments by two anonymous reviewers and the Editor L. Pfister helped us improve the manuscript substantially. C. Duvert is supported by an Endeavour Scholarship (Australian Government).

CHAPTER 8

Discussion

In this chapter, the findings of each component of the study are summarised, integrated and related to the overall aim of the dissertation (Section 8.1). Section 8.2 examines the practical implications of the study for our conceptual understanding of catchment response to rainfall, while Section 8.3 discusses how this research contributes to the improvement of existing field and analytical methodologies. The concluding chapter (Chapter 9) identifies the limitations of the study and raises new questions for future research.

8.1 Summary of the findings

In areas subjected to (semi)arid, Mediterranean and (sub)tropical climates, the main source of groundwater recharge is generally derived from a few significant rainfall pulses; therefore, understanding hydrological responses to episodic recharge is essential (Currell et al., 2015). This consideration takes on full significance in mountainous regions where greater recharge rates are expected to occur, and where the recent recharge is likely to be the main contributor to lowland groundwater resources — this process is referred to as mountain front recharge. While the development of methods aimed at quantifying aquifer

recharge has received considerable attention in the last few decades, the effects of mountain front recharge on both inter-aquifer mixing and groundwater contribution to streams remain largely undescribed.

The overall goal of this dissertation was to improve our understanding of the response of aquifers and streams to episodic recharge at different temporal scales. To address this, a range of shallow aquifers and their adjacent surface water systems were monitored in a subtropical catchment that features the interface between an igneous mountain range and a lowland alluvial valley. The component studies reported in Chapters 4 to 7 were based on an assessment of both historical data obtained from government agencies and data collected as part of this work. The results, presented as four stand-alone publications, have together contributed to a better understanding of catchment-scale hydrological response and of its predominant controls. The specific outcomes derived from each chapter are summarised below.

Chapter 4 examined the response of the river and alluvial aquifer to both low and high frequency rainfall fluctuations using multi-year hydroclimatic records. By examining the spectral information buried in precipitation and water level time-series, it was demonstrated that the alluvial aquifer in its upstream section (i.e. close to the mountain front zone) was almost as responsive to inter-annual rainfall cycles as the stream. These low frequency fluctuations in groundwater level were related to large-scale atmospheric circulations, in particular to the El Niño-driven oscillation. By contrast, both the rate and magnitude of change were lower in the downstream section of the aquifer, even during multi-year droughts that led to the drying out of streams. The use of an original sliding window cross-correlation technique allowed assessment of short-term dynamics in the response time of the aquifer to recharge. While processes were found to be complex and highly non-linear in nature, it was inferred that diffuse recharge controlled the groundwater response in the downstream part of the catchment.

These findings provided a good basis for understanding the response of the alluvial aquifer to rainfall inputs, particularly in the downstream area. However, knowledge of the response of other shallow aquifers, i.e. those in direct contact with the headwaters where the bulk of recharge may occur, was still lacking from Chapter 4. Unlike the alluvial system, other aquifers in the Teviot Brook catchment are not routinely monitored and hydraulic data remain scarce. A worthwhile alternative to water level monitoring is the measurement of naturally-occurring solutes in water, because chemical substances are indicators of water movement rather than energy propagation.

Based on the above considerations, both Chapters 5 and 6 made use of a range of environmental tracers with the aim of documenting the possible inter-aquifer and stream–groundwater processes that may be initiated by major recharge pulses.

First, conventional tracers (both hydrochemical and isotopic elements) were examined pre- and post- a major storm event that provided a unique opportunity to study the response of the catchment to episodic recharge. Tracers were measured in a number of hydrological components, including the alluvial, sedimentary bedrock and fractured igneous rock aquifers, as well as the drainage network (Chapter 5). The strong connection between the main stream and underlying alluvium, previously suggested by hydraulic gradient data, was established with confidence using the tracer approach. Importantly, several lines of evidence suggested prompt recharge of the sedimentary bedrock aquifer near the mountain front via the fractured igneous rocks. Further downstream, the hydrochemical and isotopic signatures of some alluvial waters were suggestive of mixing with the sedimentary bedrock aquifer, but it was not always clear whether this process was enhanced by recharge. Overall, while each tracer provided different insights that allowed identification of a range of within- and between-aquifer processes, the multi-tracer approach developed in Chapter 5 did not yield definitive assessments of the catchment response to episodic recharge.

Much debate still exists regarding the behaviour of rare earth elements (REEs) in groundwater, yet some research has shown that REEs may behave differently than other solutes; hence the sequence of REEs may be a good candidate to delineate processes that are not revealed when using conventional tracer methods (e.g. Tweed et al., 2006). This observation provided the motivation to examine the spatial and temporal patterns of REEs and their response to the same major recharge event (Chapter 6). The assessment of changes in REE signatures allowed evaluation of inter-aquifer mixing with more confidence: the contribution of freshly recharged waters to the deeper sedimentary bedrock groundwater flow via preferential pathways was confirmed along the mountain front, even in areas where conventional methods did not detect any change. Furthermore, post-flood contributions from sedimentary bedrock waters to the alluvium were discovered not only in the downstream part of the alluvial aquifer but also at a location upstream near the interface between the two formations.

When taken together, the findings from Chapters 5 and 6 confirmed that mountain front recharge can be a significant process in aquifers of the mountain front – alluvial valley zone, and that major recharge events can in places be a key control on inter-aquifer mixing.

While these chapters showed the effect of episodic recharge on within- and between-aquifer processes, they did not establish how the system output, i.e. groundwater discharge to streams, responded to changes in recharge. Chapter 7 addressed this last piece of the puzzle by exploring the travel time of streamwater using high-resolution time-series of a range of tracers, including tritium. Results suggested that the stream in its upper parts was dominated by short flowpaths with travel times of up to one year. By contrast, at the transition zone between mountain front and the alluvial plain, older groundwater flowpaths contributed to streamflow, likely originating from the alluvial aquifer and/or the deeper

sedimentary bedrock.

Most importantly, according to simple modelling scenarios using tritium data, the travel time of this older groundwater fraction varied substantially over time: the travel time increased (i.e. older contributions) shortly after major recharge events, and was lower (i.e. more recent contributions) under low flow conditions. This was attributed to the flushing out of older waters, possibly from the sedimentary bedrock aquifer. Further evidence from Fe concentrations independently corroborated that groundwaters from the sedimentary bedrock may have contributed to stream baseflow shortly after recharge events. Also, while the travel time of groundwater stored in the catchment was generally longer than that of the groundwater contributing to baseflow, under high flow conditions the baseflow component had travel times that approached those of stored groundwater. Another result of the modelling approach developed in Chapter 7 was that diffuse recharge was found to be a significant, although relatively young contributor to groundwater in the alluvium, which supports the earlier postulation from Chapter 4.

8.2 Implications for hydrological process understanding

The findings from this thesis have several implications for the conceptualisation of catchment processes in mountainous areas under episodic recharge. The research questions that were formulated in Chapter 1, central to this dissertation, are briefly revisited here. Details are given on how the three key questions have been answered, with a comparison to previous work and an emphasis on the contribution of this thesis to the overall body of knowledge.

(1) How do shallow aquifers and streams respond to episodic recharge at the mountain front – alluvial valley transition zone?

Looking at multi-annual time scales, the alluvial aquifer proved to be controlled by long-term variations in climate-driven rainfall fluctuations. This was especially the case at the mountain front, where water levels were more variable than in the downstream portion of the alluvium. The stream was even more responsive to a change in recharge rate, as it dried out in several instances during extended droughts. It is not known whether the other aquifers studied in this work (i.e. the sedimentary and igneous formations) were also controlled by the same global-scale fluctuations; however given the close link between different hydrological components, it is very likely that the climate-driven effects detected in the alluvium would be equally found in other groundwater systems.

The occurrence of connections between large-scale atmospheric circulations and catchment response has been documented in other parts of the world (Hanson et al., 2006; Barco et al., 2010; Holman et al., 2011; Perez-Valdivia et al., 2012; Kuss and Gurdak, 2014). In Australia, while the influence of atmospheric circulation on rainfall and streamflow pat-

terns has been well described (e.g. Chiew et al., 1998; Lau and Nath, 2000; Murphy and Timbal, 2008), most research on groundwater has overlooked climatic fluctuations and their relationship to groundwater levels. If such relationships are confirmed, large-scale climatic cycles may then provide additional constraints on groundwater level forecasting. Recently an approach of this kind has shown promise for the prediction of groundwater levels up to six months in advance (Almanaseer et al., 2014).

Looking at shorter term dynamics, recharge via the mountain front was identified as a key process during rainfall events, whereas the sections of aquifers located further away from the mountain front were controlled by diffuse recharge over the lowland plains (Figure 8.1). Most studies of mountain front recharge have focused on arid to semi-arid regions (e.g. Alford, 1985; Manning and Solomon, 2005), and only recently has this process been investigated for the first time in a humid temperate environment (Doyle et al., 2015). While it is a potentially large recharge component in areas subject to high rates of evapotranspiration, mountain front recharge remains highly uncertain and poorly documented in the tropical and subtropical regions. Yet, this information is critical for the development of sound conceptual models at the regional scale (e.g. Wilson and Guan, 2004; Wahi et al., 2008), and valuable for the calibration of numerical groundwater flow models (Doyle et al., 2015). This study has provided a first qualitative assessment of such mechanisms in a subtropical area, and the next step will be the provision of quantitative estimates of the mountain front recharge contribution to regional-scale aquifers in these regions.

(2) Can inter-aquifer mixing be initiated by episodic recharge?

Two types of recharge-driven inter-aquifer interactions have been outlined through this dissertation. First, subsurface inflow from the mostly overlying fractured igneous rocks to the sedimentary bedrock aquifer occurred post-recharge. Second, increased seepage of sedimentary bedrock waters into the alluvial aquifer was observed at different locations (Figure 8.1).

An unexpected, but apparent finding of this work was that groundwater flow in the sedimentary bedrock was highly dynamic and responded rapidly to a change in recharge conditions. This response was attributed to the occurrence of preferential flow pathways through the mountain front (i.e. focused recharge), but it was also linked to the heterogeneous nature of the sedimentary bedrock itself (Figure 8.1). It is increasingly clear that preferential flow pathways are a key mechanism to inter-aquifer mixing. Groundwater mixing has been reported to occur preferentially through fractures (e.g. Tweed et al., 2006; Hofmann and Cartwright, 2013) but also along faults (Folch and Mas-Pla, 2008; Roques et al., 2014; Moya et al., 2015) and via volcanic necks (Raiber et al., 2009, 2015). Yet, preferential flow mechanisms are challenging to measure, and the influence of hydraulic conductivity

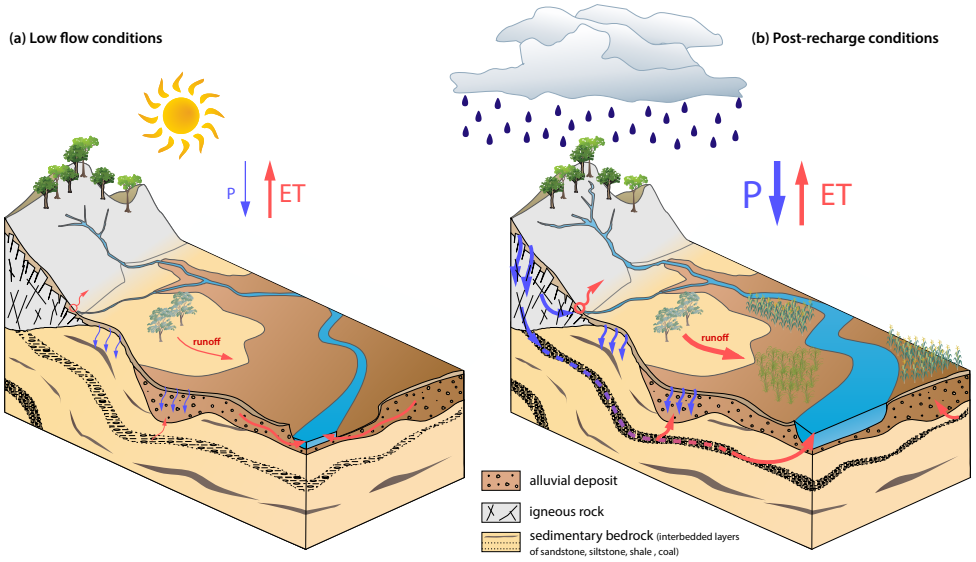

Figure 8.1: Conceptual diagram outlining the catchment processes elucidated in this thesis. Under low flow conditions (a), runoff and diffuse recharge are minimal due to high evapotranspiration rates; contributions from the igneous rock (travel times < 1 yr) and alluvial aquifers (travel times 10–20 yr) provide low baseflow to the stream; limited seepage of sedimentary bedrock waters to the alluvium occurs in the downstream region. After major recharge pulses (b), runoff and diffuse recharge are substantial; the sedimentary bedrock aquifer is rapidly recharged via the mountain front; high conductivity pathways in the sedimentary bedrock are activated, flushing out older waters into the alluvium and streams; increased contributions from the igneous rock (travel times < 1 yr) and sedimentary aquifers (travel times 20–60 yr) provide higher baseflow to the stream.

heterogeneities on flow pathways is still not well understood (Welch and Allen, 2014). Even in catchment hydrology studies, few models incorporate the effects of preferential flow (Burt and McDonnell, 2015).

While questions remain, this work has shown that the common assumption of high inertia and long response time of sedimentary bedrock aquifers may be misleading in some geological settings. This observation highlights the need for a shift in thinking on the way bedrock aquifers are conceptualised in catchment-scale studies: rather than a no-flow boundary, the interface between sedimentary bedrocks and overlying formations should be seen as a dynamic zone with potentially significant interflow where hydraulic conductivities are highest.

The findings presented here also illustrate the importance of considering nonsteady state conditions for developing sound conceptual models of the hydrological interactions between different aquifers. Clearly, repeated sampling campaigns are needed for the provision of reliable assessments of the rate and timing of recharge effects on groundwater flow. Most studies on inter-aquifer mixing have relied on single sampling campaigns (e.g. Dogramaci and Herczeg, 2002; Cartwright et al., 2010; King et al., 2015), which has often led to difficult interpretations since the involved processes are likely to be highly transient.

(3) Is the travel time of water through catchments affected by episodic recharge?

Groundwater discharge was found to account for an important portion of streamflow, even shortly after significant rainfall episodes. This finding is in agreement with most studies investigating the sources of water during high flow events (Klaus and McDonnell, 2013). Much less understood is the time needed for these groundwater contributions to exit the catchment, as is the extent of variation of their travel time with varying flow conditions. While shorter flow pathways contributing to streamflow have received considerable scientific attention in the last decade (e.g. McGuire and McDonnell, 2006; Hrachowitz et al., 2013; Harman, 2015), more work is needed to elucidate how longer, deeper flow pathways discharge into streams (Stewart et al., 2012; Frisbee et al., 2013).

It has been suggested in this study that the travel time of the groundwater component to streamflow was highly variable, and that its variability was a function of wetness conditions: interestingly, travel time estimates were positively correlated with antecedent precipitation (Figure 8.1). These results entirely contradict the few other observations available in the literature, which all revealed a larger preponderance of older waters at low flow conditions (Morgenstern et al., 2010; Cartwright and Morgenstern, 2015). Although challenging for catchment process understanding, it was proposed that the release of older groundwater shortly after recharge pulses was due to (Figure 8.1):

(i) the prompt activation of preferential flow pathways at the mountain front, where the bulk of rainfall and recharge occurred;

(ii) the initiation of a piston flow effect that may have propagated to the alluvial and sedimentary bedrock aquifers;

(iii) the generation of preferential flow in those latter systems associated with locally high hydraulic conductivities, ultimately leading to discharge of older waters into the stream.

Overall, the research developed here suggests that the concept of "old water" in storm-flow partitioning studies may be overly simplistic, and that this component should not be regarded as one single, time-invariant entity. Another important finding was that the old water fraction travel time was significantly younger than the travel time of groundwater stored in the catchment, which outlines the necessary distinction between transit and storage waters in catchment process conceptualisation. Similar observations have been reported for shallow subsurface water (Benettin et al., 2015; van der Velde et al., 2015), but had not yet been described for relatively deeper settings.

8.3 Methodological implications

Not only did the results add to our conceptual understanding of catchment hydrology in subtropical mountainous environments, they also contributed to advance certain aspects of existing methodologies and to test others. Specifically, this work demonstrated that:

1. Wavelet analysis was beneficial for the development of a temporal but also spatial understanding of aquifer response to rainfall. While this spectral approach has been increasingly applied to the characterisation of aquifers (Slimani et al., 2009; Tremblay et al., 2011; Kuss and Gurdak, 2014), most studies to date had not addressed the spatial patterns within single groundwater systems. In this study, it was shown that spatial variations in the wavelet product can be related to the local physical characteristics of aquifers.

2. Although further work is required to better constrain the physical processes responsible for the observed variations, the proposed sliding window cross-correlation method proved a valuable tool for the quantification of the aquifer response time to rainfall. Similar techniques have been developed in karstic settings (Delbart et al., 2014), and the attempt presented in this thesis was the first one for a porous aquifer. Other recent studies such as the one by Yu and Lin (2015) attest to the relevance of developing innovative approaches to characterise the spatiotemporal relationships between rainfall and groundwater levels.

3. This work has confirmed that integrated, multi-tracer studies are necessary in complex mountainous areas where the direct characterisation of geological heterogeneity is not feasible (e.g. Suecker et al., 2000; Manning and Solomon, 2005; Blumstock et al., 2015). Different lines of evidence are needed to infer hydrological processes at the catchment scale, and the combined use of multiple tracers with a repeated sampling strategy proved essential to capture the temporal variations in the involved systems. However, heterogeneity within single aquifers was a major limitation to the use of conventional tracers for delineating inter-aquifer mixing processes.

4. REEs were particularly useful to trace processes that were not detectable by more conventional tracer methods. After the original study by Möller et al. (2006), this work is the first to the author's knowledge that used REEs in a systematic way for delineating transient inter-aquifer interactions and their spatial patterns. Before the method becomes readily usable by water resource managers, further effort is required to better constrain the physical processes that control the REE behaviour in different hydrological systems.

5. The collection of tritium time-series data in streamwater was instrumental in revealing short-term variations in the older groundwater contribution to streams, which had been largely ignored in the literature so far. In the Southern Hemisphere, tritium has potential for accurately dating waters based on single measurements, and this situation may apply to the Northern Hemisphere in the next decade (Stewart et al., 2012). For a better appreciation of the time scales in catchment response, it is recommended to conduct tritium measurements – in combination with other tracers – at a range of flow conditions and at multiple nested catchment scales.

CHAPTER 9

Conclusions

9.1 Major outcomes

While the research presented in this dissertation is based on the analysis of a subtropical catchment located in southeast Queensland, Australia, the findings are applicable to other mountainous catchments worldwide, particularly those experiencing highly episodic recharge. This work has provided an improved understanding of the hydrological response of rivers and groundwater to major recharge events at the mountain front. Notable outcomes in this regard include:

- Identification of connections between large-scale atmospheric circulations and catchment response. It was suggested that climatic cycles such as the El Niño Southern Oscillation may provide additional constraints on long-term groundwater level forecasting in subtropical and tropical areas of eastern Australia.

- Provision of a first qualitative assessment of mountain front recharge in a subtropical area. It was shown that mountain front recharge was a substantial component for aquifers of the mountain front – alluvial valley zone, while diffuse recharge became an important factor in lowland areas far apart from the mountain front.

- Evidence for inter-aquifer mixing shortly after major recharge events. Due to the predominance of preferential pathways, groundwater flow was shown to be highly dynamic and to respond rapidly to a change in recharge conditions. In particular, high recharge pulses proved to be a key control on transient mixing processes between igneous, sedimentary and alluvial aquifer systems.

- Identification of substantial variations in the travel time of the groundwater contribution to streams. It was suggested that the "old water" fraction to streamflow should be regarded as a highly variable component that fluctuates through the (de)activation of different groundwater flowpaths to the stream under varying recharge conditions.

- Development and refinement of methodologies related to the assessment of hydrological processes in complex mountainous settings. Particularly, the benefits of using rare earth elements as tracers of inter-aquifer processes were evidenced; so were those of collecting tritium time-series to outline variations in the travel time of the groundwater fraction to streamflow. The importance of conducting repeated sampling campaigns in groundwater systems was also emphasised.

9.2 Limitations and recommendations for future research

This thesis answered a number of fundamental questions with respect to the hydrological response of catchments to high recharge events; yet a number of questions remain to be answered, in part due to a range of limitations in the original research design. These limitations are briefly addressed below, and some recommendations are made that will continue to improve our understanding of hydrological processes at the mountain front – alluvial valley interface.

1. On the sampling frequency

Only two sampling campaigns were conducted to investigate the effects of a recharge pulse on different aquifers. While this allowed detection of substantial changes in each hydrological component, a longer sequence of samples would have been likely to provide a broader understanding of the catchment response to recharge. This is a key aspect for future research given the highly dynamic processes in mountainous areas. Although spanning a longer period, the time-series data collected in streamwater would also have benefited from sampling at a higher frequency in order to capture the whole range of possible tracer values. New opportunities to study transient hydrological processes are emerging with recent developments in portable devices that allow near-continuous analysis of a variety of tracers in the field (Gilfedder et al., 2015; Tweed et al., 2016). These are promising tools for a more comprehensive characterisation of groundwater contributions to streams.

2. On the spatial heterogeneity

On several occasions the issue of spatial heterogeneity has been evoked in this dissertation. Spatial heterogeneity is an important source of uncertainty, with serious implications for (i) defining end-members and (ii) scaling up patterns and processes from single boreholes to the catchment scale. This has been problematic in this study, particularly in the case of the sedimentary bedrock, known to be highly anisotropic. As argued by Uhlenbrook (2006), catchment hydrology is a science in which all processes are preferential. This observation

also clearly applies to deeper geological formations, as preferential flow processes were identified as the main drivers of the hydrological response in the study catchment. Dealing with heterogeneity would require higher spatial resolution of sampling; detailed lithological description by geophysical imaging may also be needed to better appreciate possible preferential pathways (de Marsily et al., 2005). Overall, new methods need to be proposed that investigate preferential flow processes in more detail, which are then to be implemented in numerical models as these typically consider geological formations as homogeneous and isotropic.

3. On evapotranspiration effects

While evaporation is relatively well understood and can be quantified by examining the fractionation patterns of water stable isotopes, transpiration is a complex process that remains largely unknown. The potential effects of plant uptake on groundwater chemistry have long been neglected (Edwards and Webb, 2009), and this work is no exception. Yet, in tropical and subtropical areas transpiration is likely to be a major process controlling solute concentrations. Of consideration is also the influence of evapotranspiration on the estimates of travel time through catchments: a recent study has shown that younger waters in storage were more likely to contribute to evapotranspiration, which tended to result in longer travel times at the catchment scale (van der Velde et al., 2015). Generally, additional research is required to relate evapotranspiration dynamics and the hydrological response of catchments.

4. On the "hidden streamflow" problem

Baseflow waters can be very old ($> 1 \times 10^3$ yr; Gardner et al., 2011; Frisbee et al., 2013), and the use of tritium did not preclude the potential omission of contributions older than about 100 years. Other tracers that are not blind to older waters, such as terrigenic helium-4 (Smerdon et al., 2012) or carbon-14 (Bourke et al., 2014) would need to be examined in this regard. Also, a broader question that is yet to be answered is whether the increase in older contributions after recharge is a result that is merely specific to the study catchment, or if it is also applicable to other areas. Again, more work is needed in other parts of the world to determine if such processes are part of generic catchment behaviour.

5. On velocities and celerities

The time-varying cross-correlation method developed in this thesis, as well as other similar time-series approaches, may be usefully applied to environmental tracer data rather than head data to measure water movement rather than energy propagation. For instance, high-frequency electrical conductivity records may be used to make inferences on the response time of aquifers to a high flow event (e.g. Welch et al., 2014). Other methods are currently being developed, such as dynamic time warping and nonparametric deconvolution, to determine time-varying travel times between adjacent systems using tracer time-series (Schmidt et al., 2012; Liao et al., 2014). This ties in with the call for action of McDonnell and Beven

(2014) to urgently include both flux and tracer data in catchment studies for improving the understanding of hydrological processes and the ability to model them.

To conclude, this integrated study provided novel insights into the response of shallow aquifers and adjacent streams to episodic recharge. Additional research that builds upon this work to further constrain the processes of catchment response to recharge will also need to address water resource vulnerability under future climate uncertainty. This is an essential endeavour, particularly for tropical and subtropical climatic zones where climate change effects are predicted to be exacerbated.

Bibliography

Alford, D., 1985. Mountain hydrologic systems. *Mountain Research and Development* 5, 349–363.

Alley, B., Beebe, A., Rodgers, J., Castle, J.W., 2011. Chemical and physical characterization of produced waters from conventional and unconventional fossil fuel resources. *Chemosphere* 85, 74–82.

Allison, G.B., Cook, P.G., Barnett, S.R., Walker, G.R., Jolly, I.D., Hughes, M.W., 1990. Land clearance and river salinisation in the western Murray Basin. *Journal of Hydrology* 119, 1–20.

Almanaseer, N., Sankarasubramanian, A., Bales, J., 2014. Improving groundwater predictions utilizing seasonal precipitation forecasts from general circulation models forced with sea surface temperature forecasts. *Journal of Hydrologic Engineering* 19, 87–98.

Amin, I.E., Campana, M.E., 1996. A general lumped parameter model for the interpretation of tracer data and transit time calculation in hydrologic systems. *Journal of Hydrology* 179, 1–21.

Andreo, B., Jiménez, P., Durán, J., Carrasco, F., Vadillo, I., Mangin, A., 2006. Climatic and hydrological variations during the last 117–166 years in the south of the Iberian Peninsula, from spectral and correlation analyses and continuous wavelet analyses. *Journal of Hydrology* 324, 24–39.

Andreu, J.M., Alcalá, F.J., Vallejos, A., Pulido-Bosch, A., 2011. Recharge to mountainous carbonated aquifers in SE Spain: Different approaches and new challenges. *Journal of Arid Environments* 75, 1262–1270.

Arattano, M., Marchi, L., 2005. Measurements of debris flow velocity through cross-correlation of instrumentation data. *Natural Hazards and Earth System Science* 5, 137–142.

Aravena, R., Wassenaar, L.I., Plummer, L.N., 1995. Estimating ^{14}C groundwater ages in a methanogenic aquifer. *Water Resources Research* 31, 2307–2317.

Bagard, M.L., Chabaux, F., Pokrovsky, O.S., Viers, J., Prokushkin, A.S., Stille, P., Rihs, S., Schmitt, A.D., Dupré, B., 2011. Seasonal variability of element fluxes in two Central Siberian rivers draining high latitude permafrost dominated areas. *Geochimica et Cosmochimica Acta* 75, 3335–3357.

Bailly-Comte, V., Jourde, H., Roesch, A., Pistre, S., Batiot-Guilhe, C., 2008. Time series analyses for karst/river interactions assessment: Case of the Coulazou river (southern France). *Journal of Hydrology* 349, 98–114.

Bailly-Comte, V., Martin, J.B., Screaton, E.J., 2011. Time variant cross correlation to assess residence time of water and implication for hydraulics of a sink-rise karst system. *Water Resources Research* 47, W05547.

Banks, E.W., Simmons, C.T., Love, A.J., Shand, P., 2011. Assessing spatial and temporal connectivity between surface water and groundwater in a regional catchment: Implications for regional scale water quantity and quality. *Journal of Hydrology* 404, 30–49.

Barco, J., Hogue, T.S., Girotto, M., Kendall, D.R., Putti, M., 2010. Climate signal propagation in southern California aquifers. *Water Resources Research* 46, W00F05.

Barron, O.V., Crosbie, R.S., Dawes, W.R., Charles, S.P., Pickett, T., Donn, M.J., 2012. Climatic controls on diffuse groundwater recharge across Australia. *Hydrology and Earth System Sciences* 16, 4557–4570.

Barthel, R., 2014. HESS Opinions "Integration of groundwater and surface water research: an interdisciplinary problem?". *Hydrology and Earth System Sciences* 18, 2615–2628.

Bates, B., Kundzewicz, Z., Wu, S., Palutikof, J., 2008. Climate Change and Water. Technical Paper IV, Intergovernmental Panel on Climate Change, Geneva (Switzerland).

Bau, M., 1999. Scavenging of dissolved yttrium and rare earths by precipitating iron oxyhydroxide: experimental evidence for Ce oxidation, Y-Ho fractionation, and lanthanide tetrad effect. *Geochimica et Cosmochimica Acta* 63, 67–77.

Bau, M., Koschinsky, A., Dulski, P., Hein, J.R., 1996. Comparison of the partitioning behaviours of yttrium, rare earth elements, and titanium between hydrogenetic marine ferromanganese crusts and seawater. *Geochimica et Cosmochimica Acta* 60, 1709–1725.

Baudron, P., Barbecot, F., Gillon, M., Aróstegui, J.L.G., Travi, Y., Leduc, C., Castillo, F.G., Martinez-Vicente, D., 2013. Assessing groundwater residence time in a highly anthropized unconfined aquifer using bomb peak ^{14}C and reconstructed irrigation water ^{3}H. *Radiocarbon* 55, 993–1006.

Beck, M.S., Drane, J., Plaskowski, A., Wainwright, N., 1969. Particle velocity and mass flow measurement in pneumatic conveyors. *Powder Technology* 2, 269–277.

Benettin, P., Kirchner, J.W., Rinaldo, A., Botter, G., 2015. Modeling chloride transport using travel time distributions at Plynlimon, Wales. *Water Resources Research* 51, 3259–3276.

Benettin, P., van der Velde, Y., van der Zee, S.E.A.T.M., Rinaldo, A., Botter, G., 2013. Chloride circulation in a lowland catchment and the formulation of transport by travel time distributions. *Water Resources Research* 49, 4619–4632.

Bennetts, D.A., Webb, J.A., Stone, D.J.M., Hill, D.M., 2006. Understanding the salinisation process for groundwater in an area of south-eastern Australia, using hydrochemical and isotopic evidence. *Journal of Hydrology* 323, 178–192.

Bergmann, H., Sackl, B., Maloszewski, P., Stichler, W., 1986. Hydrological investigation in a small catchment area using isotope data series. In *Fifth International Symposium on Underground Water Tracing*, IAHS Publication no. 215, 255–272. Institute of Geology and Mineral Exploration, Athens (Greece).

Bethke, C.M., Johnson, T.M., 2002. Paradox of groundwater age. *Geology* 30, 385–388.

Bethke, C.M., Johnson, T.M., 2008. Groundwater age and groundwater age dating. *Annual Review of Earth and Planetary Sciences* 36, 121–152.

Biddau, R., Bensimon, M., Cidu, R., Parriaux, A., 2009. Rare earth elements in groundwater from different Alpine aquifers. *Chemie der Erde–Geochemistry* 69, 327–339.

Biddau, R., Cidu, R., Frau, F., 2002. Rare earth elements in waters from the albitite-bearing granodiorites of Central Sardinia, Italy. *Chemical Geology* 182, 1–14.

Birkel, C., Soulsby, C., Tetzlaff, D., 2015. Conceptual modelling to assess how the interplay of hydrological connectivity, catchment storage and tracer dynamics controls nonstationary water age estimates. *Hydrological Processes* 29, 2956–2969.

Birkel, C., Soulsby, C., Tetzlaff, D., Dunn, S., Spezia, L., 2012. High-frequency storm event isotope sampling reveals time-variant transit time distributions and influence of diurnal cycles. *Hydrological Processes* 26, 308–316.

Blavoux, B., Lachassagne, P., Henriot, A., Ladouche, B., Marc, V., Beley, J.J., Nicoud, G., Olive, P., 2013. A fifty-year chronicle of tritium data for characterising the functioning of the Evian and Thonon (France) glacial aquifers. *Journal of Hydrology* 494, 116–133.

Blumstock, M., Tetzlaff, D., Malcolm, I.A., Nuetzmann, G., Soulsby, C., 2015. Baseflow dynamics: Multi-tracer surveys to assess variable groundwater contributions to montane streams under low flows. *Journal of Hydrology* 527, 1021–1033.

Bouchaou, L., Mangin, A., Chauve, P., 2002. Turbidity mechanism of water from a karstic spring: example of the Ain Asserdoune spring (Beni Mellal Atlas, Morocco). *Journal of Hydrology* 265, 34–42.

Boulton, A.J., Datry, T., Kasahara, T., Mutz, M., Stanford, J.A., 2010. Ecology and management of the hyporheic zone: stream–groundwater interactions of running waters and their floodplains. *Journal of the North American Benthological Society* 29, 26–40.

Bourke, S.A., Harrington, G.A., Cook, P.G., Post, V.E., Dogramaci, S., 2014. Carbon-14 in streams as a tracer of discharging groundwater. *Journal of Hydrology* 519, 117–130.

Box, G.E.P., Jenkins, G.M., 1976. *Time series analysis: forecasting and control.* Prentice Hall, Upper Saddle River (USA).

Brenot, A., Négrel, P., Petelet-Giraud, E., Millot, R., Malcuit, E., 2015. Insights from the salinity origins and interconnections of aquifers in a regional scale sedimentary aquifer system (Adour-Garonne district, SW France): Contributions of δ^{34}S and δ^{18}O from dissolved sulfates and the δ^{87}Sr/δ^{86}Sr ratio. *Applied Geochemistry* 53, 27–41.

Brunke, M., Gonser, T., 1997. The ecological significance of exchange processes between rivers and groundwater. *Freshwater Biology* 37, 1–33.

Buishand, T.A., 1982. Some methods for testing the homogeneity of rainfall records. *Journal of Hydrology* 58, 11–27.

Burns, D.A., Murdoch, P.S., Lawrence, G.B., Michel, R.L., 1998. Effect of groundwater springs on NO_3^- concentrations during summer in Catskill Mountain streams. *Water Resources Research* 34, 1987–1996.

Burt, T.P., McDonnell, J.J., 2015. Whither field hydrology? The need for discovery science and outrageous hydrological hypotheses. *Water Resources Research* 51, 5919–5928.

Burton, N.R., 1988. Report on geological investigations – Teviot Brook dam site 88.3 km – Feasability study. Reference No. PP1765, Queensland Water Resources Commission.

Campbell, C.E., Pearson, B.N., Frost, C.D., 2008. Strontium isotopes as indicators of aquifer communication in an area of coal-bed natural gas production, Powder River Basin, Wyoming and Montana. *Rocky Mountain Geology* 43, 171–197.

Cartwright, I., Gilfedder, B., Hofmann, H., 2014. Contrasts between estimates of baseflow help discern multiple sources of water contributing to rivers. *Hydrology and Earth System Sciences* 18, 15–30.

Cartwright, I., Morgenstern, U., 2015. Transit times from rainfall to baseflow in headwater catchments estimated using tritium: the Ovens River, Australia. *Hydrology and Earth System Sciences* 19, 3771–3785.

Cartwright, I., Weaver, T.R., 2005. Hydrogeochemistry of the Goulburn Valley region of the Murray Basin, Australia: implications for flow paths and resource vulnerability. *Hydrogeology Journal* 13, 752–770.

Cartwright, I., Weaver, T.R., Cendón, D.I., Swane, I., 2010. Environmental isotopes as indicators of inter-aquifer mixing, Wimmera region, Murray Basin, Southeast Australia. *Chemical Geology* 277, 214–226.

Cartwright, I., Weaver, T.R., Fifield, L.K., 2006. Cl/Br ratios and environmental isotopes as indicators of recharge variability and groundwater flow: An example from the southeast Murray Basin, Australia. *Chemical Geology* 231, 38–56.

Cartwright, I., Weaver, T.R., Fulton, S., Nichol, C., Reid, M., Cheng, X., 2004. Hydrogeochemical and isotopic constraints on the origins of dryland salinity, Murray Basin, Victoria, Australia. *Applied Geochemistry* 19, 1233–1254.

Cayan, D.R., Redmond, K.T., Riddle, L.G., 1999. ENSO and hydrologic extremes in the western United States. *Journal of Climate* 12, 2881–2893.

Cendón, D.I., Hankin, S.I., Williams, J.P., der Ley, M.V., Peterson, M., Hughes, C.E., Meredith, K., Graham, I.T., Hollins, S.E., Levchenko, V., Chisari, R., 2014. Groundwater residence time in a dissected and weathered sandstone plateau: Kulnura-Mangrove Mountain aquifer, NSW, Australia. *Australian Journal of Earth Sciences* 61, 475–499.

Cendón, D.I., Larsen, J.R., Jones, B.G., Nanson, G.C., Rickleman, D., Hankin, S.I., Pueyo, J.J., Maroulis, J., 2010. Freshwater recharge into a shallow saline groundwater system, cooper creek floodplain, queensland, australia. *Journal of Hydrology* 392, 150–163.

Cendón, D.I., Peryt, T.M., Ayora, C., Pueyo, J.J., Taberner, C., 2004. The importance of recycling processes in the Middle Miocene Badenian evaporite basin (Carpathian foredeep): palaeoenvironmental implications. *Palaeogeography, Palaeoclimatology, Palaeoecology* 212, 141–158.

Chaffee, A.L., Lay, G., Marshall, M., Jackson, W.R., Fei, Y., Verheyen, T.V., Cassidy, P.J., Scott, S.G., 2010. Structural characterisation of Middle Jurassic, high-volatile bituminous Walloon Subgroup coals and correlation with the coal seam gas content. *Fuel* 89, 3241–3249.

Chen, Z., Grasby, S.E., Osadetz, K.G., 2004. Relation between climate variability and groundwater levels in the upper carbonate aquifer, southern Manitoba, Canada. *Journal of Hydrology* 290, 43–62.

Chiew, F., Peel, M., Western, A., 2002. Application and testing of the simple rainfall–runoff model SIMHYD. In V. Singh, D. Frevert, S. Meyer (Editors), *Mathematical Models of Small Watershed Hydrology and Applications*, 335–367. Water Resources Publications, Littleton (USA).

Chiew, F.H.S., Piechota, T.C., Dracup, J.A., McMahon, T.A., 1998. El Nino/Southern Oscillation and Australian rainfall, streamflow and drought: Links and potential for forecasting. *Journal of Hydrology* 204, 138–149.

Clark, I.D., Fritz, P., 1997. *Environmental Isotopes in Hydrogeology.* Lewis, New York (USA).

Cohen, B., 2012. The scenic rim of southeastern Queensland, Australia: a history of mid Cenozoic intraplate volcanism. *Episodes* 35, 103–109.

Commonwealth of Australia, 2014. *Aquifer connectivity within the Great Artesian Basin, and the Surat, Bowen and Galilee Basins – Background review.* Department of the Environment, Canberra (Australia).

Cook, A.G., Bryan, S.E., Draper, J.J., 2013. Post-orogenic Mesozoic basins and magmatism. In P.A. Jell (Editor), *Geology of Queensland*, 515–575. Geological Survey of Queensland, Brisbane (Australia).

Cook, P., Herczeg, A., 2000. *Environmental tracers in subsurface hydrology.* Kluwer Academic Publishers, Boston (USA).

Cook, P., Solomon, D., 1997. Recent advances in dating young groundwater: chlorofluorocarbons, $^{3}H^{3}He$ and ^{85}Kr. *Journal of Hydrology* 191, 245–265.

Cooper, G.R.J., Cowan, D.R., 2008. Comparing time series using wavelet-based semblance analysis. *Computers & Geosciences* 34, 95–102.

Cornaton, F., Park, Y.J., Deleersnijder, E., 2011. On the biases affecting water ages inferred from isotopic data. *Journal of Hydrology* 410, 217–225.

Cox, M.E., Wilson, A.S., 2006. Use of geochemical and isotope plots to determine recharge to alluvial aquifers: Lockyer Valley, Queensland, Australia. In *Fifth International Symposium on Management of Aquifer Recharge*, ISMAR 5, 253–263. Berlin (Germany).

Craig, H., 1961. Standard for reporting concentrations of deuterium and oxygen-18 in natural waters. *Science* 133, 1833–1834.

Cranfield, L.C., Hutton, L.J., Green, P.M., 1989. Queensland 1:100,000 geological map commentary. Ipswich sheet 9442, Queensland Department of Mines.

Currell, M., Gleeson, T., Dahlhaus, P., 2015. A new assessment framework for transience in hydrogeological systems. *Groundwater* in press.

Cuthbert, M.O., 2010. An improved time series approach for estimating groundwater recharge from groundwater level fluctuations. *Water Resources Research* 46, W09515.

Cvetkovic, V., Carstens, C., Selroos, J.O., Destouni, G., 2012. Water and solute transport along hydrological pathways. *Water Resources Research* 48, W06537.

Dafny, E., Silburn, D.M., 2014. The hydrogeology of the Condamine River Alluvial Aquifer, Australia: a critical assessment. *Hydrogeology Journal* 22, 705–727.

Dahm, K.G., Guerra, K.L., Munakata-Marr, J., Drewes, J.E., 2014. Trends in water quality variability for coalbed methane produced water. *Journal of Cleaner Production* 84, 840–848.

Dansgaard, W., 1964. Stable isotopes in precipitation. *Tellus* 16, 436–468.

Davranche, M., Grybos, M., Gruau, G., Pédrot, M., Dia, A., Marsac, R., 2011. Rare earth element patterns: A tool for identifying trace metal sources during wetland soil reduction. *Chemical Geology* 284, 127–137.

Davranche, M., Pourret, O., Gruau, G., Dia, A., 2004. Impact of humate complexation on the adsorption of REE onto Fe oxyhydroxide. *Journal of Colloid and Interface Science* 277, 271–279.

de Marsily, G., Delay, F., Gonçalvès, J., Renard, P., Teles, V., Violette, S., 2005. Dealing with spatial heterogeneity. *Hydrogeology Journal* 13, 161–183.

Delbart, C., Valdes, D., Barbecot, F., Tognelli, A., Richon, P., Couchoux, L., 2014. Temporal variability of karst aquifer response time established by the sliding-windows cross-correlation method. *Journal of Hydrology* 511, 580–588.

Department of Natural Resources, Mines and Water, 2006. Logan Basin Draft Water Resource Plan – Environmental Investigations Report. Volume 1: Summary Report, Queensland Government.

Dia, A., Gruau, G., Olivié-Lauquet, G., Riou, C., Molénat, J., Curmi, P., 2000. The distribution of rare earth elements in groundwaters: assessing the role of source-rock composition, redox changes and colloidal particles. *Geochimica et Cosmochimica Acta* 64, 4131–4151.

Dickinson, J.E., Hanson, R.T., Ferré, T.P.A., Leake, S.A., 2004. Inferring time-varying recharge from inverse analysis of long-term water levels. *Water Resources Research* 40, W07403.

Dogramaci, S., Skrzypek, G., 2015. Unravelling sources of solutes in groundwater of an ancient landscape in NW Australia using stable Sr, H and O isotopes. *Chemical Geology* 393, 67–78.

Dogramaci, S., Skrzypek, G., Dodson, W., Grierson, P.F., 2012. Stable isotope and hydrochemical evolution of groundwater in the semi-arid Hamersley Basin of subtropical northwest Australia. *Journal of Hydrology* 475, 281–293.

Dogramaci, S.S., Herczeg, A.L., 2002. Strontium and carbon isotope constraints on carbonate-solution interactions and inter-aquifer mixing in groundwaters of the semi-arid Murray Basin, Australia. *Journal of Hydrology* 262, 50–67.

Doyle, J.M., Gleeson, T., Manning, A.H., Mayer, K.U., 2015. Using noble gas tracers to constrain a groundwater flow model with recharge elevations: A novel approach for mountainous terrain. *Water Resources Research* in press.

Dripps, W.R., Bradbury, K.R., 2010. The spatial and temporal variability of groundwater recharge in a forested basin in northern Wisconsin. *Hydrological Processes* 24, 383–392.

Dulski, P., 1994. Interferences of oxide, hydroxide and chloride analyte species in the determination of rare earth elements in geological samples by inductively coupled plasma-mass spectrometry. *Fresenius' Journal of Analytical Chemistry* 350, 194–203.

Duncan, T., Shaw, T., 2003. The mobility of rare earth elements and redox sensitive elements in the groundwater/seawater mixing zone of a shallow coastal aquifer. *Aquatic Geochemistry* 9, 233–255.

Dunn, S.M., Birkel, C., Tetzlaff, D., Soulsby, C., 2010. Transit time distributions of a conceptual model: their characteristics and sensitivities. *Hydrological Processes* 24, 1719–1729.

Dürrenmatt, D.J., Giudice, D.D., Rieckermann, J., 2013. Dynamic time warping improves sewer flow monitoring. *Water Research* 47, 3803–3816.

Duvert, .C., Raiber, M., Owen, D.D.R., Cendón, D.I., Batiot-Guilhe, C., Cox, M.E., 2015a. Hydrochemical processes in a shallow coal seam gas aquifer and its overlying stream–alluvial system: implications for recharge and inter-aquifer connectivity. *Applied Geochemistry* 61, 146–159.

Duvert, C., Cendón, D.I., Raiber, M., Seidel, J.L., Cox, M.E., 2015b. Seasonal and spatial variations in rare earth elements to identify inter-aquifer linkages and recharge processes in an Australian catchment. *Chemical Geology* 396, 83–97.

Eadie, A., 1985. Report on geological investigations – Teviot Brook dam site 83.3 km – Feasability study. Reference No. PP989, Queensland Water Resources Commission.

Eberts, S.M., Böhlke, J.K., Kauffman, L.J., Jurgens, B.C., 2012. Comparison of particle-tracking and lumped-parameter age-distribution models for evaluating vulnerability of production wells to contamination. *Hydrogeology Journal* 20, 263–282.

Eckhardt, K., 2005. How to construct recursive digital filters for baseflow separation. *Hydrological Processes* 19, 507–515.

Edwards, M., Webb, J., 2009. The importance of unsaturated zone biogeochemical processes in determining groundwater composition, southeastern Australia. *Hydrogeology Journal* 17, 1359–1374.

Eggins, S.M., Woodhead, J.D., Kinsley, L.P.J., Mortimer, G.E., Sylvester, P., McCulloch, M.T., Hergt, J.M., Handler, M.R., 1997. A simple method for the precise determination of ≥ 40 trace elements in geological samples by ICPMS using enriched isotope internal standardisation. *Chemical Geology* 134, 311–326.

Einsiedl, F., Maloszewski, P., Stichler, W., 2009. Multiple isotope approach to the determination of the natural attenuation potential of a high-alpine karst system. *Journal of Hydrology* 365, 113–121.

Engdahl, N.B., Ginn, T.R., Fogg, G.E., 2013. Using groundwater age distributions to estimate the effective parameters of Fickian and non-Fickian models of solute transport. *Advances in Water Resources* 54, 11–21.

Engdahl, N.B., Maxwell, R.M., 2015. Quantifying changes in age distributions and the hydrologic balance of a high-mountain watershed from climate induced variations in recharge. *Journal of Hydrology* 522, 152–162.

Eriksson, E., 1958. The possible use of tritium for estimating groundwater storage. *Tellus A* 10, 472–478.

Eriksson, E., 1971. Compartment models and reservoir theory. *Annual Review of Ecology and Systematics* 2, 67–84.

ESSO Australia, 1974. Relinquishment report of A to P 131C Warrill Creek, Moreton Basin, Queensland. CR 4789, Queensland Department of Mines, Brisbane (Australia).

Ewart, A., 1982. Petrogenesis of the Tertiary anorogenic volcanic series of Southern Queensland, Australia, in the light of trace element geochemistry and O, Sr and Pb isotopes. *Journal of Petrology* 23, 344–382.

Ewart, A., Chappell, B.W., Maitre, R.W.L., 1985. Aspects of the mineralogy and chemistry of the intermediate–silicic Cainozoic volcanic rocks of eastern Australia. Part 1: Introduction and geochemistry. *Australian Journal of Earth Sciences* 32, 359–382.

Ewart, A., Chappell, B.W., Menzies, M.A., 1988. An overview of the geochemical and isotopic characteristics of the Eastern Australian Cainozoic volcanic provinces. *Journal of Petrology* 225–273.

Farge, M., 1992. Wavelet transforms and their applications to turbulence. *Annual Review of Fluid Mechanics* 24, 395–458.

Faure, G., 1986. *Principles of Isotope Geology, Second Edition.* John Wiley and Sons, New York (USA).

Fiorillo, F., Doglioni, A., 2010. The relation between karst spring discharge and rainfall by cross-correlation analysis (Campania, southern Italy). *Hydrogeology Journal* 18, 1881–1895.

Folch, A., Mas-Pla, J., 2008. Hydrogeological interactions between fault zones and alluvial aquifers in regional flow systems. *Hydrological Processes* 22, 3476–3487.

Freeze, R.A., Cherry, J.A., 1979. *Groundwater*. Prentice-Hall, Englewood Cliffs (USA).

Frisbee, M.D., Wilson, J.L., Gomez-Velez, J.D., Phillips, F.M., Campbell, A.R., 2013. Are we missing the tail (and the tale) of residence time distributions in watersheds? *Geophysical Research Letters* 40, 4633–4637.

Frost, C.D., Brinck, E.L., Mailloux, J., Sharma, S., Campbell, C.E., Carter, S.A., Pearson, B.N., 2011. Innovative approaches for tracing water co-produced with coalbed natural gas: Applications of strontium and carbon isotopes of produced water in the Powder River Basin, Wyoming and Montana. In K.J. Reddy (Editor), *Coalbed Natural Gas: Energy and Environment*, 59–80. Nova Science Publishers, New York (USA).

Frost, C.D., Pearson, B.N., Ogle, K.M., Heffern, E.L., Lyman, R.M., 2002. Sr isotope tracing of aquifer interactions in an area of accelerating coal-bed methane production, Powder River Basin, Wyoming. *Geology* 30, 923–926.

García-Veigas, J., Cendón, D.I., Rosell, L., Ortí, F., Ruiz, J.T., Martín, J.M., Sanz, E., 2013. Salt deposition and brine evolution in the Granada Basin (Late Tortonian, SE Spain). *Palaeogeography, Palaeoclimatology, Palaeoecology* 369, 452–465.

Gardner, W.P., Susong, D.D., Solomon, D.K., Heasler, H.P., 2011. A multitracer approach for characterizing interactions between shallow groundwater and the hydrothermal system in the Norris Geyser Basin area, Yellowstone National Park. *Geochemistry, Geophysics, Geosystems* 12, Q08005.

Gassama, N., Dia, A., Violette, S., 2012. Origin of salinity in a multilayered aquifer with high salinization vulnerability. *Hydrological Processes* 26, 168–188.

Gaucherel, C., 2002. Use of wavelet transform for temporal characterisation of remote watersheds. *Journal of Hydrology* 269, 101–121.

Gemitzi, A., Stefanopoulos, K., 2011. Evaluation of the effects of climate and man intervention on ground waters and their dependent ecosystems using time series analysis. *Journal of Hydrology* 403, 130–140.

Genereux, D., 1998. Quantifying uncertainty in tracer-based hydrograph separations. *Water Resources Research* 34, 915–919.

Genereux, D., 2004. Comparison of naturally-occurring chloride and oxygen-18 as tracers of interbasin groundwater transfer in lowland rainforest, Costa Rica. *Journal of Hydrology* 295, 17–27.

Geyh, M., Mook, W.G., 2000. Volume IV: Groundwater, saturated and unsaturated zone. In W.G. Mook, Y. Yurtsever (Editors), *Environmental isotopes in the hydrological cycle: principles and applications*, 317–429. UNESCO/IAEA, Paris (France).

Gilfedder, B.S., Frei, S., Hofmann, H., Cartwright, I., 2015. Groundwater discharge to wetlands driven by storm and flood events: Quantification using continuous Radon-222 and electrical conductivity measurements and dynamic mass-balance modelling. *Geochimica et Cosmochimica Acta* 165, 161–177.

Gleeson, T., Manning, A.H., 2008. Regional groundwater flow in mountainous terrain: Three-dimensional simulations of topographic and hydrogeologic controls. *Water Resources Research* 44, W10403.

Göb, S., Loges, A., Nolde, N., Bau, M., Jacob, D.E., Markl, G., 2013. Major and trace element compositions (including REE) of mineral, thermal, mine and surface waters in SW Germany and implications for water–rock interaction. *Applied Geochemistry* 33, 127–152.

Golding, S.D., Boreham, C.J., Esterle, J.S., 2013. Stable isotope geochemistry of coal bed and shale gas and related production waters: A review. *International Journal of Coal Geology* 120, 24–40.

Gonçalvès, J., Petersen, J., Deschamps, P., Hamelin, B., Baba-Sy, O., 2013. Quantifying the modern recharge of the "fossil" Sahara aquifers. *Geophysical Research Letters* 40, 2673–2678.

Green, C.T., Zhang, Y., Jurgens, B.C., Starn, J.J., Landon, M.K., 2014. Accuracy of travel time distribution (TTD) models as affected by TTD complexity, observation errors, and model and tracer selection. *Water Resources Research* 50, 6191–6213.

Green, T.R., Taniguchi, M., Kooi, H., Gurdak, J.J., Allen, D.M., Hiscock, K.M., Treidel, H., Aureli, A., 2011. Beneath the surface of global change: Impacts of climate change on groundwater. *Journal of Hydrology* 405, 532–560.

Grinsted, A., Moore, J.C., Jevrejeva, S., 2004. Application of the cross wavelet transform and wavelet coherence to geophysical time series. *Nonlinear Processes in Geophysics* 11, 561–566.

Gröning, M., Lutz, H.O., Roller-Lutz, Z., Kralik, M., Gourcy, L., Pöltenstein, L., 2012. A simple rain collector preventing water re-evaporation dedicated for δ^{18}O and δ^{2}H analysis of cumulative precipitation samples. *Journal of Hydrology* 448, 195–200.

Grossman, E.L., Coffman, B.K., Fritz, S.J., Wada, H., 1989. Bacterial production of methane and its influence on ground-water chemistry in east-central Texas aquifers. *Geology* 17, 495–499.

Gruau, G., Dia, A., Olivié-Lauquet, G., Davranche, M., Pinay, G., 2004. Controls on the distribution of rare earth elements in shallow groundwaters. *Water Research* 38, 3576–3586.

Guo, H., Zhang, B., Wang, G., Shen, Z., 2010. Geochemical controls on arsenic and rare earth elements approximately along a groundwater flow path in the shallow aquifer of the Hetao Basin, Inner Mongolia. *Chemical Geology* 270, 117–125.

Guo, Q., Guo, H., Yang, Y., Han, S., Zhang, F., 2014. Hydrogeochemical contrasts between low and high arsenic groundwater and its implications for arsenic mobilization in shallow aquifers of the northern Yinchuan Basin, P.R. China. *Journal of Hydrology* 518, 464–476.

Gusyev, M.A., Toews, M., Morgenstern, U., Stewart, M., White, P., Daughney, C., Hadfield, J., 2013. Calibration of a transient transport model to tritium data in streams and simulation of groundwater ages in the western Lake Taupo catchment, New Zealand. *Hydrology and Earth System Sciences* 17, 1217–1227.

Hagedorn, B., Cartwright, I., Raveggi, M., Maas, R., 2011. Rare earth element and strontium geochemistry of the Australian Victorian Alps drainage system: Evaluating the dominance of carbonate vs. aluminosilicate weathering under varying runoff. *Chemical Geology* 284, 105–126.

Hamawand, I., Yusaf, T., Hamawand, S.G., 2013. Coal seam gas and associated water: A review paper. *Renewable and Sustainable Energy Reviews* 22, 550–560.

Hancock, P.J., Boulton, A.J., Humphreys, W.F., 2005. Aquifers and hyporheic zones: Towards an ecological understanding of groundwater. *Hydrogeology Journal* 13, 98–111.

Hanson, R.T., Dettinger, M.D., Newhouse, M.W., 2006. Relations between climatic variability and hydrologic time series from four alluvial basins across the southwestern United States. *Hydrogeology Journal* 14, 1122–1146.

Hanson, R.T., Newhouse, M.W., Dettinger, M.D., 2004. A methodology to assess relations between climatic variability and variations in hydrologic time series in the southwestern United States. *Journal of Hydrology* 287, 252–269.

Harman, C.J., 2015. Time-variable transit time distributions and transport: Theory and application to storage-dependent transport of chloride in a watershed. *Water Resources Research* 51, 1–30.

Hattersley, P., 1983. The distribution of C3 and C4 grasses in Australia in relation to climate. *Oecologia* 57, 113–128.

Haxel, G., Hedrick, J., Orris, G., 2002. Rare earth elements: critical resources for high technology. USGS Fact Sheet No. 087-02, United States Geological Survey.

Healy, R.W., Bartos, T.T., Rice, C.A., McKinley, M.P., Smith, B.D., 2011. Groundwater chemistry near an impoundment for produced water, Powder River Basin, Wyoming, USA. *Journal of Hydrology* 403, 37–48.

Heidbüchel, I., Troch, P.A., Lyon, S.W., 2013. Separating physical and meteorological controls of variable transit times in zero-order catchments. *Water Resources Research* 49, 7644–7657.

Heidbüchel, I., Troch, P.A., Lyon, S.W., Weiler, M., 2012. The master transit time distribution of variable flow systems. *Water Resources Research* 48, W06520.

Henderson, P., 1984. General geochemical properties and abundances of the rare earth elements. In P. Henderson (Editor), *Rare Earth Element Geochemistry*, 1–32. Elsevier, Amsterdam (Netherlands).

Herczeg, A.L., Edmunds, W.M., 2000. Inorganic ions as tracers. In P.G. Cook, A.L. Herczeg (Editors), *Environmental Tracers in Subsurface Hydrology*, 31–78. Kluwer Academic Publishers, Boston (USA).

Herman, E.K., Toran, L., White, W.B., 2009. Quantifying the place of karst aquifers in the groundwater to surface water continuum: A time series analysis study of storm behavior in Pennsylvania water resources. *Journal of Hydrology* 376, 307–317.

Herrmann, A., Bahls, S., Stichler, W., Gallart, F., Latron, J., 1999. Isotope hydrological study of mean transit times and related hydrogeological conditions in Pyrenean experimental basins (Vallcebre, Catalonia). In *Integrated methods in catchment hydrology – tracer, remote sensing, and new hydrometric techniques. Proceedings of IUGG 99 Symposium HS4*, IAHS Publication no. 258, 101–110. International Association of Hydrological Sciences, Birmingham (UK).

Hofmann, H., Cartwright, I., 2013. Using hydrogeochemistry to understand inter-aquifer mixing in the on-shore part of the Gippsland Basin, southeast Australia. *Applied Geochemistry* 33, 84–103.

Holman, I.P., Rivas-Casado, M., Bloomfield, J.P., Gurdak, J.J., 2011. Identifying non-stationary groundwater level response to North Atlantic ocean-atmosphere teleconnection patterns using wavelet coherence. *Hydrogeology Journal* 19, 1269–1278.

Holman, I.P., Rivas-Casado, M., Howden, N.J.K., Bloomfield, J.P., Williams, A.T., 2009. Linking North Atlantic ocean–atmosphere teleconnection patterns and hydrogeological responses in temperate groundwater systems. *Hydrological Processes* 23, 3123–3126.

Hood, J.L., Roy, J.W., Hayashi, M., 2006. Importance of groundwater in the water balance of an alpine headwater lake. *Geophysical Research Letters* 33, L13405.

Hrachowitz, M., Fovet, O., Ruiz, L., Savenije, H.H.G., 2015. Transit time distributions, legacy contamination and variability in biogeochemical 1/fα scaling: how are hydrological response dynamics linked to water quality at the catchment scale? *Hydrological Processes* in press.

Hrachowitz, M., Savenije, H., Bogaard, T.A., Tetzlaff, D., Soulsby, C., 2013. What can flux tracking teach us about water age distribution patterns and their temporal dynamics? *Hydrology and Earth System Sciences* 17, 533–564.

Hrachowitz, M., Soulsby, C., Tetzlaff, D., Dawson, J.J.C., Malcolm, I.A., 2009. Regionalization of transit time estimates in montane catchments by integrating landscape controls. *Water Resources Research* 45, W05421.

Hrachowitz, M., Soulsby, C., Tetzlaff, D., Malcolm, I.A., Schoups, G., 2010. Gamma distribution models for transit time estimation in catchments: Physical interpretation of parameters and implications for time-variant transit time assessment. *Water Resources Research* 46, W10536.

Huang, T., Pang, Z., 2012. The role of deuterium excess in determining the water salinisation mechanism: A case study of the arid Tarim River Basin, NW China. *Applied Geochemistry* 27, 2382–2388.

Hughes, C.E., Crawford, J., 2012. A new precipitation weighted method for determining the meteoric water line for hydrological applications demonstrated using Australian and global GNIP data. *Journal of Hydrology* 464, 344–351.

Hughes, C.E., Crawford, J., 2013. Spatial and temporal variation in precipitation isotopes in the Sydney Basin, Australia. *Journal of Hydrology* 489, 42–55.

Huxley, W.J., 1982. Condamine River Valley groundwater investigation: The hydrogeology, hydrology and hydrochemistry of the Condamine River Valley alluvium. MAppSc Thesis, Queensland Water Resources Commission, Brisbane (Australia).

Imagawa, C., Takeuchi, J., Kawachi, T., Chono, S., Ishida, K., 2013. Statistical analyses and modeling approaches to hydrodynamic characteristics in alluvial aquifer. *Hydrological Processes* 27, 4017–4027.

Ingri, J., Widerlund, A., Land, M., Gustafsson, O., Andersson, P., Öhlander, B., 2000. Temporal variations in the fractionation of the rare earth elements in a boreal river; the role of colloidal particles. *Chemical Geology* 166, 23–45.

Jasechko, S., Birks, S.J., Gleeson, T., Wada, Y., Fawcett, P.J., Sharp, Z.D., McDonnell, J.J., Welker, J.M., 2014. The pronounced seasonality of global groundwater recharge. *Water Resources Research* 50, 8845–8867.

Jasechko, S., Taylor, R.G., 2015. Intensive rainfall recharges tropical groundwaters. *Environmental Research Letters* 10, 124015.

Jenkins, G., Watts, D., 1968. *Spectral Analysis and its Applications.* Holden-Day, San Francisco (USA).

Johannesson, K.H., Cortés, A., Ramos Leal, J.A., Ramírez, A.G., Durazo, J., 2005. Geochemistry of rare earth elements in groundwater from a rhyolite aquifer, central Mexico. In K.H. Johannesson (Editor), *Rare Earth Elements in Groundwater Flow Systems*, 187–222. Springer, Dordrecht (Netherlands).

Johannesson, K.H., Farnham, I.M., Guo, C., Stetzenbach, K.J., 1999. Rare earth element fractionation and concentration variations along a groundwater flow path within a shallow, basin-fill aquifer, southern Nevada, USA. *Geochimica et Cosmochimica Acta* 63, 2697–2708.

Johannesson, K.H., Stetzenbach, K.J., Hodge, V.F., 1997. Rare earth elements as geochemical tracers of regional groundwater mixing. *Geochimica et Cosmochimica Acta* 61, 3605–3618.

Johannesson, K.H., Zhou, X., 1999. Origin of middle rare earth element enrichments in acid waters of a Canadian High Arctic lake. *Geochimica et Cosmochimica Acta* 63, 153–165.

Johannesson, K.H., Zhou, X., Guo, C., Stetzenbach, K.J., Hodge, V.F., 2000. Origin of rare earth element signatures in groundwaters of circumneutral pH from southern Nevada and eastern California, USA. *Chemical Geology* 164, 239–257.

Kalbus, E., Reinstorf, F., Schirmer, M., 2006. Measuring methods for groundwater – surface water interactions: a review. *Hydrology and Earth System Sciences* 10, 873–887.

Kanduč, T., Grassa, F., McIntosh, J., Stibilj, V., Ulrich-Supovec, M., Supovec, I., Jamnikar, S., 2014. A geochemical and stable isotope investigation of groundwater/surface-water interactions in the Velenje Basin, Slovenia. *Hydrogeology Journal* 22, 971–984.

Katsuyama, M., Tani, M., Nishimoto, S., 2010. Connection between streamwater mean residence time and bedrock groundwater recharge/discharge dynamics in weathered granite catchments. *Hydrological Processes* 24, 2287–2299.

Kendall, M.G., 1975. *Rank correlation methods.* Oxford University Press, New York (USA).

King, A.C., Raiber, M., Cendón, D.I., Cox, M.E., Hollins, S.E., 2015. Identifying flood recharge and inter-aquifer connectivity using multiple isotopes in subtropical Australia. *Hydrology and Earth System Sciences* 19, 2315–2335.

King, A.C., Raiber, M., Cox, M.E., 2014. Multivariate statistical analysis of hydrochemical data to assess alluvial aquifer–stream connectivity during drought and flood: Cressbrook Creek, southeast Queensland, Australia. *Hydrogeology Journal* 22, 481–500.

Kinnon, E.C.P., Golding, S.D., Boreham, C.J., Baublys, K.A., Esterle, J.S., 2010. Stable isotope and water quality analysis of coal bed methane production waters and gases from the Bowen Basin, Australia. *International Journal of Coal Geology* 82, 219–231.

Kirchner, J.W., 2015. Aggregation in environmental systems: seasonal tracer cycles quantify young water fractions, but not mean transit times, in spatially heterogeneous catchments. *Hydrology and Earth System Sciences Discussions* 12, 3059–3103.

Klaus, J., Chun, K.P., McGuire, K.J., McDonnell, J.J., 2015a. Temporal dynamics of catchment transit times from stable isotope data. *Water Resources Research* 51, 4208–4223.

Klaus, J., McDonnell, J.J., 2013. Hydrograph separation using stable isotopes: Review and evaluation. *Journal of Hydrology* 505, 47–64.

Klaus, J., McDonnell, J.J., Jackson, C.R., Du, E., Griffiths, N.A., 2015b. Where does streamwater come from in low-relief forested watersheds? A dual-isotope approach. *Hydrology and Earth System Sciences* 19, 125–135.

Kløve, B., Ala-Aho, P., Bertrand, G., Gurdak, J.J., Kupfersberger, H., Kværner, J., Muotka, T., Mykrä, H., Preda, E., Rossi, P., Uvo, C.B., Velasco, E., Pulido-Velazquez, M., 2014. Climate change impacts on groundwater and dependent ecosystems. *Journal of Hydrology* 518, 250–266.

Koster, R.D., Broecker, W.S., Jouzel, J., Suozzo, R.J., Russell, G.L., Rind, D., White, J.W.C., 1989. The global geochemistry of bomb-produced tritium: General circulation model compared to available observations and traditional interpretations. *Journal of Geophysical Research: Atmospheres* 94, 18305–18326.

Kralik, M., Humer, F., Fank, J., Harum, T., Klammler, G., Gooddy, D., Sültenfuß, J., Gerber, C., Purtschert, R., 2014. Using $^{18}O/^{2}H$, $^{3}H/^{3}He$, ^{85}Kr and CFCs to determine mean residence times and water origin in the Grazer and Leibnitzer Feld groundwater bodies (Austria). *Applied Geochemistry* 50, 150–163.

Kundzewicz, Z.W., Robson, A.J., 2004. Change detection in hydrological records – a review of the methodology. *Hydrological Sciences Journal* 49, 7–19.

Kuss, A.J.M., Gurdak, J.J., 2014. Groundwater level response in U.S. principal aquifers to ENSO, NAO, PDO, and AMO. *Journal of Hydrology* 519, 1939–1952.

Labat, D., 2010. Cross wavelet analyses of annual continental freshwater discharge and selected climate indices. *Journal of Hydrology* 385, 269–278.

Labat, D., Ababou, R., Mangin, A., 2000. Rainfall–runoff relations for karstic springs. Part II: continuous wavelet and discrete orthogonal multiresolution analyses. *Journal of Hydrology* 238, 149–178.

Labat, D., Goddéris, Y., Probst, J.L., Guyot, J.L., 2004. Evidence for global runoff increase related to climate warming. *Advances in Water Resources* 27, 631–642.

Ladd, B., Bonser, S.P., Peri, P.L., Larsen, J.R., Laffan, S.W., Pepper, D.A., Cendón, D.I., 2009. Towards a physical description of habitat: quantifying environmental adversity (abiotic stress) in temperate forest and woodland ecosystems. *Journal of Ecology* 97, 964–971.

Ladson, A.R., 2008. *Hydrology: an Australian introduction*. Oxford University Press, New York (USA).

Lamontagne, S., Taylor, A.R., Batlle-Aguilar, J., Suckow, A., Cook, P.G., Smith, S.D., Morgenstern, U., Stewart, M.K., 2015. River infiltration to a subtropical alluvial aquifer inferred using multiple environmental tracers. *Water Resources Research* 51, 4532–4549.

Larocque, M., Mangin, A., Razack, M., Banton, O., 1998. Contribution of correlation and spectral analyses to the regional study of a large karst aquifer (Charente, France). *Journal of Hydrology* 205, 217–231.

Lau, N.C., Nath, M.J., 2000. Impact of ENSO on the variability of the Asian-Australian monsoons as simulated in GCM experiments. *Journal of Climate* 13, 4287–4309.

Lawrence, M.G., Greig, A., Collerson, K.D., Kamber, B.S., 2006. Rare earth element and yttrium variability in South East Queensland waterways. *Aquatic Geochemistry* 12, 39–72.

Lawrence, M.G., Kamber, B.S., 2006. The behaviour of the rare earth elements during estuarine mixing–revisited. *Marine Chemistry* 100, 147–161.

Lee, J.Y., Lee, K.K., 2000. Use of hydrologic time series data for identification of recharge mechanism in a fractured bedrock aquifer system. *Journal of Hydrology* 229, 190–201.

Lee, K.S., Wenner, D.B., Lee, I., 1999. Using H- and O-isotopic data for estimating the relative contributions of rainy and dry season precipitation to groundwater: example from Cheju Island, Korea. *Journal of Hydrology* 222, 65–74.

Lee, L.J.E., Lawrence, D.S.L., Price, M., 2006. Analysis of water-level response to rainfall and implications for recharge pathways in the Chalk aquifer, SE England. *Journal of Hydrology* 330, 604–620.

Leray, S., de Dreuzy, J.R., Aquilina, L., Vergnaud-Ayraud, V., Labasque, T., Bour, O., Le Borgne, T., 2014. Temporal evolution of age data under transient pumping conditions. *Journal of Hydrology* 511, 555–566.

Leybourne, M.I., Clark, I.D., Goodfellow, W.D., 2006. Stable isotope geochemistry of ground and surface waters associated with undisturbed massive sulfide deposits; constraints on origin of waters and water–rock reactions. *Chemical Geology* 231, 300–325.

Leybourne, M.I., Goodfellow, W.D., Boyle, D.R., Hall, G.M., 2000. Rapid development of negative Ce anomalies in surface waters and contrasting REE patterns in groundwaters associated with Zn-Pb massive sulphide deposits. *Applied Geochemistry* 15, 695–723.

Leybourne, M.I., Johannesson, K.H., 2008. Rare earth elements (REE) and yttrium in stream waters, stream sediments, and Fe-Mn oxyhydroxides: Fractionation, speciation, and controls over REE + Y patterns in the surface environment. *Geochimica et Cosmochimica Acta* 72, 5962–5983.

Li, J., 2001. Hydrochemical properties of the Teviot Brook catchment, South-East Queensland. unpublished report, Queensland University of Technology, Brisbane (Australia).

Li, J., Cox, M.E., 1996. Chemical character of groundwater in the Walloon Coal Measures of southeast Queensland. In *Mesozoic Geology of the Eastern Australia Plate Conference*, Extended Abstracts 43, 343–349. Geological Society of Australia, Brisbane (Australia).

Liao, Z., Osenbrück, K., Cirpka, O.A., 2014. Non-stationary nonparametric inference of river-to-groundwater travel-time distributions. *Journal of Hydrology* 519, 3386–3399.

Lyon, S.W., Desilets, S.L.E., Troch, P.A., 2009. A tale of two isotopes: differences in hydrograph separation for a runoff event when using δD versus δ^{18}O. *Hydrological Processes* 23, 2095–2101.

Machiwal, D., Jha, M.K., 2008. Comparative evaluation of statistical tests for time series analysis: application to hydrological time series. *Hydrological Sciences Journal* 53, 353–366.

Mair, A., Fares, A., 2010. Influence of groundwater pumping and rainfall spatio-temporal variation on streamflow. *Journal of Hydrology* 393, 287–308.

Maliva, R., Missimer, T., 2012. *Arid Lands Water Evaluation and Management*. Springer-Verlag, Heidelberg (Germany).

Maloszewski, P., Rauert, W., Trimborn, P., Herrmann, A., Rau, R., 1992. Isotope hydrological study of mean transit times in an alpine basin (Wimbachtal, Germany). *Journal of Hydrology* 140, 343–360.

Maloszewski, P., Zuber, A., 1982. Determining the turnover time of groundwater systems with the aid of environmental tracers: 1. Models and their applicability. *Journal of Hydrology* 57, 207–231.

Maloszewski, P., Zuber, A., 1996. Lumped parameter models for the interpretation of environmental tracer data. In *Manual on mathematical models in isotope hydrology*, TECDOC 910, 9–58. International Atomic Energy Agency, Vienna (Austria).

Mangin, A., 1975. *Contribution à l'étude hydrodynamique des aquifères karstiques.* Ph.D. thesis, Université de Dijon.

Mangin, A., 1984. Pour une meilleure connaissance des systèmes hydrologiques à partir des analyses corrélatoire et spectrale. *Journal of Hydrology* 67, 25–43.

Mann, H.B., 1945. Nonparametric tests against trend. *Econometrica* 13, 245–259.

Manning, A.H., Clark, J.F., Diaz, S.H., Rademacher, L.K., Earman, S., Plummer, L.N., 2012. Evolution of groundwater age in a mountain watershed over a period of thirteen years. *Journal of Hydrology* 460, 13–28.

Manning, A.H., Solomon, D.K., 2005. An integrated environmental tracer approach to characterizing groundwater circulation in a mountain block. *Water Resources Research* 41, W12412.

Martínez-Santos, M., Ruíz-Romera, E., Martínez-López, M., Antigüedad, I., 2012. Influence of upwelling on the shallow water chemistry in a small wetland riparian zone (Basque Country). *Applied Geochemistry* 27, 854–865.

Massei, N., Dupont, J., Mahler, B., Laignel, B., Fournier, M., Valdes, D., Ogier, S., 2006. Investigating transport properties and turbidity dynamics of a karst aquifer using correlation, spectral, and wavelet analyses. *Journal of Hydrology* 329, 244–257.

Massoudieh, A., 2013. Inference of long-term groundwater flow transience using environmental tracers: A theoretical approach. *Water Resources Research* 49, 8039–8052.

Massoudieh, A., Leray, S., de Dreuzy, J.R., 2014a. Assessment of the value of groundwater age time-series for characterizing complex steady-state flow systems using a Bayesian approach. *Applied Geochemistry* 50, 240–251.

Massoudieh, A., Visser, A., Sharifi, S., Broers, H.P., 2014b. A Bayesian modeling approach for estimation of a shape-free groundwater age distribution using multiple tracers. *Applied Geochemistry* 50, 252–264.

Matsutani, J., Tanaka, T., Tsujimura, M., 1993. Residence times of soil water, ground, and discharge waters in a mountainous headwater basin, central Japan, traced by tritium. In N.E. Peters, E. Hoehn, C. Leibundgut, N. Tase, D.E. Walling (Editors), *Tracers in Hydrology*, IAHS Publication no. 215, 57–63. International Association for Hydrological Science, Wallingford (UK).

McCallum, J.L., Engdahl, N.B., Ginn, T.R., Cook, P.G., 2014. Nonparametric estimation of groundwater residence time distributions: What can environmental tracer data tell us about groundwater residence time? *Water Resources Research* 50, 2022–2038.

McDonnell, J.J., Beven, K., 2014. Debates — The future of hydrological sciences: A (common) path forward? A call to action aimed at understanding velocities, celerities and residence time distributions of the headwater hydrograph. *Water Resources Research* 50, 5342–5350.

McDonnell, J.J., McGuire, K., Aggarwal, P., Beven, K.J., Biondi, D., Destouni, G., Dunn, S., James, A., Kirchner, J., Kraft, P., Lyon, S., Maloszewski, P., Newman, B., Pfister, L., Rinaldo, A., Rodhe, A., Sayama, T., Seibert, J., Solomon, K., Soulsby, C., Stewart, M., Tetzlaff, D., Tobin, C., Troch, P., Weiler, M., Western, A., Wörman, A., Wrede, S., 2010. How old is streamwater? Open questions in catchment transit time conceptualization, modelling and analysis. *Hydrological Processes* 24, 1745–1754.

McGuire, K.J., McDonnell, J.J., 2006. A review and evaluation of catchment transit time modeling. *Journal of Hydrology* 330, 543–563.

McGuire, K.J., McDonnell, J.J., Weiler, M., Kendall, C., McGlynn, B.L., Welker, J.M., Seibert, J., 2005. The role of topography on catchment-scale water residence time. *Water Resources Research* 41, W05002.

McMillan, H., Tetzlaff, D., Clark, M., Soulsby, C., 2012. Do time-variable tracers aid the evaluation of hydrological model structure? A multimodel approach. *Water Resources Research* 48, W05501.

McNeil, V.H., Cox, M.E., 2007. Defining the climatic signal in stream salinity trends using the Interdecadal Pacific Oscillation and its rate of change. *Hydrology and Earth System Sciences* 11, 1295–1307.

Meng, Y., Tang, D., Xu, H., Li, Y., Gao, L., 2014. Coalbed methane produced water in China: status and environmental issues. *Environmental Science and Pollution Research* 21, 6964–6974.

Meredith, E.L., Kuzara, S.L., 2012. Identification and quantification of base flow using carbon isotopes. *Groundwater* 50, 959–965.

Meredith, K.T., Hollins, S.E., Hughes, C.E., Cendón, D.I., Hankin, S., Stone, D.J.M., 2009. Temporal variation in stable isotopes (^{18}O and ^{2}H) and major ion concentrations within the Darling River between Bourke and Wilcannia due to variable flows, saline groundwater influx and evaporation. *Journal of Hydrology* 378, 313–324.

Meyers, S.D., Kelly, B.G., , O'Brien, J.J., 1993. An introduction to wavelet analysis in oceanography and meteorology: with application to the dispersion of yanai waves. *Monthly Weather Review* 121, 2858–2866.

Michel, R.L., 1992. Residence times in river basins as determined by analysis of long-term tritium records. *Journal of Hydrology* 130, 367–378.

Michel, R.L., 2005. Tritium in the hydrologic cycle. In P.K. Aggarwal, J.R. Gat, K.F.O. Froehlich (Editors), *Isotopes in the water cycle: past, present, and future of a developing science*, 53–66. Springer, Dordrecht (Netherlands).

Molénat, J., Davy, P., Gascuel-Odoux, C., Durand, P., 1999. Study of three subsurface hydrologic systems based on spectral and cross-spectral analysis of time series. *Journal of Hydrology* 222, 152–164.

Möller, P., Dulski, P., Salameh, E., Geyer, S., 2006. Characterization of the sources of thermal spring- and well water in Jordan by rare earth element and yttrium distribution and stable isotopes of H_2O. *Acta hydrochimica et hydrobiologica* 34, 101–116.

Möller, P., Knappe, A., Dulski, P., 2014. Seasonal variations of rare earths and yttrium distribution in the lowland Havel River, Germany, by agricultural fertilization and effluents of sewage treatment plants. *Applied Geochemistry* 41, 62–72.

Mook, W.G., 2000. Volume I: Introduction; theory, methods, review. In W. Mook, Y. Yurtsever (Editors), *Environmental isotopes in the hydrological cycle: principles and applications*, 1–169. UNESCO/IAEA, Paris (France).

Moore, T.A., 2012. Coalbed methane: A review. *International Journal of Coal Geology* 101, 36–81.

Morgenstern, U., Daughney, C.J., 2012. Groundwater age for identification of baseline groundwater quality and impacts of land-use intensification – The National Groundwater Monitoring Programme of New Zealand. *Journal of Hydrology* 456-457, 79–93.

Morgenstern, U., Stewart, M.K., Stenger, R., 2010. Dating of streamwater using tritium in a post nuclear bomb pulse world: continuous variation of mean transit time with streamflow. *Hydrology and Earth System Sciences* 14, 2289–2301.

Morris, B., Lawrence, A., Chilton, P., Adams, B., Calow, R., Klinck, B., 2003. Groundwater and its susceptibility to degradation: A global assessment of the problems and options for management. Early Warning and Assessment Report Series, RS 03-3, United Nations Environment Programme, Nairobi (Kenya).

Moya, C.E., Raiber, M., Taulis, M., Cox, M.E., 2015. Hydrochemical evolution and groundwater flow processes in the Galilee and Eromanga basins, Great Artesian Basin, Australia: A multivariate statistical approach. *Science of The Total Environment* 508, 411–426.

Muñoz Villers, L.E., McDonnell, J.J., 2012. Runoff generation in a steep, tropical montane cloud forest catchment on permeable volcanic substrate. *Water Resources Research* 48, W09528.

Mueller, M.H., Weingartner, R., Alewell, C., 2013. Importance of vegetation, topography and flow paths for water transit times of base flow in alpine headwater catchments. *Hydrology and Earth System Sciences* 17, 1661–1679.

Murphy, B.F., Timbal, B., 2008. A review of recent climate variability and climate change in southeastern Australia. *International Journal of Climatology* 28, 859–879.

Nakken, M., 1999. Wavelet analysis of rainfall–runoff variability isolating climatic from anthropogenic patterns. *Environmental Modelling & Software* 14, 283–295.

Nalley, D., Adamowski, J., Khalil, B., 2012. Using discrete wavelet transforms to analyze trends in streamflow and precipitation in Quebec and Ontario (1954–2008). *Journal of Hydrology* 475, 204–228.

Nathan, R.J., McMahon, T.A., 1990. Evaluation of automated techniques for base flow and recession analyses. *Water Resources Research* 26, 1465–1473.

Négrel, P., Casanova, J., Aranyossy, J.F., 2001. Strontium isotope systematics used to decipher the origin of groundwaters sampled from granitoids: the Vienne case (France). *Chemical Geology* 177, 287–308.

Négrel, P., Guerrot, C., Cocherie, A., Azaroual, M., Brach, M., Fouillac, C., 2000. Rare earth elements, neodymium and strontium isotopic systematics in mineral waters: evidence from the Massif Central, France. *Applied Geochemistry* 15, 1345–1367.

Négrel, P., Millot, R., Guerrot, C., Petelet-Giraud, E., Brenot, A., Malcuit, E., 2012. Heterogeneities and interconnections in groundwaters: Coupled B, Li and stable-isotope variations in a large aquifer system (Eocene Sand aquifer, Southwestern France). *Chemical Geology* 296, 83–95.

Noack, C.W., Dzombak, D.A., Karamalidis, A.K., 2014. Rare earth element distributions and trends in natural waters with a focus on groundwater. *Environmental Science & Technology* 48, 4317–4326.

Olivié-Lauquet, G., Gruau, G., Dia, A., Riou, C., Jaffrezic, A., Henin, O., 2001. Release of trace elements in wetlands: Role of seasonal variability. *Water Research* 35, 943–952.

Owen, D.D.R., Cox, M.E., 2015. Hydrochemical evolution within a large alluvial groundwater resource overlying a shallow coal seam gas reservoir. *Science of The Total Environment* 523, 233–252.

Padilla, A., Pulido-Bosch, A., 1995. Study of hydrographs of karstic aquifers by means of correlation and cross-spectral analysis. *Journal of Hydrology* 168, 73–89.

Papendick, S.L., Downs, K.R., Vo, K.D., Hamilton, S.K., Dawson, G.K., Golding, S.D., Gilcrease, P.C., 2011. Biogenic methane potential for Surat Basin, Queensland coal seams. *International Journal of Coal Geology* 88, 123–134.

Parkhurst, D.L., Appelo, C.A.J., 1999. User's guide to PHREEQC (v.2) – a computer program for speciation, batch-reaction, one-dimensional transport, and inverse geochemical calculations. Water Resources Investigations Report 99-4259, United States Geological Survey, Denver (USA).

Pédrot, M., Dia, A., Davranche, M., Coz, M.B.L., Henin, O., Gruau, G., 2008. Insights into colloid-mediated trace element release at the soil/water interface. *Journal of Colloid and Interface Science* 325, 187–197.

Pédrot, M., Dia, A., Davranche, M., Gruau, G., 2015. Upper soil horizons control the rare earth element patterns in shallow groundwater. *Geoderma* 239, 84–96.

Peel, M.C., McMahon, T.A., Finlayson, B.L., 2004. Continental differences in the variability of annual runoff – update and reassessment. *Journal of Hydrology* 295, 185–197.

Penna, D., Stenni, B., Šanda, M., Wrede, S., Bogaard, T.A., Michelini, M., Fischer, B.M.C., Gobbi, A., Mantese, N., Zuecco, G., Borga, M., Bonazza, M., Sobotková, M., Čejková, B., Wassenaar, L.I., 2012. Technical Note: Evaluation of between-sample memory effects in the analysis of δ^2H and δ^{18}O of water samples measured by laser spectroscopes. *Hydrology and Earth System Sciences* 16, 3925–3933.

Percival, D., Walden, A., 1993. *Spectral Analysis for Physical Applications: Multitaper and Conventional Univariate Techniques, vol.xxvii.* Cambridge University Press, Cambridge (UK).

Perez-Valdivia, C., Sauchyn, D., Vanstone, J., 2012. Groundwater levels and teleconnection patterns in the Canadian Prairies. *Water Resources Research* 48, W07516.

Pettitt, A.N., 1982. Parametric tests for agreement amongst groups of judges. *Biometrika* 69, 365–375.

Playà, E., Cendón, D.I., Travé, A., Chivas, A.R., García, A., 2007. Non-marine evaporites with both inherited marine and continental signatures: The Gulf of Carpentaria, Australia, at $\sim$ 70 ka. *Sedimentary Geology* 201, 267–285.

Please, P.M., Bauld, J., Watkins, K.L., 1997. A groundwater quality assessment of the alluvial aquifers in the Logan-Albert catchment, SE Queensland. 1996/048, Australian Geological Survey Organisation, Canberra (Australia).

Plummer, L., Busenberg, E., Böhlke, J., Nelms, D., Michel, R., Schlosser, P., 2001. Groundwater residence times in Shenandoah National Park, Blue Ridge Mountains, Virginia, USA: a multi-tracer approach. *Chemical Geology* 179, 93–111.

Poh, S.C., Gasparon, M., 2011. Rare earth elements: indicators of redox conditions and surface water–groundwater mixing in an estuarine wetland. In *Goldscmidt Conference Series*, Mineralogical Magazine 75, 1652.

Pourmand, A., Dauphas, N., Ireland, T.J., 2012. A novel extraction chromatography and MC-ICP-MS technique for rapid analysis of REE, Sc and Y: Revising CI-chondrite and Post-Archean Australian Shale (PAAS) abundances. *Chemical Geology* 291, 38–54.

Pourret, O., Davranche, M., Gruau, G., Dia, A., 2007. Rare earth elements complexation with humic acid. *Chemical Geology* 243, 128–141.

Pourret, O., Gruau, G., Dia, A., Davranche, M., Molénat, J., 2010. Colloidal control on the distribution of rare earth elements in shallow groundwaters. *Aquatic Geochemistry* 16, 31–59.

Quinn, K.A., Byrne, R.H., Schijf, J., 2006. Sorption of yttrium and rare earth elements by amorphous ferric hydroxide: Influence of solution complexation with carbonate. *Geochimica et Cosmochimica Acta* 70, 4151–4165.

Radziejewski, M., Kundzewicz, Z.W., 2004. Detectability of changes in hydrological records. *Hydrological Sciences Journal* 49, 39–51.

Raiber, M., Webb, J.A., Bennetts, D.A., 2009. Strontium isotopes as tracers to delineate aquifer interactions and the influence of rainfall in the basalt plains of southeastern Australia. *Journal of Hydrology* 367, 188–199.

Raiber, M., Webb, J.A., Cendón, D.I., White, P.A., Jacobsen, G.E., 2015. Environmental isotopes meet 3D geological modelling: Conceptualising recharge and structurally-controlled aquifer connectivity in the basalt plains of south-western Victoria, Australia. *Journal of Hydrology* 527, 262–280.

Rassam, D., Raiber, M., McJannet, D., Janardhanan, S., Murray, J., Gilfedder, M., Cui, T., Matveev, V., Doody, T., Hodgen, M., Ahmad, M.E., 2014. Context statement for the Clarence-Moreton bioregion. Product 1.1 from the Clarence-Moreton Bioregional Assessment, Department of the Environment, Bureau of Meteorology, CSIRO and Geoscience Australia, Canberra (Australia).

Reddy, M.M., Schuster, P., Kendall, C., Reddy, M.B., 2006. Characterization of surface and ground water δ^{18}O seasonal variation and its use for estimating groundwater residence times. *Hydrological Processes* 20, 1753–1772.

Redmond, K.T., Koch, R.W., 1991. Surface climate and streamflow variability in the western United States and their relationship to large-scale circulation indices. *Water Resources Research* 27, 2381–2399.

Ribolzi, O., Vallès, V., Bariac, T., 1996. Comparison of hydrograph deconvolutions using residual alkalinity, chloride, and oxygen-18 as hydrochemical tracers. *Water Resources Research* 32, 1051–1059.

Rinaldo, A., Beven, K.J., Bertuzzo, E., Nicotina, L., Davies, J., Fiori, A., Russo, D., Botter, G., 2011. Catchment travel time distributions and water flow in soils. *Water Resources Research* 47, W07537.

Roa-García, M.C., Weiler, M., 2010. Integrated response and transit time distributions of watersheds by combining hydrograph separation and long-term transit time modeling. *Hydrology and Earth System Sciences* 14, 1537–1549.

Rodgers, P., Soulsby, C., Waldron, S., Tetzlaff, D., 2005. Using stable isotope tracers to assess hydrological flow paths, residence times and landscape influences in a nested mesoscale catchment. *Hydrology and Earth System Sciences* 9, 139–155.

Roques, C., Bour, O., Aquilina, L., Dewandel, B., Leray, S., Schroetter, J.M., Longuevergne, L., Borgne, T.L., Hochreutener, R., Labasque, T., Lavenant, N., Vergnaud-Ayraud, V., Mougin, B., 2014. Hydrological behavior of a deep sub-vertical fault in crystalline basement and relationships with surrounding reservoirs. *Journal of Hydrology* 509, 42–54.

Rozanski, K., Araguás-Araguás, L., Gonfiantini, R., 1993. Isotopic patterns in modern global precipitation. In P.K. Swart, K.C. Lohman, J. McKenzie, S. Savin (Editors), *Climate Change in Continental Isotopic Records*, 1–36. American Geophysical Union, Washington D.C. (USA).

Schlegel, M.E., McIntosh, J.C., Bates, B.L., Kirk, M.F., Martini, A.M., 2011. Comparison of fluid geochemistry and microbiology of multiple organic-rich reservoirs in the Illinois Basin, USA: Evidence for controls on methanogenesis and microbial transport. *Geochimica et Cosmochimica Acta* 75, 1903–1919.

Schmidt, C., Musolff, A., Trauth, N., Vieweg, M., Fleckenstein, J.H., 2012. Transient analysis of fluctuations of electrical conductivity as tracer in the stream bed. *Hydrology and Earth System Sciences* 16, 3689–3697.

Schramke, J.A., Murphy, E.M., Wood, B.D., 1996. The use of geochemical mass-balance and mixing models to determine groundwater sources. *Applied Geochemistry* 11, 523–539.

Seccombe, D.W., 1989. Report on groundwater investigations within the Teviot Brook Irrigation Project. Water Resources Division internal report, Queensland Department of Primary Industry.

Seeger, S., Weiler, M., 2014. Reevaluation of transit time distributions, mean transit times and their relation to catchment topography. *Hydrology and Earth System Sciences* 18, 4751–4771.

SEQwater, 2013. Improving catchment health in Upper Teviot Brook. Catchment Planning Report 2013, Queensland Government.

Shah, T., Burke, J., Villholth, K., 2007. Groundwater: a global assessment of scale and significance. In *Water for food, water for life: a comprehensive assessment of water management in agriculture*. International Water Management Institute, London (UK).

Sharma, S., Baggett, J.K., 2011. Application of carbon isotopes to detect seepage out of coalbed natural gas produced water impoundments. *Applied Geochemistry* 26, 1423–1432.

Sharma, S., Frost, C., 2008. Tracing coalbed natural gas-coproduced water using stable isotopes of carbon. *Ground Water* 46, 329–334.

Shiller, A.M., 1997. Dissolved trace elements in the Mississippi River: Seasonal, interannual, and decadal variability. *Geochimica et Cosmochimica Acta* 61, 4321–4330.

Shiller, A.M., 2002. Seasonality of dissolved rare earth elements in the lower Mississippi River. *Geochemistry, Geophysics, Geosystems* 3, 1–14.

Siebert, C., Rosenthal, E., Möller, P., Rödiger, T., Meiler, M., 2012. The hydrochemical identification of groundwater flowing to the Bet She'an-Harod multiaquifer system (Lower Jordan Valley) by rare earth elements, yttrium, stable isotopes (H, O) and tritium. *Applied Geochemistry* 27, 703–714.

Simpson, H.J., Herczeg, A.L., 1994. Delivery of marine chloride in precipitation and removal by rivers in the Murray-Darling Basin, Australia. *Journal of Hydrology* 154, 323–350.

Sinclair Knight Merz, 2012. Impacts of groundwater extraction on streamflow in selected catchments throughout Australia. Waterlines Report, National Water Commission, Canberra (Australia).

Sklash, M.G., Farvolden, R.N., 1979. Role of groundwater in storm runoff. *Journal of Hydrology* 43, 45–65.

Slimani, S., Massei, N., Mesquita, J., Valdés, D., Fournier, M., Laignel, B., Dupont, J.P., 2009. Combined climatic and geological forcings on the spatio-temporal variability of piezometric levels in the chalk aquifer of Upper Normandy (France) at pluridecennal scale. *Hydrogeology Journal* 17, 1823–1832.

Smedley, P.L., 1991. The geochemistry of rare earth elements in groundwater from the Carnmenellis area, southwest England. *Geochimica et Cosmochimica Acta* 55, 2767–2779.

Smerdon, B.D., Allen, D.M., Grasby, S.E., Berg, M.A., 2009. An approach for predicting groundwater recharge in mountainous watersheds. *Journal of Hydrology* 365, 156–172.

Smerdon, B.D., Gardner, W.P., Harrington, G.A., Tickell, S.J., 2012. Identifying the contribution of regional groundwater to the baseflow of a tropical river (Daly River, Australia). *Journal of Hydrology* 464, 107–115.

Sophocleous, M., 2002. Interactions between groundwater and surface water: the state of the science. *Hydrogeology Journal* 10, 52–67.

Soulsby, C., Malcolm, R., Helliwell, R., Ferrier, R.C., Jenkins, A., 2000. Isotope hydrology of the Allt a'Mharcaidh catchment, Cairngorms, Scotland: implications for hydrological pathways and residence times. *Hydrological Processes* 14, 747–762.

Stearns, M., Tindall, J.A., Cronin, G., Friedel, M.J., Bergquist, E., 2005. Effects of coal-bed methane discharge waters on the vegetation and soil ecosystem in Powder River Basin, Wyoming. *Water, Air, & Soil Pollution* 168, 33–57.

Stephens, D.B., 1995. *Vadose zone hydrology.* CRC Press, Boca Raton (USA).

Stevens, N.C., Grenfell, A., Knutson, J., Ewart, A., 1989. Main range. In R.W. Johnson (Editor), *Intraplate Volcanism in Eastern Australia and New Zealand*, 111–112. Cambridge University Press, Cambridge (UK).

Stewart, M.K., 2012. A 40-year record of carbon-14 and tritium in the Christchurch groundwater system, New Zealand: Dating of young samples with carbon-14. *Journal of Hydrology* 430, 50–68.

Stewart, M.K., 2015. Promising new baseflow separation and recession analysis methods applied to streamflow at Glendhu Catchment, New Zealand. *Hydrology and Earth System Sciences* 19, 2587–2603.

Stewart, M.K., McDonnell, J.J., 1991. Modeling base flow soil water residence times from deuterium concentrations. *Water Resources Research* 27, 2681–2693.

Stewart, M.K., Mehlhorn, J., Elliott, S., 2007. Hydrometric and natural tracer (oxygen-18, silica, tritium and sulphur hexafluoride) evidence for a dominant groundwater contribution to Pukemanga Stream, New Zealand. *Hydrological Processes* 21, 3340–3356.

Stewart, M.K., Morgenstern, U., McDonnell, J.J., 2010. Truncation of stream residence time: how the use of stable isotopes has skewed our concept of streamwater age and origin. *Hydrological Processes* 24, 1646–1659.

Stewart, M.K., Morgenstern, U., McDonnell, J.J., Pfister, L., 2012. The 'hidden streamflow' challenge in catchment hydrology: a call to action for stream water transit time analysis. *Hydrological Processes* 26, 2061–2066.

Stewart, M.K., Taylor, C.B., 1981. Environmental isotopes in New Zealand hydrology; 1. Introduction. The role of oxygen-18, deuterium, and tritium in hydrology. *New Zealand Journal of Science* 24, 295–311.

Stewart, M.K., Thomas, J.T., 2008. A conceptual model of flow to the Waikoropupu Springs, NW Nelson, New Zealand, based on hydrometric and tracer (^{18}O, Cl, ^{3}H and CFC) evidence. *Hydrology and Earth System Sciences* 12, 1–19.

Stolp, B.J., Solomon, D.K., Suckow, A., Vitvar, T., Rank, D., Aggarwal, P.K., Han, L.F., 2010. Age dating base flow at springs and gaining streams using helium-3 and tritium: Fischa-Dagnitz system, southern Vienna Basin, Austria. *Water Resources Research* 46, W07503.

Suecker, J.K., Ryan, J.N., Kendall, C., Jarrett, R.D., 2000. Determination of hydrologic pathways during snowmelt for alpine/subalpine basins, Rocky Mountain National Park, Colorado. *Water Resources Research* 36, 63–75.

Tadros, C.V., Hughes, C.E., Crawford, J., Hollins, S.E., Chisari, R., 2014. Tritium in Australian precipitation: A 50 year record. *Journal of Hydrology* 513, 262–273.

Tang, J., Johannesson, K.H., 2005. Rare earth element concentrations, speciation, and fractionation along groundwater flow paths: the Carrizo Sand (Texas) and Upper Floridan aquifers. In K.H. Johannesson (Editor), *Rare Earth Elements in Groundwater Flow Systems*, 223–251. Springer, Dordrecht (Netherlands).

Tang, J., Johannesson, K.H., 2006. Controls on the geochemistry of rare earth elements along a groundwater flow path in the Carrizo Sand aquifer, Texas, USA. *Chemical Geology* 225, 156–171.

Tang, J., Johannesson, K.H., 2010a. Ligand extraction of rare earth elements from aquifer sediments: Implications for rare earth element complexation with organic matter in natural waters. *Geochimica et Cosmochimica Acta* 74, 6690–6705.

Tang, J., Johannesson, K.H., 2010b. Rare earth elements adsorption onto Carrizo sand: Influence of strong solution complexation. *Chemical Geology* 279, 120–133.

Taulis, M., Milke, M., 2007. Coal seam gas water from Maramarua, New Zealand: Characterisation and comparison to United States analogues. *Journal of Hydrology New Zealand* 46, 1–17.

Taylor, C.B., Wilson, D.D., Brown, L.J., Stewart, M.K., Burden, R.J., Brailsford, G.W., 1989. Sources and flow of north Canterbury plains groundwater, New Zealand. *Journal of Hydrology* 106, 311–340.

Taylor, R.G., Scanlon, B., Döll, P., Rodell, M., van Beek, R., Wada, Y., Longuevergne, L., Leblanc, M., Famiglietti, J.S., Edmunds, M., Konikow, L., Green, T.R., Chen, J., Taniguchi, M., Bierkens, M.F.P., MacDonald, A., Fan, Y., Maxwell, R.M., Yechieli, Y., Gurdak, J.J., Allen, D.M., Shamsudduha, M., Hiscock, K., Yeh, P.J.F., Holman, I., Treidel, H., 2013. Ground water and climate change. *Nature Climate Change* 3, 322–329.

Tetzlaff, D., Birkel, C., Dick, J., Geris, J., Soulsby, C., 2014. Storage dynamics in hydropedological units control hillslope connectivity, runoff generation, and the evolution of catchment transit time distributions. *Water Resources Research* 50, 969–985.

Tetzlaff, D., Seibert, J., Soulsby, C., 2009. Inter-catchment comparison to assess the influence of topography and soils on catchment transit times in a geomorphic province; the Cairngorm mountains, Scotland. *Hydrological Processes* 23, 1874–1886.

Tetzlaff, D., Soulsby, C., Hrachowitz, M., Speed, M., 2011. Relative influence of upland and lowland headwaters on the isotope hydrology and transit times of larger catchments. *Journal of Hydrology* 400, 438–447.

Timbe, E., Windhorst, D., Crespo, P., Frede, H.G., Feyen, J., Breuer, L., 2014. Understanding uncertainties when inferring mean transit times of water trough tracer-based lumped-parameter models in Andean tropical montane cloud forest catchments. *Hydrology and Earth System Sciences* 18, 1503–1523.

Torrence, C., Compo, G.P., 1998. A practical guide to wavelet analysis. *Bulletin of the American Meteorological Society* 79, 61–78.

Torrence, C., Webster, P.J., 1999. Interdecadal changes in the ENSO-monsoon system. *Journal of Climate* 12, 2679–2690.

Tremblay, L., Larocque, M., Anctil, F., Rivard, C., 2011. Teleconnections and interannual variability in Canadian groundwater levels. *Journal of Hydrology* 410, 178–188.

Tukey, J., 1968. An introduction to the calculations of numerical spectrum analysis. In B. Harris (Editor), *Spectral Analysis of Time Series*, 25–46. Wiley, New York (USA).

Tweed, S., Munksgaard, N., Marc, V., Rockett, N., Bass, A., Forsythe, A.J., Bird, M.I., Leblanc, M., 2016. Continuous monitoring of stream δ^{18}O and δ^{2}H and stormflow hydrograph separation using laser spectrometry in an agricultural catchment. *Hydrological Processes* 30, 648–660.

Tweed, S.O., Weaver, T.R., Cartwright, I., Schaefer, B., 2006. Behavior of rare earth elements in groundwater during flow and mixing in fractured rock aquifers: An example from the Dandenong Ranges, southeast Australia. *Chemical Geology* 234, 291–307.

Uhlenbrook, S., 2006. Catchment hydrology–a science in which all processes are preferential. *Hydrological Processes* 20, 3581–3585.

Ullman, W.J., Collerson, K.D., 1994. The Sr-isotope record of late quaternary hydrologic changes around Lake Frome, South Australia. *Australian Journal of Earth Sciences* 41, 37–45.

Unland, N.P., Cartwright, I., Andersen, M.S., Rau, G.C., Reed, J., Gilfedder, B.S., Atkinson, A.P., Hofmann, H., 2013. Investigating the spatio-temporal variability in groundwater and surface water interactions: a multi-technique approach. *Hydrology and Earth System Sciences* 17, 3437–3453.

Valdes, D., Dupont, J.P., Massei, N., Laignel, B., Rodet, J., 2006. Investigation of karst hydrodynamics and organization using autocorrelations and $T - \Delta C$ curves. *Journal of Hydrology* 329, 432–443.

Van Beek, C.G.E.M., Van Breemen, N., 1973. The alkalinity of alkali soils. *Journal of Soil Science* 24, 129–136.

van der Velde, Y., de Rooij, G.H., Rozemeijer, J.C., van Geer, F.C., Broers, H.P., 2010. Nitrate response of a lowland catchment: On the relation between stream concentration and travel time distribution dynamics. *Water Resources Research* 46, W11534.

van der Velde, Y., Heidbüchel, I., Lyon, S.W., Nyberg, L., Rodhe, A., Bishop, K., Troch, P.A., 2015. Consequences of mixing assumptions for time-variable travel time distributions. *Hydrological Processes* 3460–3474.

van Dijk, A.I.J.M., Beck, H.E., Crosbie, R.S., de Jeu, R.A.M., Liu, Y.Y., Podger, G.M., Timbal, B., Viney, N.R., 2013. The Millennium Drought in southeast Australia (2001–2009): Natural and human causes and implications for water resources, ecosystems, economy, and society. *Water Resources Research* 49, 1040–1057.

Van Voast, W.A., 2003. Geochemical signature of formation waters associated with coalbed methane. *AAPG Bulletin* 87, 667–676.

Venturelli, G., Boschetti, T., Duchi, V., 2003. Na-carbonate waters of extreme composition: Possible origin and evolution. *Geochemical Journal* 37, 351–366.

Vogel, J.C., 1967. Investigation of groundwater flow with radiocarbon. In *Isotopes in hydrology*, 355–369. International Atomic Energy Agency, Vienna (Austria).

Wada, Y., Wisser, D., Bierkens, M.F.P., 2014. Global modeling of withdrawal, allocation and consumptive use of surface water and groundwater resources. *Earth System Dynamics* 5, 15–40.

Wahi, A.K., Hogan, J.F., Ekwurzel, B., Baillie, M.N., Eastoe, C.J., 2008. Geochemical quantification of semiarid mountain recharge. *Ground Water* 46, 414–425.

Wang, G., Hendon, H.H., 2007. Sensitivity of Australian rainfall to inter-El Niño variations. *Journal of Climate* 20, 4211–4226.

Ward, C.R., Spears, D.A., Booth, C.A., Staton, I., Gurba, L.W., 1999. Mineral matter and trace elements in coals of the Gunnedah Basin, New South Wales, Australia. *International Journal of Coal Geology* 40, 281–308.

Weissmann, G.S., Zhang, Y., LaBolle, E.M., Fogg, G.E., 2002. Dispersion of groundwater age in an alluvial aquifer system. *Water Resources Research* 38, 16–1–16–13.

Welch, C., Harrington, G.A., Leblanc, M., Batlle-Aguilar, J., Cook, P.G., 2014. Relative rates of solute and pressure propagation into heterogeneous alluvial aquifers following river flow events. *Journal of Hydrology* 511, 891–903.

Welch, L.A., Allen, D.M., 2014. Hydraulic conductivity characteristics in mountains and implications for conceptualizing bedrock groundwater flow. *Hydrogeology Journal* 22, 1003–1026.

Wells, A.T., O'Brien, P.E., 1994. *Geology and petroleum potential of the Clarence-Moreton Basin, New South Wales and Queensland*. Australian Geological Survey Organisation, Canberra (Australia).

Whitford, D.J., Hamilton, P.J., Scott, J., 1994. Sedimentary provenance studies in Australian basins using neodymium model ages. *APEA Journal* 34, 320–329.

Willis, S.S., Johannesson, K.H., 2011. Controls on the geochemistry of rare earth elements in sediments and groundwaters of the Aquia aquifer, Maryland, USA. *Chemical Geology* 285, 32–49.

Wilson, J.L., Guan, H., 2004. Mountain-block hydrology and mountain-front recharge. In J.F. Hogan, F.M. Phillips, B.R. Scanlon (Editors), *Groundwater Recharge in a Desert Environment: The Southwestern United States*, 113–137. American Geophysical Union, Washington D.C. (USA).

Winter, T., Harvey, J., Franke, O., Alley, W., 1998. Groundwater and surface water: A single resource. USGS Circular 1139, United States Geological Survey.

Woessner, W.W., 2000. Stream and fluvial plain ground water interactions: Rescaling hydrogeologic thought. *Ground Water* 38, 423–429.

Worsley, K.J., 1979. On the likelihood ratio test for a shift in location of normal populations. *Journal of the American Statistical Association* 74, 365–367.

Yago, J.V., 1989. *Basin analysis of the middle Jurassic Walloon Coal Measures in the Great Artesian Basin, Australia*. Ph.D. thesis, University of Queensland.

Yan, Z., Liu, G., Sun, R., Tang, Q., Wu, D., Wu, B., Zhou, C., 2013. Geochemistry of rare earth elements in groundwater from the Taiyuan Formation limestone aquifer in the Wolonghu Coal Mine, Anhui province, China. *Journal of Geochemical Exploration* 135, 54–62.

Yu, H.L., Lin, Y.C., 2015. Analysis of space–time non-stationary patterns of rainfall–groundwater interactions by integrating empirical orthogonal function and cross wavelet transform methods. *Journal of Hydrology* 525, 585–597.

Zhang, Y.K., Schilling, K., 2004. Temporal scaling of hydraulic head and river base flow and its implication for groundwater recharge. *Water Resources Research* 40, W03504.

Zhou, H., Wang, Q., Zhao, J., Zheng, L., Guan, H., Feng, Y., Greig, A., 2008. Rare earth elements and yttrium in a stalagmite from Central China and potential paleoclimatic implications. *Palaeogeography, Palaeoclimatology, Palaeoecology* 270, 128–138.

Zuber, A., 1986. Mathematical models for the interpretation of environmental radioisotopes in groundwater systems. In P. Fritz, J. Fontes (Editors), *Handbook of environmental isotope geochemistry*, 1–59. Elsevier, Amsterdam (Netherlands).

Zuber, A., Maloszewski, P., 2000. Volume VI: Modelling – Chapter 2: Lumped parameter models. In W. Mook, Y. Yurtsever (Editors), *Environmental isotopes in the hydrological cycle: principles and applications*, 497–516. UNESCO/IAEA, Paris (France).

Zuber, A., Witczak, S., Rozanski, K., Sliwka, I., Opoka, M., Mochalski, P., Kuc, T., Karlikowska, J., Kania, J., Jackowicz-Korczynski, M., Dulinski, M., 2005. Groundwater dating with ^{3}H and SF_6 in relation to mixing patterns, transport modelling and hydrochemistry. *Hydrological Processes* 19, 2247–2275.

APPENDIX A

Tracer Data

Table A.1: Major ions and ionic ratios for groundwaters and surface waters collected during the dry sampling round (October 2012) in the Teviot Brook catchment.

Sampling location	Hydrological unit	TDS (mg/L)	Ca (mg/L)	Mg (mg/L)	Na (mg/L)	K (mg/L)	Alk (mg/L)	Cl (mg/L)	SO_4 (mg/L)	Si (mg/L)	molar Na/Cl (-)	r (meq/L)	CCR (-)	SI calcite	SI dolomite	SI kaolinite
T1	Main stream	272	24.4	12.2	22.9	1.1	158.7	27.3	5.4	13.2	1.2	0.4	1.5	-1.15	-2.32	4.24
T2		663	51.8	31.2	71.2	2.4	377.2	98.5	3.6	13.4	1.1	1.0	0.7	0.36	0.76	5.85
T3		618	46.8	30.7	71.0	3.4	341.0	103.4	3.1	10.4	1.1	0.7	0.6	-0.33	-0.55	3.47
T4		1573	134.0	92.7	218.2	5.0	448.1	588.7	71.1	8.3	0.6	-7.0	0.3	0.54	1.29	2.28
T5		2777	269.0	159.0	381.0	3.0	523.3	1235.6	178.1	12.2	0.5	-17.9	0.3	0.83	1.79	3.03
T6		3634	300.0	195.0	687.1	5.7	463.4	1811.4	153.6	8.3	0.6	-23.4	0.0	1.06	2.26	3.57
CCk	Tributaries	1925	66.8	94.9	357.9	5.5	826.7	500.0	59.4	10.0	1.1	2.4	-0.3	0.77	2.08	6.62
OCk		2784	162.0	120.0	548.5	3.8	577.6	1118.9	225.1	12.8	0.8	-8.5	-0.2	0.45	1.07	3.99
SG		5018	97.2	263.0	1259.0	8.3	821.1	2170.1	379.6	3.5	0.9	-13.0	-0.5	1.27	3.31	2.60
A01	Alluvium	550	61.1	31.6	38.6	0.6	314.0	61.7	7.7	23.6	1.0	-0.5	2.3	-0.60	-1.17	5.34
A02		661	67.3	36.3	54.9	0.8	393.0	70.3	4.2	22.1	1.2	0.1	2.0	-0.27	-0.51	3.88
A04		1387	29.0	17.7	358.4	0.9	648.0	306.0	10.3	10.2	1.8	7.7	-1.5	-0.16	-0.21	5.55
A05		2285	279.0	170.0	181.6	0.2	525.5	1060.6	37.5	17.1	0.3	-19.3	0.7	0.10	0.30	5.21
A06		824	87.9	31.5	124.9	0.3	279.1	258.5	19.0	10.5	0.7	-2.4	0.2	-0.42	-1.00	6.39
A07		837	79.7	39.1	81.2	0.6	557.1	41.7	15.2	15.8	2.9	1.9	3.0	0.00	0.00	7.22
A08		850	74.5	37.8	91.7	1.9	409.7	112.1	35.1	17.2	1.5	1.6	0.7	-0.21	-0.40	4.43
A09		1569	146.0	104.0	180.6	0.8	604.6	461.6	44.0	10.8	0.6	-5.9	0.6	-0.05	0.07	5.60
A10		2354	348.0	152.0	193.7	3.5	334.0	1201.8	88.7	17.4	0.2	-24.4	0.6	-0.06	-0.17	5.69
A11		1237	122.0	70.1	147.9	1.6	503.2	321.7	33.3	18.8	0.7	-3.7	0.6	-0.01	0.06	6.84
A12		3669	352.0	208.0	559.3	2.8	629.1	1819.6	50.8	17.0	0.5	-24.4	0.2	0.20	0.48	5.31
A13		2033	176.0	99.2	324.1	1.5	543.3	832.4	30.0	14.4	0.6	-8.0	0.1	0.23	0.53	4.79
A14		2282	179.0	112.0	391.2	3.5	514.4	1023.9	30.7	16.4	0.6	-9.7	0.0	0.93	1.97	3.45
B01	Sedimentary bedrock	368	16.5	9.6	67.0	1.5	214.5	24.4	9.6	17.5	4.2	1.9	-1.9	-0.17	-0.28	2.09
B02		1152	46.4	43.8	211.1	3.0	577.9	227.0	1.4	22.2	1.4	3.6	-0.5	0.89	2.06	4.79
B03		2817	23.0	15.6	775.2	6.8	1039.7	935.3	0.0	11.6	1.3	14.6	-1.2	-0.07	0.01	3.92
B04		974	68.4	42.9	138.8	2.6	556.0	118.4	7.9	21.8	1.8	2.2	0.3	0.15	0.42	6.12
B05		1743	3.1	1.6	496.0	2.6	813.6	392.0	0.0	8.9	1.9	13.0	-1.9	0.23	0.37	4.55
B06		2678	149.0	89.2	559.6	4.8	571.3	1262.1	22.2	8.7	0.7	-5.4	-0.3	-0.06	-0.04	5.05
B07		1083	48.4	60.5	159.3	3.6	623.8	131.4	13.4	24.2	1.9	2.8	0.1	-0.03	0.35	6.20
B08		2877	79.0	88.3	723.0	6.3	588.7	1278.7	74.5	20.8	0.9	-1.6	-0.6	-0.15	0.06	5.05
B09		2779	53.8	52.9	658.8	4.9	1171.3	730.3	88.2	7.5	1.4	12.2	-1.1	-0.06	0.18	6.21
B10		1262	39.3	20.7	269.2	4.7	779.2	103.0	3.4	22.2	4.0	9.1	-2.8	-0.12	-0.17	5.18
B11		2511	30.2	28.0	654.6	5.0	1005.0	754.6	5.8	11.3	1.3	12.7	-1.2	0.14	0.54	5.01
B12		1529	97.6	95.7	201.9	2.7	623.8	456.9	14.3	14.5	0.7	-2.5	0.3	-0.01	0.30	5.32
B13		4802	28.1	11.6	1698.0	8.1	414.8	2597.5	14.7	9.8	1.0	4.4	-1.0	0.15	0.20	3.21
B14		928	27.3	25.4	202.0	3.0	505.6	121.9	21.8	7.8	2.6	4.8	-1.6	-0.12	0.04	4.40
I02	Igneous springs	225	22.2	9.0	16.8	0.8	137.8	12.5	5.3	11.9	1.8	0.4	2.8	-0.11	-0.31	3.17
I03		320	7.6	7.5	84.1	2.7	72.2	118.0	12.1	7.2	1.1	0.2	-0.8	-2.97	-5.67	2.22

Alk stands for alkalinity, r for residual alkalinity, and CCR is the cation chloride ratio index (Owen and Cox, 2015). 'T' is for the samples collected from the main stream, 'CCk', 'OCk' and 'SG' are tributaries, 'A' is for alluvial boreholes, 'B' is for bedrock boreholes, and 'I' is for igneous springs. Saturation indices were calculated using PHREEQC (Parkhurst and Appelo, 1999).

Table A.2: Major ions and ionic ratios for groundwaters and surface waters collected during the wet sampling round (March 2013) in the Teviot Brook catchment.

Sampling location	Hydrological unit	TDS (mg/L)	Ca (mg/L)	Mg (mg/L)	Na (mg/L)	K (mg/L)	Alk (mg/L)	Cl (mg/L)	SO_4 (mg/L)	Si (mg/L)	molar Na/Cl (-)	r (meq/L)	CCR (-)	SI calcite	SI dolomite	SI kaolinite
T1	Main stream	234	23.3	9.3	15.0	2.7	140.2	18.9	4.3	11.2	1.3	0.4	2.4	-0.05	-0.18	3.13
T2		290	27.0	13.1	23.9	5.0	163.6	37.0	5.1	11.8	1.0	0.3	1.3	-0.39	-0.78	4.38
T3		365	35.0	18.2	32.9	3.7	207.6	46.7	6.0	11.1	1.1	0.2	1.3	0.56	1.17	2.41
T4		376	31.6	16.8	42.2	5.8	184.2	69.6	9.4	11.3	0.9	0.0	0.5	0.24	0.54	3.56
T5		504	44.6	24.6	62.0	4.3	226.8	114.6	14.4	10.3	0.8	-0.5	0.5	0.62	1.33	2.37
CCk	Tributaries	436	24.8	23.0	71.7	3.7	141.6	138.9	18.6	9.8	0.8	-0.8	0.0	-0.71	-1.14	5.92
SCk		799	59.1	32.6	143.2	4.9	311.4	218.9	11.8	13.3	1.0	-0.5	-0.1	0.47	0.98	3.84
FCk		505	31.4	27.2	75.4	4.5	195.2	137.7	9.8	14.4	0.8	-0.6	0.1	-0.04	0.17	3.76
WCk		1160	67.4	55.4	235.5	8.7	270.8	498.4	6.8	13.1	0.7	-3.5	-0.2	0.25	0.77	3.55
OCk		2417	162.2	114.6	471.0	7.5	481.8	950.0	213.7	11.5	0.8	-9.6	-0.1	0.90	1.98	3.88
SG		2502	77.7	124.3	635.0	15.5	400.0	1055.3	178.3	8.4	0.9	-7.5	-0.5	0.50	1.57	3.23
A01	Alluvium	582	64.0	34.0	32.0	1.7	339.7	65.1	7.8	22.7	0.8	-0.4	2.5	-0.28	-0.53	6.08
A02		703	73.9	41.3	48.7	1.9	424.5	71.7	4.4	22.5	1.1	-0.1	2.5	-0.08	-0.11	5.76
A03		654	63.2	35.4	55.2	2.2	423.8	47.6	1.8	18.1	1.8	0.8	2.8	0.34	0.78	4.19
A04		1255	29.4	17.5	348.3	3.2	560.9	260.9	7.5	15.0	2.0	6.3	-1.7	-0.35	-0.59	8.70
A05		1862	238.6	142.1	168.8	3.6	686.3	559.0	32.7	17.6	0.5	-12.4	1.0	0.18	0.49	6.92
A06		792	81.9	28.4	105.9	2.0	384.5	153.4	18.5	9.9	1.1	-0.1	0.4	-0.31	-0.77	5.98
A07		760	75.6	38.4	71.4	2.3	486.5	42.8	15.4	15.4	2.6	1.1	3.1	-0.19	-0.35	7.04
A08		713	64.7	34.0	82.5	4.5	381.7	97.4	20.8	18.1	1.3	0.3	0.9	-0.07	-0.10	5.67
A09		1823	202.5	130.7	202.8	2.4	690.4	518.2	47.2	13.8	0.6	-9.6	0.8	0.17	0.47	6.65
A10		2187	360.1	151.3	171.7	5.1	321.7	1077.3	72.1	16.1	0.2	-25.1	0.8	-0.01	-0.08	6.57
A11		1133	133.5	61.0	107.8	3.6	427.5	314.1	36.8	18.4	0.5	-4.7	0.8	-0.02	-0.06	7.45
A12		4211	490.9	272.9	643.5	9.0	624.1	2088.0	48.8	18.2	0.5	-36.8	0.3	0.32	0.71	6.62
A13		1805	178.8	92.0	281.5	3.5	501.6	701.3	24.6	14.5	0.6	-8.3	0.2	0.05	0.13	7.16
A14		2361	229.4	132.3	398.2	8.0	549.2	990.2	26.9	17.1	0.6	-13.3	0.2	0.30	0.70	6.36
B01	Sedimentary bedrock	489	13.2	8.1	105.1	2.7	297.6	27.2	1.1	18.2	5.7	3.6	-4.1	0.20	0.54	1.98
B02		1545	65.2	66.6	294.8	5.5	793.2	261.9	29.4	18.5	1.7	4.3	-0.6	0.40	1.16	4.38
B03		3333	28.8	19.6	1074.6	11.9	1186.6	990.4	0.0	13.6	1.7	16.3	-1.6	0.58	1.36	4.12
B04		938	90.4	54.8	87.0	3.0	580.9	74.5	9.6	23.6	1.8	0.5	2.5	0.14	0.38	5.85
B05		1941	1.5	0.8	624.1	8.3	915.1	364.2	0.0	9.2	2.6	14.9	-2.6	-0.35	-0.63	3.85
B06		2656	170.3	106.1	609.0	8.9	605.0	1118.6	24.8	9.3	0.8	-7.3	-0.3	-0.12	-0.12	6.37
B07		1116	48.2	54.7	177.1	5.0	663.0	121.1	11.0	23.2	2.3	4.0	-0.3	0.15	0.68	4.94
B08		3481	92.7	103.4	964.0	13.9	824.8	1370.7	69.9	24.0	1.1	0.4	-0.8	0.42	1.23	4.92
B09		3253	72.8	73.2	902.3	8.6	1419.5	681.7	76.6	9.4	2.0	13.6	-1.6	0.07	0.46	5.43
B10		1313	30.3	22.8	291.7	5.4	788.3	112.9	1.6	36.5	4.0	9.5	-2.9	-0.25	-0.28	5.25
B11		2516	25.6	16.9	713.3	7.5	1266.5	443.7	1.6	22.0	2.5	18.1	-2.3	0.11	0.38	4.67
B12		1712	124.8	126.2	240.7	6.6	665.7	498.8	13.5	16.5	0.7	-5.7	0.4	0.38	1.10	5.21
B13		6234	32.4	11.4	2557.3	24.2	528.3	3041.2	15.0	10.0	1.3	6.1	-1.3	0.16	0.20	2.81
B14		740	24.7	21.6	155.3	4.1	458.9	44.2	15.5	10.9	5.6	4.5	-3.2	-0.07	0.12	4.21
I01	Igneous springs	425	38.3	17.5	28.3	4.7	228.4	35.0	8.0	13.4	1.2	0.4	2.0	-0.02	0.14	3.55
I02		189	19.9	7.6	9.7	4.6	108.6	14.1	3.8	12.2	1.1	0.2	2.7	0.12	0.08	5.39
I04		272	18.1	11.9	33.2	3.2	138.2	44.0	6.1	11.3	1.8	0.4	0.3	-0.22	-0.29	2.88

Alk stands for alkalinity, r for residual alkalinity, and CCR is the cation chloride ratio index (Owen and Cox, 2015). 'T' is for the samples collected from the main stream, 'CCk', 'OCk' and 'SG' are tributaries, 'A' is for alluvial boreholes, 'B' is for bedrock boreholes, and 'I' is for igneous springs. Saturation indices were calculated using PHREEQC (Parkhurst and Appelo, 1999).

Table A.3: Isotope data for groundwaters and surface waters in the Teviot Brook catchment (dry and wet season).

		dry sampling round						wet sampling round			
Sampling location	Hydrological unit	δ^2H (‰)	δ^{18}O (‰)	*d*-excess (‰)	^{3}H (TU)	^{87}Sr/^{86}Sr	δ^{13}C-DIC (‰)	δ^2H (‰)	δ^{18}O (‰)	*d*-excess (‰)	δ^{13}C-DIC (‰)
T1	Main stream	-21.10	-4.31	13.3	nd	0.70377	-12.95	-26.57	-4.73	11.3	-10.89
T2		-12.24	-1.76	1.8	1.28	0.70395	-9.90	-24.45	-3.96	7.2	-10.67
T3		-2.26	-0.43	1.2	nd	0.70410	-9.35	-24.20	-4.38	10.8	-9.91
T4		-3.98	-0.44	-0.5	nd	0.70412	-6.86	-24.72	-4.28	9.5	-9.96
T5		-12.81	-1.98	3.1	nd	0.70397	-7.67	-22.93	-3.87	8.0	-9.34
T6		-7.16	-1.44	4.3	nd	0.70450	-7.70	nd	nd	nd	-8.90
CCk	Tributaries	-11.85	-2.39	7.2	nd	0.70383	-10.27	-30.45	-4.79	7.9	nd
SCk		nd	nd	nd	nd	*0.70430*	nd	-22.21	-3.5	5.7	-9.32
FCk		nd	nd	nd	nd	*0.70421*	nd	-24.72	-4.08	7.9	-10.14
WCk		nd	nd	nd	nd	*0.70407*	nd	-16.69	-2.64	4.4	-8.33
OCk		-13.04	-2.34	5.7	nd	0.70390	-7.57	-15.29	-2.33	3.4	-4.41
SG		-2.67	-0.28	-0.4	nd	0.70405	-5.90	-16.91	-2.95	6.7	nd
A01	Alluvium	-20.55	-3.82	10.0	1.07	0.70388	-8.01	-20.67	-3.71	9.5	-5.89
A02		-23.54	-4.15	9.6	0.77	0.70385	-8.24	-22.70	-3.97	9.1	-5.25
A03		nd	nd	nd	0.80	0.70395	nd	-23.27	-4.06	9.2	-5.93
A04		-17.44	-3.34	9.2	0.74	nd	-12.88	-19.60	-3.58	9.0	-10.41
A05		-23.32	-4.06	9.1	0.73	0.70433	-9.07	-21.87	-4.01	10.2	-1.88
A06		-14.11	-2.38	5.0	1.22	0.70417	-7.74	-27.50	-4.11	5.4	-5.05
A07		-23.71	-3.96	8.0	0.37	0.70401	-8.18	-28.71	-4.52	8.2	nd
A08		-17.64	-3.43	7.0	1.12	0.70396	-12.82	-17.19	-2.95	7.1	-11.38
A09		-18.77	-2.93	4.7	nd	nd	-10.28	-19.53	-3.37	7.4	-4.42
A10		-19.70	-2.95	3.9	0.54	0.70393	-8.00	-23.00	-3.74	6.9	-4.95
A11		-22.55	-3.59	6.2	< 0.05	0.70401	-11.35	-21.70	-3.74	8.3	-9.35
A12		-21.16	-3.61	7.7	0.43	0.70427	-6.35	-21.66	-3.67	7.7	-0.62
A13		-22.01	-3.94	9.5	0.20	0.70423	-10.49	-22.49	-3.81	8.0	-4.90
A14		-14.89	-2.84	7.8	0.55	nd	-11.22	-15.16	-2.65	6.1	-4.16
B01	Sedimentary bedrock	-21.79	-4.93	17.7	1.12	0.70383	-14.58	-21.23	-4.28	13.0	-13.62
B02		-21.07	-4.45	14.5	0.70	0.70391	-14.48	-22.27	-4.04	10.1	-11.10
B03		-25.93	-4.74	12.0	< 0.05	0.70356	-8.12	-26.07	-4.77	12.1	-6.49
B04		-22.42	-3.84	8.3	0.49	0.70423	-10.71	-24.12	-4.05	8.3	-6.37
B05		-26.26	-5.34	16.4	< 0.05	0.70383	-3.23	-24.04	-4.14	9.1	-2.72
B06		-16.90	-3.25	9.1	0.38	0.70369	-12.14	-14.68	-2.06	1.8	-5.26
B07		-25.41	-4.68	12.0	0.09	0.70366	-13.74	-26.11	-4.44	9.4	nd
B08		-22.65	-3.82	7.9	0.18	0.70378	nd	-23.73	-3.96	8.0	-9.76
B09		-20.57	-3.69	8.9	0.39	0.70364	-12.84	-19.77	-3.12	5.2	-9.87
B10		-22.43	-3.95	9.1	< 0.05	0.70353	-12.47	-23.91	-3.86	7.0	-11.16
B11		-23.30	-4.53	13.0	< 0.05	0.70350	-10.89	-23.39	-4.05	9.0	-7.11
B12		-20.30	-3.53	7.9	0.57	0.70389	-9.97	-21.38	-3.25	4.6	-5.47
B13		-25.11	-4.56	11.4	< 0.05	0.70334	-7.93	-26.70	-4.67	10.6	-8.44
B14		-12.27	-1.55	0.1	1.28	0.70431	-11.13	-14.90	-1.48	-3.0	-10.03
I01	Igneous springs	nd	nd	nd	nd	*0.70370*	nd	-26.56	-5.19	15.0	-13.43
I02		-22.13	-4.63	14.9	1.30	0.70355	-13.93	-26.95	-4.85	11.9	-11.54
I03		-17.62	-2.75	4.4	nd	0.70539	-12.97	nd	nd	nd	nd
I04		nd	nd	nd	nd	*0.70400*	nd	-28.23	-4.84	10.5	-13.43

d-excess: deuterium excess. nd: not determined. Italicised values for the strontium isotopic ratios were measured in samples collected during the wet sampling round. The δ^2H and δ^{18}O values are expressed relative to the SMOW standard. The δ^{13}C-DIC values are expressed relative to PDB standard.

Table A.4: Rare earth element concentrations in different hydrological units of the Teviot Brook catchment (dry sampling round).

Hydrological unit		pH	EC (µS/cm)	La	Ce	Pr	Nd	Sm	Eu	Gd	Tb	Dy	Ho	Er	Tm	Yb	Lu	∑ REE	Y	$R_{(M/L)}$	$R_{(H/M)}$
Igneous	I02	7.78	222	14.4	29.2	2.9	16.5	3.8	0.7	4.2	0.7	4.2	0.8	2.5	0.3	2.7	0.4	83.4	23.0	0.38	0.09
	I03	5.70	575	327.9	475.4	133.2	666.7	133.8	20.2	109.2	12.8	61.1	12.7	41.3	6.7	44.0	9.1	2054.2	364.7	0.20	0.04
Main stream	T1	6.65	345	16.5	27.2	2.9	15.9	4.3	0.7	4.4	0.7	4.3	0.9	2.9	0.4	3.2	0.5	84.7	29.5	0.37	0.15
	T2	7.58	660	45.8	88.3	10.1	49.5	12.4	3.0	13.0	2.0	10.8	2.3	6.8	0.9	6.2	0.9	252.0	63.3	0.34	-0.02
	T3	6.93	865	372.4	841.1	107.6	463.8	105.1	28.0	105.0	14.8	73.5	14.0	35.8	4.9	27.8	4.1	2197.9	nd	0.25	-0.26
	T4	7.29	1370	232.9	517.6	65.0	295.2	69.5	17.5	69.3	10.3	53.8	10.2	27.2	3.6	21.1	3.3	1396.4	319.5	0.30	-0.20
	T5	7.35	5040	233.6	545.5	65.3	295.1	69.1	17.0	72.1	10.6	56.6	11.3	31.4	4.4	24.6	4.1	1440.6	367.0	0.31	-0.13
	T6	7.66	7140	136.2	300.9	37.5	175.3	41.5	10.4	62.2	6.8	33.2	7.0	18.3	2.6	14.6	2.3	848.7	nd	0.42	-0.25
Tributaries	CCk	7.58	2850	77.5	205.7	20.1	97.3	22.3	5.2	23.2	3.8	19.3	4.2	11.1	1.5	10.3	1.5	502.9	116.8	0.34	-0.08
	SG	8.20	8130	114.0	317.8	33.8	149.2	37.7	9.6	40.4	6.1	31.3	6.7	17.1	2.5	14.3	2.2	782.9	212.1	0.36	-0.14
	OCk	7.17	4660	60.3	138.8	15.2	74.9	18.3	4.8	21.4	3.4	17.0	3.8	10.6	1.4	9.3	1.4	380.6	122.5	0.41	-0.07
Alluvium	A02	6.58	793	379.1	791.5	100.1	428.7	93.4	24.5	96.0	14.0	71.9	13.7	37.5	4.8	27.3	4.2	2086.7	nd	0.24	-0.23
	A03	6.78	959	43.0	55.3	7.4	31.6	8.7	1.3	8.7	1.1	9.9	2.1	8.1	1.2	9.3	1.2	188.9	nd	0.19	0.35
	A04	7.09	2130	611.9	833.7	172.1	639.4	146.0	28.8	116.7	21.6	119.8	24.6	68.2	9.0	65.5	9.9	2867.1	nd	0.15	0.01
	A05	6.60	4270	394.6	881.0	98.6	562.7	103.4	27.4	89.7	15.3	72.6	14.1	41.3	4.3	26.3	4.7	2335.9	nd	0.24	-0.21
	A06	6.70	1480	974.0	1397.3	288.2	1399.4	237.8	62.9	305.5	39.5	269.9	48.1	133.8	15.9	103.6	17.9	5293.6	nd	0.28	-0.10
	A08	6.61	2680	198.7	486.2	67.3	255.5	54.2	14.6	50.7	6.6	38.9	6.5	16.3	2.7	13.5	1.7	1213.6	nd	0.15	-0.27
	A10	6.55	4540	9.3	28.1	3.8	12.0	3.9	1.2	7.6	0.8	7.6	1.9	6.9	0.8	3.6	1.0	88.4	51.2	0.56	0.21
	A11	6.75	2085	13.8	32.3	2.8	11.7	3.2	0.6	3.3	1.1	7.8	1.7	7.8	0.9	7.2	1.3	95.5	95.4	0.48	0.48
	A14	7.61	4270	45.0	96.1	11.8	58.8	13.6	2.7	16.3	2.4	14.6	4.0	9.0	1.2	11.0	1.0	287.4	129.3	0.39	0.03
Sedimentary bedrock	B01	7.70	480	7.1	10.2	1.6	6.7	1.8	0.5	4.4	1.2	8.7	2.0	6.9	0.8	7.8	1.5	61.2	64.4	0.81	0.46
	B03	7.20	5000	3.4	5.7	0.7	2.7	0.7	0.2	1.2	0.3	4.4	1.5	5.0	0.8	4.9	1.1	32.6	67.1	0.52	0.93
	B05	8.33	2830	2.4	4.7	0.7	3.0	0.8	0.2	1.3	0.2	1.9	0.4	1.2	0.1	1.0	0.2	18.1	12.8	0.57	0.18
	B09	6.81	4840	65.3	114.7	20.3	114.7	33.2	7.3	37.7	6.2	39.2	6.6	15.5	2.1	11.6	2.3	476.8	nd	0.58	-0.16
	B13	7.70	10960	24.3	45.3	6.9	23.9	6.3	1.3	7.0	1.1	7.6	1.9	4.8	0.8	3.9	1.1	136.1	75.9	0.29	0.21
	B14	7.23	1470	21.8	36.7	5.6	26.1	8.4	1.3	7.3	1.6	12.9	2.8	7.4	1.0	6.4	0.9	140.2	133.3	0.47	0.13

Concentrations of rare earth elements are expressed in parts per trillion (ppt); nd: not determined. The ratios $R_{(M/L)}$ and $R_{(H/M)}$ as calculated according to equations 6.1 and 6.2 are also shown.

Table A.5: Rare earth element concentrations in different hydrological units of the Teviot Brook catchment (wet sampling round).

Hydrological unit		**pH**	**EC (µS/cm)**	**La**	**Ce**	**Pr**	**Nd**	**Sm**	**Eu**	**Gd**	**Tb**	**Dy**	**Ho**	**Er**	**Tm**	**Yb**	**Lu**	**∑ REE**	**Y**	**$R_{(M/L)}$**	**$R_{(H/M)}$**
Igneous	I01	7.10	665	4.3	9.2	1.3	5.3	1.1	0.1	1.0	0.2	0.9	0.2	0.6	0.1	0.6	0.1	25.1	6.5	0.23	0.01
	I02	7.90	250	16.5	30.1	3.5	17.1	4.1	0.9	4.6	0.8	4.7	0.9	2.8	0.4	3.1	0.4	90.0	22.7	0.36	0.08
	I04	6.64	370	53.2	135.4	10.9	53.1	11.7	2.3	11.3	1.7	9.2	1.8	4.9	0.6	3.8	0.6	300.3	46.9	0.22	-0.16
Main stream	T1	7.78	270	17.1	31.8	3.7	19.5	4.4	0.9	4.9	0.7	3.9	0.8	2.4	0.3	2.2	0.4	93.0	25.8	0.34	-0.02
	T3	8.10	490	40.3	54.9	7.8	37.8	8.8	2.3	10.2	1.5	8.7	1.7	5.1	0.6	4.1	0.6	184.3	56.5	0.30	-0.11
	T5	8.04	790	48.3	70.9	9.8	45.0	10.1	2.5	10.7	1.8	10.7	2.3	6.6	0.8	5.9	0.9	226.3	75.7	0.26	0.03
Tributaries	FCk	7.60	805	31.8	46.3	8.7	44.8	10.8	2.4	11.5	1.7	10.3	2.2	6.2	0.9	6.3	1.0	185.0	63.2	0.39	0.07
	OCk	7.67	4370	14.5	25.9	2.8	17.5	4.5	1.1	6.3	1.0	6.9	1.6	5.4	0.7	5.5	0.9	94.6	70.3	0.56	0.24
	SCk	7.70	1230	28.0	51.8	7.1	36.6	9.4	2.2	10.3	1.5	9.2	1.8	5.4	0.7	4.9	0.8	169.6	58.6	0.40	0.00
	WCk	7.48	2190	59.5	68.2	12.2	67.0	14.6	3.2	18.9	2.8	16.1	3.9	11.0	1.6	10.3	1.7	291.0	145.1	0.39	0.07
Alluvium	A01	7.35	860	10.2	19.7	2.8	11.8	2.9	0.6	4.2	1.3	6.0	1.6	4.8	0.7	5.4	0.9	73.0	68.3	0.63	0.25
	A03	6.90	955	2.6	7.7	1.3	7.1	1.2	0.2	1.2	0.2	3.6	1.3	3.6	0.4	4.7	0.9	36.0	49.6	0.39	0.89
	A04	6.95	2040	130.0	187.9	39.8	188.0	50.1	13.0	53.3	8.7	41.0	8.4	20.7	2.8	16.1	2.6	762.5	nd	0.44	-0.21
	A05	6.58	3150	50.0	121.4	15.7	85.2	19.9	5.9	23.3	3.6	20.2	4.8	13.1	1.7	10.5	1.5	377.0	nd	0.47	-0.05
	A06	6.67	1150	24.8	33.1	6.9	37.4	9.4	2.2	10.5	1.3	7.9	1.7	4.8	0.7	4.5	0.7	145.9	52.8	0.41	-0.01
	A07	6.73	980	77.1	188.2	22.2	101.6	23.7	6.6	23.0	3.6	17.5	3.6	9.8	1.2	8.0	1.1	487.3	nd	0.30	-0.17
	A08	6.65	3010	3.4	5.0	1.2	8.7	2.0	0.3	2.9	0.4	3.0	0.7	2.0	0.2	1.3	0.2	31.3	49.6	0.68	-0.03
	A09	7.01	1002	8.4	15.2	2.1	9.3	2.6	0.3	3.6	0.6	4.6	1.1	3.6	0.5	4.1	0.6	56.6	44.9	0.52	0.32
	A10	6.59	4260	0.5	0.8	0.1	0.6	0.1	nd	0.2	0.04	0.4	0.05	0.2	nd	0.1	nd	nd	6.0	0.54	0.13
	A11	6.76	1810	0.9	0.6	0.2	1.0	0.3	nd	0.3	0.1	0.6	0.2	0.6	0.0	0.6	0.1	nd	9.3	0.48	0.59
	A12	6.60	7850	13.7	18.6	3.2	20.6	4.9	1.2	7.5	1.3	9.8	2.3	7.5	0.9	6.3	0.9	98.6	116.7	0.63	0.19
	A13	6.82	3270	0.2	nd	nd	1.0	0.2	nd	0.5	0.1	0.9	0.3	1.2	0.1	1.2	0.2	nd	26.1	1.42	0.57
	A14	6.84	4320	1.9	4.3	0.4	1.6	0.4	nd	0.8	0.2	1.9	0.5	2.0	0.2	1.9	0.3	16.5	27.6	0.59	0.62
Sedimentary bedrock	B01	8.00	580	19.4	38.9	5.1	22.6	6.4	1.6	7.5	1.3	10.1	2.3	7.5	1.1	8.2	1.3	133.2	73.9	0.46	0.32
	B02	7.23	2220	18.2	21.3	2.8	14.7	4.3	0.9	8.1	1.7	12.6	3.4	12.1	2.0	13.7	2.6	118.4	150.6	0.67	0.51
	B03	7.70	5090	22.1	34.3	4.3	18.4	4.6	1.1	6.1	1.3	10.2	2.7	10.2	1.8	12.7	2.5	132.4	107.7	0.43	0.60
	B04	6.93	1180	11.9	16.6	2.0	8.0	1.7	0.3	2.6	0.4	2.6	0.6	2.0	0.2	1.8	0.3	51.2	28.2	0.30	0.15
	B05	8.12	2870	4.8	8.9	nd	3.6	0.8	nd	0.8	0.2	1.0	0.2	0.7	0.1	0.5	0.1	21.6	9.3	0.17	0.07
	B06	6.52	5020	5.8	10.8	1.2	5.7	1.5	0.2	2.2	0.4	2.8	0.7	2.1	0.2	1.7	0.3	35.5	34.4	0.51	0.15
	B07	7.16	1574	6.7	10.1	1.0	5.8	1.4	0.2	1.9	0.4	2.6	0.6	2.1	0.3	2.2	0.4	35.6	25.6	0.49	0.34
	B08	7.20	6210	12.8	21.0	2.5	11.1	2.6	0.4	3.4	0.6	4.0	0.9	2.8	0.4	3.4	0.5	66.5	35.3	0.35	0.26
	B09	6.74	5130	17.5	28.7	3.5	14.8	3.8	0.8	5.0	0.8	5.9	1.2	3.5	0.4	3.0	0.4	89.5	50.7	0.38	0.05
	B10	6.86	1770	4.5	11.6	1.8	8.9	3.3	1.1	7.6	1.4	9.1	1.7	5.1	0.6	3.6	0.5	61.0	56.1	1.00	-0.08
	B11	7.21	3870	13.5	25.8	3.2	15.0	4.0	1.5	5.4	1.0	7.0	1.4	4.5	0.6	4.4	0.8	88.2	69.3	0.52	0.19
	B12	7.05	2860	5.7	8.7	1.4	6.9	1.8	0.4	2.4	0.4	3.0	0.7	2.1	0.3	1.9	0.3	36.0	27.7	0.51	0.20
	B13	7.68	11850	10.4	20.0	2.5	10.8	2.7	0.5	3.0	0.5	3.4	0.7	2.1	0.3	1.8	0.3	58.9	22.4	0.33	0.07
	B14	7.33	970	4.8	5.0	0.7	3.8	1.2	0.2	1.6	0.3	1.5	0.3	1.0	0.1	1.0	0.1	21.6	13.6	0.49	0.05

Concentrations of rare earth elements are expressed in parts per trillion (ppt); nd: not determined. The ratios $R_{(M/L)}$ and $R_{(H/M)}$ as calculated according to equations 6.1 and 6.2 are also shown.

Table A.6: Whole-rock samples REE concentrations.

Sample location	Geological unit	Sample depth (m)	La	Ce	Pr	Nd	Sm	Eu	Gd	Tb	Dy	Y	Ho	Er	Tm	Yb	Lu
		-	82	167	nd	72	13.10	2.16	12.10	1.83	nd	nd	1.88	nd	0.75	4.75	0.74
Flinders Peak	trachyte	-	71	148	nd	67	14.40	2.28	11.70	2.08	nd	nd	2.30	nd	0.88	5.81	0.87
		-	86	176	nd	79	17.10	2.09	14.00	2.62	nd	nd	2.80	nd	1.02	6.98	1.01
Mount Alford	rhyolite	-	52	113	nd	46	8.60	0.20	6.90	1.12	nd	nd	1.20	nd	0.44	3.00	0.42
		75	25.77	56.98	7.04	27.54	5.64	1.38	4.95	0.79	4.70	24.63	0.97	2.67	0.40	2.59	0.38
Wild Horse	WCM	78	16.98	40.34	5.45	24.19	6.21	1.72	7.04	1.07	6.39	38.62	1.40	4.03	0.60	3.87	0.59
		92	21.91	49.20	6.14	23.96	4.73	1.26	4.27	0.72	4.53	23.81	0.97	2.69	0.40	2.55	0.37

Concentrations are expressed in parts per million (ppm); nd: not determined. Data for the trachyte and rhyolite samples are from Ewart et al. (1985); data for the WCM samples are from this study.

APPENDIX B

Statement of Contribution of Co-Authors

The authors listed in the following have certified* that:

1. They meet the criteria for authorship in that they have participated in the conception, execution, or interpretation, of at least that part of the publication in their field of expertise;

2. They take public responsibility for their part of the publication, except for the responsible author who accepts overall responsibility for the publication;

3. There are no other authors of the publication according to these criteria;

4. Potential conflicts of interest have been disclosed to (a) granting bodies, (b) the editor or publisher of journals or other publications, and (c) the head of the responsible academic unit;

5. They agree to the use of the publication in the student's thesis and its publication on the QUT ePrints database consistent with any limitations set by publisher requirements.

Chapter 4: Response of a Stream–Aquifer System to Low and High Frequency Rainfall Fluctuations

Contributor	Statement of Contribution*
Clément Duvert	Designed the research, carried out the data analysis, interpreted the results and wrote the manuscript.
Hervé Jourde*	Assisted with research design and data analysis, and contributed to the manuscript.
Matthias Raiber*	Contributed to the manuscript.
Malcolm E. Cox*	Contributed to the manuscript.

Principal Supervisor Confirmation

I have sighted email or other correspondence from all co-authors confirming their certifying authorship.

Name: Malcolm Cox **Signature** QUT Verified Signature **Date:** 2-04-2016

Chapter 5: Hydrochemical Processes in a River–Alluvium–Bedrock Continuum and Implications for Recharge

Contributor	Statement of Contribution*
Clément Duvert	Designed the research, carried out the field and laboratory work, data analysis and wrote the manuscript.
Matthias Raiber*	Assisted with research design and data analysis, and contributed to the manuscript.
Daniel D.R. Owen*	Assisted with data analysis and contributed to the manuscript.
Dioni I. Cendón*	Assisted with laboratory analysis and contributed to the manuscript.
Christelle Batiot*	Contributed to the manuscript.
Malcolm E. Cox*	Contributed to the manuscript.

Principal Supervisor Confirmation

I have sighted email or other correspondence from all co-authors confirming their certifying authorship.

Name: Malcolm Cox **Signature** QUT Verified Signature **Date:** 2-04-2016

Chapter 6: Linking Seasonal & Spatial Variations in Rare Earth Elements with Inter-Aquifer Processes

Contributor	Statement of Contribution*
Clément Duvert	Designed the research, carried out the field and laboratory work, data analysis and wrote the manuscript.
Dioni I. Cendón*	Assisted with laboratory analysis, interpretation of results and contributed to the manuscript.
Matthias Raiber*	Assisted with research design and contributed to the manuscript.
Jean-Luc Seidel*	Assisted with laboratory analysis and contributed to the manuscript.
Malcolm E. Cox*	Contributed to the manuscript.

Principal Supervisor Confirmation

I have sighted email or other correspondence from all co-authors confirming their certifying authorship.

Name: Malcolm Cox **Signature:** QUT Verified Signature **Date:** 2-04-2016

Chapter 7: Tritium Reveals Temporal Variations in the Groundwater Contribution to a Stream

Contributor	Statement of Contribution*
Clément Duvert	Designed the research, carried out the field work, analysed the data and wrote the manuscript.
Michael K. Stewart*	Assisted with data analysis, interpretation of results, and contributed to the manuscript.
Dioni I. Cendón*	Assisted with laboratory analysis and contributed to the manuscript.
Matthias Raiber*	Assisted with research design and contributed to the manuscript.

Principal Supervisor Confirmation

I have sighted email or other correspondence from all co-authors confirming their certifying authorship.

Name: Malcolm Cox **Signature:** QUT Verified Signature **Date:** 2-04-2016